CRPP

CENTRE DE RECHERCHES EN PHYSIQUE DES PLASMAS
FACULTÉ DES SCIENCES DE BASE
ASSOCIATION EURATOM - CONFÉDÉRATION SUISSE

ÉCOLE POLYTECHNIQUE
FÉDÉRALE DE LAUSANNE

ANNUAL REPORT

2008

Table of content

Préface

J'ai le plaisir de vous présenter le rapport annuel 2008 du Centre de Recherches en Physique des Plasmas (CRPP) incluant en particulier les activités de l'Association Euratom - Confédération Suisse.

Nos travaux couvrent les domaines d'excellences traditionnels du CRPP et je suis fier de pouvoir présenter les nombreux résultats discutés dans le rapport.

Je tiens à remercier tous les organismes suisses et internationaux qui nous ont apporté leur soutien financier. L'engagement de mes collègues est un élément essentiel de notre succès que j'aimerais souligner: je tiens ici à leur exprimer ma reconnaissance.

Prof. M.Q. Tran
Directeur Général

Forword

It is my pleasure to present to you the annual report 2008 of the Centre de Recherches en Physique des Plasmas (CRPP) including in particular the activities of the Association Euratom – Swiss Confederation.

Our work covers the traditional domains of excellence of CRPP and I am proud to be able to present to you the numerous results discussed in the report.

I wish to thank all Swiss and International organisations that have supported us financially. The commitment of my colleagues is an essential element of our success, which I would like to highlight: let me herewith express my gratitude to them.

Prof. M.Q. Tran
General Director

Vorwort

Ich freue mich, Ihnen hiermit den Jahresbericht 2008 des Centre de Recherches en Physique des Plasmas (CRPP) vorlegen zu können, der insbesondere die Aktivitäten im Rahmen der Assoziation EURATOM - Schweizer Eidgenossenschaft umfasst.

Mit unserer Arbeit decken wir Gebiete ab, auf denen das CRPP eine hervorragende Stellung erreicht hat. Ich bin stolz darauf, Ihnen in diesem Bericht eine Uebersicht der vielfältigen Ergebnisse geben zu können.

Es ist mir ein wichtiges Anliegen, bei dieser Gelegenheit allen nationalen und internationalen Organisation zu danken, die uns finanziell unterstützt haben. Meinen Kollegen am CRPP möchte ich Dank und Anerkennung aussprechen für Ihren ständigen und bereitwilligen Einsatz, der die Grundlage unserer erfolgreichen Arbeit bildet.

Prof. M.Q. Tran
General Direktor

Prefazione

E' mia prerogativa e mio onore presentare il rapporto annuale 2008 del Centro di Ricerca in Fisica dei Plasmi (CRPP) comprendenti in particolare le attività dell'Associazione Euratom – Confederazione Elvetica.

Le attività che ho il piacere di presentare in questo rapporto coprono le diverse aree d'eccellenza del CRPP.

Vorrei cogliere l'occasione per porgere i miei ringraziamenti a tutti gli organismi svizzeri e internazionali che ci hanno fornito il loro sostegno finanziario. Tengo altresì ad esprimere la mia profonda gratitudine ai miei colleghi, il cui impegno è un elemento essenziale per il successo delle nostre ricerche.

Prof. M.Q. Tran
Direttore Generale

1 INTRODUCTION

1.1 The international frame and its relation to the Swiss programme

ITER remains the focus of the international activities. The ITER Organisation with the collaboration of the participating Parties (China, EU, India, Japan, Korea, Russia and USA) is analyzing the technical, scientific and managerial impacts of the Design Review.

Switzerland has formalised its participation to ITER. This is performed by an exchange of letters between the Swiss Confederation and the EU. The Upper Chamber of the Parliament ratifies this exchange in 2008. Full ratification is expected in 2009.

In 2008 the Euratom conducts a review of its programme, known as the "Facility Review". An international panel including high-level personalities from the industrial, academic world gives clear recommendations about the European strategy for the next 20-30 years. Only a few tokamaks are expected to play a key role before the scientific operation of ITER (foreseen at this time by 2018). The CRPP tokamak is one of these few machines for which the Panel recommends the upgrades and continuation of operation.

The Fusion Research in Switzerland, since 1978, is fully integrated in the Euratom Programme via the various Agreements. In 2008, it is important to note that the European Fusion Programme has launched a new initiative to buy a 100 Teraflops high performance computer (HPC) devoted specifically for fusion. The CRPP, being traditionally a centre of excellence in numerical modelling, is expected to play an important role during the scientific exploitation phase.

1.2 A brief summary of the CRPP activities

The research at the CRPP during 2008 continued along the same lines as in the past. The Annual Report provides details on the scientific achievements and the technical developments performed. A few highlights are given below:

- on TCV a number of original results were obtained, despite a relatively short experimental campaign, resuming in March 2008 after a planned shutdown dedicated to a number of refurbishments, including the replacement of all plasma facing CFC tiles, and two unforeseen interruptions due to vacuum problems. We cite here only two of these results:
- a new divertor configuration ("snowflake") was developed on TCV, allowing a better energy flux in the divertor;
- real-time control of plasma current and elongation using ECRH actuators on TCV was demonstrated for the first time;
- for the first time, statistical steady state gyrokinetic particle simulations of turbulence could be performed thanks to the application of numerical noise control algorithms;
- a wealth of scientific results was obtained in the field of the physics of turbulence using the specialised device Torpex;

- R+D activities in view of the construction of ITER were performed in the field of heating, plasma magnetic diagnostics and qualification of superconducting cables;
- material sciences and technology were focused on the fabrication, characterisation and modelling of low activation steels and refractory alloys;
- industrial processes involving plasma remains an important line of research in collaboration with industry.

Switzerland is a "voluntary contributor" in the "Braoder Approach" activities agreed between the EU and Japan. The CRPP is the main Swiss actor for all activities decided by the government.

Finally, it is important to note that the CRPP was the local organiser of the IAEA 22nd Fusion Energy Conference. The 22nd FEC was held at the Palais des Nations in Geneva and was hosted by the Swiss Government. It commemorated the 50th Anniversary of the 2nd Conference on Peaceful use of Atomic Energy in 1958, where fusion research was declassified and which allowed international collaboration.

1. INTRODUCTION

1.1 La situation internationale en relation avec le programme Suisse

ITER reste le point focal des activités internationales. L'Organisation ITER, en collaboration avec les pays participants (la Chine, l'Union Européenne, l'Inde, le Japon, la Corée du Sud, la Russie et les USA) analyse l'impact technique, scientifique et directorial du «Design Review».

La Suisse a formalisé sa participation à ITER, par échange de lettres entre la Confédération Helvétique et l'UE. Le Conseil des Etats (chambre haute du parlement fédéral) a ratifié cet échange en 2008. La ratification complète est attendue pour 2009.

En 2008, l'Euratom a conduit un réexamen de son programme, connu sous le nom de «Facility Review». Un jury d'experts internationaux, incluant des personnalités de haut niveau de l'industrie et du monde académique, a donné des recommandations claires sur la stratégie européenne pour les 20 ou 30 prochaines années. Seul un petit nombre de tokamaks vont jouer un rôle clé avant l'opération scientifique d'ITER (prévue pour le moment en 2018). Le tokamak du CRPP, le TCV, est l'une de ces quelques machines pour lesquelles le jury d'experts recommande la revalorisation et la poursuite des opérations.

La recherche en fusion en Suisse est, depuis 1978, pleinement intégrée dans le programme Euratom par divers accords. Il est important de mentionner que le programme européen a lancé, en 2008, une initiative afin d'acquérir un ordinateur de haute performance de 100 Teraflops dédié spécifiquement à la fusion. Le CRPP, étant traditionnellement un centre d'excellence en modélisation numérique, va jouer un rôle important durant la phase d'exploitation scientifique.

1.2 Un bref résumé des activités du CRPP

La recherche au CRPP a continué en 2008 dans les mêmes lignes que par le passé. Le rapport annuel donne les détails des succès scientifiques obtenus et des développements technologiques entrepris. Quelques points marquants sont donnés ci-dessous :

- Dans le tokamak TCV, un certain nombre de résultats originaux ont été obtenus, malgré une campagne expérimentale relativement courte, qui n'a pu débuter qu'en Mars 2008 à cause d'une ouverture de la machine planifiée pour différentes interventions techniques, y compris le remplacement de toutes les tuiles en carbone, et qui a été interrompue à deux reprises à cause de problèmes de vide. Nous ne citons ici que deux exemples de ces résultats :
- Dans TCV, une nouvelle configuration du divergeur, baptisée «snowflake», a été développée, permettant une meilleure répartition de l'énergie sortante ;
- Le contrôle en temps réel du courant et de l'élongation du plasma en utilisant des actuateurs ECRH a été démontré pour la première fois.
- Pour la première fois, des simulations gyrocinétiques particulaires de la turbulence ont pu être obtenues en état stationnaire du point de vue statistique, grâce à l'application d'algorithmes de contrôle du bruit numérique.

- Quantité de résultats scientifiques ont été obtenus dans le domaine de la physique de la turbulence en utilisant l'expérience spécialisée Torpex.
- Des activités de R&D en vue de la construction d'ITER ont été accomplies dans les domaines du chauffage du plasma, des diagnostics magnétiques et de la qualification des câbles supraconducteurs.
- La science et la technologie des matériaux se sont focalisées sur la fabrication, la caractérisation et la modélisation des aciers à faible activation et des alliages réfractaires.
- Les procédés plasmas pour l'industrie restent une ligne de recherche importante, en collaboration avec des sociétés privées.

La Suisse est un contributeur volontaire aux activités dites de « Broader Approach » agréées entre l'UE et le Japon. Le CRPP est l'acteur principal Suisse pour toutes les activités décidées par le gouvernement.

Pour terminer, il est important de mentionner que le CRPP a été l'organisateur local de la 22^{e} Conférence sur l'Energie de Fusion de l'Agence Internationale de l'Energie Atomique (AIEA). Cette conférence s'est tenue au Palais des Nations à Genève sous les auspices du gouvernement suisse. Elle commémorait le 50^{e} anniversaire de la 2^{e} Conférence sur l'Utilisation Pacifique de l'Energie Atomique de 1958, au cours de laquelle la recherche en fusion fut rayée de la liste des activités secrètes, ce qui permit la collaboration internationale.

1 EINLEITUNG

1.1 Der internationale Rahmen und der Bezug zum Forschungsprogramm in der Schweiz

Das Projekt ITER steht weiterhin im Brennpunkt der internationalen Forschungsaktivitäten zur Kernfusion. Zur Zeit werden die Auswirkungen des "design reviews" im technischen, wissenschaftlichen und organisatorischen Bereich von der ITER-Organisation und den beteiligten Partnern (China, Europäische Union, Indien, Japan, Korea, Russische Föderation und USA) analysiert.
Die Schweiz hat ihre Beteilung am ITER-Projekt durch einen Briefaustausch zwischen der Schweizer Konföderation und der Europäischen Union nun auch formell geregelt. Der Ständerat hat diesen Briefwechsel im Jahr 2008 bestätigt; mit der vollen Ratifizierung wird für das Jahr 2009 gerechnet.

Im Jahre 2008 wurde von EURATOM unter dem Titel "Facilities Review" eine Bestandsaufnahme des wissenschaftlichen Programms durchgeführt. Eine Auswahl internationaler Experten aus dem industriellen und akademischen Bereich gab Empfehlungen zur Strategie für die nächsten 20-30 Jahre ab. Nur wenigen Tokamak-Experimenten wird für die Zeit vor der Inbetriebnahme von ITER (erwartungsgemäss im Jahr 2018) noch eine bedeutende Rolle zugemessen. Der Tokamak TCV des CRPP ist eine der ausgewählten Maschinen, für die von der Expertengruppe die Fortsetzung des Betriebs sowie ein weiterer Ausbau ("upgrade") empfohlen wird.

Seit 1978 ist die Fusionsforschung in der Schweiz durch mehrere Abkommen in das EURATOM-Programm integriert. Ein bedeutendes Ereignis im Jahr 2008 innerhalb des Europäischen Programms zur Fusion war die Entscheidung zum Erwerb eines neuen Hochleistungsrechners (HPC, mit 100 Teraflops). Es ist zu erwarten, dass dem CRPP als Expertenzentrum auf dem Gebiet von numerischen Modellrechnungen bei der wissenschaftlichen Nutzung dieser Anlagen eine bedeutende Rolle zukommen wird.

1.2 Eine kurze Zusammenfassung der Forschungsarbeiten am CRPP

Im Jahr 2008 folgte die Forschungstätigkeit am CRPP den bereits vorgezeichneten Linien. Dieser Jahresbericht enthält Einzelheiten der wissenschaftlichen Ergebnisse und technologischen Entwicklungen. Einige Punkte verdienen besondere Erwähnung :

- Trotz der relativ kurzen Betriebsperiode von TCV im Jahr 2008, wurden neue und herausragende Ergebnisse erzielt, wie die folgenden Beispiele zeigen. Eine Unterbrechung des Betriebs bis März 2008 war geplant, um eine Reihe von Umbauten vorzunehmen, z.B. den Austausch sämtlicher CFC-Ziegel mit denen die Gefässwand von TCV ausgekleidet ist. Allerdings kam es durch zwei technische Zwischenfälle mit Vakuumproblemen zu unerwarteten Verzögerungen.
- Die Entwicklung einer neuartigen Divertorkonfiguration (sogen. "snowflake") ermöglicht eine bessere Verteilung des Energieflusses im Divertor.

- erstmalig konnten Plasmastrom und –elongation durch gezielte Einkopplung von Elektronzyklotronheizung in Echtzeit kontrolliert werden.
- Durch die Anwendung verbesserter Algorithmen zur Kontrolle von "numerischem Rauschen" ist es erstmals gelungen, Plasmaturbulenz mit Hilfe von statistischen gyrokinetischen Methoden zu simulieren.
- Am Experiment TORPEX wurde bei Untersuchungen zur Plasmaturbulenz eine Vielfalt neuer Ergebnissen erzielt.
- zur Vorbereitung von ITER wurden auf den Gebieten Plasmaheizung, magnetische Sonden und bei der Qualitätsprüfung von Supraleitern wichtige Forschungs- und Entwicklungsarbeiten durchgeführt.
- In der Materialforschung lag der Schwerpunkt bei der Entwicklung und Untersuchung von Stahllegierungen mit geringer Aktivierung durch Neutronen.
- Die Anwendung von Plasmen in industriellen Prozessen bleibt eine bedeutende Aktivität am CRPP, bei der die Zusammenarbeit mit der Industrie eine wichtige Rolle spielt.

Die Schweiz leistet einen freiwilligen Beitrag im Rahmen des Abkommens zum "broader approach" in der Fusionsforschung, das zwischen der Europäischen Union und Japan abgeschlossen wurde. Sämtliche diesbezügliche Aktivitäten, zu denen die Schweizer Regierung zugestimmt hat, werden vom CRPP koordiniert.

Letztlich sollte nicht unerwähnt bleiben, dass vom CRPP, als zuständigem Institut des Gastlandes, bei der Durchführung der 22. IAEA Konferenz zur Kernfusion wesentliche organisatorische Aufgaben übernommen wurden. Die Schweizer Bundesregierung war Gastgeber dieser Konferenz, die im Palast der Nationen in Genf abgehalten wurde. Der Konferenz kommt eine besondere Bedeutung zu, denn sie erinnert an die 2. Konferenz über die friedliche Nutzung der Kernenergie, die 50 Jahre früher (1958) am selben Ort abgehalten wurde. Damals begann mit dem Verzicht auf Geheimhaltung die internationale Zusammenarbeit bei der Fusionsforschung.

1. INTRODUZIONE

1.1 La situazione internazionale

ITER rimane il punto focale delle attività internazionali. L'organizzazione ITER sta analizzando le implicazioni tecniche, scientifiche e decisionali del processo di riesame del design di ITER, insieme ai suoi membri costituenti (Cina, Unione Europea, India, Giappone, Corea, Russia e Stati Uniti).

La Svizzera ha formalizzato la sua partecipazione a ITER attraverso uno scambio di lettere fra il governo della Confederazione e la Commissione dell'Unione Europea. La camera alta del Parlamento ha ratificato tale scambio nel 2008. La ratificazione completa avverrà nel 2009.

Nel 2008, Euratom ha condotto un esame del suo programma nel campo della fusione, noto sotto il nome di 'Facilities Review'. Un comitato internazionale comprendente personalità di alto livello del mondo industriale e accademico ha fornito chiare raccomandazioni sulla strategia da seguire in Europa per i prossimi 20-30 anni. Soltanto un numero molto ristretto di tokamaks sono stati giudicati in grado di fornire un contributo rilevante prima dell'operazione di ITER (prevista per il 2018). Il tokamak del CRPP, TCV, è fra questi, per i quali il comitato raccomanda ulteriori sviluppi ed una continuazione dell'operazione.

Dal 1978, la ricerca nel campo della fusione in Svizzera è integrata nel programma Euratom attraverso vari accordi ufficiali. Nel 2008, un'iniziativa importante è stata lanciata dal programma europeo per acquisire un computer ad alta capacità di calcolo (100 Teraflops), specificamente dedicato alla fusione. Il CRPP, tradizionale centro di eccellenza per il calcolo numerico, giocherà un ruolo importante nell'utilizzo di tale computer.

1.2 Breve riassunto delle attività del CRPP

Le attività del CRPP durante 2008 sono proseguite secondo le linee di ricerca stabilite negli anni precedenti. Questo rapporto annuale fornisce i dettagli dei risultati scientifici e degli sviluppi tecnologici ottenuti durante l'anno. Fra questi, segnaliamo:

- Nonostante una campagna sperimentale di durata ridotta, cominciata in Marzo 2008 dopo una lunga apertura pianificata per diversi lavori di miglioria, compresa la sostituzione di tutte le tegole di carbonio all'interno della camera da vuoto, e interrotta a due riprese a causa di problemi di vuoto, diversi risultati originali sono stati ottenuti su TCV. Fra questi, citiamo due esempi:
- un nuovo concetto di divertore 'a fiocco di neve', potenzialmente importante per alleviare il problema dell'interazione plasma-parete, è stato sviluppato e dimostrato sperimentalmente su TCV;
- il controllo in tempo reale della corrente e dell'elongazione del plasma tramite attuatori ECRH è stato dimostrato sperimentalmente per la prima volta;
- per la prima volta, simulazioni statistiche stazionarie basate su un modello di plasma giro-cinetico sono state condotte, grazie a nuovi algoritmi di controllo del rumore numerico;

- un gran numero di risultati sperimentali su fenomeni di base nella turbolenza dei plasmi magnetizzati sono stati ottenuti utilizzando l'esperimento di base Torpex;
- attività di ricerca e sviluppo sono state condotte in vista della costruzione di ITER, nel campo del riscaldamento addizionale del plasma, delle diagnostiche magnetiche e della qualifica dei cavi superconduttori;
- attività nell'ambito della scienza e tecnologia dei materiali, focalizzate sulla fabbricazione, la caratterizzazione e la modellizzazione di acciai a bassa attivazione e leghe refrattarie;
- attività importanti nell'ambito dei processi industriali basati sull'utilizzo dei plasmi, in collaborazione con l'industria privata.

La Svizzera è fra i contribuenti volontari al cosiddetto accordo di 'Broader Approach' fra Unione Europea e Giappone. La messa in pratica delle attività legate a tale accordo e decise dal governo federale è responsabilità del CRPP.

Infine, notiamo che il CRPP ha agito come organizzatore locale della 22esima conferenza sull'energia di fusione dell'IAEA ('Fusion Energy Conference', FEC). La FEC si è tenuta al Palazzo delle Nazioni a Geneva, ed è stata ospitata ufficialmente dal governo federale. La FEC ha anche fornito l'occasione per una celebrazione del 50esimo anniversario della seconda conferenza sull'uso pacifico dell'energia atomica, tenuta sempre a Ginevra nel 1958, durante la quale la ricerca in fusione fu de-classificata, il che diede il via a tutte le collaborazioni internazionali.

2 RESEARCH ACHIEVEMENTS OF THE CRPP IN 2008

2.1 The TCV tokamak

The first part of 2008 was dedicated to the completion of the TCV shutdown started in March 2007, with plasma operation re-starting only in spring 2008. During the shutdown, as detailed in Section 3 dedicated to technical achievements, several repairs and upgrades were implemented to the TCV device and its ancillaries, including a complete dismounting and cleaning of the more than 1600 graphite tiles forming the first wall, upgrades of existing diagnostics, installation of new diagnostic systems and new plasma control hardware, and the repair of a gyrotron source for third harmonic EC plasma heating.

Despite a short experimental campaign, a growing complement of diagnostics, analysis and modelling tools has led to significant new results in a variety of areas in the period covered by this Report.

For the campaign starting in 2008, specific topical areas to address on TCV were defined and agreed during discussions within the TCV Team and with its European and International collaborators at the beginning of the year. These topical areas form the TCV general scientific programmeme, which aims at broadening the physical parameter range of reactor relevant regimes for ITER and DEMO, by exploring fundamental tokamak plasma physics questions and by investigating new plasma shapes and control tools. The programmeme aims at exploiting TCV unique capabilities, such as plasma shaping and EC tools, and is structured according to five themes:

- Advanced scenarios with internal transport barriers and large bootstrap currents (of interest for a steady-state operation of tokamaks)
- H-mode (the reference scenario for Q=10 operation in ITER)
- Transport and rotation
- ECH and ECCD physics
- Real time control of plasma and heating systems

As this Report discusses achievements that are primarily based on data collected during the campaigns ending in 2007, the text is organized according to he structure of the experimental programmeme of 2006-2007, encompassing the study of scenarios with internal transport barriers, the characterisation and modelling of edge plasmas, and in particular Scrape-Off-layer flows, the physics of H-modes, including magnetic triggering of ELMs, the physics of plasma rotation and of heat and particle transport, the physics of ECH, ECCD and related control methodologies, an assessment of the potential of Electron Bernstein waves for heating and current drive, and the exploration of new plasma shapes and configurations.

In parallel with the scientific exploitation of TCV, based on both the short 2008 campaign and on the analysis and theoretical modelling of TCV databases, part of the team dedicated some efforts in exploring possible medium term developments and upgrades, in conjunction with the recently conducted European facilities review. These studies address the possibility of direct ion heating by NBI, of increasing the ECRH X3 power, of installing additional tools for error fields and

ELM control, and of performing fast ion physics experiments on TCV, and are detailed in Section 3.5.

2.1.1 Scenarios with internal transport barriers

Global plasma oscillations in eITB regimes

In TCV, global plasma oscillations affecting several plasma parameters, including the total current and the line-averaged density, are observed in fully non-inductively driven plasmas featuring eITB with strong ECH/ECCD (Fig. 2.1.1). It has been demonstrated that these oscillations are linked to the destabilization and stabilization of MHD modes near the foot of the eITB. Here, large pressure gradients are present in a region of low magnetic shear; as a consequence, the ideal MHD stability limit is more easily reached, i.e. infernal modes can become unstable at a lower normalised β value than in standard scenarios. Depending on the proximity to the ideal limit, small crashes or resistive modes can be destabilized, which affect the time evolution of the discharge. Being near marginal stability, the modes can be stabilized by slight modifications of the local pressure and safety factor (q) profiles. If this is the case, the plasma confinement recovers, the shear reverses and the internal transport barrier builds up, until a new MHD mode is destabilized again.

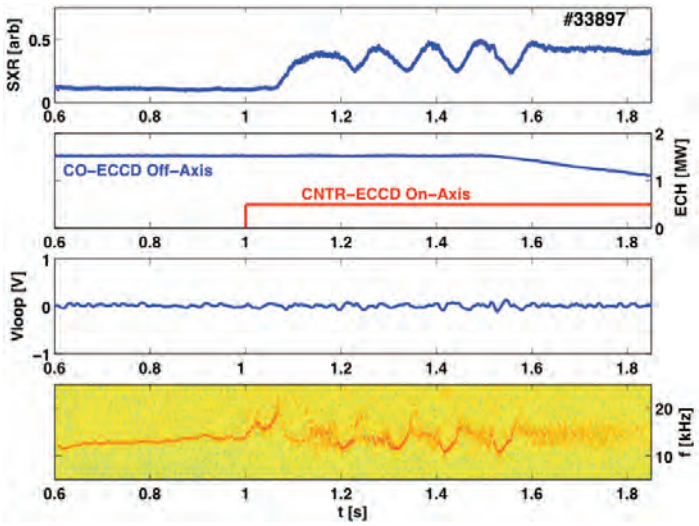

Fig. 2.1.1 *Evolution of line-integrated soft x-ray signal, EC power in the off-axis and on-axis beams, V_{loop} and MHD spectrogram in a fully non-inductive discharge with global plasma oscillations in TCV. At 1.5s, the off-axis power is reduced which changes the q profile, stabilizing the low frequency mode and resulting in a non-oscillating high performance eITB.*

A hollow current density profile and the proximity to the infernal mode ideal limit are inherent to these scenarios, which makes it is very likely that such oscillations will occur in ITER, leading to the loss of a transport barrier and to a confinement degradation. This is why it is important to develop a current density perturbation technique using various actuators that mitigate the deleterious effects of MHD activity.

TCV results show that this cyclical behaviour can indeed be controlled by modifying the current density or pressure profiles, either with Ohmic current density

perturbations or by modifying the ECH/ECCD power. Figure 2.1.1 provides an example of the latter, showing the time evolution of a discharge fully sustained by 1.35MW off-axis co-ECCD. At t=1s an EC beam of 0.45MW is injected on-axis with a counter-CD component, which triggers an eITB with a strong pressure gradient near the q_{min} region. At 1.2s, and regularly afterwards, a large tearing mode at a frequency ~12kHz is generated, reducing the confinement, as indicated by the reduction in the central soft x-ray (SXR) emission (top trace). The q and pressure profiles are modified by the magnetic island and the mode is stabilized; the barrier forms again until the instability boundary is reached and the mode is once more driven unstable, restarting the cycle. At t=1.5s, the off-axis co-ECCD power is reduced progressively, which changes the q profile. After 1.6s, the profiles are such that the low frequency tearing mode is stable and the discharge performance remains high, as seen from the SXR trace, despite a lower total EC power injected.

Transport in the presence of eITBs

Simulations of experiments in which small perturbations to the core current were applied using the ohmic transformer in steady-state eITBs have unambiguously demonstrated that the confinement improvement is directly linked to the local magnetic shear becoming more and more negative. The results of these simulations are shown in Fig. 2.1.2 in terms of reconstructed q profiles and of the confinement improvement as a function of the value of the magnetic shear.

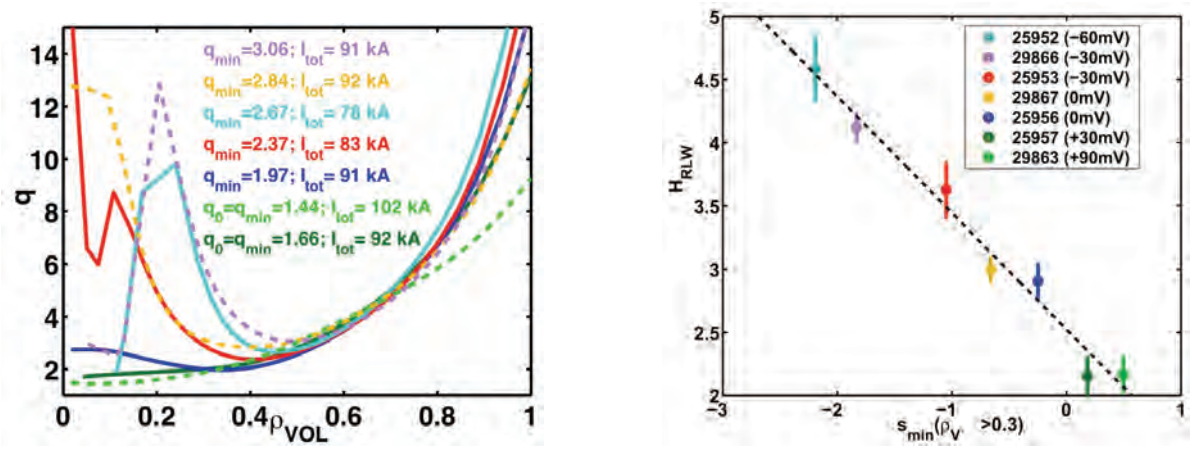

Fig. 2.1.2 *Left: safety factor profiles in steady-state eITB scenarios, showing that q_{min} is varied between 1.97 and 3.06. The plasma current values are also indicated. Right: the factor describing the confinement improvement in TCV over the L-mode value, H_{RLW}, as a function of the minimum value of the reconstructed magnetic shear outside ρ_V=0.3, where the reconstruction is reliable. The value of the small additional loop voltage for the different cases is also indicated. A linear trend is clearly visible, indicating a smooth confinement improvement.*

The study of the particle transport properties of eITBs in TCV has shown that linear gyrokinetic theory can explain why a dominant thermo-diffusive pinch is observed and leads to very peaked density profiles. For the latter studies a new method to obtain particle pinch contributions from linear gyrokinetic simulations was developed. Using this method, it has been shown that the collisionality dependence of density peaking in monotonic q profile discharges can also be qualitatively explained. The peaking reaches its maximum near the transition from ITG to TEM turbulence.

2.1.2 Plasma edge characterisation and modelling

The study of Scrape-Off Layer (SOL) transport, both steady state and transient, is a key element of the edge physics research programmeme on TCV. Recent efforts have concentrated on the study of parallel SOL flow, cross-field turbulence driven particle transport, the link between parallel and cross-field transport and the physics of ELM transport.

Radial profiles of parallel SOL ion flows have been measured in both lower and upper single-null (SNL and SNU) diverted configurations using a reciprocating Mach probe on the machine mid-plane in a series of experiments in which closely matched ohmic density scans are performed for both toroidal field (B_φ) directions (FWD-B and REV-B, where, for FWD-B, the ion $\nabla B \times \mathbf{B}$ drift is directed towards the X-point in SNL). Strong flows are observed at low density ($M_\parallel \sim 0.5$); the flows decrease with increasing density, are co-current directed and reverse direction with B_φ. Remarkably good agreement in both magnitude and direction is found between these measured flows and the neoclassical Pfirsch-Schlüter ion flow estimated on the basis of a large aspect ratio approximation, as shown in Fig. 2.1.3. Taking the mean value of the FWD-B and REV-B flows at any given density reveals a small, yet significant, field independent component when the probe measurement is made either poloidally above or below the mid-plane. This offset clearly depends on the radial position and density (it increases with density) and is always directed away from the mid-plane. When the same exercise is performed for a magnetic equilibrium such that the probe reciprocates precisely on the plasma mid-plane, the offset disappears at all densities within the measurement error. The fact that roughly the same offset appears above the mid-plane in SNU and below it in SNL eliminates the divertor sink as a potential contributor to this offset, while the absence of an offset at the mid-plane is direct evidence for a ballooning type origin of the flow.

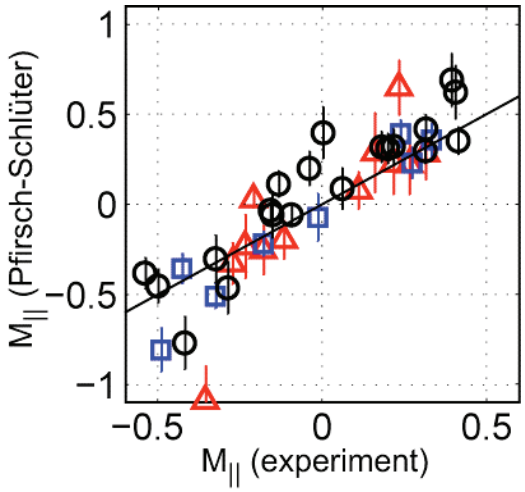

Fig. 2.1.3 *Comparison between the measured (field direction dependent) flows and the neoclassical Pfirsch-Schlüter prediction, estimated on the basis of a large aspect ratio approximation*

This field independent flow on TCV has been clearly identified with the time average of transient over-pressure generated in field aligned filaments ("blobs") driven by interchange mechanisms. These structures, identified as high relative fluctuation levels on the Mach probe particle flux time series, increase in number with plasma

density, similarly to the observed flow offset behaviour. They are also observed more frequently with decreasing plasma current (at fixed density) and are responsible for the SOL density profile broadening, which is seen either with increasing density or decreasing current. This is consistent with an increase in fluctuations and turbulence driven radial transport as the plasma collisionality increases, and is evidently related to the blob formation process.

Filamentary structures are also commonly observed in tokamaks during ELM activity. Direct evidence for this has been seen on TCV in high time and space resolution IR images of the outer divertor target in ohmic H-modes (Type III ELMs). An example of these observations is reported in Fig. 2.1.4. Field line tracing demonstrates that these filaments are consistent with a release of energy in the outer mid-plane region from a number of discrete toroidal locations, giving mode numbers in the range n~10-20. A filamentary structure is also seen by Langmuir probes in the SOL and at the outboard mid-plane main chamber walls. In the case of Type III ELMs, radial propagation velocities are in the range ~1kms^{-1} and no acceleration or deceleration is seen in the main SOL within experimental error. On average, between 5-8 substructures are detected at the wall for each ELM (for both Type III and Type I ELMs) and, interestingly, the fluctuating parallel particle flux statistics during the ELM filaments appear very similar to those observed in the inter-ELM phases. A new array of fast radiation detectors based on AXUV diodes has been used to obtain tomographic reconstructions of the radiation distribution during ELMs on a fast (~5μs) timescale. During Type I ELMs, evolution of radiation in the X-point and inner divertor regions, coincident with the start of Mirnov coil activity, is clearly seen before any particle flux reaches first wall surfaces. Shortly afterwards bright lobes are seen in the outer mid-plane regions (coincident with the detection of filaments at the wall) and later (on the ion transit timescale along field lines) in the outer target vicinity.

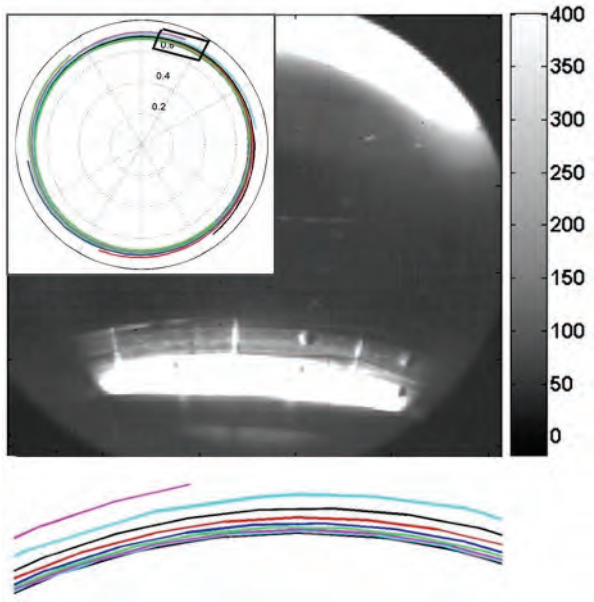

Fig. 2.1.4 *Fast IR images of the outer divertor target (TCV vessel floor tiles) in ohmic H-modes, for Type III ELMs, with the temperature in C on the right hand side. The IR data shows qualitative agreement with post-explusion filament propagation along open magnetic field lines, as demonstrated by the correspondance with the calculated deposition pattern shown at the bottom of the figure for six toroidally localized divertor filaments at the mid-plane (superimposed on top left corner of the IR camera image).*

The majority of the ELM energy reaching the targets does so in the separatrix vicinity, both for Type I and Type III, similarly to JET observations for Type I ELMs. The linear relationship between ELM rise time at the target, τ_{IR}, and parallel transit time from mid-plane to target, $\tau_{||}$, seen elsewhere is also observed on TCV Type III ELMs, but not for the larger (Type I) ELMs seen in X3 heated H-modes, where $\tau_{IR} >> \tau_{||}$. Modelling of the ELM parallel transport is progressing, using the 2D edge code package SOLPS5 and the 1D particle-in-cell kinetic code BIT1. The numerical results are being tested both against measurements of particle and heat fluxes at the targets and against each other, in particular to better quantify the consequence of fixing heat and particle flux limiters in fluid simulations.

2.1.3 H-mode physics

H-mode target development

The cleaning of the TCV C-tiles was expected to strongly influence the plasma edge conditions and therefore on the H-mode accessibility in the first TCV discharges after the plasma restart. The first goal of the H-mode physics programmeme was to recover a stationary ELMy H-mode with Ohmic heating only since such ohmic H-modes could subsequently be used as targets for X3 heating experiments.

In TCV ohmic plasmas studied in previous campaigns, H-modes were usually obtained during the divertor formation if the plasma current and density were set above a given value. With the cleaned tiles, that minimum value of the plasma current appears to have decreased from about 320kA to 260kA. The discharges then enter either short H-mode phases followed by back-transitions to L-mode or ELM free H-mode phases leading to an unavoidable disruption.

The search for the stationary ELMy H-mode was pursued by varying the plasma shape together with the plasma current and density. A discharge with almost regular ELMs was obtained.

Contribution to L-H transition threshold database

The analysis of the power requirement to obtain a good H-mode in ITER has been finalised, based on a multi-machine database including TCV results. The influence of the device size on the density dependence of the threshold power as well as the relationship between the magnetic field and the density threshold or rollover have been addressed in detail. A new recommended scaling for the H-mode threshold power has been released under the form:

$$P_{Thresh} = 0.0488\ n_{e20}^{0.717}\ B_T^{0.803}\ S^{0.941}$$

where P_{Thresh} is the threshold power expressed in MW, n_{e20} the plasma density in $10^{20}m^{-3}$, B_T the magnetic field in Tesla and S the plasma outer surface area in m^2. With this scaling, the predicted threshold power for ITER reaches 52MW and 86MW for low and high density respectively (0.5 and $1\times10^{20}m^{-3}$). Since these power values correspond, by definition, to the entry into the H-mode only, a discussion followed on the power required to access an H-mode of adequate performance (H factor~1). It was shown that the power at which confinement studies were performed in the different devices was generally larger than 1.5 times the threshold power. Since ITER cannot be operated at such required power, a multi-machine joint experiment

was launched to investigate the possibility of accessing a good performance H-mode with power levels close to the threshold.

Magnetic triggering of ELMs in TCV and ASDEX Upgrade

Given the importance of improving our understanding of the physics of ELMs and their control for ITER, magnetic triggering of ELMs in TCV and ASDEX Upgrade was re-investigated in detail to find a clue for the observed opposite behaviour between the two tokamaks. ELMs are triggered in ASDEX Upgrade when the plasma is moved down towards the X-point with a consequent decrease of the plasma current density in the edge region. This is contrary to the observation on TCV, in which ELMs are triggered when the edge current is increased by an upward plasma movement. In the previous simulation study using a free-boundary tokamak simulator, DINA-CH, similar local plasma shape deformations were observed near the upper G-coil set in TCV and near the upper passive stabilization loop (PSL) in ASDEX Upgrade for opposite plasma movement, as shown in Fig. 2.1.5. In particular, a local flux surface expansion was observed when ELMs are triggered in the experiments. A stability analysis conducted by using the ideal MHD stability code KINX shows that the squareness increase in the low field side (LFS) and upper half plane of the poloidal cross-section in ASDEX Upgrade can destabilise the edge. These observations give us a clue for understanding the opposite behaviour observed in the two devices. However, this shape deformation effect was found to be much weaker in TCV, therefore the edge current increase induced by the upward plasma movement is still an important candidate as the mechanism responsible for triggering ELMs in TCV.

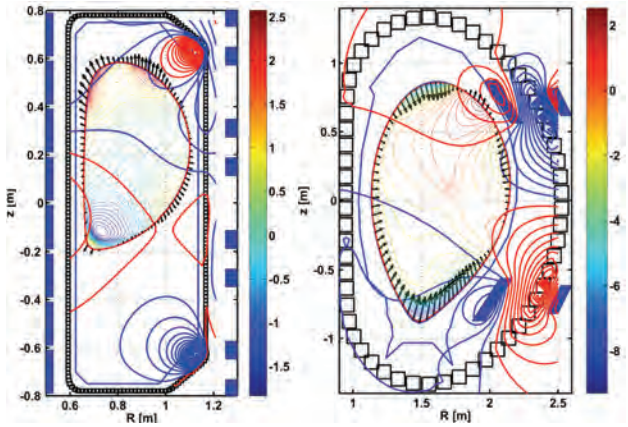

Fig. 2.1.5 *Flux surface deformations and vacuum flux changes are shown for upward plasma movement in TCV discharge #20333 (left) and downward plasma movement in ASDEX Upgrade discharge #18343 (right). ELMs are triggered in the experiments for these plasma movements. The arrows are amplified by a factor 20 for visibility.*

To investigate further the plasma shape deformation effect, additional experiments were conducted in ASDEX Upgrade. In these experiments, radial plasma movement was pre-programmemed to produce a larger plasma shape deformation and to minimise fluctuations in the edge plasma currents, as shown in Fig. 2.1.6. Although the plasma shape was easily deformed with the radial plasma movement, ELMs were not triggered. KINX stability analysis on this plasma showed that the plasma boundary curvature change is related to the edge stability. Compared to the vertical plasma movement, during which the plasma column size varies during the movement, the radial plasma movement has little influence on the plasma

boundary curvature and column size. The observations from the two experiments, DINA-CH free-boundary simulations and KINX stability analysis are summarized in Table 1. This work is the result of a collaboration with the Keldysh Institute, the Kurchatov Institute, the TRINITI Institute and the CEA Cadarache.

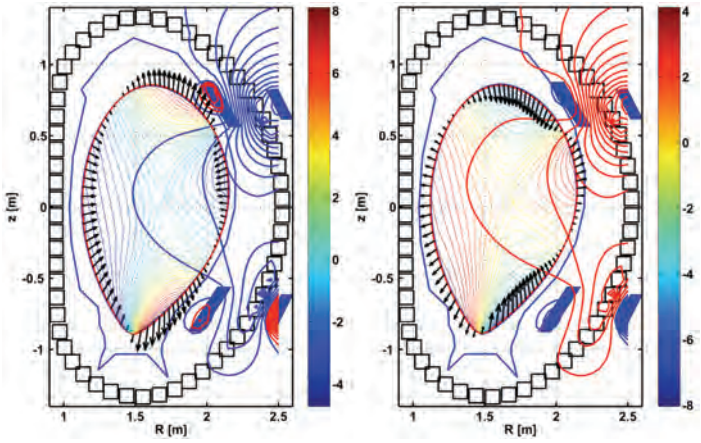

Fig. 2.1.6 *Flux surface deformations and vacuum flux changes are shown for inward (left) and outward (right) radial plasma movements in ASDEX Upgrade. The arrows are amplified by a factor 20 for visibility.*

Observations	TCV	ASDEX Upgrade		Comments
Plasma movement	Upward	Downward	Inward	
Type of natural ELMs	Type III	Type I	Type I	
Triggered ELMs	Observed	Observed	Not observed	
Edge current density	Increased[b]	Decreased	-	
Edge current gradient	Decreased (locally increased)	Increased (locally decreased)	-	Mixed contributions
Edge pressure gradient	Decreased	Increased[b]	-	
Plasma area	Expanded	Shrunk[b]	-	
Shape deformation	Locally expanded in upper LFS[b]	Locally expanded in upper LFS[b]	Elongated	
Squareness (upper LFS)[a]	Decreased	Increased[b]	-	Squareness decrease in TCV is not yet clearly explained
Curvature (upper LFS)[a]	-	Locally increased or decreased	Locally increased or decreased	Similar patterns
Curvature (lower LFS)[a]	-	Increased[b]	Decreased	Systematic differences in the stability margin behaviour

[a] Observations from the KINX analysis
[b] Possible candidates for triggering ELMs.

Table 1 *Summary of the observations in the experiments and simulations of magnetic triggering of ELMs.*

2.1.4 Plasma rotation

Following the observation of toroidal rotation reversal in TCV for a relatively small change in the plasma parameters, the conditions for rotation reversal were reproduced on the C-Mod Tokamak (MIT, USA), where a toroidal rotation reversal phenomenon was also observed. In the absence of new experimental data during the prolonged 2008 TCV machine refurbishing, analysis was concentrated on the role of sawteeth in determining the plasma rotation profiles.

It was initially concluded that the maximum toroidal rotation in TCV L-mode discharges was inversely proportional to the plasma current. Experiments on TCV, in which the position of the sawtooth inversion radius was changed using X2 heating, indicate that the rotation profile outside the sawtooth inversion radius remains approximately constant, with no significant dependence upon the details of the core plasma current profile. By extrapolating the core toroidal rotation from the rotation profile outside the sawtooth inversion radius, we obtained evidence for a considerably weaker dependence of the core rotation on I_p for both positive and negative plasma current directions (Fig. 2.1.7). By normalising to the ion temperature, as previously concluded, one can also compensate for the additional heating effect of the plasma current (Fig. 2.1.8). In the absence of sawteeth, there is little dependence of the extrapolated toroidal rotation upon plasma current above an edge safety factor ~3. Discharges with higher plasma current display a decreasing plasma rotation with increasing plasma current. It is interesting to note that it is these configurations that exhibit the toroidal rotation reversal effect.

Since sawtooth relaxation is divided into a long period in which the pressure builds up, followed by a relatively short crash, recent work has focused on measuring the toroidal rotation profile evolution within a sawtooth period. To this end, the recently commissioned real-time digital control hardware has been programmemed to identify the sawtooth crash and generate timing events for the Charge Exchange Spectroscopy hardware that is used to measure the ion rotation profiles.

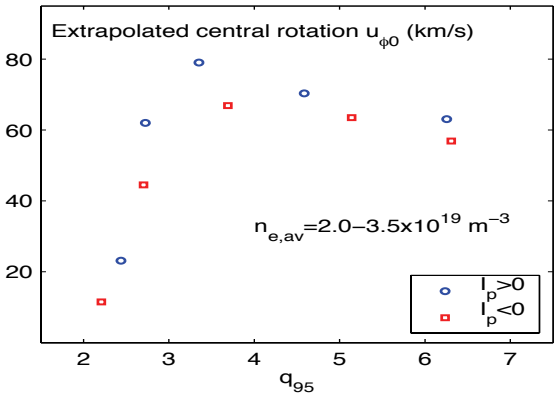

Fig. 2.1.7 *Extrapolated value of the rotation at the plasma centre from the rotation gradient outside the sawteeth inversion radius.*

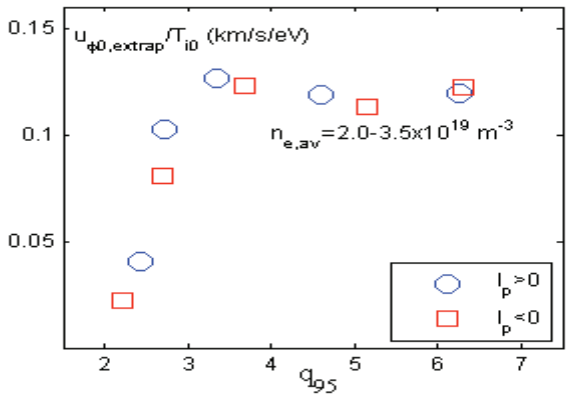

Fig. 2.1.8 *Extrapolated central toroidal rotation normalised to the measured ion temperatures. Above q=3, there is little remaining evidence of a plasma current dependence.*

2.1.5 Heat and particle transport in TCV

Effect of triangularity on heat transport in ECH L-mode discharges

The investigation of the effects of plasma shaping serves two main purposes: it provides stringent tests for transport and stability theories, thus a valuable tool for model validation, and it gives crucial information for the design of future devices beyond ITER, since plasma shape can have a strong influence on confinement, MHD stability and performance. Recently, it has been shown that plasma triangularity can strongly affect confinement and transport: core energy confinement is improved with increasingly negative triangularity in L-mode, whereas confinement in H-mode increases with increasingly positive triangularity.

The role of plasma triangularity on heat transport was investigated in L-mode plasma shaping experiments, combined with gradient variation experiments using ECRH, to find out the relevant variables and decorrelate the experimental parameters. For a fixed shape, the heat diffusivity χ_e was found to mainly scale with T_e, density and effective charge, through the *effective collisionality* ν_{eff}, defined as the electron–ion collision frequency normalized to the electron curvature drift frequency, $\nu_{eff}=\nu_{ei}/\omega_{De}\sim 0.1\ R_0 n_e Z_{eff}/T_e^2$. This clarification led to a clear determination of the impact of triangularity on χ_e. The electron heat diffusivity evaluated from experimental data at mid-radius is represented as a function of $1/\nu_{eff}$ in Fig. 2.1.9, for positive and negative δ. The decrease in χ_e with increasing ν_{eff} is confirmed for both plasma shapes, along with a clear decrease in χ_e with decreasing plasma triangularity.

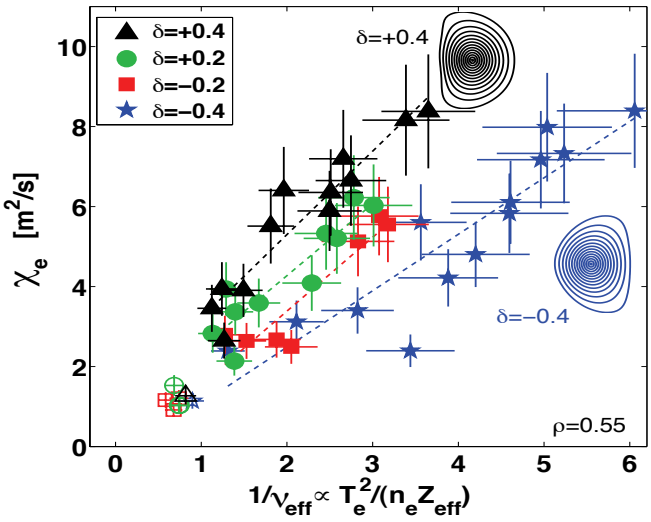

Fig. 2.1.9 *Effect of shape and collisionality on the heat diffusivity measured in TCV (ρ=0.55).*

Gyro-kinetic simulations have been performed on the basis of self consistent MHD equilibrium reconstructions, focusing on these L-mode TCV discharges with δ=±0.4. Both GS2 (local) and LORB5 (global) linear simulations indicate that, for the experimental parameters, the dominant instability is a Trapped Electron Mode (TEM). In the δ<0 case, the growth rate of the most unstable mode is found 10% lower than in the δ>0 case. More importantly, the "transport effective" perpendicular wave vector of the mode, defined as the average along a field line of

the local perpendicular wave vector $k_\perp$ weighted by the energy of the fluctuations, is found significantly higher at δ<0 than at δ>0 in the region of low poloidal wave vectors ($k_\theta \rho_i$<0.6). These two effects result in a lower mixing length heat diffusivity $\gamma / < k_\perp^2 >$ for the δ<0 case, as detailed here below.

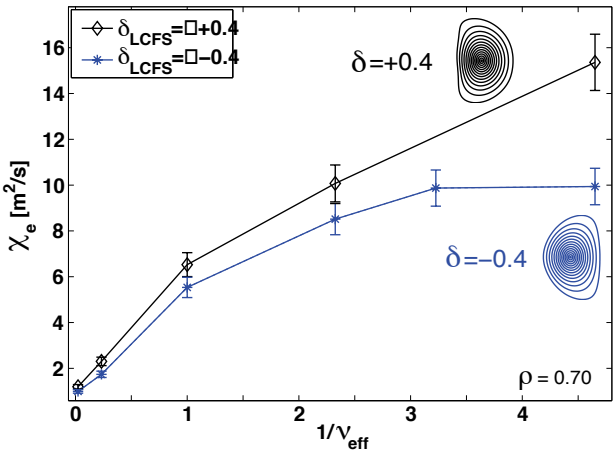

Fig. 2.1.10 *Corresponding non-linear results of heat diffusivity simulated with GS2 for the two extreme triangularities δ=±0.4 (ρ=0.7). Note that the radius of investigation has been chosen further out to get heat diffusivities as high as in experiment.*

Two different mechanisms can be invoked to explain these results. First, the local shear, s, is higher in the tips of the negative triangularity plasma compared to the positive triangularity case at the same LFS location. As the local perpendicular wave vector scales as $k_\perp^2 = k_\theta^2(1 + s^2\theta^2)$, with θ the poloidal angle, an increase in the local shear contributes to an increase of the effective $k_\perp$. The effect of the shear is also qualitatively observed in the global simulations, Fig. 2.1.11, where the eddies of the electrostatic potential appear to be more tilted in the δ<0 case. Second, the change in the curvature and ∇B drifts modifies the toroidal precession drift of the trapped particles. As the TEM is intrinsically linked to the resonance with the toroidal precession drift, this modification can significantly affect the radial transport. The variation of the toroidal precession drift with the plasma triangularity is rather complex and depends on the pitch angle and energy of the trapped particles. For the particle energies at which most transport occurs, typically 2-3×T_e, the toroidal precession frequency is closer to the resonance condition at δ>0 than at δ<0 over a large portion of the pitch angle domain.

The non-linear simulations performed with the GS2 code confirm the TEM nature of the most unstable modes, proving that trapped electrons carry most of the heat flux. The reduction of transport at negative triangularity is notably stronger than in the linear simulations and in fair agreement with the experimental results (Fig. 2.1.10). The effect of plasma collisionality is also investigated for comparison with the experiment. As shown in Fig. 2.1.12, the relative contribution of the trapped particles to the total heat flux decreases at high collisionality. By displacing the particles in phase space, collisions can indeed disrupt the resonance between the precession drift of the trapped electrons and the TEM wave. Note that at high collisionality (Fig. 2.1.12, left), the difference in heat flux between positive and negative triangularity is reduced, as in experiment.

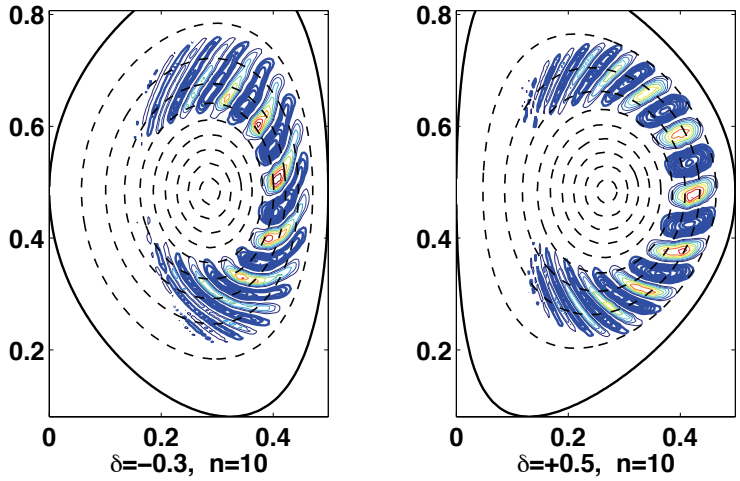

Fig. 2.1.11 *Global linear gyro-kinetic simulations (LORB5) showing the impact of the plasma triangularity for δ = -0.3 (left) and δ = +0.5 (right) on the TEM electrostatic potential cell orientation, for the n = 10 mode*

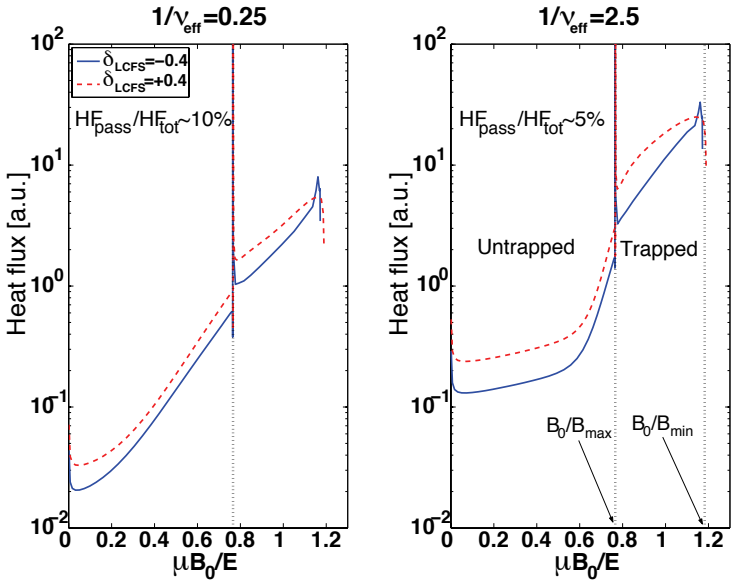

Fig. 2.1.12 *Heat Flux vs. pitch angle for two values of collisionality. At higher ν_{eff} the relative contribution from passing electrons to the total flux increases. Even though their contribution to the total flux is small, note how negative δ "stabilizes" also passing electrons (reduces the heat flux of passing electrons).*

Impurity transport

There have been no new results on impurity transport, due to the long shutdown and the involvement of staff in other areas. However, it is worth mentioning that a fast gas valve was installed on TCV in collaboration with HAS, which should become a key tool for impurity transport studies in the near future.

2.1.6 Physics of ECH, ECCD and of suprathermal electrons

Real-time control of plasma current and elongation with ECRH actuators

The linear analogic control system used since the inception of TCV is based on matrix multiplication of signals and on a PID controller, and has been limited to the control of the plasma current and density and of the poloidal and Ohmic field coil currents. This system was recently extended to include the EC system (power and launcher angle) actuators for the first time, to control the plasma current and elongation. With the development and integration of new, digital real time control hardware, TCV now has the capability to extend real-time control techniques to nonlinear algorithms for its multiple EC actuators, including independent power supplies and launchers, with reactor-relevant applications particularly in the realm of MHD stability control (e.g. sawteeth and NTMs). A new 36-channel digital-signal-processor (DSP) controller has been tested successfully to replace the analogue PID system with its discretized digital-filter counterpart. A parallel development has occurred to address the need for real-time processing of massively multi-channel diagnostic signals, such as the 200 channels acquired by the soft X-ray tomography system. A 96-channel compact-PCI acquisition and real-time unit has been prototyped and applied to MHD stability control through EC actuators. Integrating this system with Simulink® development and visualisation leads to a powerful, simple controller which may be directly exploited by TCV users, providing an intuitive way to simulate the controller based upon models of the plasma response.

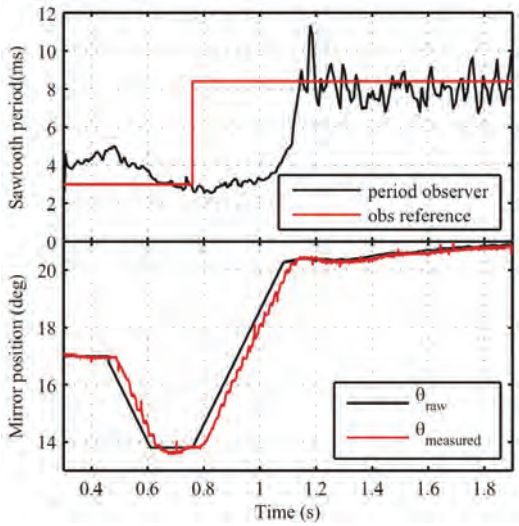

Fig. 2.1.13 *Sawtooth control using the ECRH launcher angle to control the ECRH deposition around the q=1 surface for shot 35833. The top trace shows the period reference signal together with the measured sawtooth period. The lower trace shows the mirror position.*

Initial applications have focused on the control of the sawtooth period, which was changed by modifying the current profile in the vicinity of the q=1 surface. The difficulty with this scheme is that the plasma response is non-linear. Only within a very small angle range does the sawtooth period respond to (small) changes in the launcher orientation, where the controller gain must be low, as opposed to outside this region where the gain should be large. A sawtooth crash detection algorithm was developed for the compact-PCI controller, operating on several core soft X-ray channels. The period was then calculated, averaging over two sawteeth to form the observer. Figure 2.1.13 shows the reference and measured sawtooth period signals, as well as the requested and measured mirror positions for a first proof of principle. To provide a convincing demonstration, the target sawtooth period was not set to a constant value, but to a step function. As the control request increases from 3 to 8ms, the mirror moves to larger angles, which correspond to deposition at smaller

minor radii, until the reference is reached. Such systems are also being developed for real-time equilibrium reconstruction, plasma shape control, real-time tomography, profile control, NTM suppression and for triggering diagnostics.

2.1.7 Electron Bernstein Wave Heating

Following the first successful demonstration of Electron Bernstein Waves (EBW) absorption at the edge via O-SX-B double mode conversion in TCV, initial core deposition experiments have started. For an optimum coupling of the O2 power to the Bernstein mode in these experiments, the required normalized density scale length is $k_0 L_n \approx 4$, where the wave number k_0 of the incident wave in vacuum is fixed by the ECRH system. This yields an optimum value of the density scale length $L_n = \frac{n_e}{|\nabla n_e|}$ at the mode conversion layer (between the plasma cutoff and the upper hybrid resonance). Values of L_n larger than this optimum decrease the width of the O-X conversion angular window, whereas lower values of L_n allow tunneling of the slow X-mode (SX) to the fast X-mode (FX) through the evanescent layer (between the upper hybrid resonance and the X-mode R-cutoff) and cause a power loss at the SX-B conversion. Edge Thomson Scattering measurements show that optimum values of L_n are obtained in the pedestal of low-q shaped H-mode plasmas in ELM-free phases.

Unfortunately, operating at low-q implies strong central sawtooth activity, which makes the deposition location of modulated EBW heating obtained from the standard Fast Fourier Transform (FFT) analysis unreliable. Recently, the Break-In-Slope (BIS) analysis method has been investigated to circumvent this difficulty: if the microwave power applied to the plasma is modulated fast enough, the diffusion and convection processes as well as the other power sinks and sources can be assumed to vary on a much slower time scale. If in addition the density remains constant during the power steps, the electron local energy conservation equation can be simplified to $\Delta \frac{\partial W_e}{\partial t} \approx \frac{3}{2} k_B \Delta \frac{\partial T_e}{\partial t} \approx \Delta P_{ECH}$, where ΔP_{ECH} is the jump in local absorbed power at the EC power breaks. In other words, the simplest form of the BIS analysis assumes that, if the heating power modulation is fast enough, the electron temperature T_e has a prompt linear response to the steps in the ECH power. At each ECH power step time, the jump in the slope of simple linear fits of a T_e time trace gives thus an estimation of the local variation of the absorbed power. The BIS analysis allows resolving the power deposition location with a time rate as high as the power modulation frequency, whereas FFT analysis needs longer time intervals. Moreover, the BIS analysis allows selecting EC power pulses at times without sawtooth perturbations, yielding an estimation of the deposition profiles where the FFT and correlation analyses fail due to the presence of sawteeth.

In view of future modulated EBH central deposition experiments, the BIS method has been successfully tested on X2 heating scenarios. The experimental power deposition location results are in very good agreement with the TORAY ray-tracing code as well as with the LUKE ray-tracing and Fokker-Planck-Equation-solver code (Fig. 2.1.14 and 2.1.15).

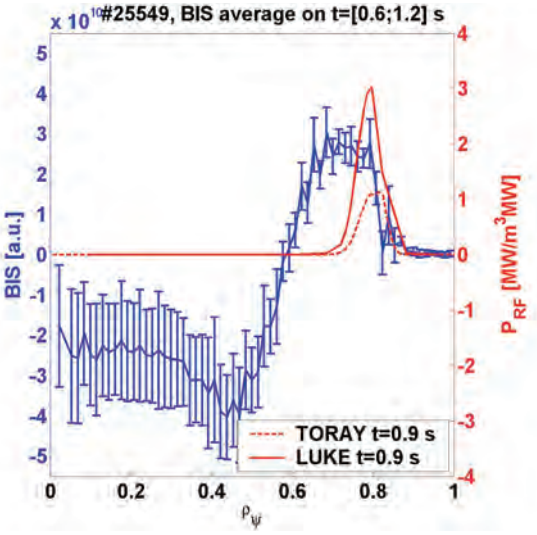

Fig. 2.1.14 *Break-in-Slope (BIS) analysis of 166 Hz modulated X2 heating experiment in a stationary plasma (TCV #25549). Time-average BIS amplitude profile versus radial coordinate ρ_ψ (blue) after tomographic inversion of the experimental soft X-ray profiles. The maximum BIS amplitude indicates the power deposition location and is in good agreement with the TORAY (red dashed) and LUKE (red solid) simulation codes.*

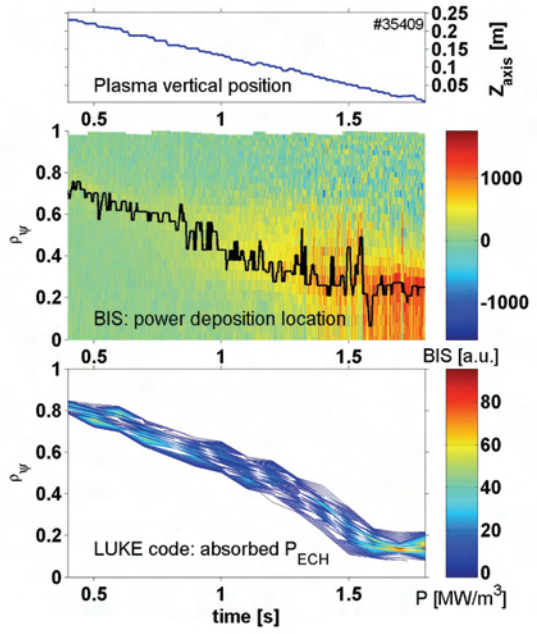

Fig. 2.1.15 *BIS analysis of a 500 Hz modulated X2 heating experiment in a plasma which vertical position is swept down in front of a fixed EC power launcher (TCV #35409). Top: Magnetic axis vertical position sweep. Center: BIS amplitude versus radial coordinate ρ_ψ and time. The maximum of BIS (in black) gives an estimate of the power deposition location as a function of time. Bottom: Power deposition location from the LUKE code versus radial coordinate ρ_ψ and time. Both experiment and simulation show the expected displacement of the power deposition location from the edge to plasma center.*

2.1.8 Exploration of new plasma shapes and configurations

Optimizing performance, stability and confinement is vital in the search of an economical tokamak reactor. Plasma shaping is one of the important free operational parameters, strongly influencing plasma properties and performance, stability and transport. Among the subjects not yet addressed in TCV, is the effect of shape, and in particular negative triangularities, on the H-mode properties, such as ELM stability (see Fig. 2.1.16). The calculated ideal stability of negative triangularity H-modes is significantly different from that of positive triangularity, which should lead to different pedestal parameters and ELM behaviour, with a reduced operation range in β. The comparison with experiments will allow a test of edge stability models over an unprecedented triangularity range. Confinement studies aim at better characterizing the role of edge pedestal and core confinement in H-mode at negative triangularity, potentially combining improved core confinement and reduced ELM heat load relaxations. In addition, negative triangularity plasmas would allow the test of β–limits and operation in a domain prone to resistive wall modes (RWM) at lower β.

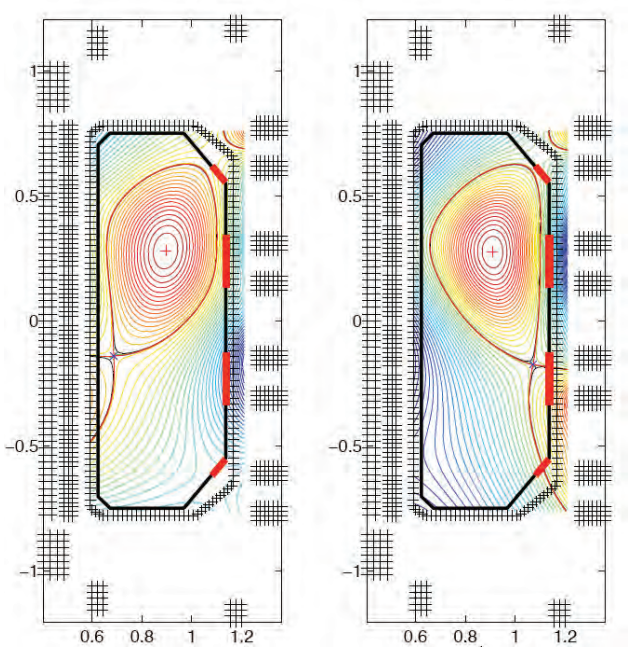

Fig. 2.1.16 *Negative upper triangularity plasmas with X-point on the HFS (left) and on the LFS (right). The proposed equilibrium on the left enables the test of a partly negative triangularity plasma using the present heat load resistant carbon wall on the HFS. The LFS wall has yet to be equipped with a similar optimized carbon wall for long pulse operation*

The ELM power load can also be mitigated in new advanced divertors, like the "snowflake divertor", using a hexapole null configuration instead of the conventional quadrupole, allowing a broader expansion of the flux surfaces. A preliminary study on the possibility to create a snowflake divertor on TCV has shown the compatibility of our tokamak with such innovative configuration. An example of a model shot is shown in Fig. 2.1.17.

Different innovative shapes can be studied on TCV, such as the doublet, with an X-point inside the plasma, a configuration obtained earlier transiently only, that needs adequate control tools to be developed into a stable stationary configuration. The axisymmetric stability of a doublet configuration was studied using the CAXE free-boundary equilibrium code. A rigid plasma model has been developed to analyse the stability of the plasma displacement (RZIP2 model). The results have then been compared with the KINX code. There are mainly two vertically unstable modes. The first one, characterised by two plasmas moving in the same direction, is well represented with the rigid model. The results in the second unstable mode (two plasmas moving in opposite direction) are not in a good agreement with the KINX results. Further studies are necessary to understand this particular instability for a doublet.

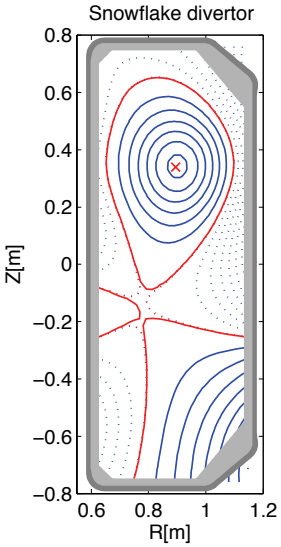

Fig. 2.1.17 *Example of a pre-programmemed snowflake divertor to be tested in TCV.*

A reliable breakdown is essential both for an efficient tokamak operation and for developing doublet plasmas from the growth of two separate discharges. The magnetic field structure during the breakdown phase can be analysed using an electro-magnetic model of TCV. The main parameters that characterise the breakdown are estimated for different configurations (single-null, double-null for doublet shaped plasmas), using a database of 15000 breakdown experiments. The reliability of the breakdown is found to increase with the connection length.

2.2 Theory and numerical simulation

Theory and numerical modeling activities cover the following main areas of research: first principle based simulations of turbulence, MHD analysis of tokamaks, application of RF waves, and investigations of 3D magnetic confinement configurations. In addition, the CRPP has made contributions to the Integrated Tokamak Modelling Task Force.

2.2.1 Physics underlying anomalous transport

Global gyrokinetic simulations (ORB5 code)

Nonlinear turbulence simulations have been performed with the global gyrokinetic code ORB5. Among the highlights is the application of a noise control technique acting also as source/sink operators that preserve the long term structures such as zonal flows while allowing for the gradient to be maintained in quasi-steady state well above marginal stability. An entropy balance relation has been introduced, allowing for a verification of the numerical quality of the simulation from a physical point of view and demonstrating that the noise control technique enables ORB5 simulations to reach steady state.

A careful verification of the influence of the parallel velocity nonlinearity on ITG turbulence has been preformed. The recent results show that previous studies that had concluded to a strong effect on the zonal flow structure were probably affected by numerical noise accumulation. The effects on zonal flow structures and on heat flux are in fact weak, if any, when the signal to noise ratio is sufficiently high.

Progress has been made with linear and nonlinear simulations of Trapped Electron Modes (TEMs). An approach keeping all electrons in phase space but considering passive tracers in the passing portion of phase space has been verified. A new particle orbit integrator in magnetic coordinates has been introduced in the ORB5 code and numerical tests have been performed, showing that the time step could be increased by a large factor, thus reducing the computational cost. Other improvements have been introduced in ORB5, in particular a scheme for avoiding spurious zonal flows to be created by the boundary conditions.

An investigation of the bursty nature of Ion Temperature Gradient (ITG) driven turbulence has been undertaken. The bursts are characterized by abrupt peaks in the energy flux and in zonal flow amplitude. These bursts propagate radially inwards or outwards (Fig.2.2.1). We could evidence a correlation of the direction of propagation with the sign of the underlying zonal flow velocity shear. The resulting statistics (probability distribution function of heat flux) has a marked non-Gaussian component. One-dimensional models have been investigated which provide a simplified description of the avalanche dynamics.

In collaboration with the CEA in Cadarache, an investigation of the role of plasma elongation on the damping of Geodesic Acoustic Modes (GAM) and on residual undamped Zonal Flows has been made. Analytical dispersion relations have been derived and compared with the results of ORB5 simulations. Both results show a decrease in GAM frequency with elongation, an increase in GAM damping rate, and an increase in undamped zonal flow residual. Linear and nonlinear ORB5 simulations of ITG turbulence in a sequence of ideal MHD tokamak equilibria of varied elongation have yielded the following results: linear growth rates and marginal stability points of all cases coincide with each other when expressed in terms of a renormalized temperature gradient that takes into account the flux surface expansion due to elongation. In nonlinear runs, the critical upshifted (Dimits shift) renormalized gradient is the same for all elongations. However, a decrease of heat flux with elongation, thus a decrease of profile stiffness, has been evidenced. All nonlinear results were obtained by sequences of noise-controlled simulations.

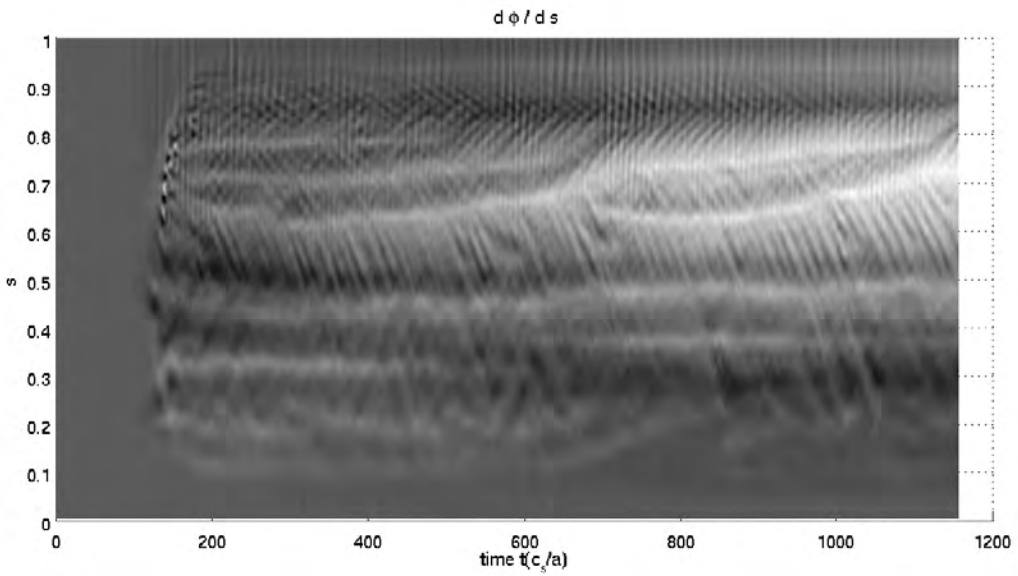

Fig. 2.2.1 *Contours of zonal flow amplitude versus radius and time in a global nonlinear gyrokinetic simulation of ITG turbulence using the ORB5 code. Avalanches appear as oblique streaks, quasi-steady zonal flows as nearly horizontal features. The vertical, quasi-periodic lines are due to Geodesic Acoustic Modes oscillations.*

Electron-ion collisions have been implemented in the ORB5 code using a Langevin (random walk) approach. In order to avoid the numerical noise generation due to this type of method, an alternative route is being explored that is acting on the marker weight evolution in a deterministic way rather than on the marker trajectories with a random generator.

Several technical improvements have been implemented in the ORB5 code. A new interface with the MHD equilibrium code CHEASE has been written and tested that allows better accuracy. Also, the massive parallelism scalability has been demonstrated up to 32768 cores on a BG/P platform, with efficiencies as high as 84% in strong scaling tests and 94% in weak scaling tests. The ORB5 code is considered for the benchmarking in the frame of the Partnership for Advanced Computing in Europe (PRACE) initiative.

A DECI (DEISA Extreme Computing Initiative) project proposed by the CRPP, with IPP Garching and the University of Warwick as co-PI's, has been approved. The allocation granted is 1.1 million CPU-hours on the Blue Gene / P at the Rechenzentrum Jűlich. We are currently making use of this computing power for studies of size scaling of ITG-induced transport, Trapped Electron Mode, and ETG turbulence using the ORB5 code.

Grid-based gyrokinetic simulations

Further linear and nonlinear simulations for analyzing the effect of order $\varepsilon=r/R$ (aspect ratio) inconsistencies in the standard implementation of the s-α equilibrium model in flux-tube codes were carried out using the grid-based gyrokinetic code GENE. This study pointed out strong differences between simulations using the s-α model and a corrected equilibrium model for Cyclone base case parameters, thus providing important clarifications for this benchmark. Using an interface between the equilibrium code CHEASE and GENE, a study of the effects of plasma shaping

on microinstabilies was initiated. In the case of ITG-type modes, the main dependence of both the linear growth rate and the ion heat flux on elongation was identified to result from the modification of the spatial profile gradients, confirming similar results obtained with the particle code ORB5. In close collaboration with IPP-Garching, a global version of the GENE code is under development, with the goal of addressing non-local effects in turbulent transport. As a first step in this direction, and in order to allow for radial variation of equilibrium quantities, the original Fourier representation for the radial direction was replaced by a real space treatment. This change of representation involved addressing various issues, such as the field solvers (Poisson and Ampere), the gyro-averaging operators, and the anti-aliasing technique.

A semi-Lagrangian code solving the drift kinetic equation in straight slab geometry using cubic spline interpolation has been implemented and parallelized with MPI considering a two-dimensional domain decomposition. The code has been benchmarked in the linear regime. Perpendicular (i.e. ExB), as well as parallel non-linearities have been validated separately by considering respectively the Kelvin-Helmholtz instability and the propagation of Ion Acoustic Waves along the magnetic field as test problems. The next development stage for this code shall be towards a sheared slab, followed by cylindrical geometry. Exploration of alternative semi-Lagrangian schemes has been carried out, in particular Galerkin-based methods using spectral elements (high order piecewise polynomial representation).

A collaboration with the CASC (Center for Applied Scientific Computing), and funded by LLNL, has been initiated for investigating the opportunities of applying Adaptive Mesh Refinement techniques for evolving Vlasov-type advection equations. A code design has been formulated for developing a spatially 2-dimensional Vlasov simulation code, with first applications to the study of Laser Plasma Interaction. This code will heavily rely on the SAMRAI (Structured Adaptive Mesh Refinement Application Infrastructure) library, and in its first implementation will make use of a semi-Lagrangian advection scheme. Implementation is under way.

Turbulent transport of fast ions

Previous studies using the GENE code on fast ion transport induced by micro-turbulence have been pursued. Several plasma configurations have been investigated, and a possible impurity pinch has been observed at low temperatures in Helium distributions with a steep temperature gradient. Thanks to a flattening of the Helium temperature profile, this pinch is not likely to occur in an expected ITER-like plasma. A non-vanishing diffusivity however persists at high temperatures ($D_{fast} = 0.15*D_i$ at $T_{fast} = 50*T_e$, as from Fig. 2.2.2). Further analysis by means of GENE phase space diagnostics will shed light on whether the high particle flux is driven by resonant mechanisms, or low energy interaction. Moreover, the single particle pushing code HMGC has been adapted to operate with GENE's turbulent fields, numerically mapped from a flux tube to a toroidal geometry for this purpose.

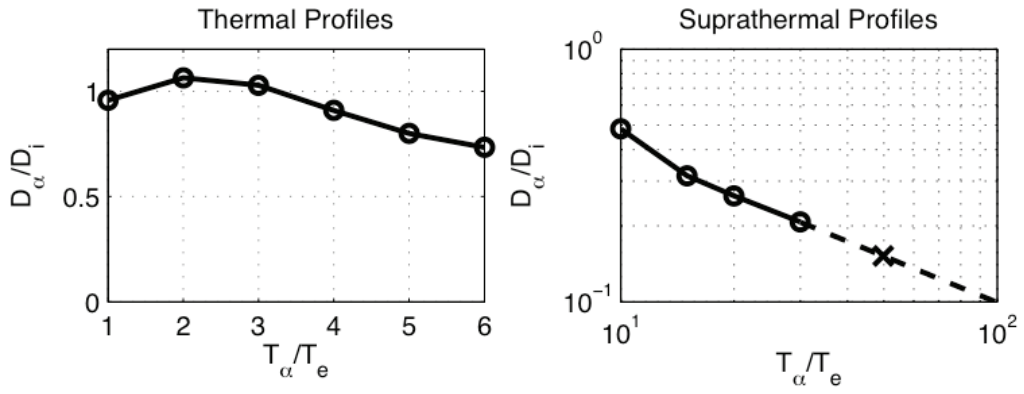

Fig. 2.2.2 *Diffusivity D_α versus temperature of Maxwellian distributions of Helium impurities (left) and alpha particles (right) in ITER, relative to the bulk ion diffusivity D_i.*

Studies of ECH/ECCD for scenario control

Safety-factor profile tailoring for sawtooth control and reverse shear scenarios

The activity has focused this year on the control of the current density profile in ITER using the EC launchers, both equatorial (EL) and upper launchers (UL). A coherent strategy has been proposed and analyzed in detail, consisting of one row in counter-CD and 2 rows in co-CD for the EL, and an extended functionality range for the UL. The study shows that with such a set-up, significant and sufficient flexibility is obtained for all the scenarios foreseen on ITER. By extending the functionality range of the upper launcher, significant control capabilities of the sawtooth period can be obtained. The upper launcher improvement enables enough margin to exceed the requirements for neoclassical tearing mode stabilization, for which it was originally designed. The analysis of the sawtooth control was carried out with the ASTRA transport code, coupled with the threshold model by Porcelli, to study the control capabilities of the improved upper launcher on the sawtooth instability. The simulations take into account the significant stabilizing effect of the fusion alpha particles. The sawtooth period can be increased by a factor of 1.5 with co-ECCD outside the q=1 surface, and decreased by at least 30% with co-ECCD inside q=1.

The present ITER base-line design has the electron cyclotron launchers providing only co-ECCD. The variant for the equatorial launcher proposes the possibility to drive counter-ECCD with 1 of the 3 rows of mirrors: the counter-ECCD can then be balanced with co-ECCD and provide pure ECH with no net driven current. The difference between full co-ECCD off-axis using all 20MW from the equatorial launcher and 20MW co-ECCD driven by 2/3 from the equatorial launcher and 1/3 from the upper launcher has been shown to be negligible. Counter-ECCD also offers greater control of the plasma current density, therefore this analysis addressed the performance of the equatorial launcher to control the central q profile. The equatorial launcher has been shown to control very efficiently the value of $\Delta q = q(\rho=0.2) - q_{min}$ in advanced scenarios, if one row provides counter-ECCD.

Neoclassical tearing modes (NTM)

The effect of changing the current density profile with ECCD on the stability of the cylindrical tearing mode stability limit has been analyzed. The difference between

driving current inside and outside the resonant surface, as well as between Co- and Counter- current drive has been detailed. This is performed in preparation of specific experiments that are foreseen on TCV to study the effect of ECCD on Δ' and the destabilization/stabilization of tearing modes observed with local Co-/Counter-current drive, respectively.

ASTRA simulations of the effect of an island on heat transport have also been started, in this case related to the global oscillations observed on TCV. The latter are triggered by MHD modes and the aim is to simulate the full cycles in order to better understand the dynamics. These will also be useful for the integration of NTM modules into transport simulations in the ITM-TF activities.

Particle transport modeling

A quasi-linear gyrokinetic model is developed to predict stationary values of the logarithmic density gradient for electrons and ions. The contributions to the off-diagonal convective term composing the turbulent particle flux are derived from first principles and evaluated with numerical parameter scans. The application of the model together with the numerical scans have yielded a comparison between theory and experiment showing qualitative agreement. A "universal" behaviour of the density peaking resulting from the pinch coefficients has been thoroughly analyzed in terms of the dominant microinstabilities. The model has also been successfully applied to interpret the observations on particle transport from the eITB scenario in TCV.

2.2.2 RF waves

Alfvén and ICRF waves in 2D and 3D configurations

The improvements done in the warm version of the LEMan code with consistent computation of the parallel wave vector have permitted to perform simulations of an LHD configuration in the Alfvén domain and thus to point out a temperature dependence of the global modes (TAE's) frequencies. In a JET-like geometry, such phenomenon was not observed. One explanation for this behaviour is a coupling with waves converted at the Alfvén resonances due to the increased complexity of the spectrum from 3D effects. Numerical convergence has been demonstrated for a three-dimensional case for both the cold and warm models with consistent computation of the parallel wave vector. Furthermore, the contribution of fast ions in the dielectric tensor has been added by introducing a bi-Maxwellian distribution function. The latter permits to take into account anisotropy in the velocity space. Tests have shown that even a small density of fast particles have an effect on the absorbed power. Finally a new iterative method has been implemented. The idea here is to reduce the computation time and to enable simulations in the ICRH domain where convergence of the full model with consistent computation of the parallel wave vector is hard to complete. This method was successfully benchmarked in 2D configurations (circular and JET-like cross section) in the Alfvén domain against the full model.

For a numerical study into the effects of ion cyclotron resonant heating (ICRH) on the fast particle distribution function in general plasma geometry, three codes have been coupled. The general (2D or 3D) MHD equilibrium generated by VMEC (including full shaping and pressure anisotropy) is interfaced with two codes. The full-wave code LEMan uses the equilibrium to calculate the power deposition and electromagnetic field strength of a wave field generated by a chosen antenna using

a warm model. The dielectric tensor makes use of a realistic bi-Maxwellian representation for the distribution of fast ions. The single particle Hamiltonian code VENUS combines the outputs of VMEC and LEMan in order to calculate the evolution of the distribution function. Within VENUS, Monte Carlo operators for Coulomb collisions of the fast particles with the background plasma have been implemented, accounting for pitch angle and energy scattering. Also, ICRH is simulated using Monte Carlo operators on the Doppler shifted resonant layer. The latter operators act in velocity space and induce a change of perpendicular and parallel velocity depending on the electric field strength and the corresponding wave vector. Ultimately, the change in the distribution function will then be fed into VMEC for generating a new equilibrium and thus a self-consistent solution can be found via multiple iterations. So far, we have succeeded in attaining one iteration.

2.2.3 Operational limits

MHD Stability and Kinetic effects

Studies continue in order to identify kinetic modifications to modes which are essentially of MHD origin. An analytical calculation of average toroidal drift orbits in an anisotropic plasma has been made. Solutions are obtained for both trapped and passing orbits in general shaped geometry. The results are important for studies into electron and ion fishbone instabilities with various mode numbers and in a variety of equilibria. Furthermore, the inclusion of shaping effects could help to explain contrasting anomalous transport phenomena in, for example TCV, with differing geometry. Work in this area has demonstrated good agreement with flux tube simulations, which in turn has explained improved trapped electron mode stability for negative triangularity.

Stability criteria for electron fishbones in tokamaks are being developed in order to be relevant for baseline, hybrid and advanced scenarios. The two latter scenarios are dependent on recent analytical work undertaken on infernal modes and Mercier modes for vanishing magnetic shear. It is expected that the work will be used to interpret electron fishbones observed in tokamaks, including possibly TCV. For this purpose, a user-friendly interface (GUI) has been developed enabling the spectral analysis of ECE signals, accounting for various functions such as detrending, filtering, cross-correlation analysis. This tool is particularly useful for the discovery of weak or localized modes in signals with high noise levels.

Sawtooth behaviour and internal ideal stability

The sawtooth control mechanism in plasmas employing off-axis toroidally propagating ion cyclotron resonance waves in tokamaks has been reinvestigated. The radial drift excursion of energetic passing ions distributed asymmetrically in the velocity parallel to the magnetic field is found to determine stability when the rational q=1 surface resides within a narrow region centred about the shifted fundamental cyclotron resonance. This work employs RF wave-field and fast ion distribution function simulations applied to a key demonstration JET discharge with localised off-axis ion cyclotron current drive (ICCD) counter to the Ohmic current. Analytical and full numerical calculations of the internal kink mode with the simulated JET ICRH distribution function demonstrate ideal instability when the deposition of the resonating ions is very close to the q=1 radius. Such is the sensitivity to the location of deposition, and the magnitude of the effect, that this fast ion mechanism, i.e. non-MHD mechanism, dominates over the previously

assumed classical mechanism relating to the change in the magnetic shear due to the fast ions, and the resulting effect on MHD stability.

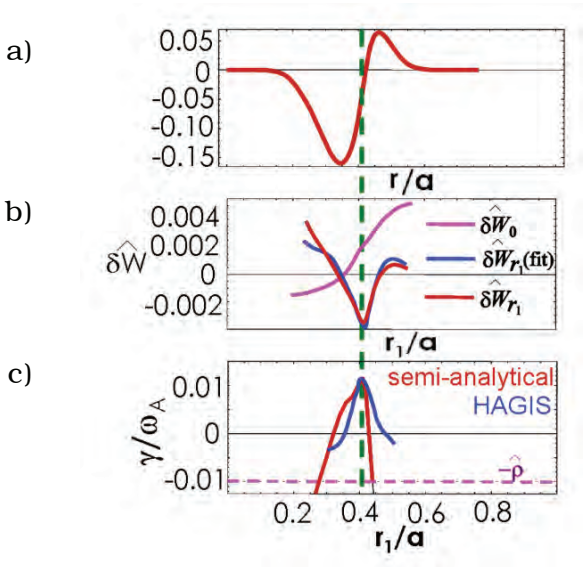

Fig. 2.2.3 *Showing (a) the fast ion current for a key JET demonstration discharge, (b) analytical calculation of the potential energy for the internal kink mode as a function of the normalized q=1 radius, r_1/a, for the above fast ion current profile, and (c) a comparison of the analytical growth rate with HAGIS numerical simulation.*

As shown in Fig. 2.2.3, it is found that maximum instability occurs when the q=1 radius is located where the radial gradient of the passing fast ion current dipole is largest. Furthermore, unlike the classical sawtooth control mechanism, the fast ion mechanism derived here is independent of the electron drag, which is expected to limit the current drive efficiency of the proposed ICRF system for ITER. In order to distinguish between the two mechanisms, and test the prospects of sawtooth control in ITER using ICCD, experiments at JET using minority He3 are planned in December (see section on JET in this report).

MHD equilibria and stability computations of TCV plasma

In view of supporting possible doublet plasma experiments in the TCV tokamak, the doublet version of the CAXE-F free boundary equilibrium code and the KINX-NW resistive wall n=0 stability code have been updated and installed. Free-boundary doublet equilibria with the TCV PF coils were computed and an interface to the rigid plasma displacement code has been developed. The most unstable n=0 mode features displacements in reverse directions in the two regions inside the separatrix. The perturbed surface current at the edge of the plasma outside the separatrix (mantle or common flux region) strongly stabilizes the mode. The growth rate for a reference TCV doublet configuration changes from ~300 1/s to ~3000 1/s with and without mantle respectively (still being ideally stable). It is worth to note that even a strong increase of the wall poloidal resistance results in a weak (few percent) increase of the growth rate. We conclude that the rigid displacement model should include the effect of surface current in order to produce realistic estimates of the most unstable mode growth rates for doublet configurations.

In view of forthcoming TCV experiments, free boundary equilibria with negative triangularity have been computed using the real PF coil configuration. Equilibria

with negative x-point triangularity and with negative or positive triangularity on the other side were both found significantly less stable against high-n ballooning modes near the edge (as compared to positive triangularity configurations). Access to second stability region is practically removed. This may result in differences in the ELM behaviour for the negative triangularity configurations. The pressure driven n=1 kink limits are lower compared to the positive triangularity equilibria. The value of the n=0 growth rate is very high for the negative triangularity equilibria in TCV with the reference elongation 1.75: ~1500 1/s. The growth rate is further increased when taking into account the ports (modeled as very high resistivity axisymmetric pieces of the wall): ~3000 1/s in the reference plasma position (i.e. plasma center aligned with the F6 coil) and can even go ideally unstable when the plasma is shifted inside farther from the LFS wall. It confirms the conclusion about the high sensitivity of the vertical stability in negative triangularity configurations to the proximity to the outer wall of the plasma. A lower elongation is needed for the negative triangularity configurations to be vertically controllable. The axisymmetric growth rates were computed for an equilibrium series with negative triangularity and elongation from 1.4 to 1.75. An elongation 1.4 corresponds to a reasonable growth rate ~700 1/s without ports and a factor of 2 larger with ports modelled as axisymmetric openings.

Tokamak stability in the presence of axisymmetric islands

Numerical studies of tokamak stability in the presence of axisymmetric islands have been pursued. Several improvements have allowed us to use much finer grids. Convergence studies confirmed the existence of non-dipole equilibria stable against n=0 modes, at least with fixed boundary. An analytic dipole-type free-boundary equilibrium configuration in slab geometry was investigated. Axisymmetric stability calculations showed a tilt instability very similar to that found in nonlinear modeling.

2.2.4 Optimization of 3D configurations

Optimization of quasi-isodynamic stellarator configurations

The existence of small ripple in quasi-isodynamic stellarators with poloidally closed contours of the magnetic field strength has been explored. This has been verified in configurations with large number of field periods and high aspect ratio which are stable to ballooning modes. A reduction of the aspect ratio retains the small ripple properties, but the ballooning modes are destabilized.

Ballooning eigensolver with COOL finite elements

A 3D ballooning eigensolver based on the COnstraints Oriented Library (COOL) finite elements has been developed (the BECOOL code). The discretized system reduces to a special block pentadiagonal eigenvalue equation that is solved with an inverse vector iteration method. Numerical computations reveal that BECOOL recovers precisely the eigenvalues calculated by the VVBAL shooting code when using second order Legendre polynomials. Further tests portray a time-based need to find an optimal Legendre polynomial order for intensive computations. It is determined that the ballooning mode equation discretized with cubic Legendre polynomials appears to be the optimal case to consider.

MHD stability analysis of LHD

The MHD stability of LHD plasmas with internal diffusion barriers (IDB) produced with rapid fueling in the core region through pellet injection is investigated. The high central density plasmas have steep core pressure gradients which become shallow in the plasma periphery. Ideal and resistive MHD modes are stable in the central plasma region. However, the resistive MHD mode, investigated with an MHD turbulent transport model applied at NIFS, becomes unstable near the edge. The theoretical results and experimental observations suggest that the formation of the electron density profile in the IDB plasma is more likely influenced by resistive than ideal MHD.

Neoclassical transport in 3D stellarators

The VENUS - δf code has been applied to calculate the bootstrap current in the LHD device. In the extremely long mean-free-path regime, the results obtained agree reasonably well with the quasi-analytic predictions of the Shaing-Callen theory. In this regime, the computational demands of the VENUS - δf code to obtain a steady state solution are large. In the collisional regime, the outward-shifted LHD configuration displays a negative bootstrap current (that unwinds the rotational transform). The magnetic island structures in high density IDB plasmas complicate the determination of bootstrap currents in the core region of the plasma.

Fluid MHD stability in a Heliotron with anisotropic fast particles.

Two anisotropic pressure models for global fluid stability implemented in the TERPSICHORE code have been applied to the LHD Heliotron, considering a sequence of equilibria with fixed diamagnetic beta ~5% (of which the fast particles contribute a 1/3 fraction) and varying the parallel to perpendicular temperature ratio of hot particles. The rigid hot particle stability model predicts quasi-stability to global modes. The fully interacting model shows stabilization with increasing parallel to perpendicular hot particle temperature ratios until the transition from an external ballooning to an internal kink mode takes place. The prospects of beam driven-fusion in a Heliotron system have been considered.

Free-boundary, 3D, anisotropic pressure, stellarator equilibria

The ANIMEC code has been developed as an extension of the most recent free boundary version of the VMEC equilibrium code for three-dimensional plasmas with nested magnetic flux surfaces. This includes a preconditioning algorithm that is exploited to allow the computation of equilibrium states with radial force balance error improvements exceeding 4 orders of magnitude compared with the non-conditioned results. The variant of a bi-Maxwellian distribution function is invoked to determine the anisotropic pressure moments generated by energetic particle species. To obtain the vacuum magnetic field, a Green's function method is employed. Off-axis energetic particle deposition in a 2 field period quasi-axisymmetric stellarator reactor system has shown that for large parallel anisotropy the energetic particle pressures vary weakly around the flux surfaces, but the perpendicular hot particle pressure localizes in the region of the fast particle deposition layer for large perpendicular anisotropy.

2.2.5 Integrated Tokamak Modelling

In the frame of the EFDA Integrated Modelling Task Force (ITM) project no.4, we have participated in a wide benchmarking exercise with various gyrokinetic and gyrofluid codes. A good agreement has been found for the computed heat flux for core ITG turbulence. However, there is still some disagreement on the zonal flow saturation level.

In the frame of the EFDA Integrated Tokamak Modeling Task Force project no.1, new versions of the CHEASE and CAXE equilibrium codes, as well as of the KINX stability code (with a possibility to work either in a standard stand-alone mode with input files in XML format or interfaced to the MDSplus database and Kepler) were developed and presented at the EFDA ITM-TF general meeting (10-12 September, Frascati, Italy). The CHEASE, CAXE and KINX actors were developed for the Kepler work flow manager and installed on the ITM TF gateway computer. The work flows with the code actors, including the actors for code parameters input and equilibrium plotting, were tested. The codes are ready for verification and validation exercises.

There has been a significant involvement to provide HDF5 (Hierarchical Data Format) support to the TF-ITM and in particular to the project IMP no.4. [HDF5 is a unique, completely portable, open source technology that makes possible the management of extremely large and complex data collections.]

In the frame of the project IMP no.5 the RF global code LION for fast ICRF wave computations was upgraded resulting in a reduction in CPU time by 20-50%.

2.3 Operation of a specialised basic plasma physics device, TORPEX

The CRPP Basic Plasma Physics group aims at improving the understanding of fluctuations, turbulence and related transport phenomena in toroidal magnetised plasmas. The experiments are conducted on the TORPEX device, characterized by low plasma densities and temperatures, allowing high temporal and spatial resolution measurements throughout the plasma cross-section. Plasmas are confined by a toroidal magnetic field up to B_T=0.1T, and a smaller vertical component, $B_z \leq 50$mT, corresponding to a simple configuration incorporating the main ingredients for drift wave instabilities and turbulence also observed in magnetic fusion experiments, namely pressure gradients and magnetic field line curvature. Highly reproducible discharges of different noble gases with electron density and temperature in the range $n_e \sim 10^{16}$-$10^{17} m^{-3}$ and T_e~5-10eV are driven during more than 2s by microwaves (P<50kW) at f=2.45GHz, in the electron cyclotron (EC) range of frequencies. Parameters as the neutral gas pressure, the location of the EC resonance and the amount of injected power can be varied to influence density and temperature profiles.

The progress achieved in 2008 includes hardware developments and tests for the study of the interaction of fast ions with turbulence, the development of a gas puffing and fast imaging system for a non-perturbative reconstruction of turbulent structures, the development of a new 3D fluid code for a full description of plasma dynamics in TORPEX, a comprehensive characterisation of the propagation of plasma filaments (or blobs), the investigation of the existence of an improved confinement regime, the identification of differences in the turbulence in the

presence of closed field lines, the investigation of the existence of a critical gradient for turbulence onset, measurements of the plasma flow in different conditions, the discovery of universal aspects of fluctuations, and specific advances in the simulation and in the methodology for comparing numerical with experimental data. All of these aspects are discussed in the paragraphs here below, along with a short summary of more technical achievements.

2.3.1 Fast ions physics

The effort to investigate the interaction between highly energetic ions and small-scale (drift wave-like) turbulence in TORPEX plasmas progressed in 2008.

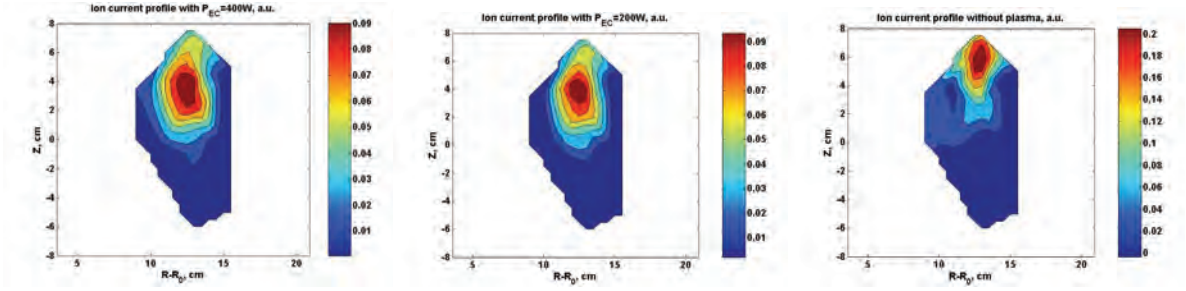

Fig. 2.3.1 *Fast ion current profiles: (left) for a magnetron power of 400W, (middle) 200W, (right) without plasma.*

The system developed for this task, comprising the fast ion source, the detector and the control system, has been assembled, commissioned and is now fully integrated into the TORPEX environment. In 2008, the fast ion source and detector (double gridded energy analyzer) were installed on a 2D movable system in order to cover an entire poloidal cross-section. The electronics for the source (two remotely controllable high voltage power supplies) was built and tested on a small vacuum chamber. These tests indicated an ion current on an external grid of the source higher than 1μA. Tests of source and detector were then conducted on TORPEX without plasma but with both toroidal and vertical magnetic field, indicating only a weak dependence of the fast ion current on the magnetic field. The bias voltage on the collecting grid was optimized for better focusing of the fast ion beam. First experiments with plasma were conducted with fast ion energies 300eV and 600eV, in a plasma regime in which the dominating instability leading to turbulence is of pure interchange type. The fast ion current profile was measured with the detector using synchronous detection to increase the signal to noise ratio. With respect to the beam propagation in vacuum, in the plasma the fast ion current profile is broader and more elongated vertically (Fig. 2.3.1). This behaviour was qualitatively predicted with simulations (Fig. 2.3.2) and could be explained by a toroidal drift of the scattered fast ions.

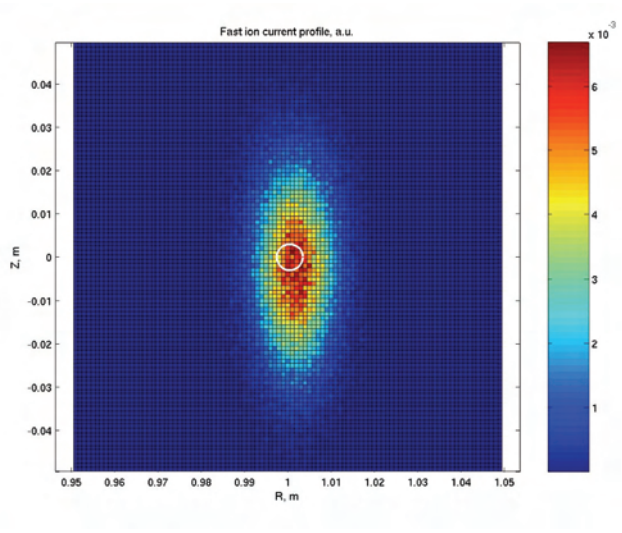

Fig. 2.3.2 *Simulation of the fast ion current profile (the white circle is the initial position of the beam).*

2.3.2 Gas puffing and fast imaging of structures

Ideally, the investigation of turbulence in plasmas would require a full spatio-temporal imaging of fluctuations of the relevant fields, as well as of the particle response, with enhanced spatial and temporal resolution, and without perturbing the plasma. Fast framing cameras are one of the most recent diagnostics to monitor light emission from magnetically confined plasmas and are now commonly used to study turbulence in plasmas. Recently, a Photron Ultima APX-RS fast framing camera has been acquired to complement the extensive set of Langmuir probes in TORPEX, namely the 86 probe array HEXTIP, which enables the comparison of statistical and spectral properties of visible light and electrostatic fluctuations. The Photron Ultima APX–RS camera detector consists of 1024×1024 CMOS diodes. At maximum resolution, the frame rate can be increased up to 3kf/s. By choosing lower resolutions, higher frame rates up to 250kf/s are possible. Sequences of thousands 8-bit digital images can be captured into the temporary memory for later slow play-back and/or storage into computer archives. The camera is controlled by a programme having extensive graphical user interface, which has been fully integrated into the TORPEX shot cycle through a client-server technology.

Preliminary measurements of visible light emission were made in a variety of plasmas and the influence on the light emission of various parameters such as vertical magnetic field, magnetron power and neutral gas pressure was studied. The results clearly show a dependence of the mean values of the light intensity on neutral gas pressure and plasma density. The quality of the imaging was improved by cooling the camera with continuous air flow and by using optical fibres. Due to the low light levels, the first attempts to interpret the light fluctuations with the plasma density fluctuations were only partially successful. To overcome this problem, a development of a gas puffing system was undertaken. A first gas puffing system including a fast piezoelectric valve and a ceramic tube with a 200μm nozzle was built, calibrated in a test bench and installed in TORPEX. The first results clearly confirm the expected improvement, enabling acquisition at frequencies up to 50kf/s. An example of this method is illustrated in Fig. 2.3.3, which shows a maximum correlation between fluctuating part of the camera and probe signals of about 0.7, in the gas puffing cloud just in front of the nozzle.

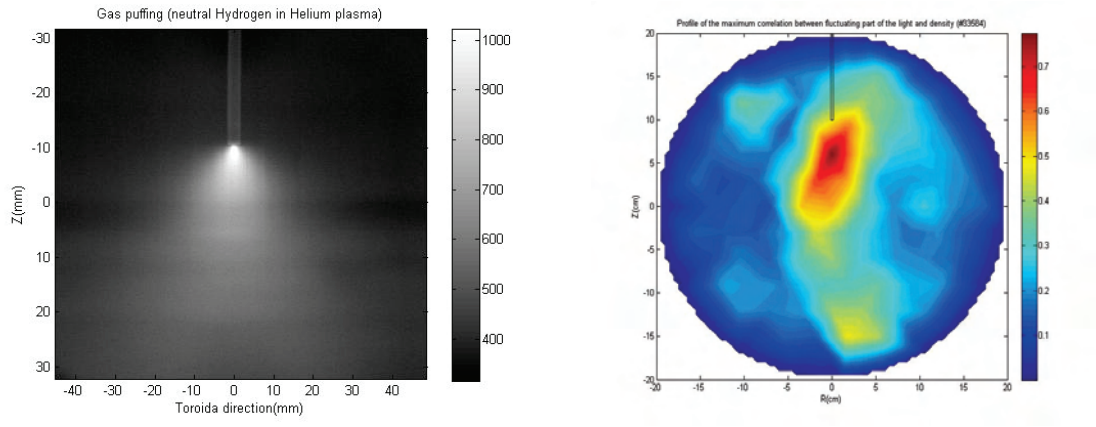

Fig. 2.3.3 *Gas puffing cloud image (left); profile of the maximum correlation between fluctuating part of the light and density (right).*

2.3.3 Development of a new 3D fluid code

In the past year, a new three-dimensional code has been implemented to follow the TORPEX plasma dynamics. The code is written making use of the Message Passing Interface, is adapted to the architecture of Pleiades2, the Linux cluster in use at CRPP, and adopts a finite difference algorithm to solve the electrostatic drift-reduced Braginskii equation. The fluid equations are solved in a flux tube geometry that follows a magnetic field line that wraps around TORPEX. The 3D code extends the previously developed 2D code, which led to the discovery of the high and low confinement modes in the TORPEX configuration, by taking into account the parallel plasma dynamics (i.e., turbulence driven by drift-waves), the effect of parallel resistivity, and finite electron mass. At low parallel resistivity, the 3D simulations confirm the picture obtained by the 2D code: the plasma profiles remain quasi two dimensional, a high confinement mode is reached if the vertical magnetic field is decreased, the source strength is increased, or the mass ratio is increased. At high parallel resistivity, a fully 3D plasma dynamics is observed, with the core plasma decoupled from the dynamics at the sheath edge. In particular, at high parallel resistivity a transition to a high confinement mode is observed, characterized by different properties than the 2D high confinement mode. The threshold condition to access this new turbulence regime has been evaluated analytically and is in good agreement with the simulation results. This project has been completed with the implementation of a simulation code able to follow the global TORPEX geometry, overcoming the assumptions of the flux-tube geometry. The analysis of the results of this comprehensive code has just started.

2.3.4 Propagation of plasma filaments in TORPEX

Filamentary structures of increased plasma density, appearing like blobs in the plane perpendicular to the magnetic field, are observed in virtually all toroidal confinement devices. At the edge of magnetic fusion devices, such as tokamaks and stellarators, a large fraction of the anomalous particle and heat transport is due to the presence of filaments. Filament transport is convective and may extend to the far Scrape-Off Layer (SOL), typically yielding flat density profiles and a significant particle flux near the wall of the device, affecting divertor heat loads and wall recycling and possibly the overall performance of ITER.

A clear picture of filament formation in TORPEX has emerged in past two years. Using previously developed experimental scenarios, in 2008 we have undertaken dedicated experiments to study the propagation properties of these plasma filaments. We have inserted limiters of different materials (conducting or insulating) to study the role of the boundary conditions on blob motion. Furthermore, we have varied parameters such as the ion mass, the neutral background pressure and the pitch angle of the magnetic field. While not all the experimental findings are yet understood, we achieved a good understanding of blobs limited by the conducting plate, for which both currents along the magnetic field and perpendicular to it play a significant role. We have derived a theoretical scaling that relates the vertical size of a blob to its radial speed. This formula, which interpolates between previously published expressions for blob speed versus size, displays a very good agreement with experimental results (Fig. 2.3.4).

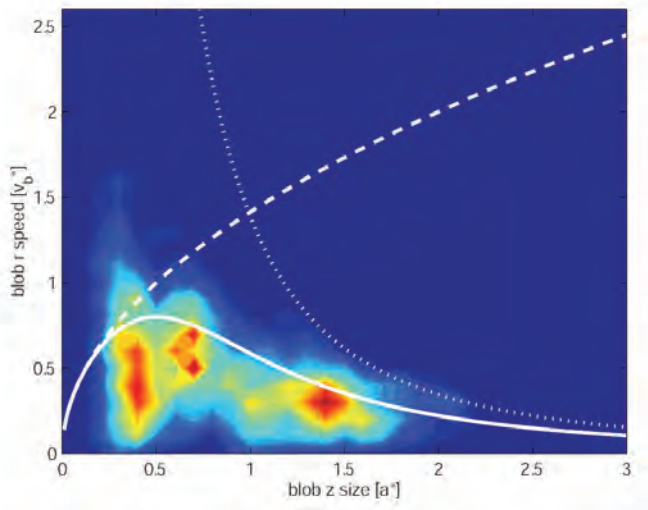

Fig. 2.3.4 *Histogram of blob radial velocity versus its vertical size for discharges in H_2, He, Ne and Ar. The solid line is the scaling derived from theory. Dashed and dotted lines are previously published scaling laws.*

2.3.5 Investigation of the existence of an improved confinement regime

Recent numerical simulations together with an analytical theory predict the existence of two confinement regimes in simply magnetized toroidal plasmas with some common features to tokamak observations. By increasing the plasma source strength, by reducing the vertical magnetic field, or by increasing the ion mass, a transition from a low to a high confinement mode regime is predicted to occur. In high confinement mode, a strong shear of the ExB velocity limits the perpendicular transport, leading to steeper gradients and larger peak values of density and temperature. A higher mode of confinement is obtained when the ratio of the linear interchange growth rate, γ, to the E×B shearing rate, $v'_{E\times B}$ is smaller then unity. We used the flexibility of TORPEX to explore the accessibility of the high confinement mode by varying various experimental parameters (vertical magnetic field, ion mass and microwave source power). The dependence of the temperature and density gradients upon the E×B velocity shear is investigated and compared with theoretical predictions. Fig. 2.3.5 shows the dependence of the experimental inverse gradient scale length of temperature and density upon $\gamma/v'_{E\times B}$. As predicted, for $\gamma/v'_{E\times B}<1$ a steepening of T_e and n_e profiles is observed.

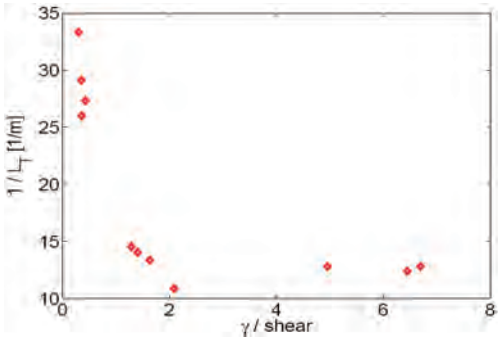

Fig. 2.3.5 *Dependence of inverse gradient scale length upon γ/v'_{ExB}. for different gases (H_2, He, Ne)*

2.3.6 Changes in turbulence character in closed field line configurations

Recently, an Ohmic transformer system has been added to TORPEX, which induces a toroidal electric field to produce a plasma current and to close magnetic field lines in the plasma. The plasma equilibrium and stability are provided by vertical magnetic field coils. During 2008, we have optimized the coil configuration against plasma current stability, resulting in a stable period of closed magnetic field lines in a large portion of the vacuum chamber. This is shown in Fig. 2.3.6. In this optimized configuration, preliminary measurements with magnetic and electrostatic probes suggest that the plasma dynamics is characterized by turbulent structures, which are associated with electromagnetic waves. This configuration represents, therefore, a unique starting point to investigate the physics of turbulent transport in tokamaks with unprecedented diagnostics capabilities.

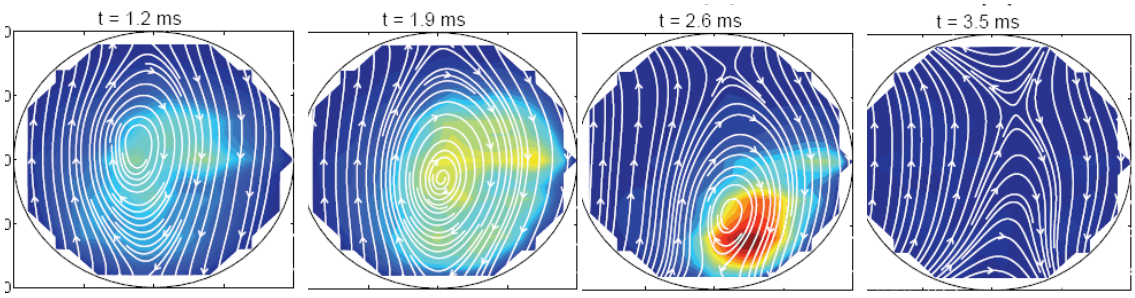

Fig. 2.3.6 *Time evolution of the closed flux surfaces obtained in TORPEX using the optimized Ohmic system.*

2.3.7 Existence of a critical gradient for the onset of drift/interchange turbulence

A theoretical analysis has shown that the interchange mode can be stabilized for very small normalized pressure gradients, which cannot be achieved in practice in TORPEX. Therefore, interchange modes are always unstable and become dominant at large vertical magnetic field. Conversely, the drift mode can be stabilised if the (e,i)-n collisions frequencies are strong enough. We tried to verify this prediction experimentally. For hydrogen plasmas, we didn't succeed to change the collisions frequencies over a wide enough range, and drift waves were still present. Similar investigations have started in argon plasmas. Preliminary results show that it

should be possible to change sufficiently the collisions frequencies, by changing the neutral gas pressure, hence to reduce the normalized pressure gradient (Fig. 2.3.7).

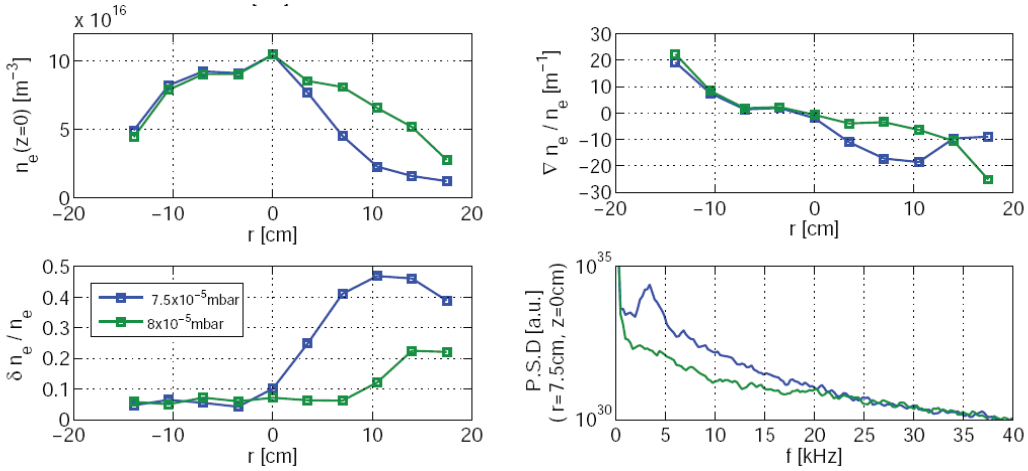

Fig. 2.3.7 *For two different neutral gas pressures (green and blue curves), radial profiles of (a) electron density, (b) inverse gradient scale length, (c) normalized density fluctuations. (d) Power spectral density of ion saturation at r=7.5cm.*

2.3.8 Measurements of the intrinsic plasma flow and rotation

A new method for toroidal velocity measurements with Mach probes has been explored. The technique is based on the conditional sampling technique, the triggering events being density blobs. The method has been therefore applied to the regime where blobs are generated from an interchange wave: the mode at 4kHz being located at -5<r<5cm and the blob region corresponds to r>7cm. A reconstruction of the time resolved two-dimensional profiles of electron density, electron temperature, plasma potential, and toroidal velocity is now possible with a single point measurement on a shot-to-shot basis. In more details, the idea was to apply a varying voltage on both sides of the Mach probe and then, using a conditional sampling method, to reconstruct the I-V Langmuir characteristic over many blob events detected with a reference Langmuir probe, for each Mach tip. A similar method has already been successfully applied to density, temperature, and plasma potential measurements with a standard Langmuir probe. The time evolution of the estimated plasma parameters is reported in Fig. 2.3.8. In the subplots a) and b), the electron density n_e measured by both Mach tips is shown. The difference in the time averaged value between both time traces already indicates a non-zero toroidal flow. The coherent oscillations at 4kHz (interchange mode) and the density blob are well captured by the Mach probe. The electron temperature is remarkably similar on both sides of the Mach probes (subplot c)). The interchange mode is still visible while there is not a clear signature of the blob in Te. In Fig. 2.3.8.d), the time evolution of the toroidal velocity in the mode region and at the edge is represented. The coherent oscillations associated with the interchange mode are clearly visible and highlighted by the thick line, which corresponds to the low-pass filtered signal. It has to be noted that V_Φ and n_e are evolving almost out of phase. In the edge region, we see that when a density blob is detected, the toroidal velocity decreases a few μs later. So, a positive n_e burst carries a positive V_Φ burst. The perturbation associated with the density blob on the toroidal velocity is much weaker (20%) than on the density itself (80%). Finally, Fig. 2.3.8(e-f) show the 2D profiles of the fluctuating density and toroidal velocity when

the blob is detected (τ=0). The mode is visible around r=-5cm and the blob is seen at the very edge (r=14 cm).

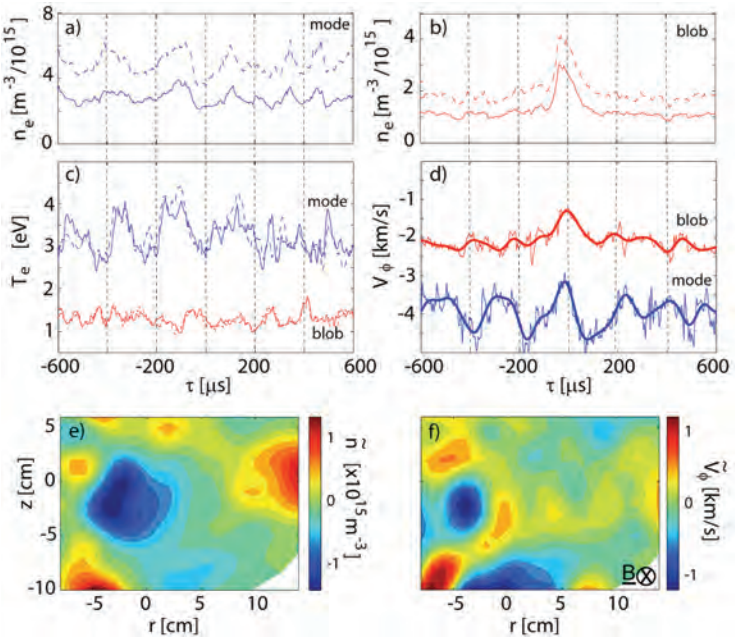

Fig. 2.3.8 *Time evolution of (a) the electron density in the mode region, measured by two Mach probe, and (b) in the blob region (r=12cm, z=0cm); (c) the electron temperature measured in both regions by two Mach probe tips (solid and dashed); (d) the toroidal velocity measured in both regions. The thick lines are data filtered with a low-pass filter at 10kHz. Example of a 2D snapshot taken when the blob of (e) the density fluctuations and (f) the toroidal velocity fluctuations is detected.*

2.3.9 Universal aspects of TORPEX plasma fluctuations

Complementing previously reported results for density fluctuations, we have shown in 2008 that the statistical properties of the floating potential fluctuations have also a universal character. In particular, the unique quadratic relationship that links the skewness S and the flatness F is still observed, though with different coefficients than for plasma density fluctuations. This observation allows us to exclude trivial effects in the observed universality due to the fact that the plasma density is a positive defined quantity.

2.3.10 Theory simulation and comparison with experimental data

TORPEX constitutes the ideal environment to perform a plasma turbulence code validation project: the magnetic geometry is relatively simple and, contrary to typical fusion devices, the diagnostics provide a full picture of the plasma dynamics that can be compared with the simulation results. The validation project started by considering the turbulence regime easier to simulate: the one dominated by the interchange dynamics and characterized by low confinement properties. For this scenario, a long 2D simulation has been performed to provide the time series and the statistics necessary for a quantitative comparison with TORPEX data. The comparison has been performed across a broad range of experimental

measurements, starting from the analysis of quantities that are directly measured in TORPEX (e.g., I_{sat} measurements), to quantities that require a sophisticated statistical treatment to be obtained from the direct experimental data (e.g., particle flux). For the purpose of code validation, the turbulence analysis techniques that had been developed to study TORPEX plasmas (e.g., structure analysis) have been applied to the simulation data.

2.3.11 Hardware upgrades

Mobile sectors

Three new mobile sectors have been manufactured (by Romabau) and delivered to CRPP after successful vacuum and mechanical tests in 2008. Two of these have been installed on TORPEX, furthering the device flexibility and reducing the shutdown time required to install new or upgraded diagnostics.

Limiters

Limiters made out of conducting (steel) and insulating (glass) material have been designed, manufactured, and installed on TORPEX. Preliminary measurements of blob propagation in the presence of the limiters have stimulated new ideas for a limiter, which allows varying the angle between the limiter and magnetic field lines. This limiter is presently being designed.

Ohmic system

A new Ohmic power supply has been studied and designed to supply the D1,E1,D2,E2 coils of TORPEX, connected in series in order to impose a vertical magnetic field inside the vacuum vessel. Since an important point was to reuse as far as possible existing material at CRPP, the energy source is based on HV capacitors of 62.5μF each. Two sets of 20 paralleled capacitors referred to ground formed a bank of 625μF in total. This bank, charged at a maximum DC voltage of 20kV, will be connected to the TORPEX coils through a HV thyristor switch (ABB), which will be triggered by fibre optic to allow a damped oscillatory current circulating through the coils and generating the required flux. The first peak current obtained is 4500A and the oscillation frequency is ~70Hz. An AC regulator (made of two thyristors connected in inverse parallel), powered from the mains (400VAC), applies an AC voltage to the primary of HV transformer (ratio 1÷35). The secondary AC voltage is rectified by a diode bridge that supplies the capacitor bank with a constant, regulated current.

Additional protection systems have been installed to insure a safe operation of this power supply. The power supply has been manufactured and the components have been installed. Commissioning on resistive load and on the TORPEX coils has been completed. Remote control and the signal acquisition are under way.

2.4 Materials research

The main objective of the Fusion Technology Materials (FTM) group of the Centre of Research in Plasma Physics (CRPP, EPFL) is to investigate the effects of the damage produced by irradiation in a variety of materials, in particular candidate structural

materials for plasma facing (first wall, divertor) and breeding blanket components of the future fusion reactors but also pure metals and model alloys. This group is located at the Paul Scherrer Institute (PSI) in Villigen.

Main R&D activities of the FTM group include development and characterization of advanced metallic materials for fusion power reactors, in particular reduced activation, oxide dispersion strengthened ferritic steels and tungsten-base materials, modelling of radiation damage and radiation effects, qualification of metallic materials for the International Thermonuclear Experimental Reactor (ITER), and small specimen test technology for the future International Fusion Materials Irradiation Facility (IFMIF). The scientific approach adopted by the FTM group to understand the fundamentals of radiation damage in metals and alloys is based on investigating the structure/mechanics relationships at different length scales (micro-, meso-, and macroscopical). A range of experimental and numerical tools is used to reach these objectives. For simulating experimentally the effects of 14MeV neutrons, that will be the product, together with 3.5MeV helium nuclei, of the envisaged fusion reactions between deuterium and tritium nuclei, the FTM group is involved in irradiation experiments performed in the target of the Swiss Spallation Neutron Source (SINQ) as well as in neutron irradiations performed in reactors in Belgium, the Netherlands and Hungary.

2.4.1 Emerging technologies

Development of material science and advanced materials for DEMO

Irradiation Experiments

A number of specimens of various materials have been irradiated in the Swiss Spallation Neutron Source (SINQ) for two years in 2004-2005. The cooling phase took place in 2006. Post-irradiation experiments should be performed in 2009. A new irradiation campaign was started in April 2007 and will be achieved in December 2008.

Development of ODS ferritic steels

Six different oxide dispersion strengthened (ODS) reduced activation ferritic (RAF) steels, with the compositions of Fe-(12-14)Cr-2W-(0.1-0.3-0.5)Ti-0.3Y_2O_3 (in weight percent), were produced by mechanical alloying, canning and degassing of the milled powders, and compaction of the powders by hot isostatic pressing (HIPping). Mechanical alloying was performed by milling either elemental Fe, Cr, W, and Ti powder particles (up to 10μm in size) or pre-alloyed, gas atomised, Fe-14Cr-2W-0.3Ti powder particles (up to 50μm in size) with 0.3%Y_2O_3 particles (20-30nm in size). Two types of ball mill have been used, namely a planetary ball mill and a high-energy ball mill, as well as two different milling atmospheres: argon and hydrogen. Various mechanical alloying conditions have been investigated (ball-to-powder ratio, speed, time, atmosphere) as well as various degassing conditions of the powders (temperature, time, vacuum) and HIPping conditions (pressure, temperature, time). The various powders and compacted ingots have been characterized in terms of density, microstructure, chemical composition, microhardness, tensile and Charpy impact properties. The obtained results allowed us to extract optimal manufacturing conditions for ODS ferritic steels (Fig. 2.4.1).

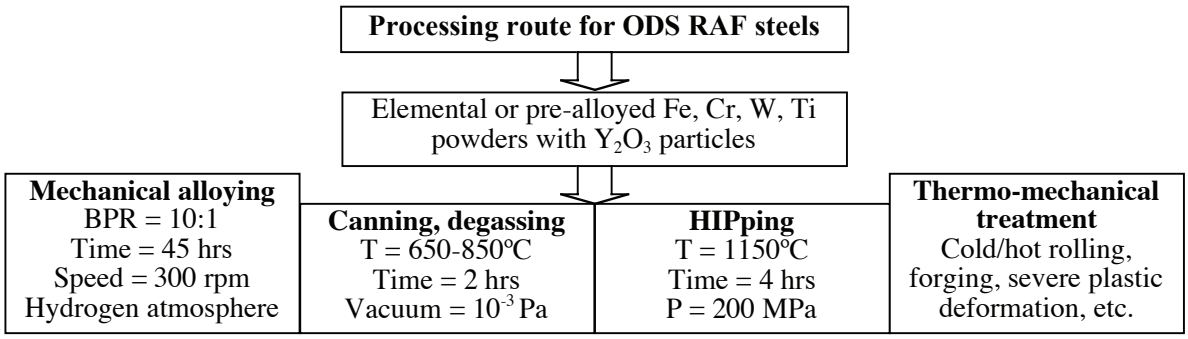

Fig. 2.4.1 *Main manufacturing conditions for ODS reduced activation ferritic steels.*

Development of tungsten-based materials

W-2.0Y and W-2.0Y_2O_3 materials (in weight percent) have been manufactured by conventional powder metallurgy methods including dry mechanical alloying in an argon or a hydrogen atmosphere of a powder of pure W (99.9%), with particle sizes in the range of 1-5μm, either with a pure Y powder (99.99%), with particle sizes below 40μm, or with Y_2O_3 particles with sizes in the range of 20-40nm, followed by degassing at 450°C for 24 hours in vacuum and hot isostatic pressing at 1350°C under 200MPa for 3 hours (Fig. 2.4.2, left). High density and microhardness values were measured, equal to 97.50% and 97.37% and to 1050$HV_{0.2}$ and 1460$HV_{0.2}$ (Hardness Vickers units) for the case of the W-2.0Y and W-2.0Y_2O_3 materials, respectively. Both materials exhibit a dense and homogeneous microstructure composed of small-sized grains (Fig. 2.4.2, right).

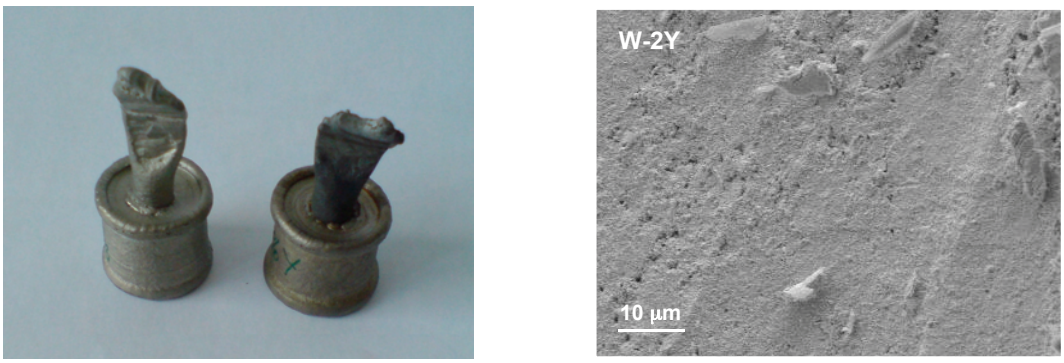

Fig. 2.4.2 *Left: Hot isostatic pressed ingots of W-2.0Y and W-2.0Y_2O_3 materials. Right: Microstructure of a hot isostatic pressed ingot of the W-2.0Y material.*

Materials modelling

Primary state of damage in Fe-He by MD simulation

The presence of helium plays a significant role on the damage production in iron by influencing the number of generated defects but also their clustering, relative to pure iron (Fig. 2.4.3). On the one hand, substitutional helium atoms tend to

decrease the number of interstitial-vacancy pairs produced within the atomic displacement cascades, playing the role of sources of vacancies easily available for the recombination with self interstitial atoms (SIAs) by a kick-out mechanism involving a substantial energy gain of around 4eV. On the other hand, interstitial helium atoms help the formation of SIAs by inducing an additional stress in the lattice, thus increasing the production of Frenkel pairs. Substitutional and interstitial helium atoms have thus antagonist roles, which would occur simultaneously in a real material. As expected, the number and size of SIA clusters are highly dependent on the Primary Knock-on Atom (PKA) energy, as they are directly related to the production of Frenkel pairs. The increase of helium concentration from 0.1at.% to 1.0at.% exacerbates the observed effects (Fig. 2.4.3). Besides the production of defects, the presence of interstitial helium atoms, and to a lesser extent of substitutional He atoms, favours the formation of SIA clusters during atomic displacement cascades. Their number and size clearly increase in presence of helium compared to pure iron (Fig. 2.4.3). This effect is easily explained by the high binding energy of interstitial helium atoms with SIA clusters of about 1.2-1.4eV. Substitutional He atoms have also non negligible binding energies with SIA clusters but their reduced mobility leads to lesser effects. The irradiation temperature plays a major role in the defect production and the clustering in presence of helium (Fig. 2.4.3). The strong binding energy and the very high mobility of interstitial helium atoms lead to the formation of SIA clusters that are surrounded at their periphery by small He clusters. Therefore, SIA clusters appear as heterogeneous nucleation sites for helium bubbles.

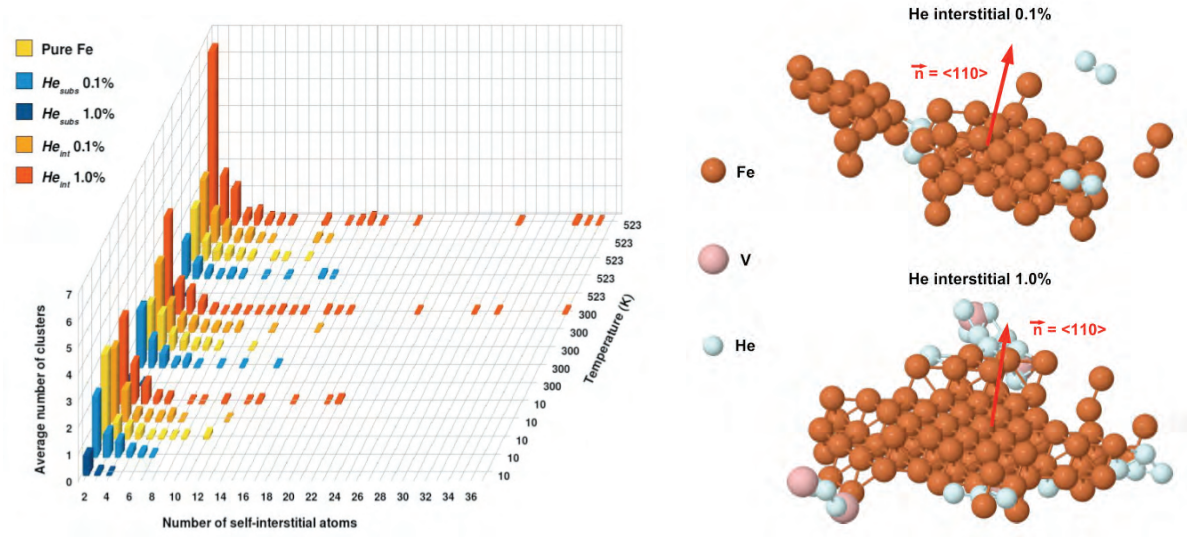

Fig. 2.4.3 *Left: Average number distribution of Fe interstitials in the clusters in pure Fe and Fe-He following 10keV cascades at 10K, 300K, and 523K. Right: Typical structure of large SIA clusters obtained at 523K following 20keV cascades in Fe containing initially 0.1at.% or 1.0at.% of He interstitials.*

2.4.2 EFDA Technology Tasks

Long Term Tasks

TW2-TTMS-004b deliverable 3 : Development and testing of coatings to improve the corrosion resistance vs Pb17Li at T>450°C

Eighteen specimens of the Reduced Activation Ferritic/Martensitic (RAFM) steel EUROFER 97 have been sent to three different European companies for deposition of W and Cr coatings using three different techniques. Six specimens have been coated with a 10μm-thick Cr coating using a galvanic technique. Six specimens have been coated with a 18-22μm-thick W coating using a physical vapour deposition (PVD) technique. Six specimens have been coated with a 120μm-thick W coating using a plasma spraying technique. Corrosion experiments for corrosion times of 500 and 1'000 hours have been completed. The corrosion attack of reference specimens of EUROFER 97 seems to present an incubation time of at least 1'000 hours. The galvanic Cr coating dissolved very rapidly in flowing Pb-17Li at 550°C. After the exposure time of 500 hours no remaining trace of the galvanic coating could be found, which indicates that such a coating does not provide any good corrosion barrier for EUROFER 97. An oxide layer was observed between the EUROFER 97 substrate specimen and the plasma sprayed W coating. The thickness of that layer increases with exposure time, while the plasma sprayed coating is gradually dissolved. This might be due to the porous nature of such a coating. The thickness of the PVD W coating was found constant up to the exposure time of 1'000 hours. No oxide layer was observed between the PVD coating and the EUROFER 97 substrate specimen. Therefore, PVD W coatings appear to be much more promising protection barriers against corrosion by flowing Pb-17Li at 550°C than galvanic Cr and plasma sprayed W coatings. Corrosion experiments for exposure times of 2'500 and 5'000 hours are in progress. They will be completed at the end of 2008.

TW3-TTMS-005 deliverable 2 : Investigation (tensile and Charpy testing) of PHT and PWHT to improve the design limits and to define the acceptable temperature range

This Task was originally planned to take place from 01.01.2003 to 31.12.2003, but no activity could be undertaken since post-weld heat-treated plates were not available from the EFDA. In June 2007, FZK agreed to produce two electron beam welds, 40mm deep, for mechanical investigations to be performed by the CRPP. Unfortunately, at the beginning of 2008 FZK announced us that the quality of the welds is too weak for further characterization by the CRPP. Therefore, this Task has been re-defined in agreement with the F4E Leadership. It is now entitled: 'Investigation of irradiated fracture mechanic samples by ball indentation/punch tests'. For the time being, a finite element model for an indentor with a spherical tip has been developed. Activities will be completed at the end of 2008.

TW4-TTMS-005/D4 & TW5-TTMS-005/D10 : Support in development of design rules for structural materials with low ductility

After irradiation the RAFM steels exhibit a very limited amount of ductility, often characterized by a very small uniform elongation, defined as the locus of the tensile curve where the maximum load is reached and where necking starts. The major drawback of this phenomenon is that it prevents converting easily load-displacement (L-D) curves into true stress-strain $\sigma(\varepsilon)$ curves due to the complex stress state that develops in the neck region. However, the $\sigma(\varepsilon)$ curves can be

indirectly determined by adjusting the few parameters defining the σ(ε) curves (typically the yield stress and two strain-hardening coefficients) used as input in finite elements simulations. From the point of view of the simulations, the necking must be artificially initiated. Some investigators introduced a small notch in the middle of the specimen while others considered a very large curvature of the gage length. In this work, we used another technique that does not rely on the introduction of a small geometrical imperfection along the specimen gage length. We defined a thin layer with an overall flow stress only 1MPa lower than that in the rest of the specimen. Note that the flow stress is of the order of 600-700MPa. The layer thickness is 40μm in the middle of the specimen having a total gage length of 13.2mm. This thin layer and minimal reduction of the flow stress are sufficient to trigger the necking in the middle of the specimen. The calculated maximum load was found very similar to the measured one.
The shear punch test consists in clamping a disk specimen between two dies and deforming it with a flat indentor. A narrow circumferential shear band develops in the disk, and over a small displacement range of the flat indentor it is possible to calculate analytically the shear stress and strain as a function of the load on the indentor and of its displacement, respectively. Then, the so-calculated shear stress and strain components are converted into the von Mises stress and plastic strain for direct comparison with the true stress and true plastic strain curve deduced from a tensile test. The axisymmetric finite element model for a deformed disk and the converted load-displacement curve (P-D curve), which is compared to the true stress-strain curve obtained from a tensile test, are shown in Fig. 2.4.4. A very good agreement was found up to about 3-4%, i.e., at small deflections for which the plastic region remains a narrow band.

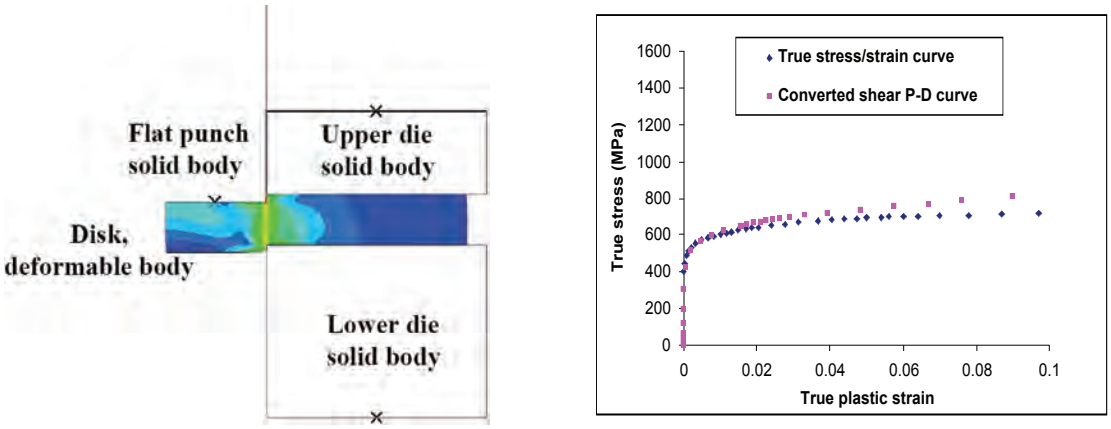

Fig. 2.4.4 *Left: Finite element model for a shear punch test. Right: Example of conversion of a load-displacement curve (P-D curve) into a true stress-strain curve.*

TW5-TTMS-001/D7 : Assessment of irradiations performed on EUROFER 97
The available fracture toughness data for the F82H-mod and EUROFER 97 RAFM steels have been compiled from the literature. Our analysis focused on the transition region between the ductile and brittle modes of fracture. Owing to the unavoidable effects of specimen size and geometry on the measured fracture toughness, a significant discrepancy in the measured and analyzed fracture toughness data was found. The general framework to analyze the fracture data in the transition region was the master-curve methodology as described in the ASTM-E1921 standard, which allows determining the reference temperature T_o that characterizes the transition.

For the unirradiated RAFM steels, it was concluded that the dependence of the fracture toughness on temperature can be described by the master-curve, provided that the measured fracture toughness data are properly corrected accounting for specimen size effects using an adjustment procedure based on a local approach for fast fracture. Such corrections are more severe than those recommended in the ASTM-E1921 standard, but the general methodology of the standard still holds. Data for the two available heats of F82H-mod were evaluated as well as those available for the various plates and bars of the EUROFER 97 heat produced by Böhler. No significant difference in the fracture properties of the two F82H-mod heats was evidenced, while the thicker plate of the EUROFER 97 was found to exhibit a lower toughness and higher T_o than all the other products.
The degradation of the fracture toughness properties of the two steels was determined following irradiations performed at T < 400-450°C. The irradiation-induced embrittlement, characterized by a shift of the reference temperature to higher temperatures, ΔT_o, was shown to scale with the irradiation-induced hardening, $\Delta\sigma_y$, defined as the increase of the yield stress at room temperature. One found $\Delta T_o/\Delta\sigma_y \cong 0.6$°C/MPa for the F82H-mod steel and $\Delta T_o/\Delta\sigma_y \cong 0.38$°C/MPa for the EUROFER 97 steel.

TW5-TTMS-005/D2 : SSTT: Model the brittle transition region - continuation of TW2-TTMS-005b/D6

The behaviour of the fracture toughness of the EUROFER 97 RAFM steel as a function of temperature has been modelled using a local approach for fracture. It was previously found from experiments that the median fracture toughness-temperature curve in the lower brittle-to-ductile transition region deviates somewhat from the master-curve as described in the ASTM E1921-03 standard. In order to model the fracture toughness behaviour, finite element simulations of compact tension specimens have been performed. The analysis of the stress fields around the crack tip has been used to define a local criterion for cleavage based upon the attainment of a critical stress over a critical area. This local criterion has been used to reconstruct the lower bound of the fracture toughness-temperature behaviour of the EUROFER 97 RAFM steel in the transition region, as shown in Fig. 2.4.5. The calibration procedure of the critical parameters has been discussed in detail. It was shown in particular that the critical stress mainly mediates the steepness of the toughness-temperature curve, while the critical area controls the vertical position of this curve in the toughness-temperature plane.

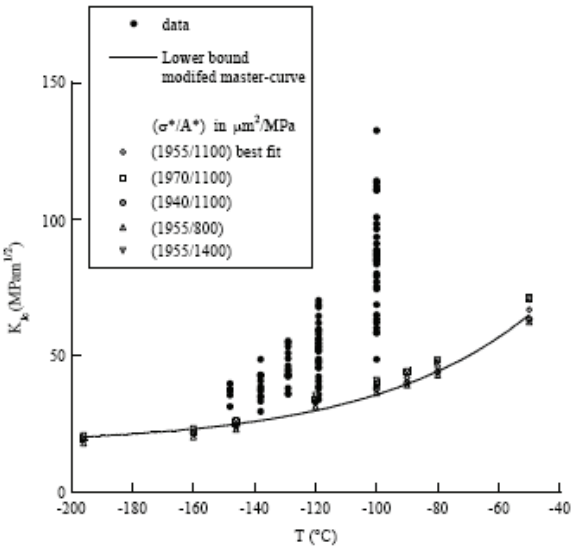

Fig. 2.4.5 *Reconstruction of the lower bound of the fracture toughness-temperature behaviour of the EUROFER 97 RAFM steel in the brittle-to-ductile transition region.*

TW5-TTMS-005/D11 : Experiments in support of TW5-TTMS-005/D2

The fracture toughness behaviour of the EUROFER 97 RAFM steel was investigated in the lower to middle ductile-to-brittle transition region. From a comparison of the failure probability diagrams of two different specimen sizes, it was concluded that constraint loss begins at rather low deformation level, characterized by a M value of about 80, while the ASTM E1921 standard recommends M = 30. By determining the reference temperature T_o in the middle transition region with 0.87T compact tension (C(T)) specimens, it was found that in the lower transition region the ASTM E1921 master-curve does not predict satisfactorily the temperature dependence of the median fracture toughness and the scatter. In order to improve the description of the data near the lower shelf region, two parameters of the master-curve were fitted using the method of maximum likelihood, namely the athermal component, A, and the reference temperature, T_o. The athermal part was found significantly lower (13MPa.$m^{1/2}$) than the recommended value of the ASTM E1921 master-curve (30MPa.$m^{1/2}$). For self-consistency, the minimum fracture toughness value was chosen equal to 10MPa.$m^{1/2}$. Thanks to the adjustment of the coefficient A, it was demonstrated that the modified master-curve allows determining accurately T_o from tests at temperatures near the lower shelf region. Indeed, the T_o value was found almost independent of the dataset temperature used to determine it when using the single temperature T_o determination method. Therefore, it is of primary importance not to overlook such shape adjustment if small specimens are used near the lower shelf to determine T_o.

TW5-TTMS-007/D15 : Dislocation-defect interaction and the evolution of the deformed microstructure in Fe (development of dislocation dynamics methods)

This work is aimed at simulating the effects of irradiation-induced defects like dislocation loops and/or cavities, such as voids or helium bubbles, on the plasticity of iron by dislocation dynamics simulations. The code microMegas from LEM-ONERA was successfully compiled and implemented on our computers. This code is based on the network approach, whereby each dislocation segment belongs to a node of a network with a specific glide system, including its glide plane, direction and Burgers vector. Results of tests showed that the code is appropriate to simulate the plasticity of a cubic sample of pure iron, 5μm a side, containing a dislocation density of $10^{12}m^{-2}$ and a defect density of $10^{21}m^{-3}$. Indeed, deformation in the presence of obstacles causes an increase in dislocation density and then in yield stress, as expected. Recently, the pertinence of linking the results of Molecular Dynamics (MD) simulations of the dislocation-defect interaction with higher-scale Discrete Dislocation Dynamics (DDD) simulations was studied in collaboration with the CNRS in Grenoble, France. Simulations using elasticity of the continuum were performed to study the validity of elasticity at the near-atomic level. As a benchmark the interaction of an edge dislocation with a 2nm void in iron was considered. It was found that there is a fair match between MD and DDD simulations at the 1 to 2nm level. Also, DDD simulations prove that image forces due to the internal free surface of the nanometric void have a significant impact on the dislocation mobility.

TW6-TTMS-007/D12 : Selection of experimental methods in JANNUS for 2007

This work was aimed at preparing a detailed scientific programmeme of ion implantation of ferritic/martensitic materials, in collaboration with a number of other European partners, in view of validating the European effort of modelling radiation damage and radiation damage effects on fusion materials using the future JANNUS facility (France). Some of the features of the JANNUS facility are illustrated in Fig. 2.4.6. An evaluation of Transmission Electron Microscopy (TEM) techniques

was made, in particular for the imaging of nanometric crystalline defects and for the chemical analysis (identification, quantification) of helium and chromium. Electron energy loss spectrometry appears to be the most adapted method for that purpose. Infrared spectroscopy was also considered, as an interesting non-destructive method to probe near-surface damage, and evaluated.

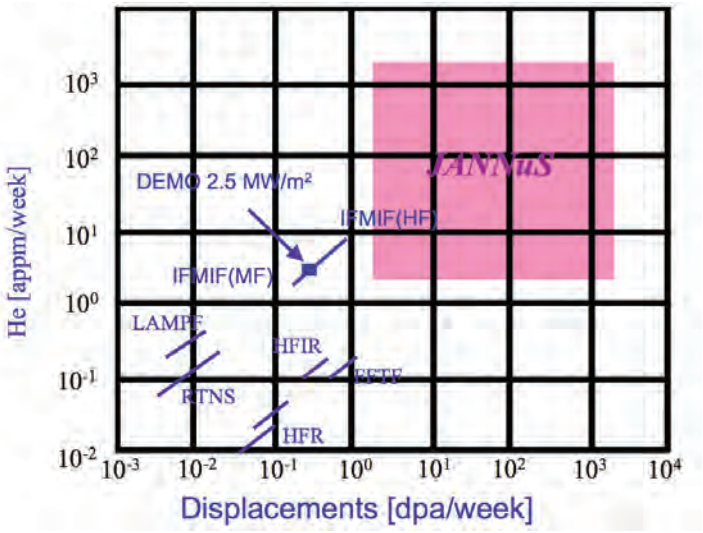

Fig. 2.4.6 *Displacements per atom (dpa) and He production rates provided by the JANNUS facility, as compared to those provided by various neutron sources and DEMO.*

TW6-TTMS-001/D4 : PIE SINQ irradiation

The irradiation rig containing specimens of EUROFER 97 RAFM steel and ODS EUROFER, which have been irradiated in the SINQ facility in 2004/2005, has been transported to the Hot Laboratory of the PSI in Spring 2007. Unfortunately, due to a lack of technical manpower at the PSI, the irradiated specimens have been extracted from the rig only in spring 2008. According to the availability of the hot cells at the PSI, Charpy impact testing of irradiated specimens should be performed at the end of 2008, while tensile testing and TEM observations of irradiated specimens should be performed in 2009.

TW6-TTMA-002/D10 : Development of W-TiC and W-Y_2O_3 alloys

W-(0.3-1.0-2.0)Y_2O_3 and W-(0.3-1.0-2.0)Y materials (in weight percent) have been manufactured by conventional powder metallurgy methods. The optimal mechanical alloying time was determined to be about 15 hours, in order to achieve relatively small and homogeneous particle and crystallite sizes and to avoid important oxygen and carbon contamination as well as contamination by the jar and the balls, leading to the formation of WC impurities in the mechanically alloyed powders. The mechanical alloying atmosphere was found to have no significant impact on the microstructure and the properties of the powders.

After cold pressing using the maximal pressure of 250MPa the density of all preliminary compacted specimens was only about 65% of the theoretical density. Sintering increased the density of all materials significantly. The density and microhardness of the sintered specimens was found to increase with the Y_2O_3 or Y content, with a slight advantage exhibited by the W-Y materials in terms of density (Fig. 2.4.7, left) and by the W-Y_2O_3 materials in terms of microhardness (Fig. 2.4.7, right). This might be due to the hardening effects engendered by the addition of Y_2O_3 nanoparticles in the latter materials. However, full density could not be achieved by cold compaction and sintering, even performing a cold re-pressing at

250MPa and a subsequent sintering at 2000°C. Scanning electron microscopy observations revealed that sintering occurred, at least partially, from liquid phase, the amount of the corresponding dense regions increasing with the Y_2O_3 or Y content. The W-2Y material appears slightly better than the W-2Y_2O_3 material, as it contains a higher amount of dense regions, in agreement with density measurements. Sintering in an argon atmosphere instead of vacuum had no significant impact on the density, microstructure and microhardness of the sintered specimens. All the obtained results indicate that another consolidation method, such as hot isostatic pressing, or hot extrusion, or spark plasma sintering, could be more appropriate than sintering for compacting such W-base materials.

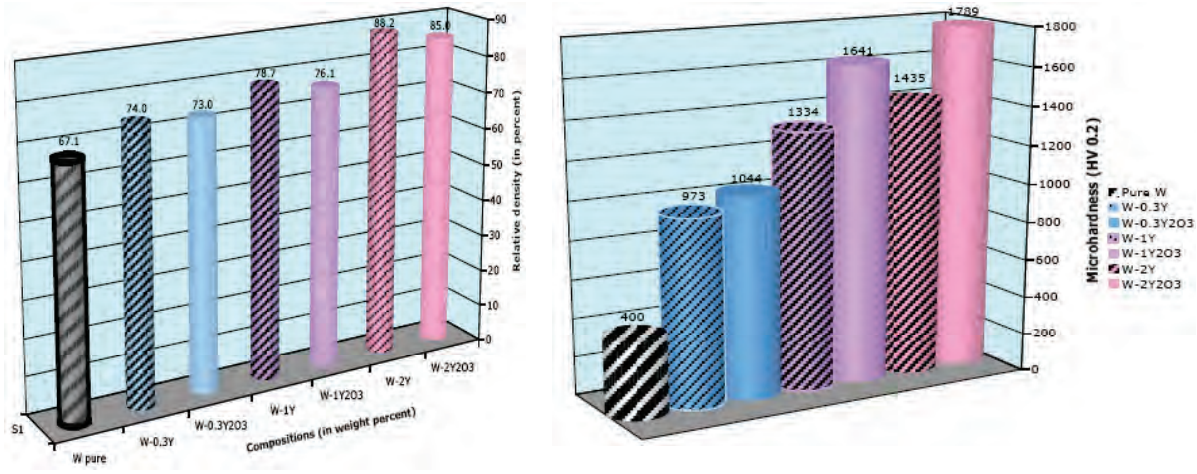

Fig. 2.4.7 *(Left) Density and (right) microhardness of the sintered W-Y and W-Y_2O_3 materials of various chemical compositions.*

Next Step Tasks

TW4-TVM-CUSSPIT : Testing of irradiated CuCrZr/SS joints produced under different blanket manufacturing conditions

CuCrZr/SS joints, where CuCrZr refers to a precipitation strengthened Cu-base alloy and SS to the 316LN austenitic stainless steel, are part of the current ITER design. Their final applicability in ITER will depend on their mechanical properties before and after neutron irradiation, with respect to those of the base materials. This work is aimed at investigating the effects of two different heat treatments on the mechanical properties (joint strength, fracture toughness) of unirradiated and neutron-irradiated CuCrZr/SS joints and base materials. The work is being performed by three partners: SCK-CEN (Belgium) is responsible for the neutron irradiations, VTT Manufacturing Technology (Finland) is in charge of testing the joints, and CRPP is in charge of measuring the fracture toughness of the CuCrZr base material. Two series of six specimens of the CuCrZr base material, having withstood two different heat treatments, have been irradiated with neutrons at SCK/CEN to three different doses of 0.001, 0.01 and 0.1dpa. The fracture toughness of the specimens will be measured at the beginning of 2009.

TW5-TVM-COMADA: Investigation of the effect of creep fatigue interaction on the mechanical performance and lifetime of CuCrZr

The CuCrZr alloy is a candidate heat sink material for the first wall of ITER. Therefore, extensive research was conducted in the past on the fatigue properties of the CuCrZr alloy, under ITER-relevant operating conditions. Unfortunately, only few

data exist concerning its creep-fatigue behaviour, mainly due to the very costly testing involved, as the tests may run for months. Therefore, an experimental testing programme was prepared with the aim of producing the additional data points needed to make reliable predictions for the first wall of ITER. A Cu-Cr-Zr alloy has been ordered by CEA (Grenoble) from the KME company and heat treated to reproduce the manufacturing route for the first wall sections of ITER. Unfortunately, the resulting grain size was up to 20mm and, therefore, of the order of the size of the test specimens. As a consequence, a new material was prepared by using another heat treatment: solutioning at 980°C for 30min, air-cooling at a rate of 50-60°C/min, ageing at 580°C for 2hrs. The new material was found to have the right microstructure with grain sizes ranging between 100 and 250μm, some of them reaching a size of 500μm (Fig. 2.4.8). However, as a result from ageing, the coherency of the precipitates with the matrix was lost, and the strength of the material was partially lost. 40 fatigue specimens and 12 creep specimens have been manufactured from that material. Preliminary creep experiments have been performed at 300°C and 350°C using a constant stress creep machine and applied stresses ranging between 190 and 200MPa. The creep times to rupture have been found to range between 334 and 526 hours. Further creep experiments will explore the effects of lower and larger applied stresses. Creep tests and fatigue tests will be achieved at the end of 2008.

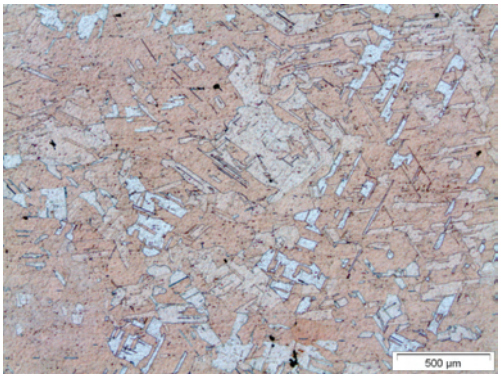

Fig. 2.4.8 *Optical micrograph of the heat-treated CuCrZr material.*

2.4.3 Broader Approach activities[*]

IFMIF-EVEDA: Design of a test module for in-situ creep-fatigue tests to be performed in the IFMIF facility and construction of a mock-up of the test module

The creep-fatigue test module will consist of three testing machines deforming independently three creep-fatigue specimens. A preliminary design of the testing machines and creep-fatigue specimens has been done (Fig. 2.4.9). The specimen will be part of an elongated assembly with two inside boreholes in which a helium coolant with a pressure of 7 bars will flow. The specimen will constitute the central part of it and the bars will serve as loading elements and pipes for cooling the bottom of the specimen. The heat will be deposited by gamma heating. Sleeves of high-density material will be inserted close to the specimen and serve to generate the required power. The temperature control will be achieved in varying the helium mass flow. First results of thermo-dynamical calculations showed that variations of approximately 150°C can be obtained by varying the helium mass flow. This should be enough to cope with usual accelerator power fluctuations. It is hoped that additional heaters will not be necessary. The geometry and temperature distribution

[*] Part of Swiss voluntary contribution to Broader Approach. Not part of the Association activities.

in the components surrounding the creep-fatigue test module, including the test cell interfaces, are necessary for final design (nuclear responses and temperature control). The mass flow needed to cool the testing machines themselves, especially the loading bars, will be assessed soon. A helium mass flow of 20g/s should be sufficient. The design will evolve in parallel with fluid dynamics and heat transfer calculations.

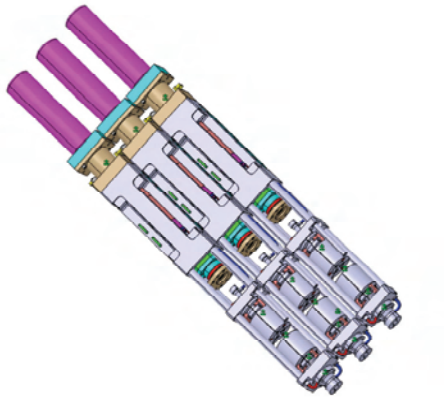

Fig. 2.4.9 *Preliminary design of the in situ creep-fatigue test module to be irradiated in the medium flux area of IFMIF. The module consists of three independent testing machines mounted together in the same frame.*

IFERC: Contribution to the definition of irradiation matrices for IFMIF by means of development of new methods for testing and analysing subsized specimens

Recent activities have been focused on the design of thermo-mechanical treatments (heat treatment and cold rolling) for plates of the EUROFER 97 RAFM steel, in order to simulate the irradiation-induced hardening and strain-hardening reduction observed for irradiated RAFM steels. A heat-treatment was applied to one plate in the as-received condition to increase the yield stress while keeping a parabolic strain hardening. This heat treatment consisted in an austenitization at 980°C for 30 minutes and a tempering at 650°C for 1.0 hour. This yielded a flow stress increase of about 250MPa without any reduction of strain hardening, as evidenced from tensile tests. On the other hand, a cold rolling was applied to another plate, yielding a thickness reduction of 10%, which should increase the yield stress also by about 250MPa but with a reduction of strain hardening. Tensile tests on specimens from this plate are in progress.

2.4.4 Supporting research

Modelling of the fracture toughness-temperature curve of the EUROFER 97 RAFM steel in the ductile-to-brittle transition region

In order to define the minimum specimen size required to get a conservative estimate of the ductile-to-brittle transition temperature of the EUROFER 97 RAFM steel, three dimensional finite element simulations of compact tension (C(T)) specimens tested at -60ºC have been performed. The code used for the simulations was ABAQUS/Standard 6.7. Symmetry conditions allowed solving only one quarter of the mesh elements. It was found that the 3D finite element simulations reproduce very well the load-displacement curves of the specimens up to the point were stable crack growth starts (ductile tearing). A finite initial crack tip radius, ρ_0, was used in the simulations. No appreciable effect of the initial crack tip radius on the load-displacement curves was observed for the investigated ρ_0 values. In Fig. 2.4.10 (left) the experimental and simulated load-displacement curves for 0.35T CT

specimens tested at -60°C are compared. There is very good agreement for clip gage openings (displacements) below 1mm.

An analysis of the local stress field at the crack tip at various temperatures allowed calibrating the critical fracture stress value, σ*, acting in a critical volume, V*, necessary to trigger macro-failure. σ* and V* are material properties controlling fast fracture in the transition region. They were used to predict the specimen size effects on the measured fracture toughness. This is illustrated in Fig. 2.4.10 (right), where the predicted increase in toughness between 0.18T and 0.36T C(T) specimens is shown, for different σ* values. The points along the black line represent the increase as expected from the ASTM-E1921 standard. Clearly, the corrections provided by this standard are not sufficient to account for specimen size effects in the case of RAFM steels, like EUROFER 97, exhibiting a low to moderate strain hardening. The dependence of the fracture toughness on temperature is fairly well reconstructed using σ*=1955MPa and V*≅4x10^{6}μm^3, as well as the observed increase in fracture toughness from the 0.36T to the 0.18T C(T) specimens.

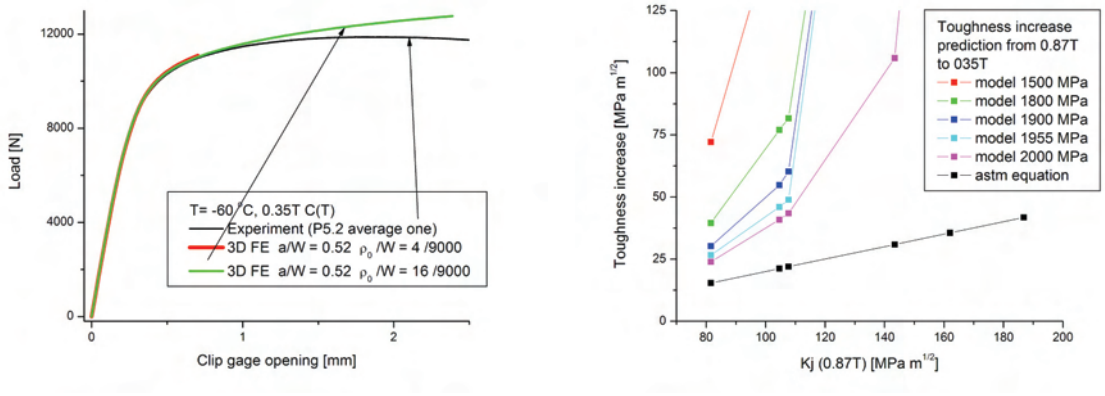

Fig. 2.4.10 *Left: Experimental and simulated load-displacement curves at -60°C for 0.35T CT specimens of EUROFER 97. Right: Increase in fracture toughness between 0.18T and 0.36T C(T) specimens, for different σ* values.*

On the relationship between the mechanical properties and microstructure of an oxide dispersion strengthened ferritic/martensitic steel

An Oxide Dispersion Strenghtened (ODS) steel for structural application in fusion power reactors up to 750°C, with the EUROFER 97 RAFM steel as matrix material and 0.3wt.% Y_2O_3 particles as reinforcement material, has been manufactured by dry mechanical alloying of elemental powders in a hydrogen atmosphere and hot isostatic pressing. With respect to the reference European ODS EUROFER, the mechanical alloying process was optimized, the evolution of the Y_2O_3 particles during mechanical alloying was studied in detail, and the irradiation-induced hardening was measured and modelled. In particular, a focused ion beam (FIB) device and its energy dispersive spectrometry (EDS) chemical analysis system were used to study the evolution of the Y_2O_3 particles during mechanical alloying. It was found that as a result from mechanical alloying for 20 hours the Y_2O_3 particles are not dissolved in the matrix but become embedded in the EUROFER 97 steel powder particles (Fig. 2.4.11).

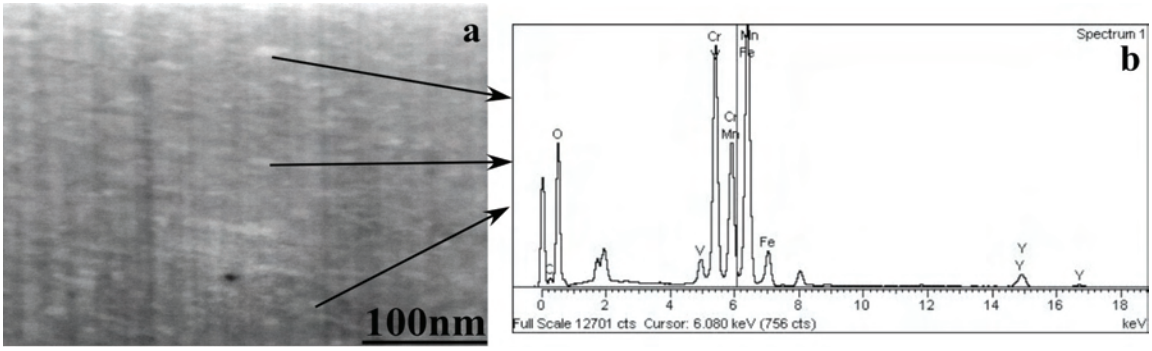

Fig. 2.4.11 *Left: FIB/SEM image of a cross-section of a EUROFER 97 steel particle, following mechanical alloying for 20 hours: light contrasts, 10-30nm in size, can be seen. Right: EDS chemical analysis of the light contrasts: these are Y_2O_3 particles embedded in the EUROFER 97 steel particle.*

Analysis of nano-sized irradiation-induced defects in Fe-base materials by means of small angle neutron scattering and molecular dynamics simulations

This work was aimed at investigating how far the Small Angle Neutron Scattering (SANS) technique can be used for detecting and characterizing nano-sized irradiation-induced defects in RAFM steels for structural application in future fusion reactors. Indeed, the resolution limit of Transmission Electron Microscope (TEM) is about 1nm in weak beam imaging mode, while it is usually thought that a large number of irradiation-induced effects in RAFM steels have a size below 1nm and that these very small defects actually contribute to the irradiation-induced hardening and embrittlement of RAFM steels occurring at irradiation temperatures below about 400°C. The aim of this work was achieved by combining SANS experiments on unirradiated and irradiated specimens of RAFM steels with MD simulations of the main expected nano-sized defects in irradiated pure Fe and Fe-He alloys, as model materials for RAFM steels, and simulations of their corresponding TEM images and SANS signals. The SANS technique has been proven to be a very powerful tool for detecting nano-sized irradiation-induced defects and a tool well complementary to TEM for characterizing such very small irradiation-induced defects.

It was found in particular that a large part of the defects produced in RAFM steels (EUROFER 97, F82H, OPTIMAX A) by 590MeV proton irradiations, at temperatures in the range 50-350°C to doses in the range 0.3-2.0dpa, have a size below 1nm, i.e., below the resolution limit of the week beam TEM imaging technique. The mean size of these small irradiation-induced defects tends to decrease with increasing the irradiation dose and to increase with the irradiation temperature, while their number density tends to increase with the irradiation dose and to decrease with increasing the irradiation temperature. TEM appears most adapted to investigate structural defects, such as dislocation loops and helium bubbles with high helium concentration, which yields a lattice deformation of the surrounding matrix, while SANS is most adapted to investigate phase defects, such as voids, helium bubbles with low helium concentration and chromium precipitates. By combining the results of SANS experiments with those of MD simulations, TEM image simulations and SANS signal simulations, the nano-sized irradiation-induced defects were identified as small helium bubbles. While the radiation hardening measured for RAFM steels cannot be explained by accounting only for the defects observed in TEM, it could be successfully modelled by also accounting for a reasonable number density of the nano-sized defects evidenced using the SANS technique.

EXTREMAT Integrated Project (IP) of the Sixth European Framework Programmeme*

Modelling of radiation damage and radiation effects on pure tungsten: Edge and screw dislocations in pure tungsten have been simulated by MD using four different interatomic potentials: the Finnis-Sinclair (1984), Ackland-Thetford (1987), Juslin (2005) and Derlet-Nguyen-Dudarev (2006) potentials. It was found in particular that the Ackland-Thetford potential provides a compact edge dislocation core (Fig. 2.4.12, left), allowing moving the dislocation for an applied stress above 100MPa, while the Derlet-Nguyen-Dudarev potential yields an extended edge dislocation core (Fig. 2.4.12, right), making impossible to move the dislocation. A new method for setting-up asymmetric screw dislocation core configurations was introduced. The most energetically favourable screw dislocation core configuration was found to be the easy asymmetric one, whatever the potential being used, while density functional theory calculations indicate that it should the easy symmetric one. This reveals that none of the four potentials being used provides an adequate screw dislocation core configuration. In addition, the Derlet-Nguyen-Dudarev potential yields a very large screw dislocation core of roughly 30*b* in radius, *b* being the magnitude of the Burgers vector.

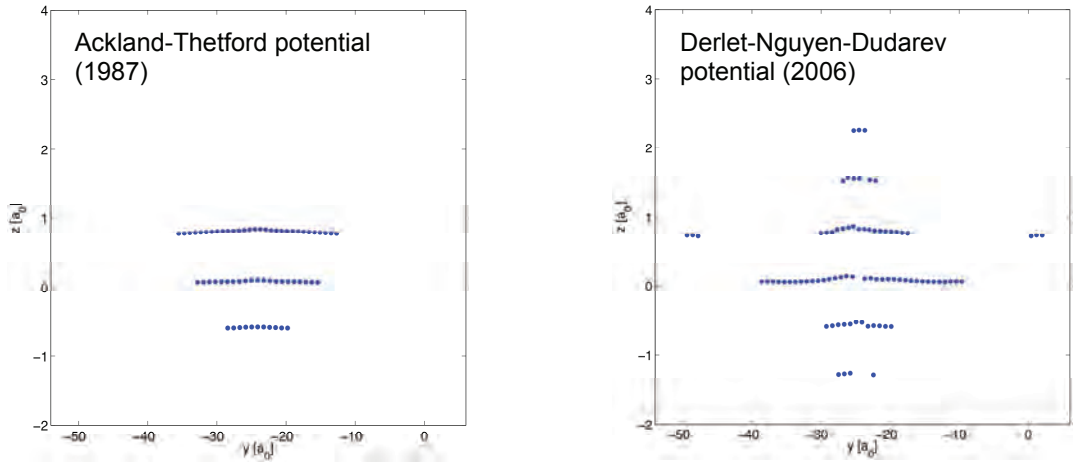

Fig. 2.4.12 *(Left) Compact and (right) extended dislocation core edge provided by the Ackland-Thetford (1987) and Derlet-Nguyen-Dudarev (2006) interatomic potentials, respectively.*

Development of Oxide Dispersion Strengthened (ODS) reduced activation ferritic (RAF) steels: An ODS RAF steel with the composition Fe-14Cr-2W-0.3Ti-0.3Y_2O_3 (in weight percent) was produced by mechanically alloying a pre-alloyed, gas atomized Fe-14Cr-2W-0.3Ti powder (Aubert&Duval, France) with Y_2O_3 particles (about 20nm in diameter) at the Plansee company (Austria) in an attritor ball mill for 48 hours in a hydrogen atmosphere, followed by degassing at 300°C and hot extrusion at 1100°C (CEA-Saclay, France). The square-shape cross-section extruded bar was then hot rolled at 700°C (CEA-Saclay, France), to get a thickness reduction of 20%, and annealed at 1050°C for 1 hour. The microstructure of the ODS RAF steel appears composed of elongated grains in the rolling direction (Fig. 2.4.13, left) and equiaxed grains in the transverse direction (Fig. 2.4.13, right). The microstructure also contains a high dislocation density and a high density of nanoclusters enriched with Y, Ti and O. Coarse particles, which were identified as Ti and/or Al oxides and

* Not part of the Association Workprogrammeme.

are preferentially located at the grain boundaries, were also observed in both directions. Both the yield strength and the ultimate tensile strength (UTS) decrease as the test temperature is increased (Fig. 2.4.14), and this decrease in strength is accompanied by an increase in total elongation, at least at temperatures above 300°C. At room temperature the material exhibits high yield strength and ultimate tensile strength values of about 1340MPa and 1420MPa, respectively, in the transverse direction. In the longitudinal direction the values are about 10% lower, due to the anisotropy of the microstructure. At 750°C the material still presents relatively high yield strengths of about 325MPa and 305MPa in the longitudinal and transverse directions, respectively. The material exhibits reasonable uniform and total elongation values over the temperature range RT-750°C, in both transverse and longitudinal directions (Fig. 2.4.14). The uniform elongation of the material decreases continuously with increasing temperature in the longitudinal direction, whereas in the transverse direction a continuous increase in uniform elongation with temperature takes place. The material exhibits weak Charpy impact properties in the transverse direction. Charpy impact properties are slightly better in the longitudinal direction, with an upper shelf energy of about 4.2J and a ductile-to-brittle transition temperature of about 8.8°C.

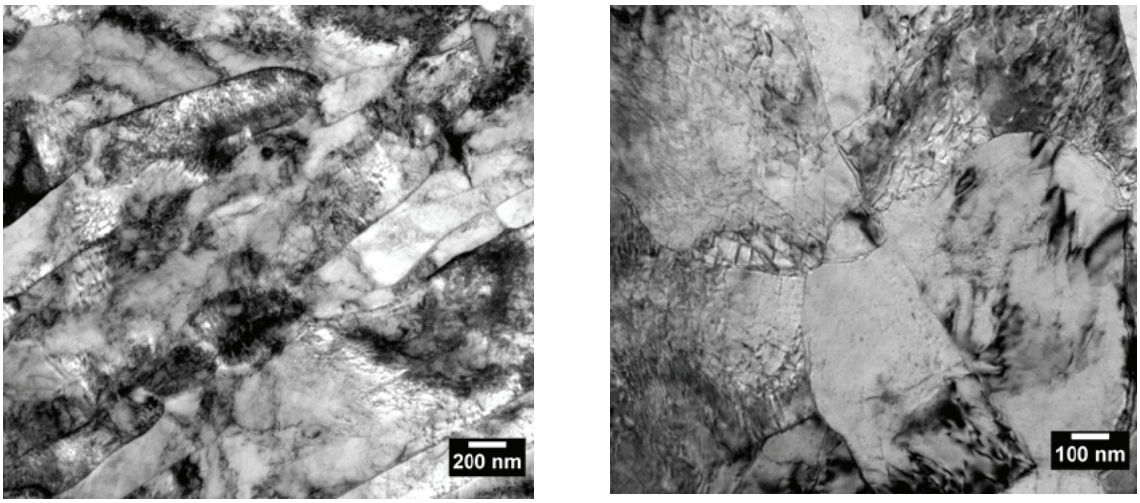

Fig. 2.4.13 *TEM images of the microstructure of the ODS RAF steel Fe-14Cr-2W-0.3Ti-0.3Y_2O_3 (left) in the longitudinal direction and (b) in the transverse direction.*

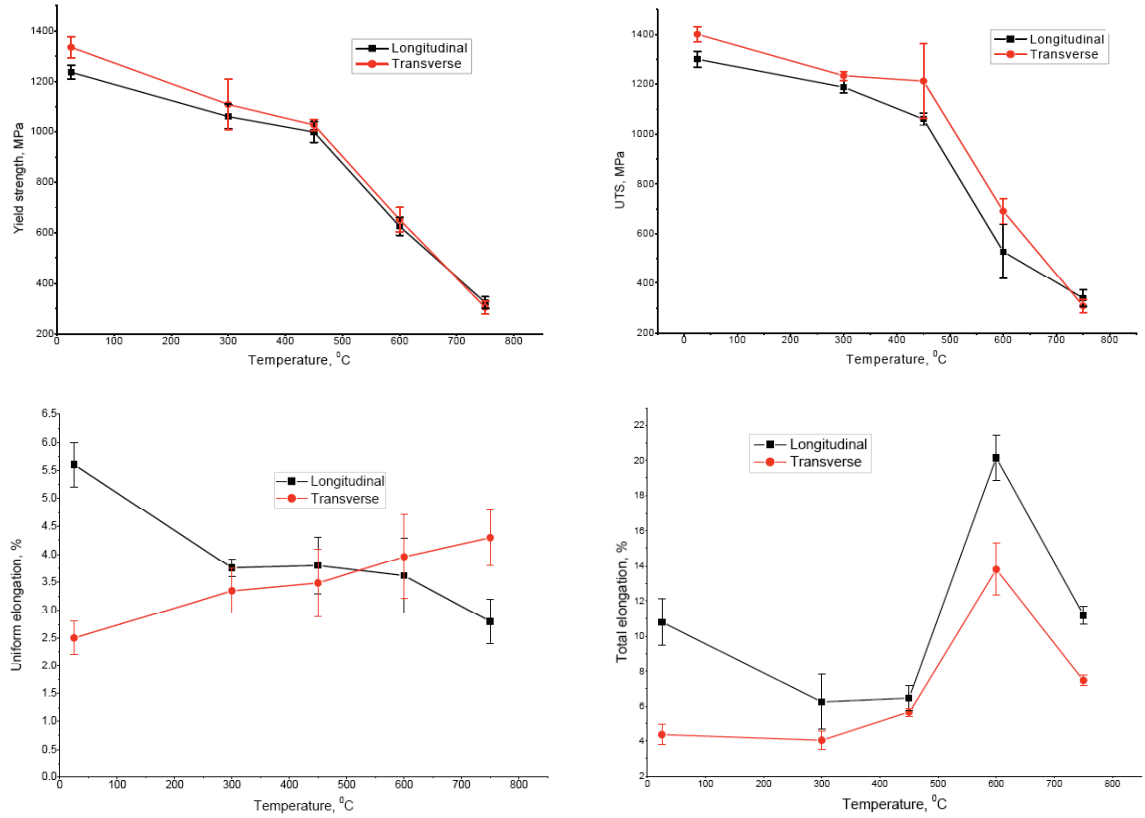

Fig. 2.4.14 *Tensile properties of the ODS RAF steel Fe-14Cr-2W-0.3Ti-0.3Y_2O_3 in the longitudinal and transverse directions.*

2.5 Superconductivity

Beside the test of the TF conductors of ITER in SULTAN, reported in section 4.5, the measurement of inter-strand resistance at the electrical connections, the participation to the PFIC test in Naka, the test of Nb_3Sn strands extracted from the Cable-in-Conduit-Conductors (CICC), the AC loss calculation and the buoyancy experiment (thermal-hydraulic behaviour) are strictly in support of ITER and have been carried out sometimes with very short notice and under various kind of agreements.

The preparation work for the European Dipole (EDIPO) test facility at CRPP has progressed in 2008 with procurement of long lead items (power supplies and High Temperature Superconductor (HTS) current leads), the completion of the design activities and the assembly of the windings of the superconducting transformer. Due to the delayed delivery of the main dipole winding from EFDA, the overall schedule of the EDIPO project has been updated and the EFDA contract extended.

The slow transition in the organization of the funding agencies (from the old EFDA to the new EFDA and F4E) caused discontinuities in the flow of contracts. In order to react timely to the urgent requests of R&D work from the European agencies, some activities, including the SULTAN operation during several months, had to be moved from “technology tasks” to “basic support”. The Underlying Technology programmeme has disappeared. The activity on High Temperature Superconductors (HTS) suffered from the lack of coordination from the new EFDA.

2.5.1 Activities in support of ITER Magnet Technology

Inter-strand resistance in the termination of ITER conductors

The non-homogeneity of the contact resistance distribution in the terminations of large CICC's leads necessarily to a certain level of current unbalance among the strands in DC operation. The overloaded strands or groups of strands hit first the critical surface in the high field region and a current re-distribution process is thus driven by the initial current sharing voltage to minimize the energy of the system. This process takes place preferably at the electrical connections where the inter-strand resistance is lower.

The inter-strand resistance is measured on three CICC terminations used in ITER TF conductors samples with different termination layout (USTF1, USTF2 and TFPR01). An inter-strand resistance experiment consists of selecting two strands or two groups of strands at a time in different configurations, feeding them with a current of the order of 50A or 100A, sensing the voltage between them and deriving the equivalent resistance. The experiment is carried out in liquid helium, with and without a background field of 0.5T.

The three termination samples differ because of the solder applied to the strand bundle. In TFPRO1, a solder coating is applied to the cable surface, in USTF2 the cable is dipped in a solder bath (full wetting) and in USTF1 the cable is filled by solder. The sub-cable wraps are fully removed only in USTF1. The inter-strand resistance results obtained are reported in Table 2.5.1.

	Without Field			With Field		
Resistance between: [nΩ]	USTF1	USTF2	TFPRO1	USTF1	USTF2	TFPRO1
Triplets in adjacent 4 stages	<3.2	2.3-4.1	12.6-16.9	1.0-4.5	2.1-5.7	16.5-22.9
Not adjacent triplets, same sectors	<3.1	1.8-5.9	12.5-20.7	1.8-4.4	4.6-7.2	17.6-28.2
Triplets in adjacent sectors	<3.2	4.6-6.8	17.2-19.9	2.4-5.0	4.7-8.3	25.7-28.3
Triplets in not adjacent sectors	<3.0	7.1-10	12.6-17.5	1.0-4.2	7.6-11.6	18.1-24.0

Table 2.5.1 *Inter-strand resistance measured on the TFUS1, TFUS2 and TFPRO1 terminations*

The inter-strand resistance values reflect the differences in the joint manufacture. The presence of the solder, even in small quantity, notably lowers the inter-strand resistance of the termination (USTF1 and USTF2). The removal of the sub-cable wraps guarantees a flat resistance distribution with very low values also between triplets in different sectors (USTF1). The magnetic field determines an increase of the resistances, which, in the case of TFPRO1 reaches 50%, and enhances also the noise level and the error bar of the measurements.

The inter-strand resistance results provide a valuable feedback for the selection of the termination layout and a quantitative input for the models of current re-distribution used in the analysis of SULTAN tests.

AC Loss Measurements in CICC with Different Aspect Ratio

The coupling loss in CICC is strongly affected by the cable geometry. Besides cable pattern, twist pitch, wrapping and void fraction, also the aspect ratio has a non

negligible role in the loss. In fact, it defines the area crossed by the flux variation and it determines therefore the entity of the coupling current between strands.

An AC loss experiment on two Nb_3Sn CICC samples (PITSAM II and PITSAM III) is carried out with a calorimetric method in the SULTAN test facility, in order to investigate the impact of the conductor aspect ratio on the loss. The two conductors, identical for cable pattern, void fraction and characteristics of both superconducting and copper strands, differ only in the aspect ratio, having PITSAM II and PITSAM III a square (9.2mm x 9.2mm) and a rectangular (12mm x 7.1mm) cable cross-section respectively. Each sample is tested in a sinusoidal field (±0.3T) perpendicular both to the background field (2T) and to the conductor axis. The AC frequency ranges between 0.2Hz and 6Hz. The rectangular PITSAM III is tested with sinusoidal magnetic field perpendicular first to the wide then to the narrow side of the conductor (90º), so that the loss relative to three different aspect ratios, 0.59/1/1.69, is compared, see Fig. 2.5.1. The coupling loss increases with the area linked to the changing magnetic field. A non-linear relation between the time constants of the cables and their aspect ratio is found, showing the possibility to predict AC loss as function of the aspect ratio of the cable even in case of complex cable geometry as multistage CICC's. The results of AC loss vs. aspect ratio are also compared with existing models for monolithic rectangular conductors.

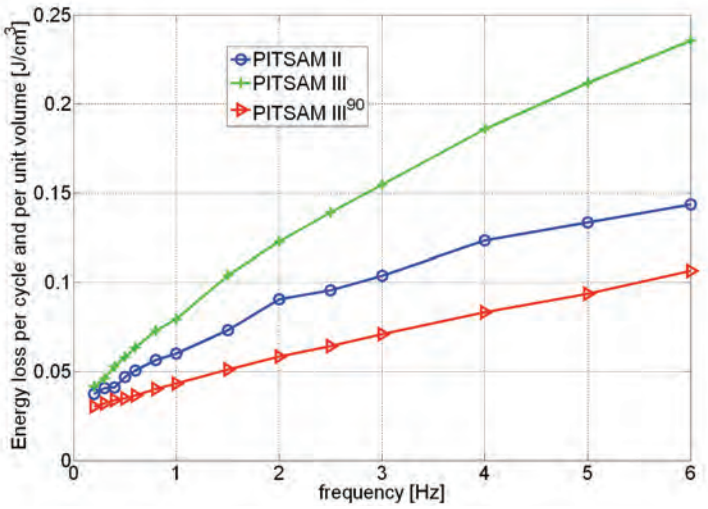

Fig. 2.5.1 *The coupling loss curve for the three conductors with different aspect ratios.*

AC Loss at random Field Change

Beside the generation of the poloidal component of the field, the main function of the poloidal field coils in a tokamak is the control of the shape and the position of the plasma, according to the chosen plasma scenario. The control currents create magnetic fields having complex trends, being almost random waveforms with frequencies in the range between 0.1Hz and 10Hz. As a consequence, AC loss is generated in the superconducting coils exposed to those signals, and the feasibility of a plasma scenario is strictly related to the ability to withstand and remove the heat coming from the AC loss.

In order to study what the behaviour of the loss is in random magnetic fields and to define the operating margins of the ITER magnetic control action, a SULTAN sample is tested under two kinds of random field signals. The first signal ("1") is obtained by adding several harmonic frequency components, in the range between 0.2 Hz and 6 Hz, having random amplitude. The second waveform ("2") is generated by a

random function generator and it has a much broader spectrum of frequencies. The tests have been carried out by varying also the maximum amplitude of the signals between 0.05T and 0.35T, while the SULTAN background field, which is perpendicular to the random field, is kept constant at 2T.

The results of the experiments suggest that in the case of signals characterized by limited spectrum of frequencies (similar to the signal 1) the loss can be approximated by the sum of the contributions estimated for each component. If the signal is characterized by a broader range of frequencies (similar to the signal 2) the power loss is higher than in the previous case and dominated by the higher frequency components. This case is likely pessimistic for the actual PF coils, as the attenuation and filtering coming from the physical components are heavier than in the small AC coils of SULTAN.

AC Loss model for control optimization (EFDA task TW6-TPO-ACCOMP)

A recent study has shown that AC loss calculation in the ITER magnets can be performed using a model with a high level of complexity and completeness. This method is however too large and computationally expensive for the inclusion in a fast control optimization procedure. The goal of the task TW6-TPO-ACCOMP is to define a simplified, fast parametric AC loss calculation algorithm whose size allows integration in the control design procedure.

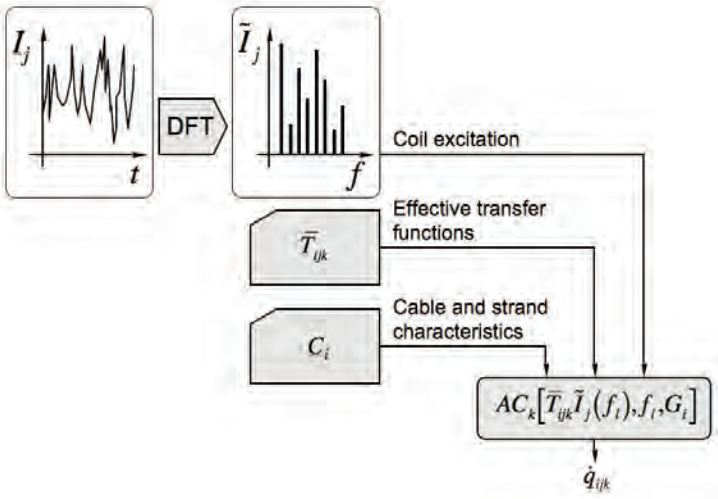

Fig. 2.5.2 *Block diagram of the AC loss calculation method.*

The basics of the method is to decompose an arbitrary current waveform in its Fourier components, compute the AC loss for each of the components independently, and then add the loss contribution (i.e. hysteresis and coupling losses, in parallel and normal field) to give an estimate of the total loss. For the calculation of the AC loss we use established formulae for hysteresis and coupling loss in strands and cables subjected to a sinusoidal field change. In particular, the formulae contain explicitly as parameters the field amplitude and frequency, which are necessary for the analysis of the Fourier components. Additional parameters describe the AC loss properties of the strand and cable (i.e. the critical current, the effective filament diameter and the coupling loss time constant), and can be used to explore parametrically the effect of design variations in the coil windings. The block diagram is depicted in Fig. 2.5.2.

In order to obtain the effective transfer functions, which are the only parameters that are not determined in the model, we perform a set of AC loss calculations for a

series of harmonic excitations with a given amplitude and frequency (the coil excitation is arbitrary, which is the scope of the plasma control algorithm).

Friction Factor in CICC

The pressure drop in forced-flow conductors is one of the key parameters for the design and operation of a magnet system. The relation between mass flow $\dot{m}$ and pressure drop Δp determines the maximum heat that can be extracted and affects the efficiency of the cryogenic system through the pumping work necessary to circulate the coolant.

The correlations for friction factor f used so far are in the form $f = f(\mathrm{Re}, \varphi)$, where φ is the void fraction, and Re the Reynolds number. They make reference to the specific conductor design only through the definition of the hydraulic diameter. The analysis of available experimental data shows however that conductors with very similar void fraction are characterized by a friction factor that differs by about a factor 2 at the same Re.

We propose to follow an alternative approach to the analysis of the friction factor data, namely to consider the cable bundle in the CICC as a porous medium, which is defined macroscopically by its porosity, i.e. the fraction of the total volume occupied by void and free to the flow. The cabled strands form the packed solid phase and the pores are the interstices between strands, and the coolant flows in the tortuous path connecting the interstices. A new fit with 3 free parameters has been obtained. The results are shown in Fig. 2.5.3. The friction factors predicted with the new approach are within 20% error from those computed *a posteriori* from the pressure drop measurements.

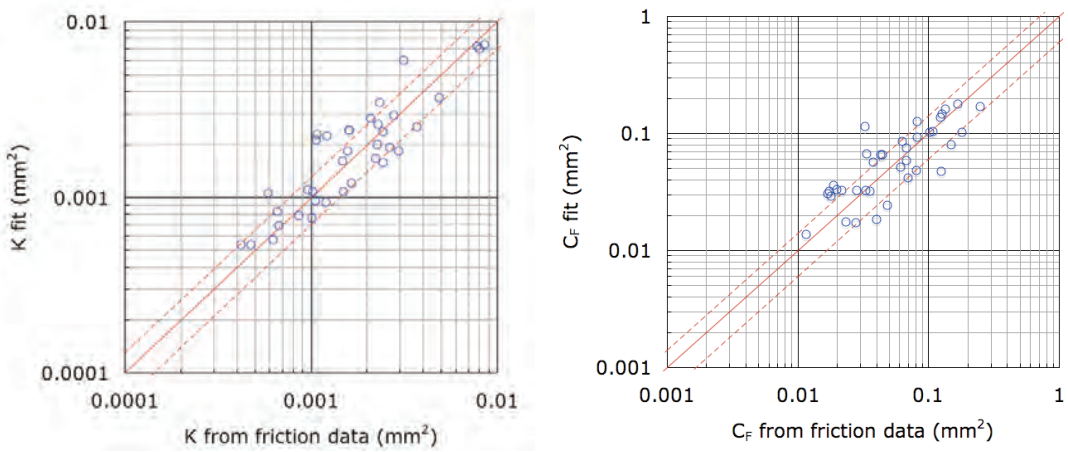

Fig. 2.5.3 *Comparison between permeabilities (left) and drag coefficients (right) derived from pressure drop measurements and computed with the new proposed fit.*

Participation to the testing of the Poloidal Field Insert Coil (PFIC)

The PFI is the last in a series of Insert Coils tested within the ITER R&D framework from year 2000 on and the only one using NbTi. The PFCI is a single-layer solenoid, wound from a 45m long ITER-type NbTi dual channel CICC. An Intermediate Joint (IJ) connects the main winding to a second piece of the same conductor, which is called the upper busbar. The conductor is representative of the one currently

proposed for the ITER PF1&6 coils. The PFI main winding and upper busbar are cooled by two separate hydraulic circuits using supercritical helium at nominal 4.5K and 0.5MPa inlet conditions.

The PFCI was fabricated by Tesla Engineering, UK, starting from a cable produced in Russia by VNIIM/VNIIKP and jacketed at Ansaldo Superconduttori, Italy. It was installed in the bore of the ITER Central Solenoid Model Coil (CSMC) at JAEA Naka, Japan. The CSMC provides the nominal background field of 6T, whereas the nominal operating current of 45kA adds a non-negligible self-field contribution, leading to a significant field variation (~ 1T) over the cross section of the conductor, similar to that in the ITER PF coils. The PFI was tested during about two months until mid-August 2008. An international testing group was set up by the ITER Organization and the Domestic Agencies.

The results of the test broadened the database for the ITER PF coils already available after the test of the PFI short sample performed in 2004 in SULTAN. In particular, the tests confirmed that:

- While sudden quenches still occur above a certain current threshold, because of (self-field) gradient on the CICC cross section, the PFI could operate in DC conditions with no premature quenches with respect to its strand at peak magnetic field, as opposed to the case of the short sample – an indirect indication of improved current uniformity.
- The resistance of the IJ (and lower termination) was much lower than in the case of the short sample thanks to improved manufacturing. However, the performance of the joint itself was degraded with respect to the conductor.

Test of a Broader Approach prototype conductor in SULTAN

A NbTi, 20kA CICC with round cross section, named SU-TFCS1, was tested in SULTAN under bilateral agreement with CEA in June 2008. The conductor was based on the original (before November 2007) design of the JT60SA magnets. Although the conductor is totally out of date compared to the updated magnet design agreed in November 2007, CEA decided to test it in SULTAN to gain experience with NbTi CICC.

The SULTAN sample, prepared by CEA under industrial contract, has a hairpin shape, with a U-bend at the bottom. In the region of the U-bend, the conductor jacket is removed and the bent cable is encased in a steel box. The test programme was agreed with CEA and included DC performance, AC loss, transient field stability and a limited extent of cyclic load. The test lasted about two weeks of SULTAN operation. The results were consistent with others of medium size NbTi CICC hairpin samples tested in SULTAN in the past years.

A thermal-hydraulic experiment about buoyancy in ITER CICC

The observation of an upward counter flow of helium in the outer annulus of a vertically oriented and top-to-bottom cooled ITER PF Coil conductor sample in 2002 stimulated closer experimental as well as theoretical investigations of the effect because it may lead to a reduction of the operational margin of the ITER TF coils. A 3.5m long dual-channel CICC section, made to the “Option1” TF conductor design, is used for dedicated thermal-hydraulic experiments in SULTAN. The objective of the test is the exploration, under various heat-load conditions, of the flow perturbation in cable. Since the sample does not carry any electrical current, intrusive sensors are attached in order to measure the radial temperature profile

(see Fig. 2.5.4 left). Small spot heaters, also installed inside the cable, heat small volumes of helium by ≈0.1K. The propagation of a small hot slug downstream of the heater permitted the direct measurement of the flow velocities in the bundle region and in the central channel.

The sample was heated by coupling current loss induced in the strands by an applied AC magnetic field as well as by strip heaters mounted on the outside of the conductor jacket. The 22 temperature sensors mounted on the sample revealed a detailed picture of the temperature distribution at different mass flow rates and heat deposition modes.

The experiments showed (see Fig. 2.5.4 right) that temperature differences between bundle and central channel downstream of a heated region vanish exponentially with the distance from that region, because the helium of the two channels mixes with a characteristic length of about 40cm. The temperature differences depend linearly on the heat loads well beyond the expected loads for ITER. With the measured parameters it is thus possible to estimate the expected temperature increase beyond the 1D model with an accuracy of about 20mK.

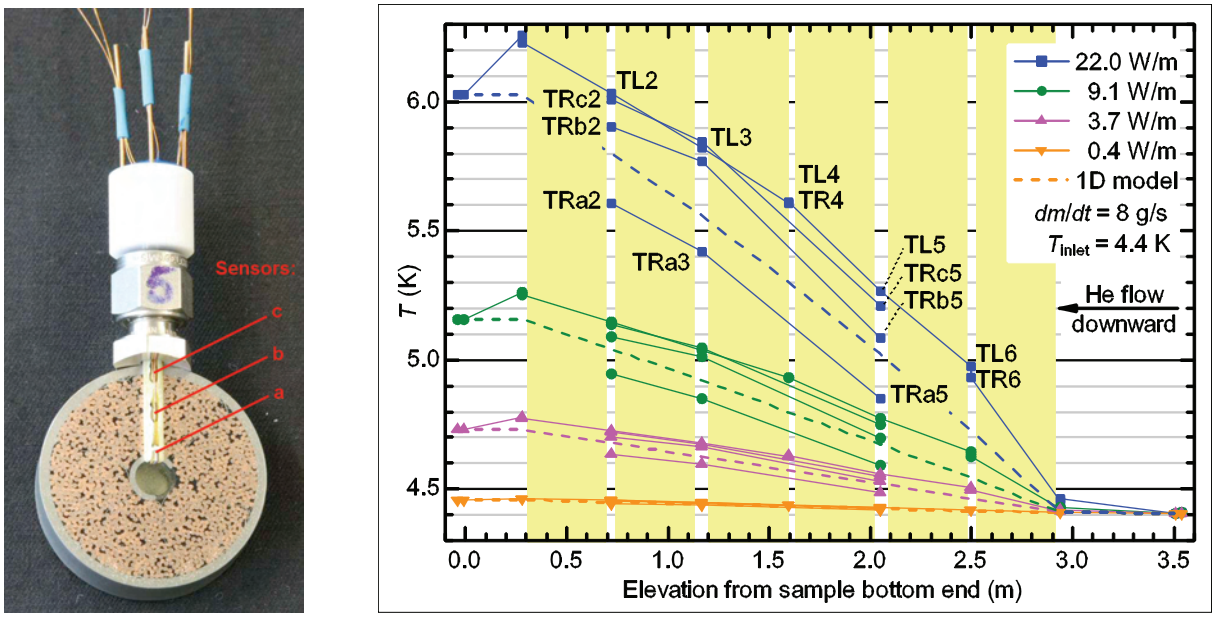

Fig. 2.5.4 *Left: Photograph of a TF conductor cross section with the holder of three temperature sensors.*
Right: Temperature profiles along the sample for four different power levels in all six strip heaters. The sensors 'a' are mounted close to the central channel, 'b' in the centre of the bundle region and 'c' close to the jacket. The dashed lines were calculated assuming a homogeneous temperature at each cross-section (1D model).

The flow velocity measurements showed that in the investigated conductor the helium velocity in the central channel is about five times larger than the one in the bundle.

Test of Nb_3Sn strands extracted from ITER CICC samples

The unexpectedly low DC performance of some ITER prototype CICC led to the question whether it arises from a reversible transverse strain in the strands caused

by the transverse Lorentz force or from a damage of filaments in the strands. Measurements of the critical current of ~8cm long strand sections extracted systematically from prototype samples were performed to see if and by how much the critical current dropped relative to the one of the reference, intact strand sample.

The sample holder shown in Fig. 2.5.5 (left) enables the mounting of the three-dimensionally distorted wires emerging from CICC extraction, while keeping them firmly supported mechanically. For the voltage measurements two sets of voltage pairs were used, one 1cm apart, the other 3cm, both centred on the sample centre. The outer voltage taps have a better resolution but are too close to the current contacts and are affected by the junction voltage, see Fig. 2.5.5 right. As the noise on the voltage tap pair already corresponded to the generally used field criterion of 0.1μV/cm, 1μV/cm was used to compare the critical current of the extracted samples and of the 1m long witness strands.

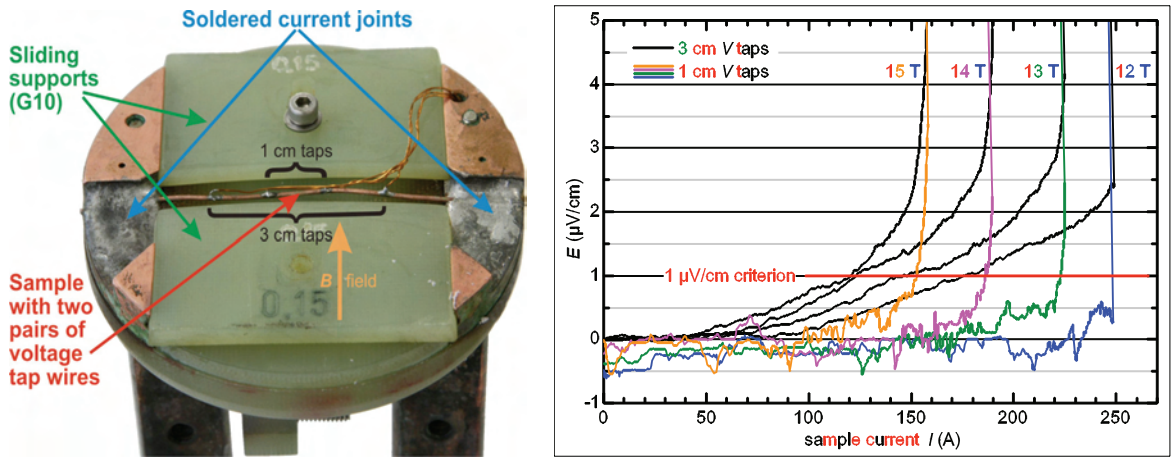

Fig. 2.5.5 *Left: Sample holder with extracted strand. Note the two sets of V taps. Right: EI curves of the resistive transition at four different applied fields (black: 3cm taps, colour: 1cm taps).*

To explore a wide range of behaviour, strands were extracted from prototype CICC representing the various types of samples tested in SULTAN: The current sharing temperature T_{cs} values of the TFPRO2 sample's two legs, dubbed OST1 and OST2, differed by more than 1K after load cycling. The strands extracted from OST2 remain only slightly below the critical current of the witness strands. The strands originating from OST1, on the other hand, show – on average – some clear degradation.

The USTF1 baseline conductor had a very stable performance. The "alternate" conductor of USTF2 did not reach its potential performance and T_{cs} dropped after load cycling. Some strands of USTF1 baseline and USTF2 alternate reach their potential, some others not quite.

The behaviour of the SULTAN samples after cyclic loading – one conductor with constant, high performance (OST2), two with lower and decreasing one (OST1, US2 alternate) – is thus reflected in the critical current measurements on strands extracted from these conductors.

2.5.2 High Temperature Superconductors

In the last few years, the "old" EFDA supported by technology tasks the development of high temperature superconductors for future use in fusion applications (TW5-TMS-HTSPER, TW5-TMS-HTSMAG, TW4-TDS-CLDES). Fusion for Energy (F4E) has taken on the responsibility for all European contributions to ITER, but is not involved in the future support of the development of HTS for fusion applications, which is in the Workprogrammeme 2008 of the "new" EFDA. As September 2008, no initiative was taken by the "new" EFDA to launch a programmeme for HTS. In the first version of the EFDA Workprogrammeme 2009, the HTS was not even mentioned.

In collaboration with other associations (Atominstitut Wien (ATI), ENEA, Forschungszentrum Karlsruhe, IEE Bratislava) a joint proposal for the future development of HTS for DEMO has been worked out in September 2008. On behalf of this cluster of associations, the head of ATI presented in October 2008 this proposal to the new EFDA, which will become responsible for the support of all new technologies for fusion.

Final Design of HTS Current Leads for ITER (TW4-TDS-CLDES)

In the task TW4-TDS-CLDES, a thermodynamic optimization study for ITER HTS current leads, consisting of a conduction-cooled HTS part and a heat exchanger cooled by helium gas, was performed and a possible design of pulsed 45kA HTS current leads was proposed. A sketch of the HTS module of an ITER pulsed 45kA HTS current lead is shown in Fig. 2.5.6.

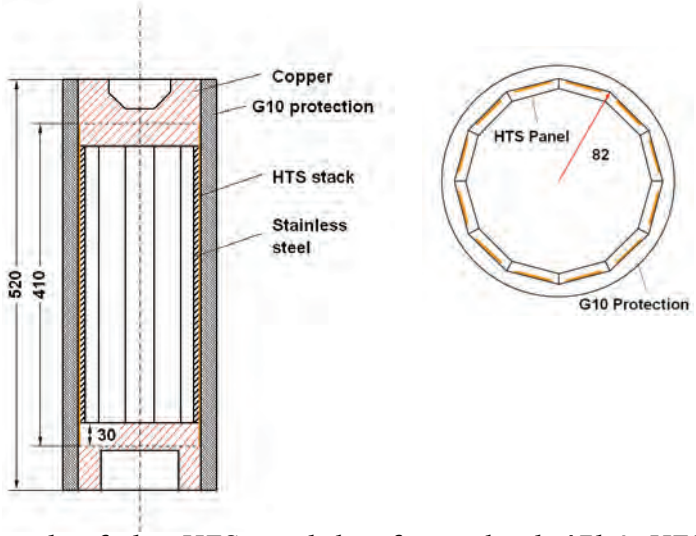

Fig. 2.5.6 *Sketch of the HTS module of a pulsed 45kA HTS current lead for ITER.*

Based on the test of the European 70kA HTS current lead demonstrator the minimum instrumentation required for the test of ITER prototype current leads has been defined. Furthermore, a procedure for the test of the ITER HTS current leads has been proposed.

Replacement of the SULTAN Current Leads by HTS Current Leads

In order to reduce the fraction of the refrigerator power required to cool the current leads it would be desirable to replace the conventional current leads of SULTAN by HTS current leads. In general, AgAu/Bi-2223 HTS tapes were used for the fabrication of high current (I > 10kA) HTS current leads. Because of the strong dependence of the critical current of AgAu/Bi-2223 tapes on magnetic fields perpendicular to the broad face of the tapes this field component has been estimated at the positions of the SULTAN current leads. First preliminary results suggest that the perpendicular field at the positions of the SULTAN current leads can reach values as high as 80mT. The use of helium gas available for the cooling of the thermal shields would lead to temperatures of 80K at the warm ends of the HTS parts of the current leads. The use of AgAu/Bi-2223 tapes for SULTAN HTS current leads would therefore require a shielding of the magnetic stray fields. Second generation HTS (YBaCuO or rare earth based RBaCuO coated conductors), characterized by a less pronounced field dependence of the critical current, could be considered as an alternative for the manufacture of the SULTAN HTS current leads. However, the use of coated conductors has not yet been demonstrated for 10kA class current leads.

2.5.3 The European Dipole (EDIPO) Project

Progress in preparation of the EDIPO test facility

The drawings of the *Vacuum Vessel* (including all flanges, the support structure of the cold mass, the thermal shield and the telescopic enclosure for the transformer lift out) are completed. The layout of the steel framework for personnel access and of the transformer lifting gear on top of EDIPO will complete the mechanical design effort soon. The procurement orders will be placed early in 2009.

All components of the new 100 kA *Transformer and Sample Holder* are in house, except the secondary coil. The cable-in-conduit conductor for the latter was manufactured in August 2008 and is currently prepared for coil winding and vacuum impregnation in December 2008. The final assembly work is planned at CRPP in the first half of 2009.

The procurement order for the main *18kA, ±10V Power Supply* was placed at Danfysik in January 2008 and updated in September 2008 after a technical design review. The delivery date is now June 2009. The EDIPO energy extraction switches, part of the *quench protection system*, must be able to break currents up to 17kA at voltages up to 2kV. The switches will be procured by CRPP and integrated in the Danfysik power supply. No individual switch satisfying these requirements is on the market. Because the straightforward solution with at least three available DC breakers in parallel (times two for redundancy) is expensive, a number of alternative configurations were studied: a high-current low-voltage bypass switch (BPS) in parallel with a 2kV circuit breaker; a BPS in parallel with a thyristor switch and a BPS in parallel with an insulated-gate bipolar transistor (IGCT) switch. The discussions with external experts will be completed shortly and a decision in favour of one solution made.

The *±300A, ±40V Power Supply* for the transformer, including the quench protection components supplied by CRPP, was ordered at Danfysik and will be delivered at CRPP in November 2008. Danfysik also implemented the requested two modes for primary and secondary current control.

To reduce the refrigeration load, it is foreseen to use 17kA *High-Temperature-Superconductor Current Leads* (HTS leads) in the EDIPO facility. These current leads will consist of a conduction-cooled HTS module, made of industrially fabricated AgAu/Bi-2223 tapes, and a gas-cooled copper part, see Fig. 2.5.7 top. Available 75K-helium gas will cool the cryogenic shields as well as the copper parts of the HTS leads. At 80K, the design temperature of the HTS modules warm end, the critical current of the AgAu/Bi-2223 tapes depends strongly on the magnetic field component perpendicular to the broad face of the tapes. Detailed field calculations, taking into account the leads self fields and the stray fields of the EDIPO magnet and of the transformer secondary winding, indicate that the peak field at the HTS stacks will reach 46mT (at I = 17kA) for a module consisting of 65 HTS stacks. A total of 150 HTS stacks, each consisting of eight solder-bonded AgAu/Bi-2223 tapes, have been procured at Bruker HTS (formerly EHTS) and delivered them to CRPP in early October 2008. Figure 2.5.7 (left) shows the distribution of the stack critical currents, measured at 77K in self-field. The final design of the HTS modules has been adjusted to the measured performance of the 65 stacks needed per lead to reach a temperature margin of at least 4K. The calculated temperature profile is shown in Fig. 2.5.7.

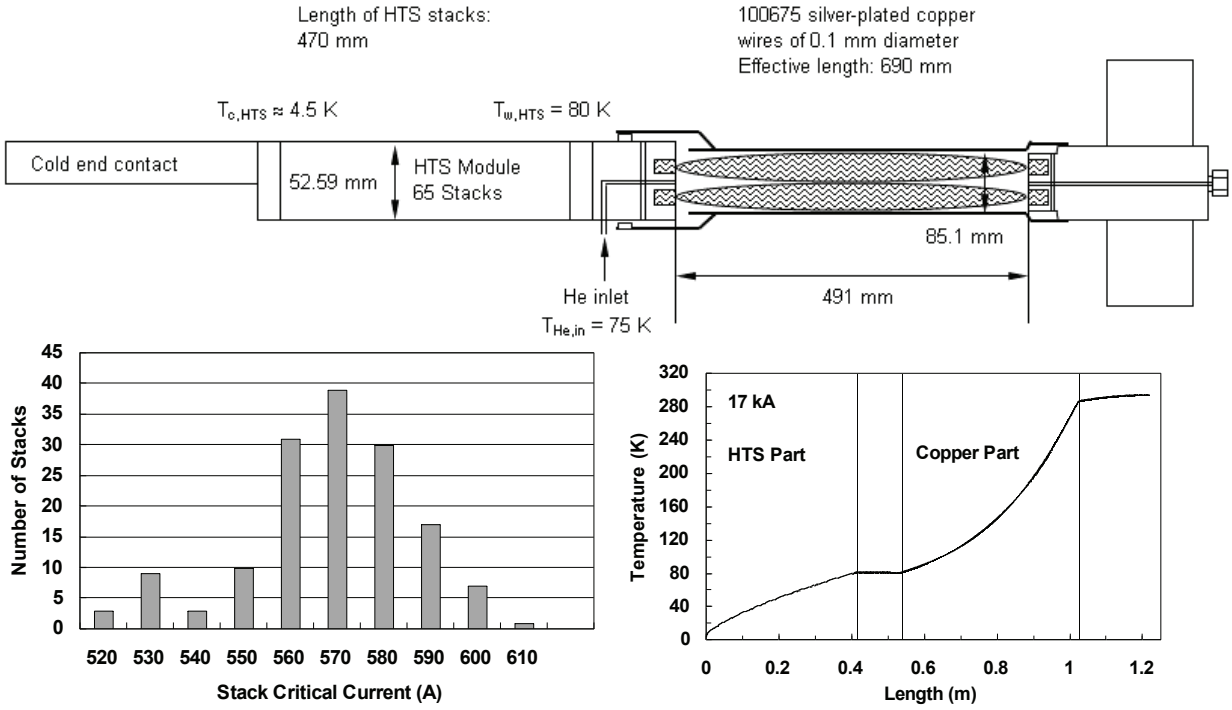

Fig. 2.5.7 *Top: Sketch of the HTS module of a 17kA HTS current lead for EDIPO. Left: Distribution of the stack critical currents measured at 77K in self-field. Right: calculated temperature profile along the current lead at 17kA (note different sections).*

A copper *thermal screen*, cooled to about 75K and surrounding the magnet cold mass inside the vacuum vessel, will reduce the radiation heat flow into the cold mass. This cylindrical screen is around 4m long and 2mm thick, and it has a diameter of 1.6m. During a fast discharge of the dipole, eddy currents are induced in the copper, and a Lorentz force, due to the interaction between the current and the magnetic field, acts on the screen. In order to reduce the eddy currents and the forces on the structure to acceptable levels, the screen needs to be segmented

longitudinally and circumferentially. To estimate these forces and to verify the effectiveness of the segmentation, 2D and 3D magnetic and mechanical analyses have been done. The number of segments along the dipole axis has been optimized and fixed to 5. Along the perimeter the screen is divided into 4 parts each covering 90º. A 3D electromagnetic analysis showed that with this configuration the current is limited to 19kA and the forces in each segment are lower than 8kN in all directions. The mechanical analysis showed deformations of the order of 100μm in the lateral surface of the screen.

Conductor Development for EDIPO – The role of cable twist pitches

The performance degradation under electro-magnetic, transverse load is a key issue for the performance of Nb_3Sn CICC. A sequence of "long" twist pitches in the early stages of a multi-stage cable is credited to mitigate the degradation compared to "short" pitches. To assess quantitatively the effect of long/short pitches maintaining constant all other conductor parameters, a short length of EDIPO medium field conductor is prepared, where the first half length (Pitsam5L) has long pitches (83/140/192 mm) in the first three cable stages and the second half length (Pitsam5S) has short pitches (34/95/139 mm). The last stage pitch is 213 mm for both lengths. The conductor is assembled into a SULTAN hairpin sample where the two branches have respectively long and short pitches.

The current sharing temperature T_{cs} is measured at the nominal operating condition for the EDIPO medium field conductor, 17kA - 8T, as a function of the load cycles. The performance evolution is summarized in Fig. 2.5.8 left. Since the first cycle, Pitsam5L has superior T_{cs} performance, about 0.5K higher than Pitsam5S. After the thermal cycle, the difference in T_{cs} grew to 1.5K. The Pitsam5L lost 0.5K overall. The process of degradation is continuous and likely not completed at the end of the test campaign.

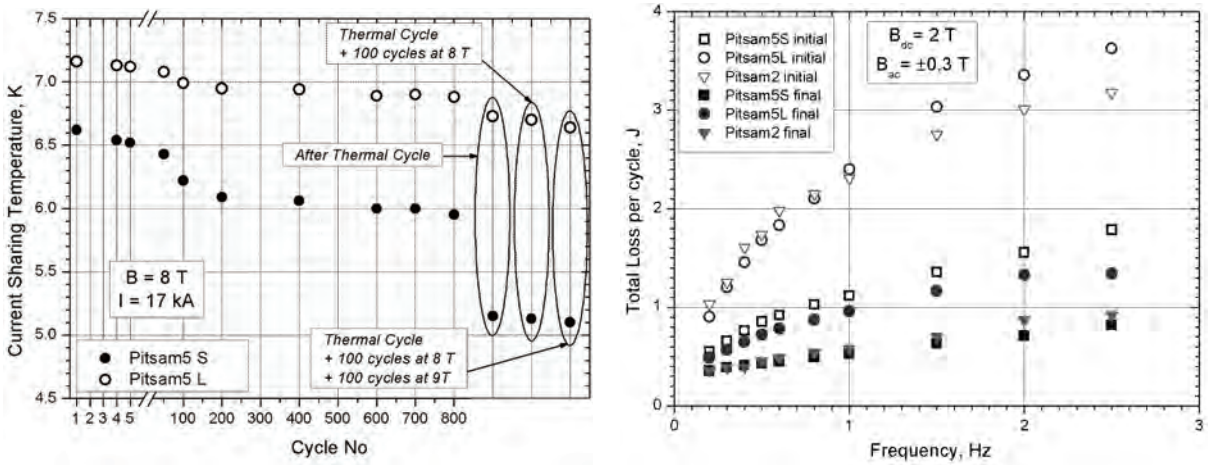

Fig. 2.5.8 *Left: Evolution of the DC performance for both Pitsam5 conductors. Right: AC loss curve before and after cyclic load for the Pitsam5 and Pitsam2 conductors.*

The impact of the twist pitch sequence on the ac loss is investigated by comparing the two Pitsam5 conductors with the reference EDIPO medium field conductor, Pitsam2, which has the same pitch sequence as Pitsam5S, except a longer pitch in the first triplet. After cyclic loading, the loss curves of Pitsam2 and Pitsam5S are identical, see Fig. 2.5.8 right, suggesting that the twist pitch of the first cable stage

has marginal impact on the loss. The slopes of Pitsam5S and Pitsam5L differ by over a factor of two, suggesting that the intermediate pitches have a substantial weight in the ac loss balance.

When all other conductor parameters (void fraction, strand, geometry) are kept constant, a sequence of long cable pitches is beneficial to mitigate the irreversible, transverse load degradation in Nb_3Sn cable-in-conduit. A long pitch in the first triplet is the main driver to reduce the degradation. The sample with long cable pitches has over twice as much ac loss compared to the sample with short cable pitch. However, a long pitch in the first triplet has not substantial impact on the ac loss.

All the conductor layout variations for EDIPO medium field conductor stay substantially below the potential dc performance expected from the strand properties. The best conductor degrades by ≈20% since the beginning of the test campaign and ends up with 30% degradation.

2.6 Industrial process plasmas[1]

The situation in academia has led to a substantial reduction of the R&D activities of the industrial plasma group. The number of projects and in particular the manpower have decreased, which will strongly influence the future output of the group. The number of the research topics has been considerably reduced.

For several plasma processes used in industry, higher deposition rates are necessary. This trend leads to the development of new plasma sources and novel processing techniques. One of the most interesting topics is the development of plasma sources and its integration into a future industrial high deposition rate plasma reactor. The industrial plasma group is particularly active in this expanding field. One CTI project, started this year together with Sulzer Metco, aims at combining plasma spraying and high rate thin film deposition with one tool: the plasma torch. For SiOx deposition as used mainly in the packaging industry, developments to increase the deposition rate are also made either by new processing or by the development of a novel plasma source.

The diversification of the R&D activities is ongoing and long-term topics have been initiated. A particular weight shall also be given to discharge physics and arcing under various conditions.

Discharge physics is still a key issue in the world of industrial plasmas. Fundamental studies to understand breakdown and discharges are still a necessity. One of the main problems in industrial reactors is the occurrence of arcing and parasitic discharges, which can hinder a successful introduction into industrial production lines. Arcing starts to be the limiting factor in several plasma applications, thus triggering intense research and development on this topic.

The study of arc phenomena is one of the oldest topics in plasma physics. In our opinion arcing is at present a key issue in the application of plasma in industry for the coming years. Research and development of Electrical Discharge Machining is another important point in the research of the industrial plasma group. (The basic behaviour of the plasma during electrical discharge machining will be studied in collaboration with Charmilles SA.)

[1] Work not belonging to the EURATOM Association's work programmeme.

During the year meetings and discussions with various industries on other new plasma processing issues have been made and will give new R&D topics and interesting science for the industrial plasma group of the CRPP in the future.

2.6.1 Thin and thick film coating using liquid and gaseous precursors with low pressure plasma spraying (LPPS)equipment

Conventional plasma spraying provides rapid coating due to the high enthalpy and high velocity of the plasma jet. Metal and also ceramic powder material can be melted and deposited in the form of splats which produce thick and porous coatings as required. A process called LPPS-Thin Film was developed a few years ago which can deposit dense layers at low pressure with thicknesses as low as ~ 10-20 μm with high deposition rates. However, there are applications where dense and thin (submicron) coatings are required, which can not be obtained either by conventional thermal spray techniques nor by the LPPS-Thin Film process. These coatings are usually produced at low deposition rates (<10nm/s) by Physical or Chemical Vapour Deposition (PVD, CVD) processes.

In this CTI project, started this year, we show that it is possible to deposit thin and dense layers from liquid or gaseous precursors at high deposition rates using conventional plasma spraying equipment operated at low pressure (mbar range). With this approach it is possible to combine the conventional thermal spray coating with the newly-developed thin film deposition using the same equipment to obtain multilayer deposits with special functionalities and properties.

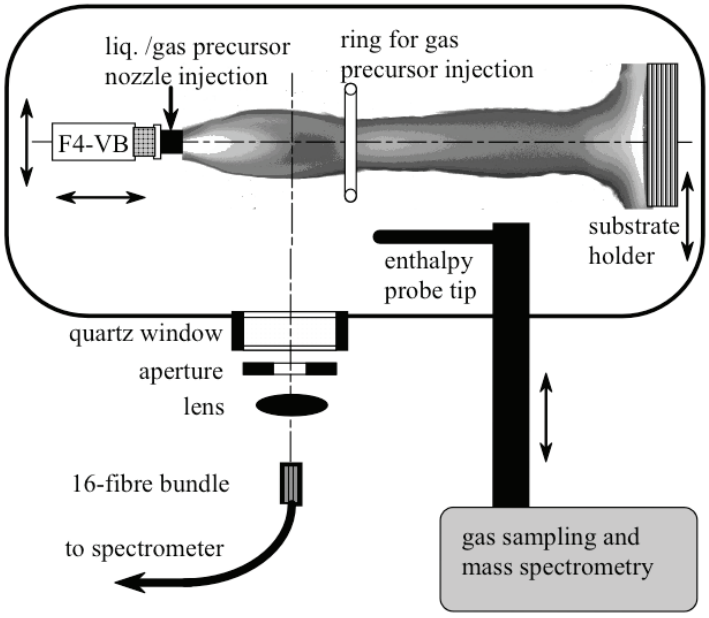

Fig. 2.6.1 *Experimental arrangement for thin film deposition using a F4 plasma gun.*

The process used is based on a Sulzer Metco Multicoat System with a F4-VB plasma torch mounted inside the vacuum chamber (Fig. 2.6.1). A movable, water-cooled substrate holder is positioned downstream of the torch nozzle. The gas precursors presently used are either hydrocarbons or organosilicon such as hexamethyldisiloxane (HMDSO, $C_6H_{18}OSi_2$) diluted with O_2. These are injected either inside the torch nozzle or through a perforated ring downstream, or at both places,

depending on the requirements of the process. Liquid precursors are injected inside the torch nozzle downstream of the arc, either directly through small holes or by using a nebulizer. The efficiency of the gas or liquid precursor penetration, the homogeneity of mixing, as well as the transport and decomposition inside the plasma jet were measured by optical emission spectroscopy (OES) and mass spectrometry (MS). SiO_x layers were deposited with up to 35nm/s from a mixture of oxygen and HMDSO. The O_2 gas is injected inside the torch nozzle whereas the HMDSO vapour produced by a Controlled Evaporation Mixer is injected with an Ar carrier gas flow rate through the ring.

The deposition rate of SiO_2 was observed not to saturate with increasing the HMDSO mass flow rate within the parameter window investigated. Since the conditions have not yet been optimized, this suggests that this process has a high potential for very fast deposition of thin and dense films. The gas sampled from the plasma jet at different locations is analysed by mass spectrometry to estimate the efficiency of precursor conversion (depletion). It appears that more than 95% of the gas precursor is used. The location where the gas precursor is injected has a strong influence on its conversion efficiency and also on the mixing homogeneity in the plasma jet flow. The precursor transport and mixing in the plasma jet are also strongly influenced by the flow properties. In particular, there might be a recirculation of the gas outside the plasma jet, induced by shear forces at the jet fringes. Another effect, due to a chamber volume much larger than the plasma jet volume, is that there might be some regions where the gas stagnates. These flow effects are influenced by the presence or absence of a substrate in the plasma jet. When the jet is impacting on the substrate, there is a strong modification of the recirculation flow topology, which hence influences the precursor transport, mixing and chemical reactions.

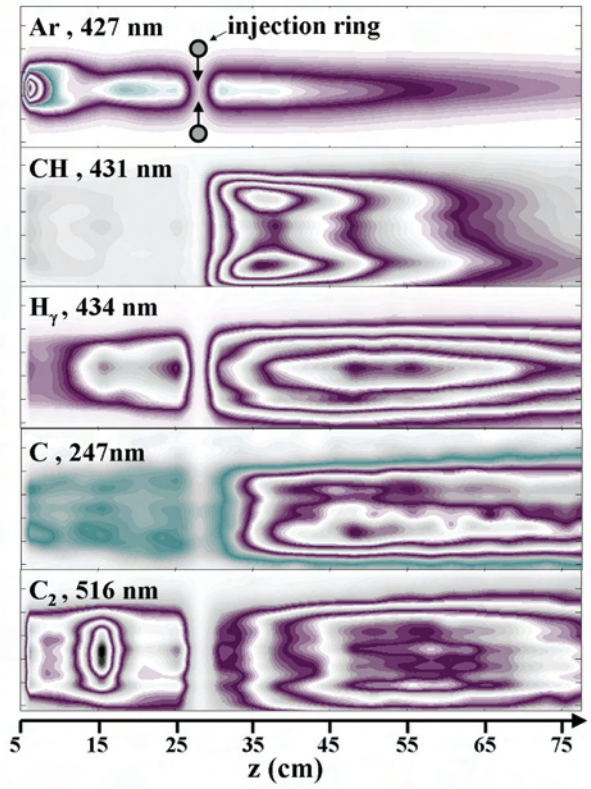

Fig. 2.6.2 *Light emission during injection of gaseous precursor.*

Light emission of the plasma jet, either from the plasma forming gas (in our case, argon), or from the injected precursors can be used to monitor the chemical reactions, mixing and transport of the excited species. Figure 2.6.2 shows a mapping of the emission from the above lines and bands in the form of images. The radial profiles are not Abel-inverted and therefore represent the lateral profiles of light emission integrated along the line of sight. The typical flow pattern of supersonic under-expanding plasma jets can be identified from the intensity variations of the Ar emission, which is higher in the compression zones and barrel shocks, and weaker in the expansion regions.

The emission from CH(A-X) is remarkably concentrated very close to the injection ring, with a sharp increase as the jet flow passes the ring. This suggests that the excitation mechanisms occur directly from the injected CH_4 and that it is a very fast process. In addition, the emission from CH decays relatively fast downstream of the flow and is not observed upstream of the injection ring, as for all the other species. This shows that the source for CH emission, namely CH_4, is rapidly depleted.

A very different behaviour is observed for the emission from C_2 which is slowly increasing downstream of the injection ring. It is also observed upstream, with a maximum close to the torch nozzle at z=15 cm. This shows that the creation mechanism of C_2 emitting species is slow since they are formed by secondary reactions from the dissociated CH_4 products along the flow.

The source of emission from excited C atoms seems quite similar to the one producing CH, except that it is probably slower, as suggested by the smoother increase of atomic carbon emission downstream the injection ring. Note also the very low C emission upstream of the ring which suggests that it is weakly produced from the species which re-circulate.

2.6.2 Arcing and parasitic discharges in RF plasma reactors

In the frame of the CCEM project “Cost efficient thin film photovoltaics for future electricity generation” funded by Swisselectric, the arcing and the appearance of parasitic discharges in high power RF plasmas have been investigated.

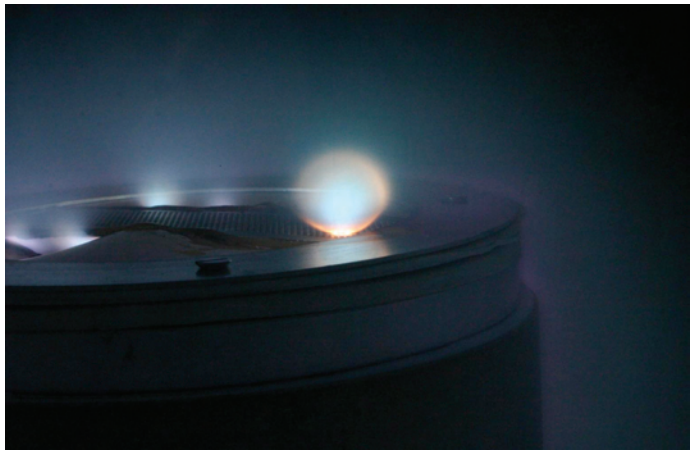

Fig. 2.6.3 *Close-up of a hollow cathode in the arcing testbed.*

The need for more powerful and larger area reactors for plasma enhanced chemical vapour deposition brings current designs to their limits. Parasitic plasmas and arcing become more common and can damage or even destroy these reactors. A

better understanding of these phenomena is crucial for the development of new reactor generations. In a very large area reactor many types of arcs and parasitic plasmas can coexist, possibly influencing each other. Since such a reactor is a very complex system, it is difficult to develop simple models explaining the cause of the damage observed in industry. After listing rough subgroups of arcing damage, the first step has been to try and reproduce these discharges in a small research reactor, with a simple geometry. This procedure will then allow us to isolate the underlying fundamental physical principles. Once the types of discharges behind the arcs and parasitic plasmas are known, methods to prevent damage to the reactor can be developed. A short term solution would be to find real-time diagnostics to detect damaging arcs during operation. It is important to note that to be of use for the industry, such diagnostics have to be relatively cheap and easy to implement.

Another, long-term solution is to find design rules to completely prevent the identified arcs and parasitic plasmas from forming in the first place, or at least to shift the onset to higher power regimes.

One important group of discharges are hollow cathode discharges (Fig. 2.6.3) which are very intense discharges burning in holes or slits, mainly due to an electron pendulum effect. Hollow-cathode like, brightly burning plasmas can sometimes be observed in the holes of the showerhead and the grids covering the pumping line. These discharges can degrade the deposition material, and might lead to high-current arcs capable of melting and destroying reactor parts.

Teflon was used as a spacer to separate the pumping grid of a commercial large area reactor from the aluminium base plate. Discharges in 1mbar argon resulted in yellow hollow cathode discharges. Analysis via optical emission spectroscopy showed that the yellow light was due to a chemiluminescence continuous spectrum from 500 to 700nm.

Another group is RF breakdown across gaps (mm, cm) in the absence of plasma. In the reactor there are a few areas where no plasma should ignite, but where the surfaces are still exposed to high RF voltages and the gases used during deposition and cleaning. Inside the showerhead distances are kept below the minimum necessary for breakdown, to avoid the formation of plasma and/or arcs. Nevertheless, breakdown can and does occur and leads to damaged components. To understand the possibly complex reasons for the occasional arcing event, parallel plate breakdown experiments were made and the complexity of the geometry increased until finally arriving at an exact copy of the suspender screw used in the commercial plasma reactor.

The experiment consisted of two aluminium plates of 13cm diameter, separated by Teflon or perspex rings with an inner diameter of 11cm. The gap separating the electrodes (i.e. the thickness of the separator-rings) was varied between 1 and 5mm. Decreasing the gap-size from 5 to 1mm lead to a flattening of the breakdown curve. Adding a small cone on the parallel plates did not change the breakdown curve, but a cylinder configuration tends to lower the breakdown voltage, especially in the left-hand branch of the curve.

With the present test bed we have a very versatile tool for testing various geometries in view of arcing and parasitic discharges.

2.6.3 Plasma Edge Simulations by Finite Elements using COMSOL

Capacitively-coupled RF plasmas play an important role in industrial applications such as the production of flat displays and thin film solar cells. In these prominent applications, large area coatings with homogeneous film thickness and film structure over large substrate areas must be obtained. Large efforts have been made to obtain several square meters of surface coatings with sufficient homogeneity in thickness and film structure by careful design of the electrode of the RF reactor. However, the reactor edges and the resulting edge plasma still can lead to considerable perturbations in the coating properties. Inhomogeneities of plasma parameters lead to imperfection on the film and can also be responsible for the occurrence of nonlinear effects such as nano-particle formation in the plasma. In addition, the edge plasma is susceptible to triggering parasitic discharges leading to inhomogeneities, severe perturbations of the coating process, or even to the destruction of reactor components. The physics and chemistry induced by particular reactor edge designs are still unknown and not yet well investigated. Numerical simulations of the edge plasma produced in simplified reactor geometries has been chosen to reduce the complexity of the numerical calculation and moreover to investigate the basic plasma physics of the reactor edge and its dependence on typical design parameters.

The COMSOL Multiphysics software is used to simulate the RF edge plasma in the mbar pressure range with a simplified reactor geometry. At present an electropositive plasma excited by a RF frequency of 13.56MHz is modelled by the well-known continuity equations for the electron and ion densities and energy conservation equations closed by the Poisson equation and the corresponding boundary and initial conditions. The typical geometrical dimensions of the investigated plasmas were chosen to be comparable to industrial RF plasma reactors. Several simplified edge geometries (Fig. 2.6.4) such as an open electrode geometry, electrodes with corners and angles and also (a)symmetrical electrode configurations have been studied.

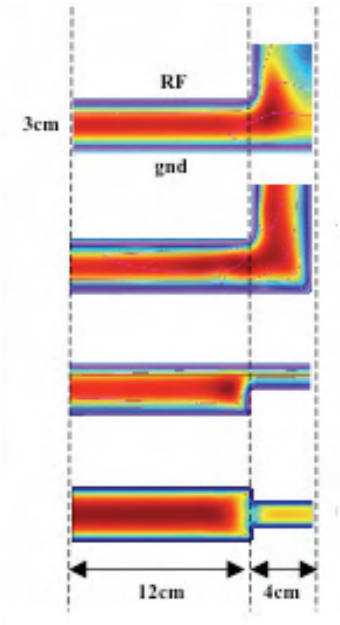

Fig. 2.6.4 *The different RF reactor geometries investigated. (Surface plot of the electron density and the contour plot of the electrical potential).*

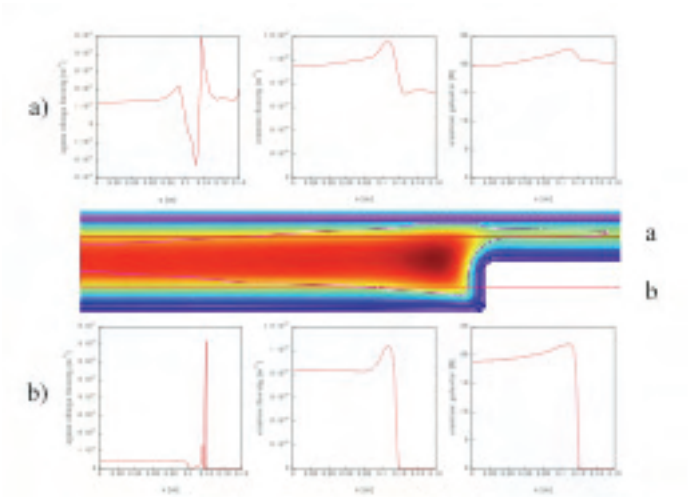

Fig. 2.6.5 *Presence of electrostatic double layers along two different heights within the discharge shown. The inserts show the space charge density, electron density and electrical potential at each height.*

Figure 2.6.5 shows the surface plot of the electron density and the contour plot of the electrical potential for an asymmetrical electrode case. The inserts show the space charge density, the electron density and electrical potential along the indicated lines. The space charge density shows the typical behaviour found in earlier investigations on electrostatic double layers. The presence of the double layer in these RF plasmas has been reported earlier and is still a point of ongoing research.

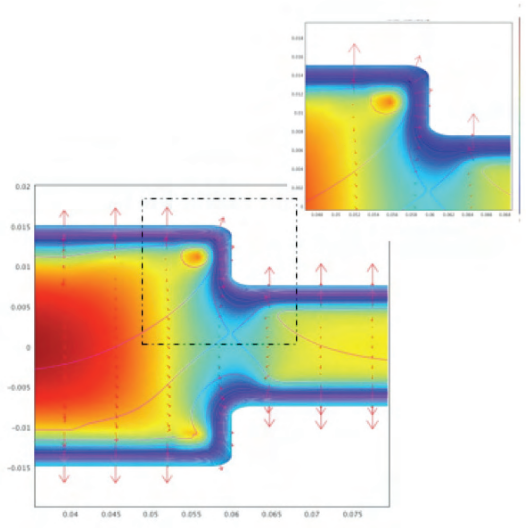

Fig. 2.6.6 *Influence of corners in the reactor wall on the edge RF plasma. Surface plot: electron density, contour plot: electrical potential, and arrows: total electron density flux.*

In this case, a local electron density maximum is found near to the two concave corner walls (see also Fig. 2.6.6). Post processing also shows that the ionization rate is also peaked at this place. The present simulations might be considered as a first step towards more detailed calculations of the plasma parameters in the RF reactor edge. This includes the simulations of more realistic reactor walls including metallic and dielectric elements.

All the various simulations of edge plasmas revealed the importance of corners in the metallic reactor wall. A concave corner leads to a strong increase of the electrical potential amplitude as well as to a peaking of the particle densities and therefore to a focalization of the ionization rate. Conversely the convex corner leads to a decrease of the electrical potential and consequently to a decrease of the local electron density.

The plasma sheath thickness, the electron density and the step size are important parameters governing the plasma physics around corners. If the plasma sheath thickness is much smaller than the step dimensions, the plasma sheath follows the step conformally. However, if the sheath thickness and the step size are comparable, large changes in the plasma are expected. The behaviour of the plasma sheath around a corner is a basic feature of plasma physics and of first importance for the design of RF plasma edge in modern plasma processing. The present simulations revealed the very basic influence of the reactor boundaries on the local plasma environment. Roth & Rau (Switzerland), OC Oerlikon, the IMT (Neuchatel) and other companies showed clear interest in applying of the simulation to their particular deposition problems

2.6.4 Optimization of the plasma enhanced chemical vapor (PECVD) process for the deposition of SiO_x barrier coatings on polymers.

The main technologies for the deposition of oxide barrier such as SiO_x on polymer films are based on vacuum web coating methods. In the so-called PECVD (plasma enhanced chemical vapour deposition) the organosilane is decomposed, and fragments attached at the polymer film surface react with oxygen atoms to form SiO_x layers.

During SiO_x deposition, production of fine sized (micrometer or even nanometer sized) powder is a great disadvantage of the process. First, the powder damages equipment such as vacuum pumps, leading to costly maintenance and repairs. Furthermore, powder might be a potential health risk and should therefore be reduced or completely avoided. Strong powder production is also a sign that the process could have much higher deposition rate since much of the available monomer is transformed into fine-sized SiO_x powder instead of being used for the coating. The mechanism of powder formation in deposition plasmas with hexamethyldisiloxane (HMDSO), oxygen and noble gases is completely unknown.

In the present CTI project in collaboration with Tetra Pak the basics of the SiO_x powder formation is investigated and ways are studied in order to strongly reduce the powder formation. The basic research is made in a small RF reactor at the CRPP whereas the test for high deposition rate/low powder formation shall be tested later in a semi-industrial reactor. In order to understand better the different mechanisms and processes leading to powder formation, we analyzed plasmas fed by three organosilicon compounds, such as HMDSO, TMS and HMDSN, with various amounts of oxygen admixture. These three monomers have a similar chemical structure. The analysis are performed with time resolved in-situ Fourier Transform Infrared Absorption Spectroscopy (ATR-FTIR) in the spectral range between 4000-600cm^{-1}. The choice of the plasma parameters was made to have large powder formation in order to investigate the history and chemistry of the particles. In the gas mixture $HMDSO/O_2$ we observed the typical peaks for $HMDSO/O_2$ plasmas, such as the SiOSi bend at 830cm^{-1}, the SiOSi stretch at 1073cm^{-1}, the $Si(CH_3)_x$ stretch at 1263cm^{-1}, formaldehyde at 1725cm^{-1}, formic acid at 1783cm^{-1}, CO at 2140cm^{-1}, CO_2 at 2340cm^{-1}, CH_3 (symmetric and asymmetric stretch. respectively at 2910 and 2966cm^{-1}), the OH stretch of hydrogen-bonded

OH and in free SiOH. Other peaks have been identified by the deconvolution of the spectra. The bending and stretching peaks evolve in time, showing an increase of their width. For the case of equal gas mixture we do not observe significant differences in the plasma spectra compared to the spectra recorded for pure HMDSO plasma. By comparing the two conditions it has been deduced that a high oxygen amount is responsible of big particle production. Furthermore, the time evolution of each peak reveals that at the beginning of the process the particle formation is induced by polymerization, after that the particles grow and are coated with a $SiO_xC_yH_z$ layer. These first considerations have been confirmed by studying plasmas with TMS and HMDSN as monomer with oxygen admixture.

The acquired plasma spectra are due to contributions from the plasma, monomer and the powder. It is possible to calculate the real plasma spectrum removing the contribution of the gas and afterwards that of the powder, whose spectrum has been recorded by a ex-situ ATR-FTIR. The calculation made for the $HMDSO/O_2$ plasma spectra at the steady state show an interesting peak dominating at 980 cm^{-1}; it is the oxygen asymmetric stretching vibration which seems to play an important role.

2.6.5 Plasma diagnostics for electrical discharge machining (EDM)

Electrical Discharge Machining (EDM) is a widely-used machining technique. With this technology, numerous industries produce moulds, dies and finished parts with complex shapes. The process consists in successively removing small volumes of workpiece material, molten or vaporized during a discharge. The sparks are created in a flowing dielectric, generally water or oil. The liquid dielectric plays a crucial role for the electrode cooling and for the material removal: it increases the removing force on the molten metal when the plasma collapses, then it solidifies the molten metal into small particles, and finally it flushes them away.

During 2008 the CTI project in collaboration with Charmilles Technologies SA, the Ecole d'Ingénieurs de Genève and Micron SA has been continued. The project is dedicated to the development and investigation of EDM milling. In the frame of this project, fundamental experiments on the behaviour of the spark in EDM milling have been performed. This includes statistical investigations of the random EDM discharges. These studies have been performed directely on an industrial tool with a newly developed pulse generator delivered by Charmilles SA. An additional important point for the future development of EDM with Charmilles SA is the development of advanced plasma diagnostic methods. Plasma diagnostics of the spark is a challenge since the discharge immersed in a dielectric is small, typically far less than one millimetre, complicated by the poor reproducibility from spark to spark. New innovative plasma diagnostic methods are absolutely necessary if the EDM discharge or other micro-discharges are to be understood. Therefore the development of advanced plasma diagnostics is also as a prime point in a planned future project.

In addition, first experiments on Dry EDM have been performed. In this process the oil or water dielectric is replaced by air or some reactive or inert gases. These first experiments indicate that Dry EDM is quite a difficult process and its industrialization is still far from being achieved. The investigation will be continued in an additional CTI project in collaboration with Charmilles SA and the ETHZ.

2.6.6 Design, characterisation and modelling of new advanced plasma sources

In the frame of an industrial mandate the development and use of advanced high current DC arcplasma reactor for high rate microcrystalline silicon deposition has been investigated. The aim of the proposed mandate was to establish a catalogue of advantages and problems related with new plasma sources in an advanced plasma reactor for the production of microcrystalline silicon at very high deposition rate. The research lead to interesting new insights in the construction and design of novel plasma reactors and the plasma physics and plasma chemistry involved in these devices.

2.6.7 Helyssen SARL, a start-up company in the CRPP

Helyssen SARL, a start-up company, uses a test bed in the laboratories of the industrial plasma group to evaluate the performance of an industrial Birdcage antenna as Helicon source. The magnets and the necessary equipment for benchmarking and infrastructure have been lent to Helyssen SARL by the CRPP. This includes equipment also for plasma diagnostics and equipment and know-how in order to quantify the performance of high power RF plasma sources.
In collaboration with Tetra Pak Romont and the CRPP a new project has been elaborated which will investigate the application of the Helicon RF Plasma source developed by Helyssen SARL in the packaging industry. The application of this plasma source seems to be promising since very high deposition rates could be achieved during first tests performed at the CRPP site.

2.6.8 Future and future projects

During the year a new CTI project dealing with the development of a novel PECVD reactor for the deposition of thin film silicon for solar cell applications has been accepted by the CTI. The project will start on January 1st 2009 in collaboration with OC Oerlikon Solar in Neuchatel.

Furthermore, a continuation of the former project with RUAG (formerly Mecanex) on the basics of the physics of arc triggering in slip-rings has been elaborated. The project is funded by ESTEC ESA.

In collaboration with Charmilles SA, Inspire AG at the ETHZ, Balzer Technik and Carbagas, a project concerning DRY Electrical Machining has been elaborated and submitted to the CTI.

During 2007 the FP7 project PLASMAERO has been accepted. Within this European project (participating institutions and Universities from France, Great Britain, Italy, Poland, Germany, Holland and Russia) problems related to the application of plasmas in aerodynamics are investigated. The CRPP participates together with the Laboratoire de Thermique Appliquée et de Turbomachines (LTT) and the Laboratoire d'Ingénierie Numérique (LIN) of the Energy Institute (ISE) from the Faculty of Engineering (STI) in this programmeme. In addition the CRPP will also be work package manager of the important work package “Plasma devices”.

During the last year numerous discussions with interested industries have been made resulting in many small experiments and tests which have been performed on the various plasma reactors at the CRPP.

New contacts with interested industries as well with other university institutes have been established with the aim to diversify the activities of the group. The diversification towards new collaborations and topics has been started and new proposals will be discussed between the industry and the CRPP.

Besides the difficulties of obtaining funding for the different projects, the problem of manpower is the most difficult one. The lack of suitable PhD students and Post Docs is a big problem in recruiting manpower for the projects of the industrial plasma group.

Finally, it is a real pleasure to note that a high degree of confidence exists between all the collaborating industries and the plasma processing group, thereby establishing a stimulating and interesting working ambiance.

3 TECHNICAL ACHIEVEMENTS

3.1 TCV operation

TCV operation was resumed early March 2008, following the major shutdown initiated in 2007. The scientific programmeme was interrupted by two major vacuum leak incidents: the first one happened on a freshly boronised wall and resulted in considerable problems in the plasma breakdown reliability; the second incident was a destruction of a diagnostic window by an uncontrolled ECH beam, resulting in projections of melted brazing material on the carbon tiles and took two months to repair.

3.2 TCV ECH systems

The X2 system for TCV restarted after a 1 year shutdown. The oldest gyrotron magnet no longer operates due to quenching at low current. The cause is being investigated, but may require repair at the factory: the associated gyrotron will not be available for experiments at least until winter 2008-2009.

To save on running costs and optimize the use of resources, the X3 system was not used in 2008. TCV will have ≈1.45MW third harmonic ECRH power available at the plasma and experimental work on the quasi-stationary, high performance ELM-free regime will resume in 2009. The 5 X2 systems will also be available.

The window of the vertical ECE system was damaged during an experiment in September due to excess refraction of an EC beam, leading to a vacuum leak. The protection system related to EC operations is being reviewed by the TCV operations team to avoid this type of event in the future.

All ECH launchers (X2 and X3) on TCV can be steered in real time, and experiments were carried out during the 2008 TCV campaign to control the X2 launchers using the new digital control system. In preparation for this, a detailed characterization of the mirror transfer functions was carried out. The response properties were measured in open loop using a chirp driving function as well as pseudo-random binary noise, both with the vessel at air and under vacuum. The transfer functions of all six launchers were found to be well approximated by a single two-pole function. Possible variations of the time constants with vessel conditions, e.g. as influenced by baking, are being monitored and documented. One gyrotron and launcher were successfully used for real-time feedback control of the sawtooth period and for control of the central x-ray emission.

In addition, a proof-of principle experiment of feedback control of the polarization of ECH waves by rotating polarizers in the transmission line was carried out in collaboration with NIFS-Japan. A series of algorithms were developed both for the control of the polarization state and for the maximization of ECH absorption. Both variants were successfully tested in a low-power set-up, and thus provide good prospects for being applied to the Large Helical Device (LHD) in the near future. This collaboration fits well with a task launched by EFDA for experimental investigation of real-time control of EC polarization on European machines. CRPP will be the coordinator of this work, including purchase of fast polarizers for one X2 transmission line, low power measurements of the 170GHz MOU (RFCU of the 2MW

TED gyrotron) polarizer setup in the European Gyrotron Test Facility, IR measurements of wall heating as a function of polarization and 'data mining' of existing 'sniffer probe' signals.

3.3 Diagnostics

3.3.1 Thomson Scattering

The basic data analysis routines, providing spatial profiles at multiple times of the electron temperature and density in TCV plasmas immediately after each shot, have been revised. With the present computing power available for TCV, more evolved methods may now be used without the penalty of long execution times.

Previously, a fast, lookup-table based, search algorithm based was used to convert different spectral channels ratios into electron temperature values (REM, ratio evaluation method). Although this procedure often provided satisfactory results, under conditions of low signal-to-noise or in case of systematic errors (e.g. caused by variations in detector sensitivity), the REM produced biased or even faulty results, requiring a further analysis.

3.3.2 X-Ray Tomography

During 2008, the soft X-Ray camera was partly redesigned and major changes were implemented. The system comprises of 9 physical cameras with 200 lines of sight. These lines of sight were modified to optimise their étendue and to increase the number of chords intercepting a typical TCV plasma configuration, thus improving the tomographic reconstructions. Figure 3.3.1 shows a tomographic inversion superposed with the flux surfaces reconstructed by the LIUQE Grad-Shafranov solver (right). On the left-hand side, the core peaked emission is observable. This state represents the ramp between two sawtooth crashes. Thanks to the number of chords, it is possible to increase the spatial resolution of the reconstruction, in comparison with the previous system. For the same discharge, TCV #35944, a mode is identified in the form of sawteeth precursor (Fig. 3.3.2), which can be analyzed with XTOMO. This is an m=1 mode, as expected in the case of q=1 sawteeth activity.

The previous aged detectors were replaced. The new detectors preserve the geometry and size and benefit from a new manufacturing process that is expected to prolong their relative calibration factor (between detectors) for a larger number of pulses. The new detectors were calibrated using a X-ray medical source and their pre-amplifier electronics update to use state-of-the-art operational amplifiers that increase the bandwidth of the system.

The data acquisition system was also upgraded, allowing 250kHz sampling rates (routinely acquired at 100kHz). The improved time resolution will be invaluable for diagnosing fast MHD events and edge instabilities like ELMs.

A comparative study showed that non-linear least-square fitting methods will produce more reliable reconstructions by making use of the information from all signal channels with the advantage of being less vulnerable to "outliers". Using tailored weighting factors in the evaluation of the error cost function, the influence of "bad signals" and systematic errors in calibration data was reduced. Persisting

incompatibilities are detected by reverse processing of the results via a comparison of the expected with the measured signals in each spectral channel.

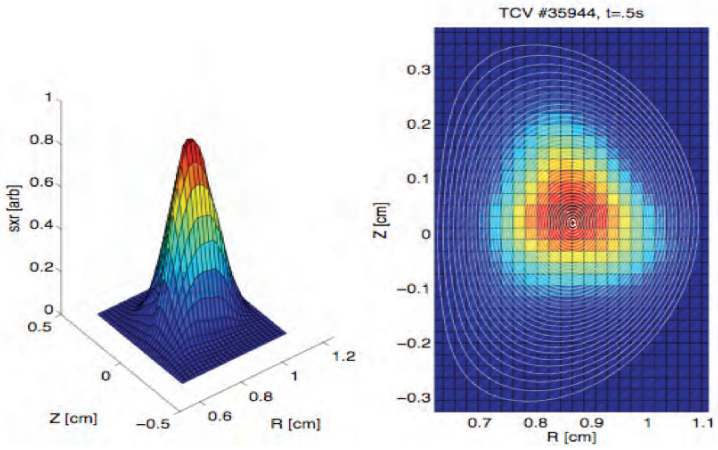

Fig. 3.3.1 *TCV shot #35944, SXR tomographic inversion between two sawteeth crashes. On the left hand side the peak in the core is visible, whereas on the right a cross section of the emission is reported (red = higher emission) with LIUQE reconstruction superposed.*

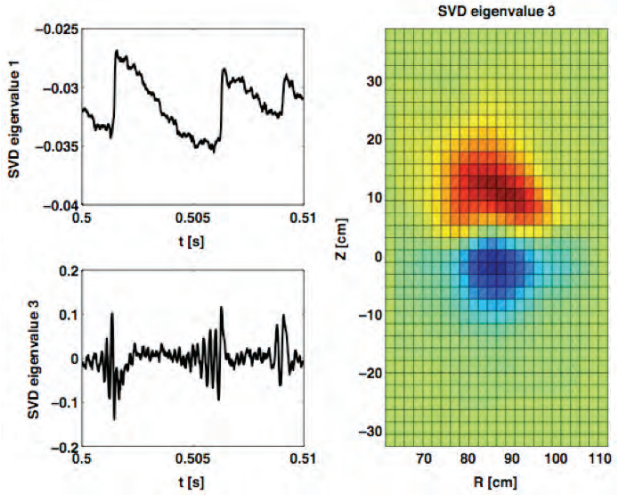

Fig. 3.3.2 *TCV #35944, identification through SVD of inverted SXR system of a m=1 precursor-type mode.*

3.3.3 FIR Polarimeter

A new far-infrared (FIR) polarimeter diagnostic is currently under construction and installation on TCV using a recycled dual cavity far infrared laser pumped by a CO_2 laser. The diagnostic will be used for measurements of the magnetic field distribution and hence the current density in the TCV plasmas.

During 2008, work has been directed mostly toward component manufacturing, testing, installation, alignment and system integration. This work includes the waveguides from the laser room to the torus, a 5-way beam splitter below the TCV vessel and a detector assembly above (Fig. 3.3.3). The detector electronics and the control system for semi-automatic operation of the CO_2-FIR laser system have been

designed and built. The commissioning of the system has unfortunately been delayed by a major failure of the CO_2 pump laser, which necessitates partial rebuilding and retrofitting of additional safety interlocks. The diagnostic is planned to be operational in early 2009.

Fig. 3.3.3 *Detector and focussing lens assembly for the FIR polarimeter diagnostic. There are 2 detectors and 2 lenses for each of the 5 beams crossing the plasma.*

3.3.4 Diagnostic Neutral Beam

Following the replacement of the DNBI RF-plasma generator by an arc-plasma source in October 2006 a re-optimised ion optical system (IOS) was installed in DNBI-TCV in February 2008. The optimisation of the regime of the ion source resulted in a reduction of the beam size in the plasma from 7 to 4cm (beam radius on 1/e level), Fig. 3.3.4. This upgrade is expected to increase the upper plasma density range of CXRS measurement from ~$7\times10^{19}m^{-3}$ to $10^{20}m^{-3}$.

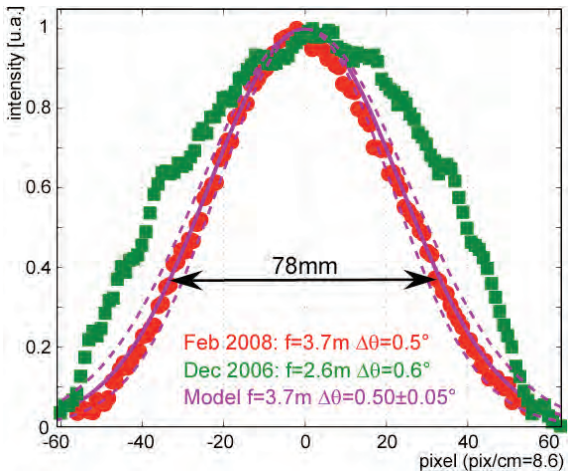

Fig. 3.3.4 *Beam profiles in the TCV at 420cm from Ion Optical System (IOS).*

The DNBI on TCV was delivered together with a local control system (LCS). All functions necessary for safe DNBI operation are included in the LCS which is designed to protect itself from externally generated dangerous situations. The DNBI can operate either under supervision of the TCV central control system, or independently (in local mode), controlled from a local PC for tests and

commissioning. About 40% of beam discharges are used for conditioning, optimisation and tests without TCV activity. To date, the DNBI LCS was housed in CAMAC modules, with the timing and other beam parameters pre-set by the DNBI control software. The introduction of the arc discharge plasma source required changes in the control and acquisition and modification of the LCS. A new control system, based on industrial PCI cards of National Instruments Corporation and LabView, was developed, comprising ~140 input/output channels. The timing panel of the new DNBI-TCV Local control programme interface is shown in Fig. 3.3.5.

Fig. 3.3.5 *Timing panel of the DNBI Local Control Programme*

3.3.5 Tangential X-Ray detector array

A 6-detector, tangential X-ray diagnostic has been designed and built in collaboration with RRC-Kurchatov Institute (Moscow, Russian Federation). The goal of the diagnostic is to investigate the dynamics of suprathermal electron generation, with special emphasis on fast transient events, such as runaway electron production and electron acceleration during magnetic reconnection processes associated with resistive MHD phenomena (primarily sawtooth crashes and disruptive instabilities). The diagnostic assembly can be rotated in two directions, using motorized drives coupled to vacuum bellows (Fig. 3.3.6), effectively enabling observation along virtually any chosen direction for the vast majority of TCV plasma discharge configurations.

The diagnostic was installed in late 2007 and the TCV-side vacuum interface, provided by a 0.127mm thick Beryllium window, was added in April 2008. The data acquisition units and attendant cabling were installed and tested in July 2008. In October 2008 the controller unit for the motorised drives, as well as the detector amplifiers, were calibrated and tested, and the system is now ready for operation.

Fig. 3.3.6 *View of the X-ray diagnostic.*

3.3.6 Hard X-ray camera

A multi-chord CdTe hard X-ray (HXR) camera (Fig. 3.3.7), used on TCV during several separate periods between 1999 and 2005 on loan from CEA-Cadarache, is set to return once again to TCV at the end of 2008 following an agreement between CEA and CRPP. The instrument is planned to remain at CRPP until Autumn 2009, with a further extension possible. The camera is employed as a spectroscopic system with energy resolution ~8keV in the 10-200keV range and is used to diagnose the suprathermal electron population generated by electron cyclotron heating and current drive. Important results on the spatial transport of suprathermal electrons were obtained using this diagnostic in the past, and the instrument remains extremely valuable both as a survey diagnostic and for further physics studies, particularly in the upcoming campaign of third harmonic EC heating.

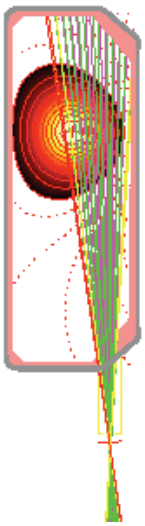

Fig. 3.3.7 *Geometry of the hard X-ray camera on loan from CEA.*

3.3.7 Hard X-ray tomography

The conceptual design of a spectroscopic hard X-ray tomography diagnostic has been completed in 2008. This envisioned system comprises up to 4 cameras of typically 20 detectors each, distributed around the poloidal plane to provide the possibility of tomographic inversion. The primary goal is to extend the studies of suprathermal electron dynamics performed previously on TCV to a full 2D

reconstruction. It is expected theoretically, and has been seen experimentally, that Bremsstrahlung emission from the suprathermal population is not poloidally symmetric, owing primarily to the presence of trapped particles. A full experimental study of this asymmetry would be performed for the first time on TCV with such a system. The design uses CdTe detector technology, with typically 7-8keV resolution in the 5-200keV energy range, and a novel radial Soller collimator concept to maximise the étendue uniformity across the arrays. We have now moved to the final production design stage for the first camera, to be located in a port on the TCV midplane (Fig. 3.3.8). The design incorporates up to 36 selectable Al attenuator thicknesses, to obtain unsaturated signal rates for the highly variable fluence range observed in TCV. In addition, the whole port assembly can be rotated by 90 degrees, to switch between poloidal and toroidal lines of sight, for greatly increased physics potential in the study of distribution function anisotropies. It is planned to build and commission this first camera during 2009.

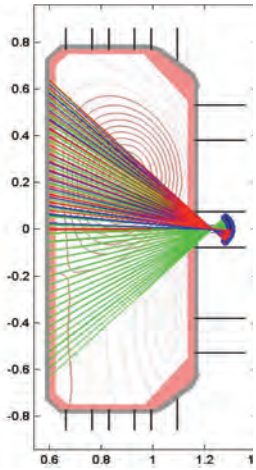

Fig. 3.3.8 *Geometry of the first component of a planned hard X-ray tomography system.*

3.3.8 Tangential phase contrast imaging

A laser imaging apparatus has been installed on TCV to study core density fluctuations with high spatial localisation (down to 1% of the minor radius), thanks to a tangential viewing arrangement (Fig. 3.3.9). The diagnostic is based on a 7-cm wide, 10.6-μm wavelength CO_2 laser beam launched through the plasma and subsequently analysed through a phase-contrast filter and imaged onto a 30-element photoconductive detector array. The accessible wave-number range, from 0.9 to 60cm^{-1}, spans the spectrum of ion- to electron-dominated turbulence (ITG, TEM and ETG modes), opening for the first time the possibility of a thorough study of core turbulence in plasmas with strong electron heating.

All the in-vessel components were installed in the course of 2008 with the design of the imaging optical system completed in early 2008. The remaining components have been procured, including the external optics and attendant supports, an optical table, a laser focus stabilisation system and the data acquisition electronics. The final optics supports will be installed in 2008 and alignment and commissioning will immediately follow, with first data expected before the end of 2008.

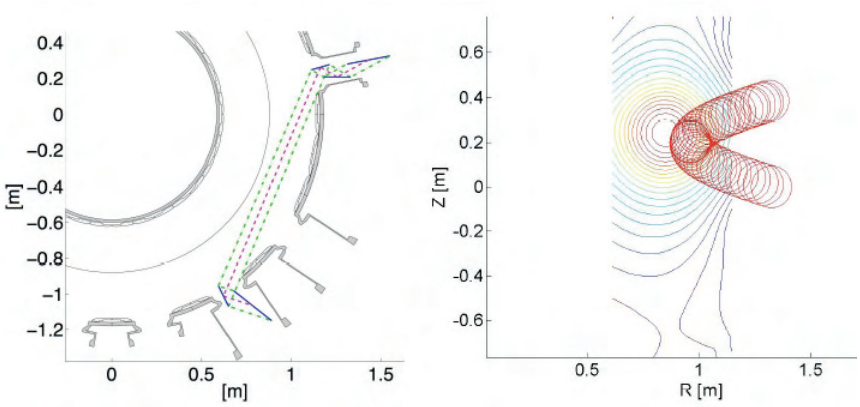

Fig. 3.3.9 *Typical laser beam trajectory in the tangential phase contrast imaging diagnostic: top (left) and poloidal (right) views*

3.3.9 Microwave reflectometer

The single-frequency homodyne reflectometer recently installed on TCV has been equipped with a new microwave coupler and mechanical support system. The microwave coupler consists of a telescope and scalar horn to convert efficiently from a fundamental W-band waveguide to an overmoded 63.5mm diameter HE11 waveguide, and vice versa. The HE11 mode is in turn optimised for coupling to the spare 2nd harmonic steerable ECRH launcher that is used as the single monostatic antenna for this system. The support system is a more robust, easy-to-align structure than the temporary one used in the initial tests. The diagnostic is now ready for operation.

3.3.10 Lower-Hybrid Parametric Instability Probe

An antenna for EM waves in the 0.5-1.5GHz range (and in particular the Lower-Hybrid Parametric Instability range) has been recently installed on TCV. The probe is directly connected to an analogic spectrum analyser. The analyser operation and analogic acquisition parameters are remote-controlled by a GUI interface via a PC. The local oscillator sweep and the amplitude signal are then digitized at a 200-kHz rate. The full equipment has been successfully tested with test signal.

3.3.11 Correlation ECE Diagnostic on TCV

The two-channel correlation ECE diagnostic on TCV has been upgraded to improve its performance in diagnosing the broadband temperature fluctuations, as well as high-frequency MHD and/or fast particle driven modes.

At the intermediate frequency stage, each of two correlation ECE channels is detected by means of Schottky diode detectors, and then split into three independent branches with different video filter characteristics: 0–600kHz, 4th order; 40–250kHz, 4th order; 0–40kHz, 3rd order.

New measurements performed by the upgraded correlation ECE diagnostic showed the presence of broadband temperature fluctuations with their amplitude increased

from the plasma centre towards the edge (Fig. 3.3.10). Measurements were taken in Ohmic and ECRH plasmas.

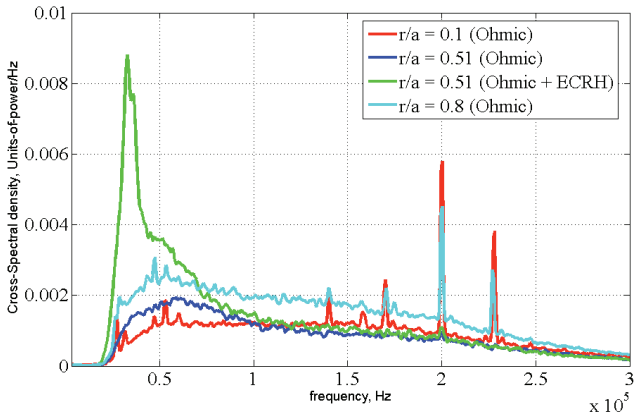

Fig. 3.3.10 *Measurements of the broadband electron temperature fluctuations by means of the upgraded correlation ECE diagnostic on TCV.*

3.3.12 Compact NPA

The compact NPA spectrometer is now installed on a port that does not directly see the DNB neutral beam and can be positioned to observe the plasma along a radial or a tangential chord in the TCV chamber midplane. This arrangement will be used to measure the fast ion distribution during strong ECH heating.

3.3.13 Charge Exchange Spectroscopy

The charge exchange spectroscopy diagnostic has been upgraded with new fibre optic bundles permitting up to 40 chords for both the toroidal and poloidal observation cameras (Fig 3.3.11). The recently implemented RealTime control system has been programmemed to detect the time of the X-ray sawtooth crash and provide a series of trigger pulses to a fast acquisition algorithm on the CXRS diagnostic (Fig 3.3.12).

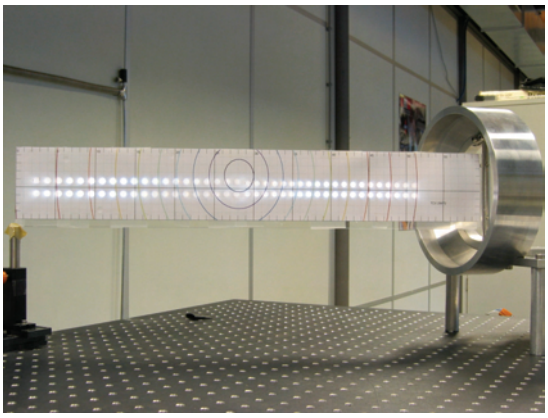

Fig. 3.3.11 *Backlit projection of the fibre optic observation chords onto a paper target that indicates the position of a centred configuration's flux surfaces.*

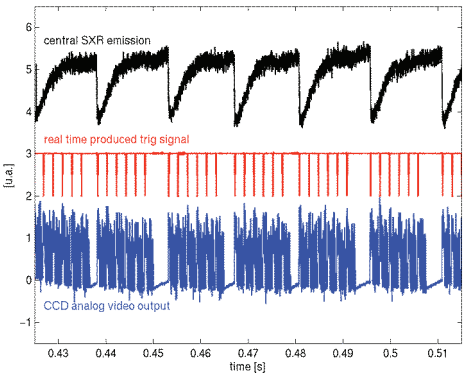

Fig. 3.3.12 *Control of CXRS acquisition. The sawtooth crash is detected generating the CXRS trigs (red)*

3.3.14 SPRED UV-Spectrometer

A soft iron cage has been successfully installed around the MicroChannel based detector on the SPRED spectrometer. The proximity of the detector to the TCV magnetic field was resulting in focussing errors and a dynamic displacement of the spectrum across the detector during plasma discharges.

3.3.15 Fast Injection Valve

The disruption mitigation valve (DMV) is a fast gas injection system capable of delivering short (down to 1 ms) gas pulses with a repetition rate up to 1 kHz. Key elements of the system are a solenoid valve, a bell shaped exit nozzle and a skimmer. The gas, after exiting the valve, is collimated by the nozzle and is subsequently "peeled" by the skimmer, i.e. the cutting the turbulent edge of the mainly laminar main beam. The result is a well collimated gas pulse with fast rising and falling edges. The number of particles contained in one pulse depends on the gas type, backing pressure and pulse length, and is typically around 10^{20} in a 5 ms pulse. Four gases are planned for initial operation: deuterium, helium, neon and argon.

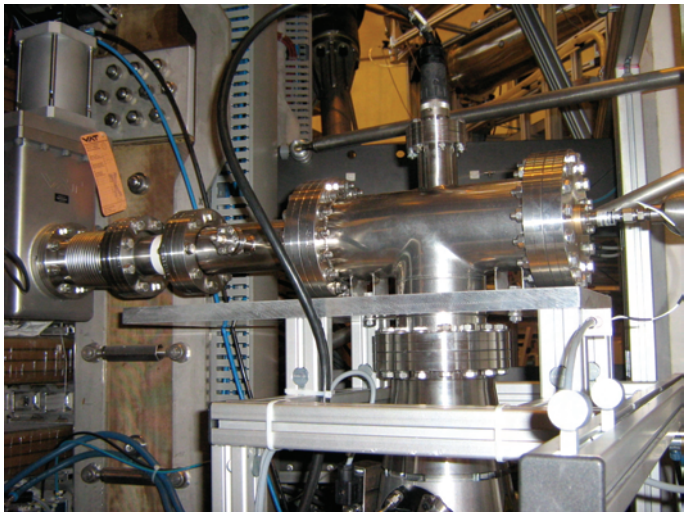

Fig. 3.3.13 *DMV installation on TCV*

3.4 TCV control and acquisition

TCV is developing pre-programmemed and real time control tools for optimising plasma performance in advanced tokamak scenarios, through manipulation of the pressure and current profiles and of the plasma shape. Two new real time controllers have been developed and installed.

3.4.1 Advanced Plasma Control System (APCS) Digital Signal Processor (DSP) system

The final version of the hardware and firmware of the 36 DSP system built by the IST (Lisbon, Portugal) was delivered in December 2007. Since then this system has been fully integrated in the TCV plasma control system, with appropriate electronics and wiring to accommodate additional input and output signals. Its integration in the TCV plant control is finished and reliability tests are presently carried out in parallel with the old control system and was used in several TCV plasma shots. Progress has been made in the definition and implementation of the required data structure to incorporate the new programmeming capabilities in the plasma design phase of the shot preparation. Particular care was given to implement a structure that can easily evolve to follow changes in the control system hardware and to incorporate new control strategies and algorithms. This will facilitate setting up real time control tools of the plasma shape and of the ECH system to optimise the plasma performance in advanced scenarios. The focus has now switched to optimizing the plasma control algorithms for digital control.

3.4.2 Real Time massive diagnostic analysis

The second system provides a distributed massive real time analysis at the diagnostic level to generate elaborated physical quantities for both the supervision and the control of the plasma as well as for the study of advanced operation modes.

Two DTACQ 196 channel acquisition cards were purchased, together with a modern Intel dual-core cPCI computer card. This system has been extensively tested and was shown able to acquire 196 channels and provide up to 32 output signals with an ~10us cycle time. By acquiring a single X-ray diode signal from TCV, this system has been successfully used to measure the sawtooth period in real-time and generate a proportional signal to change the angle of an ECH X2 mirror. Other projects are being developed around this hardware base, from the control of the TCV breakdown phase to a real time magnetic surface reconstruction (real-time LIUQE).

The first application of digital ECRH launcher control was carried out by employing an algorithm to control the characteristics of sawtooth relaxations. ECRH deposited in the vicinity of the q=1 surface is well known to strongly affect the sawtooth period and amplitude, depending on the exact radial location relative to the surface. Algorithms were developed to control the sawtooth period and were successfully tested online in experiments demonstrating real time control of the sawtooth period: the system adjusted the EC launcher angle until the observed period obtained the requested value.

3.4.3 Data acquisition evolution

Data acquisition on TCV has been a combination of well tested CAMAC based systems and considerably more recent multichannel systems for the acquisition of many channel diagnostics. The legacy CAMAC equipment that provides highly modular and distributed acquisition using EtherNet or SerialLink communications now accounts for a large proportion of the total acquisition time for a TCV discharge. Reducing this acquisition time allows the operators more time to design the following experiment and thus increase productivity i.e. more plasma discharges per working day.

Simultaneously, TCV's initial choice of computing hardware is approaching the end of its useful life so a solution to acquiring the legacy CAMAC faster and current hardware was sought. The final solution involved a relatively cheap X86 based computer connected to the CAMAC crate using a SCSI-based crate controller from Jorway (USA). Since these computers are essentially lower power PCs, they could be operated using the same software as that used to run TCV with a high degree of autonomy. In contrast to the serial CAMAC controllers, noted above, that acquire each CAMAC crate in turn, each of our ~20 crates can be acquired simultaneously.

To date ~9 of the most populated CAMAC crates have been equipped with these SCSI controllers that routinely achieve transfer rates of ~1.3Mbytes/second compared to the old serial system that achieved only 0.3Mbytes/second. The final goal is to equip the remaining CAMAC crates to achieve a total data acquisition time of less than 2 minutes to be compared with acquisition times that can exceed 12 minutes.

3.5 TCV upgrades

The TCV team is currently investigating a range of possible upgrades to further enhance the potential of the facility for delivering fusion relevant research in the medium and long term. The issues CRPP wishes to address include ELM control, heating at high density and to high plasma pressure, ion heating, fast ion physics, as well as confinement and stability of shaped plasmas potentially able to provide superior performance, such as presented in section 2.1.9. The systems under consideration include a saddle coil system useable for resonant magnetic field perturbations, error field correction and fast vertical position control, an upgrade to the X3 heating power, a neutral beam heating system, active MHD antennae and a set of low field side heat load tiles allowing for negative triangularity divertor configurations. Three of these systems will require a complete refurbishment of the inside of the low field side vessel walls (the saddle coils, high heat load tiles and the active MHD antennae) and are being considered as a package. Design of the tiles will be carried out after the completion of the conceptual design of the saddle coils and the active MHD antennae.

The projects detailed below are to become proposals for preferential support. Implementation of all or part of the projects will depend on the availability of financial support at Swiss and European levels.

3.5.1 Saddle coil system

The upgrade project for TCV includes the installation of an ITER-like set of saddle coils for ELM control, error field correction and vertical control. A large variety of geometrical arrangements have been qualified, including ex-vessel and in-vessel coils. The ex-vessel solution was discarded due to a large distance from the plasma and the screening of the conducting vessel for AC operation, both implying an excessively large coil current. For the in-vessel option, given the toroidal periodicity of TCV and the large variation in the plasma shape and position, a set of three rows of 8 coils is envisaged. This coil configuration was shown to produce the adequate edge magnetic ergodisation and to offer the required flexibility for an experimental approach of the ELM control and mitigation method using saddle coils. Experimental values provided by DIII-D and JET and island overlap calculations indicate that ELM control would require 4kA-turn, while for vertical stabilisation currents of the order of 5kA-turn are required. Error field measurements indicate that its correction would also require 3kA-turn. The power supply system necessary to provide these features is still under study, but the actual approach is based on a single fast power supply, providing the vertical control, combined with multiple slow power supplies for the other features.

An electrical model combining the coils, the vessel and the plasma has been developed and used to calculate the magnetic screening due to the vessel, the effective inductance of the coil system and the forces applied on them during operation. A Lagrange method has been developed to determine the optimal current distribution between coil rows. Due to the impact of the installation of these new coils on the low field side wall of TCV, the conceptual design is developed together with other modifications of the LFS components of the TCV vessel, namely, the replacement or the suppression of the internal vertical stabilisation coils, the compatibility with the TAE excitation antennas, the upgrade of the carbon tiles to sustain divertor strike points with negative triangularity shapes.

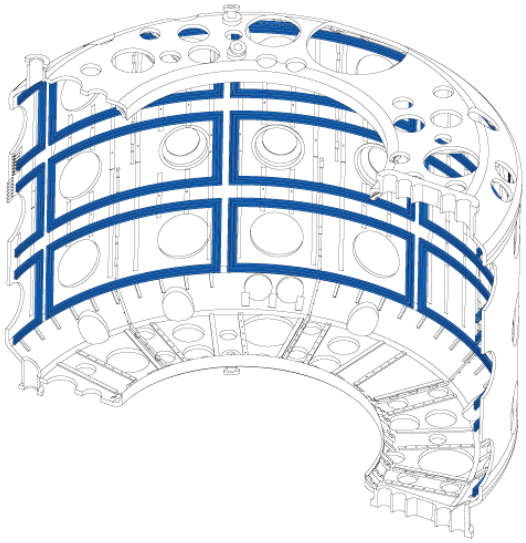

Fig. 3.5.1 *Saddle coil system for TCV*

3.5.2 Upgrade of X3 heating systems

With regard to the study presented in 2007, the reference plan for the upgrade is maintained and basically consists in adding, to the existing 0.5MW/118GHz gyrotrons, 3 additionnal 1MW gyrotrons operating at 126GHz and injected in TCV with the present top-launcher. This frequency is compatible with an operation on a different cavity mode of the 140GHz gyrotron developed and manufactured within the EU for the electron cyclotron heating of the W7-X stellarator.

The three existing 118GHz gyrotrons would be connected, via new microwave switches, to the X2 transmission lines for an X3-LFS injection. It is foreseen that the superconducting magnets (SCM) needed for operating the 3 new 126GHz/1MW gyrotrons would be cryogen-free, hence, compared to SCM's with a liquid helium bath, the operational costs would be significantly lowered. Cryogen-free SCM's are also ITER relevant since they are required by the new reference design for the ITER ECRH-ECCD system.

3.5.3 Feasibility studies for neutral beam injection in TCV

An important requirement for TCV is to become capable of heating plasmas at relatively high density and β and to be able to vary the Ti/Te ratio over a wide domain including the case of equal temperatures. The only way this can be achieved in a relatively small device is to supplement the existing electron heating with direct ion heating in the form of neutral beam injection (NBI). In addition, the availability of neutral beam heating enables the pursuit of physics investigations in several areas of MHD (fast particle modes, Neoclassical Tearing Modes, Resistive Wall Modes) , heat transport and momentum transport.

TCV presently has two 15cm diameter ports available, with access to the plasma at an angle of 11.5 degrees (measured at the port centre) for a neutral beam, like the existing diagnostic neutral beam. In addition we are considering using a near-tangential injection geometry trough a 10cm diameter port with an axis having a tangency point a few millimetres outside of the inner wall tiles, which define the inner vessel aperture radius (R_{IW}=64.5cm). Preliminary contacts with one potential supplier suggest that the 15cm port may be equipped with injectors capable of delivering up to 1MW at vessel entry, while the smaller near-tangential port may be suitable for up to 600kW.

Heating of the inner wall tiles as a result of shine-through is a serious limitation in the case of the near–normal injection. As a result, operation of the beam would have to be restricted to electron densities in excess of about $5\times10^{19}m^{-3}$ with the present un-cooled tiles at the inner high field side vessel wall. Replacement of these tiles with high heat flux components would somewhat alleviate this constraint.

Figure 3.5.2 shows the heating efficiency for a 20keV deuterium beam as a function of line average density for currents from 95kA (blue) to 500kA (black) for three tangency radii. It is determined by both shine through and orbit losses calculated using a Monte-Carlo orbit code following the ions as they slow down and undergo pitch angle scattering. The two figures on the top correspond to the tangential system and a practical tangential system would have en efficiency between those two cases. The efficiency of a tangential system would lie between those shown for R_{tan}=60 and 70cm (upper left and right of Fig. 3.5.2). Typically X2 experiments are performed at $\langle n_e \rangle < 2\times10^{19}m^{-3}$ and I_p<200kA. A tangential system would allow

experiments at the lowest currents and densities, as used in much of the steady state scenarios with X2 ECCD, at efficencies of around 50%. Near-normal injection (bottom of Fig. 3.5.2) is suitable for H-modes and shaped plasmas at high density and current. In these plasmas it can be used together with X3 ECH. However, this geometry is unsuitable for low densities and for low plasma currents, i.e. for synergetic experiments with X2 ECH and ECCD.

At the lowest densities, fast particle residence times can be of order of 100ms, leading potentially to the build-up of substantial fast ion populations corresponding to a normalised fast beta $\beta_{Nf}=\beta_{Tf}I_p/(aB_T)\sim1$ for 0.5MW using tangential injection, which is highly likely to lead to fast particle instabilities. At the high density, high current end of the TCV operating domain, an injection of 2.6MW (of which 2MW with $R_{tan}=0.23$) would lead to β_{Nf} of around 0.4, which is a substantial contribution to the plasma normalized pressure. Hence there is a potential for investigation fast particle physics in TCV, including in plasmas where localised X2 ECCD can be used to counteract the stabilising effect of fast particle on sawteeth. The tangential system could also be used for the study of TAE modes excited by the $v_{bT}=v_A/3$ resonance and even the $v_{bT}=v_A$ resonance, if the injector can be designed to operate also at 50keV with hydrogen. The injectors can provide a torque of some 0.3Nm, which is estimated to be sufficient for rotation and RMW control experiments, if the two near-normal injectors are installed such as to provide opposite torques.

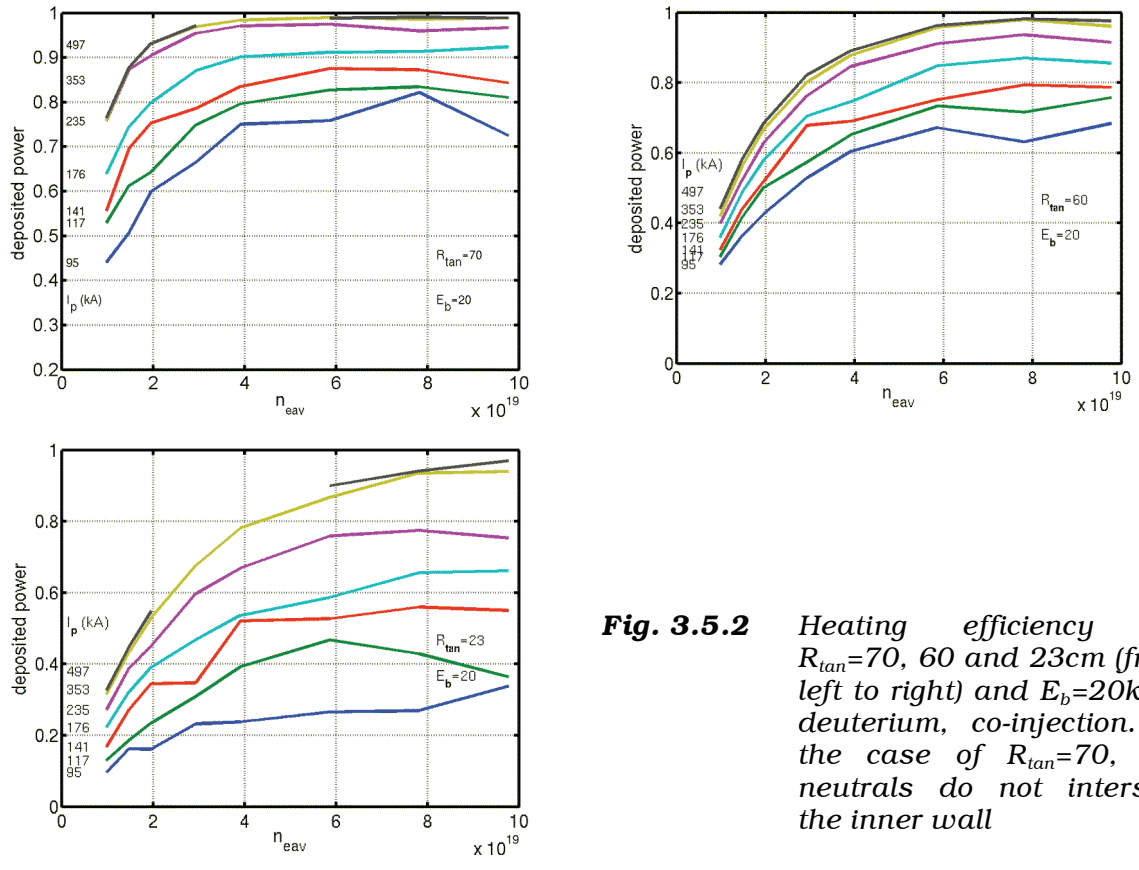

Fig. 3.5.2 *Heating efficiency for R_{tan}=70, 60 and 23cm (from left to right) and E_b=20keV, deuterium, co-injection. In the case of R_{tan}=70, the neutrals do not intersect the inner wall*

3.5.4 Active MHD antennae

A proposal has been made to develop fast ion physics tools for TCV, which may involve a set of antennas for heating in the Ion Cyclotron range of frequencies (ICRF) and another set of antennas for the excitation of waves in the Alfvén

frequency range. The study of the ICRF system has been put on hold because of concerns about system intergration in the TCV vessel and orbit confinement of fast ions. However, if a tangential NBI systems is implemented, large populations of fast particles susceptible of resonating with Alfvén waves will be produced at the appropriate plasma density and field. The proposed system would use a set of AW antennae placed on the low field side wall such as to excite a broad range of radially overlapping modes with intermediate toroidal mode numbers, aimed at producing a controlled redistribution of the fast ion population, such as to avoid deleterious MHD instabilities. In a reactor, such a system could serve to prevent the occurrence of potentially dangerous alpha particle driven modes and hence assist in burn control.

3.6 Superconductivity

3.6.1 Improvement of the measuring technique accuracy in the Sultan samples

The current sharing temperature, T_{cs}, detection by voltage taps is affected by the presence of *early voltages* roughly proportional to current (*voltage slopes*). The slopes change in amplitude as a function of the background field, loading history and operating temperature. In the worst cases, the voltage at nominal current is comparable or even higher than the voltage criterion for T_{cs}. No measurable power (temperature increase) is associated to such voltages (*transverse voltages*) and post-processing methods have been proposed to reduce the impact of these slopes on the assessment of the T_{cs}.

In the assumption that the strands inside a sub-cable are at the same potential and the early voltage arises from current unbalance only among sub-cables, pairs of *voltage stars* were introduced in the sample instrumentation, see Fig. 3.6.1, to detect the voltage along each individual sub-cable. The results showed that the slopes do not disappear, but the average of six signals has a slope that is always lower than the maximum slope of a single voltage pair. Several distances among the taps have been implemented to test the impact of this parameter. The best results have been obtained with the taps closest to the high field region. For longer length the noise is higher and the measured VT transition is highly distorted.

The average signal of the stars after the subtraction of the slope is retained as the best guess to evaluate the T_{cs}. The assessment of the linear slope is limited to the low current level, $\leq$ 30 kA, and its accuracy varies from sample to sample. The standard deviation of the different T_{cs} evaluated with the individual star signals after the subtraction of the individual slopes, in the range of ±0.04 K to ±0.2 K, gives a measure of the advantage of using the average of six signals rather than a single voltage pair.

Two main hypotheses have been formulated to explain the origin of the slopes. The first assumes that the current redistribution, responsible of the slopes, happens in the joint and is caused by the current unbalance among the strands. In this sight the cure would be reducing the current unbalance or/and the inter-strand resistance inside the joint. In summary this first hypothesis states that the slopes are an artifact of the SULTAN sample and no information related to the cable or strand performance is carried by those signals. The second hypothesis invokes the presence of filament breakages randomly distributed along the strands, which may cause voltage traces similar to the ones usually measured, even if the sample is

equipped with an ideal zero resistance joint. In this case the slopes would bring highly relevant information about the status of the strands in the cable.

To investigate this latter hypothesis inter-strand resistance measurements in Nb_3Sn cable terminations prepared with the same procedure were performed and showed very low resistance, assuring therefore an effective current redistribution at the joint at voltages below the criterion. Some simple circuital models confirm this statement.

Continuous improvement of the temperature sensors and their installation on SULTAN samples for reliable temperature readings over the last two years led to a sound mounting method of commercial zirconium oxynitride films (Cernox™), which enssures an optimal thermal contact between the conductor and the sensor. All Cernox™ sensors used on SULTAN samples are calibrated by the manufacturer with an accuracy of ±5mK. An evaluation of the precision and reproducibility of the current sources and the amplification chain up to the analogue to digital converter, as well as potential thermal voltages, led to the conclusion that the absolute error of the temperature readings is typically ±30mK, primarily originating from offset errors of the amplifiers and thermal EMFs, the last one assessed by switching the polarity of the sensor current. The Cernox™ sensor magneto-resistance at 9T is -0.6% at 8K (50mK) and -0.26% at 4.2K (11mK). Observations of the temperature reading variations from run to run (possibly separated by days) showed that the measurements typically lie within a range of ±10mK, at the same operating conditions. The reproducibility of the readings is thus significantly higher than the absolute accuracy, allowing detailed observations of relative temperature changes, in the range of few mK.

Such an enhancement in the thermometry accuracy has made viable an alternative method for the assessment of the conductor performance, based on the calorimetric evaluation of the Joule power generated during the current sharing regime, W_{cs}. The governing relation for the W_{cs} in steady state and neglecting the conductivity of Cu along the strands is

$$W_{CS} = \dot{m}\left[h\left(p,T\right)_D - h\left(p,T\right)_U\right], \qquad (1)$$

where $\dot{m}$ is the He mass flow rate, h is the He enthalpy as a function of the pressure p and temperature T. The subscripts "U" and "D" refer to the upstream and downstream location, respectively. In the nominal conditions for the T_{cs} tests, E=10μV/m $\dot{m}$=2g/s, I=68kA, the power generated by current sharing at the 0.45m conductor length exposed to high field is 306mW, which corresponds to a temperature rise of 30mK.

The temperature is measured by thermometers installed at ± 400mm from the field center, at 9T magnetic field. Four sensors are applied at the same longitudinal location, see Fig. 3.6.1 middle, and the average temperature ($T_{ave,U}$, $T_{ave,D}$) among them is retained for the analysis. The redundancy in the thermometry is aimed to smooth thermal gradients across the cable. The measured average temperature differences in controlled conditions (i.e. B=11T and I=0kA when the power generated in the HFZ is null) are base-lined to zero by subtracting a 3rd degree polynomial fit of $T_{ave,D}$–$T_{ave,U}$. Such a procedure limits the deviation from the zero power level to few tens of mW. The uncertainty on the mass flow rate, estimated to be 5%, is also taken into account.

The agreement between the calorimetric and voltage methods, see Fig. 3.6.1 right, is very good, especially at the T_{cs} criterion, where the discrepancy is <0.1K. The error bar for the calorimetric method in this case is ±0.1K, since the cable n index is 16 and the transition is moderately sharp.

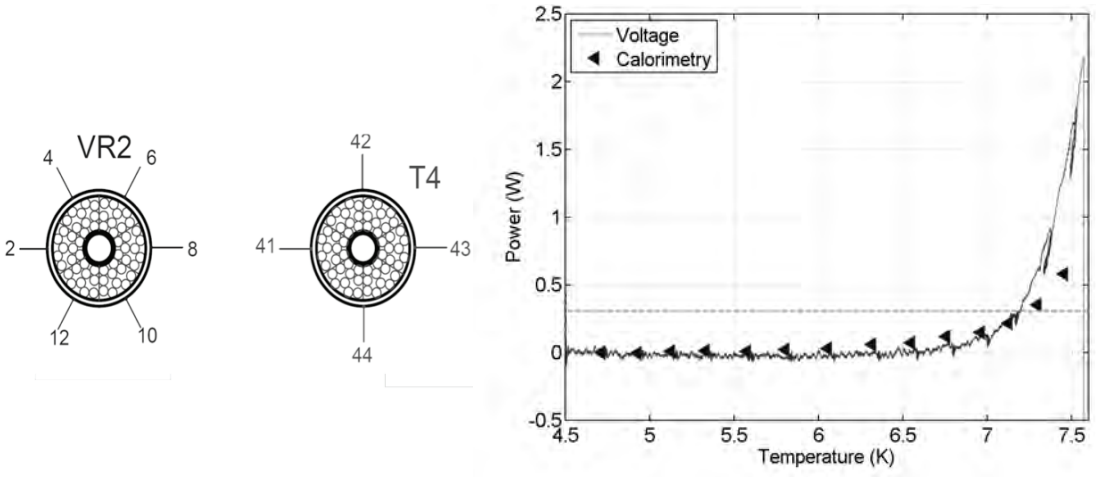

Fig. 3.6.1 *Left: Location of the voltage stars (e.g. VR2) and of the temperature sensors (e.g. T4) in the SULTAN samples Right: Comparison of electric field vs. temperature for calorimetric and voltage taps method.*

3.7 Gyrotron for Dynamic Nuclear Polarization Enhanced Magic Angle Spinning Nuclear Magnetic Resonance[1]

The project, started in 2007 and aimed at a preliminary design of a frequency tunable gyrotron for Dynamic Nuclear Polarization (DNP) enhanced Magic Angle Spinning (MAS) Nuclear Magnetic Resonance (NMR) Spectroscopy, has been intensively pursued in 2008.

Based on this preliminary design it has been decided, beginning of 2008, to submit two research proposals to the Swiss National Science Foundation (SNSF).

The first proposal entitled 'Gyrotron for Dynamic Nuclear Polarization Enhanced Magic Angle Spinning Nuclear Magnetic Resonance Spectroscopy' has been submitted as a 'Requip' request to SNSF for financing the hardware (gyrotron, superconducting magnet, HV power supplies and diagnostics) needed to develop and integrate the frequency tunable gyrotron oscillator into a 400MHz NMR spectrometer.

The second proposal, entitled 'Dynamic Nuclear Polarization Enhancement of Magic-Angle-Spinning Nuclear Magnetic Resonance Spectroscopy using gyrotrons', consists in a three year research programmeme aimed to the development of the RF sources for this type of application (including oscillators and amplifiers) and, in addition, to the development of the associated spectroscopy techniques used in DNP-MAS/NMR. To carry out this research programme a 'Sinergia' grant request has been submitted to SNSF for essentially covering two post-doc positions to conduct the necessary R&D.

These SNSF funding requests have been jointly submitted by three laboratories within EPFL (Centre de Recherche en Physique des Plasmas, Laboratoire de

[1] Work not belonging to the EURATOM Association's work programmeme.

physique des matériaux nanostructurés and Laboratoire de résonance magnétique biomoléculaire) and both have been awarded by SNSF.

Presently, the detailed specifications of the major components of the gyrotron (gyrotron and superconducting magnet) have been finalized and the associated tendering procedures have been initiated. The complete gyrotron source is planned to be fully characterized in the fall 2009 and the integration on a NMR spectrometer shall be completed in the first quarter of 2010. In parallel, the procedure for hiring two post-docs is under way.

4 DIRECT SUPPORT FOR ITER BY CRPP

4.1 Introduction

In this section we assemble a large fraction of the work performed by the CRPP in 2008 for the ITER project, in view of the increasing importance of the work undertaken over the last few years. Since most of the research programmeme of CRPP is linked to fusion development in general, and therefore to ITER in particular, the distinctions are sometimes artificial and work for ITER still appears throughout the report. However, we have identified those areas in which the work carried out is clearly in direct support of the project, including:

2 The development of the European Gyrotrons
3 The ITER Gyrotron test stand at CRPP
4 The ITER Upper Launcher for Electron Cyclotron Waves
5 The use of SULTAN for developing and testing ITER superconductors
6 The development of the ITER magnetics diagnostic
7 The development of the ITER CODAC design
8 Contributions to the International Tokamak Physics Activities, now under ITER authority
9 Contributions to ITER committees
10 Development of ITER full tokamak simulations

4.2 Development of the European gyrotrons

4.2.1 Summary of the results

The first prototype 2MW/170GHz/CW Coaxial gyrotron was tested for a period of 11 months extending from November 2007 to September 2008, under the EFDA task agreement TW6-THHE-CCGT1. Due to the delay in the delivery of the superconducting magnet (SCM), the initial planning had to be revised, and it was decided to renounce some of the tests, involving the RF Conditioning Unit (RFCU) or the transmission lines. Figure 4.2.1 is a view of the experiment with the CNR Short Pulse Load installed (CNR-SPL).

The target we were aiming at with the first prototype was 2MW/1s at 170GHz.
The performance level which could be reached was

- 1.4MW/0.5ms in a very short pulse,
- 0.5MW/60ms after pulse extension.

The power level limitation could be due to a poor electron beam quality, possibly setting an upper bound to the accessible range of the electron beam pitch angle parameter, β_{perp}/β_{ll}, and consequently of the voltage and RF power. In addition the high level of stray radiation (originating at the launcher system and possibly at the beam tunnel, as well as the reflections from the dummy load) can limit the oscillation range.

Fig. 4.2.1 *The gyrotron with the CNR SPL installed.*

A few factors can be invoked to explain the limitation of the pulse length, such as low frequency oscillations in the range of a few hundred MHz or the existence of a Penning-like discharge between the cathode and the corona ring surrounding it. The cause is not yet identified with certainty.

4.2.2 Tube performance for short pulses

An extensive experimental campaign was conducted to characterise the gyrotron and optimise the output power. Parameters such as the magnetic field in the cavity region, in the gun region, and its derivative were varied, as well as the beam voltage, current and radius.

The main observation is that due to arcing in the tube and/or to mode loss, it was not possible to reach the nominal design parameters in terms of beam energy.

In the best case, the design $TE_{34,19}$ mode was observed up to an acceleration voltage of 82-83kV instead of 90kV (the nominal operating voltage), at a cavity magnetic field of 6.80T instead of the nominal 6.86T. Due to the lower acceleration voltage, the pitch angle was limited to a value a ~1.0.

By using a very short pulse load (VSPL) on loan from FZK, the highest recorded output power in a 1ms pulse was 1.4MW for a beam acceleration of 81.5kV, at a current of 82A, slightly higher than the 75A design value, corresponding to an efficiency of 21.6%.

The experiments were repeated after installation of the CNR Short Pulse Load. Figure 4.2.2 presents the measured output power as a function of the acceleration voltage, for two different magnetic fields, using the FZK VSPL (red curves) and using the CNR SPL (green curves) for magnetic fields of 6.80T (continuous lines) and 6.82T (broken lines).

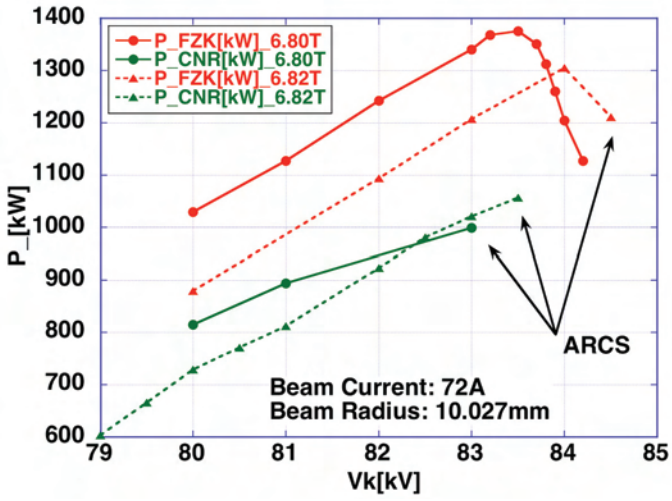

Fig. 4.2.2 *Output power measured in short pulses with the FZK VSPL (red curves) and the CNR SPL (green curves) for a magnetic field of 6.80T (continuous lines) and 6.82T (broken lines).*

It appears that the power measured with the FZK-VSPL is higher than that measured with the CNR-SPL. Previous comparative experiments performed in 2006 at FZK with the same two loads showed that the FZK-VSPL can be considered as a matched load, whereas the CNR-SPL, which was designed for a perfect Gaussian beam, reflects of the order of 3%. This value is very small, but can account for the performance change.

In order to understand the experimental results, extensive simulations were carried out by FZK and CRPP. A more detailed analysis of the gun using the code Ariadne++ indicated that the spread in perpendicular velocity is higher than initially estimated using the code Daphne, and is probably of the order of $d\beta_{perp}$=10%. Further multimode self-consistent simulations were performed at FZK. They indicate that the effects of a velocity spread of the order of 10% are a lowering of the ouput power, and a reduction of the upper limit range of excitation from 90kV to 87kV, in agreement with the experiments. Moreover, Rieke diagrams (not shown here) indicate that the gyrotron operates close to the stability limit for the experimentally optimised parameters, making the output power very sensitive to any reflections.

4.2.3 Beam radiation profile

The RF beam radiation profile was measured and the amplitude and phase profiles were reconstructed. In order to do that, the temperature elevation of a partially absorbing target located in the microwave beam path was recorded by an infrared camera once the correct $TE_{34,19}$ operating mode was established. Images were taken in a few planes along the microwave beam path, and used as the input of an iterative reconstruction algorithm

Figure 4.2.3a) shows the intensity recorded at 664mm from the window, after perspective correction, background removal and filtering, in 3dB steps. Three planes, in this particular case located at 464mm, 564mm and 664mm, were used in the retrieval analysis, and the result is shown in Fig. 4.2.3b). The fact that the

reconstructed amplitude compares very well (>99%) to the measurement constitutes a validation of the technique.

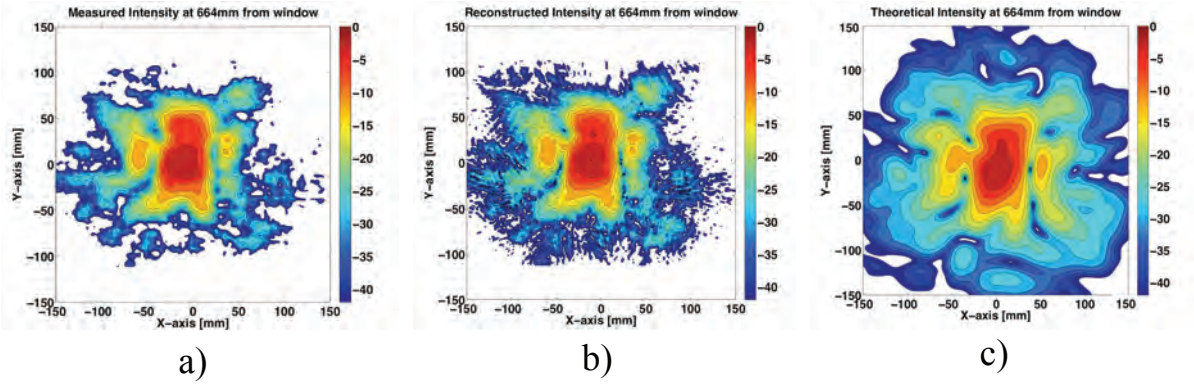

Fig. 4.2.3 *a) Measured (shown after pre-processing) and b) reconstructed intensity patterns at 664mm from the window. The theoretical pattern is shown on c). All data shown in 3dB steps down to -40dB.*

Moreover, there is very good agreement between the measured/reconstructed amplitude, and a theoretical simulation provided by FZK and depicted in Fig. 4.2.3c). The obviously moderate Gaussian content of the output beam is the result of a design option: since the mode $TE_{34,19}$ is not optimal for the quasi-optical mode launcher, it was decided to minimise the stray radiation inside the gyrotron (still while providing an approximately circular beam cross-section at the gyrotron window), at the cost of Gaussian content.

4.2.4 Other observations

Beside the results presented above, the main other results of the experimental period were:

Low frequency oscillations in the range of a few hundred MHz were observed, as on the FZK pre-prototype. They were not identified as a limiting factor, since they usually disappeared after a few ms. Nevertheless, they still need more investigation.
Bursts of oscillations at 5MHz, coming with a period of 200ms, and possibly associated to the High Voltage Power Supply were observed.
Some initial calorimetric measurements indicate that the amount of stray radiation could be as high as 12% (9% of the output power is measured in the internal loads circuit, and it is estimated that 75% of the stray radiation is dissipated by this way).
The collector conditioning was straightforward and successful up to 2MW/10s (in the absence of gyrotron oscillations, pulse length limited by the HVPS), and up to 2.4MW/2s (not limited).
The collector thermal foot-print (showing the deposition location of the electron beam on the collector in a very short pulse) was measured with an IR camera and suggests that the electron beam alignment and the electron beam uniformity are satisfactory.
The short pulse performance of the tube suffered a dramatic decrease in rf power at some point of the testing period. This is not explained yet, but might be due to the plastic deformation of some internal subassembly.

4.2.5 Prospects

Following the original planning, the experimental period is complete, the tube has been sent to the manufacturer to be opened, inspected, and refurbished with the possible implementation of some changes to the gun geometry and the mode launcher. The tube is expected to be back at the beginning of the fourth quarter 2009, to allow a further experimental campaign before the end of 2009.

4.3 The ITER gyrotron test stand at CRPP

4.3.1 Power supplies

Following the delivery and installation of the SCM on-site, the preliminary tests with the gyrotron have started without delay. A supply structure based on the existing HV power supplies at CRPP (RHVPS) has been studied and designed. Figure 4.3.1 presents the HV room where the additional electrical components, connected downstream the HV coaxial cable drawing the energy from the RHVPS, have been installed. Particularly, one can observe:

- The matching passive components (1) adapting the coaxial cable impedance to damp the HV reflection in case of fast HV transients
- The thyristor crowbar (2) used as a backup protection in case of an arc occurring during the gyrotron conditioning
- The gyrotron filament power supply (3) isolated at the cathode potential (-90kV)

During the first phase of the tests, the gyrotron has been operated without depressed potential applied to the body. The beam voltage was delivered by the RHVPS only. This period of tests has been successful, the acceleration voltage has been gradually increased up to this nominal value: -85kV. The protections and the warning signals have interrupted faulty pulses inside the time delay required for safe gyrotron operation. In this supply configuration, a regular and reliable working period of ~5 months with the test facility allowed us to investigate the RF capability of the gyrotron.

Body Power Supply (BPS) operation

The second phase of the tests focused on the gyrotron ability to be operated in the depressed collector mode, requiring to apply a decelerating potential on the body made of two separated parts: a central part named “the insert” and an external circular part named “the body”. For this purpose, a second HV power supply, named BPS, is mandatory. This equipment had been commissioned by the end of Year 2006, and regularly used on a dummy load along 2007, during the acceptance tests of the C-GT170 test facility by TED (the gyrotron manufacturer).

After a commissioning time of the whole HV supply system (RHVPS, BPS, the crowbar and the control), the latter has been operated continuously and successfully during three months in 2008, in order to investigate the RF domain limits of the gyrotron with a depressed collector. Although the working environment was in particular case hard to sustain (repetitive arcs occurrence), the BPS has shown reliable behaviour, which allows us to be confident in the next working step integrating the Main HV Power Supply (MHVPS) to be procured from industry.

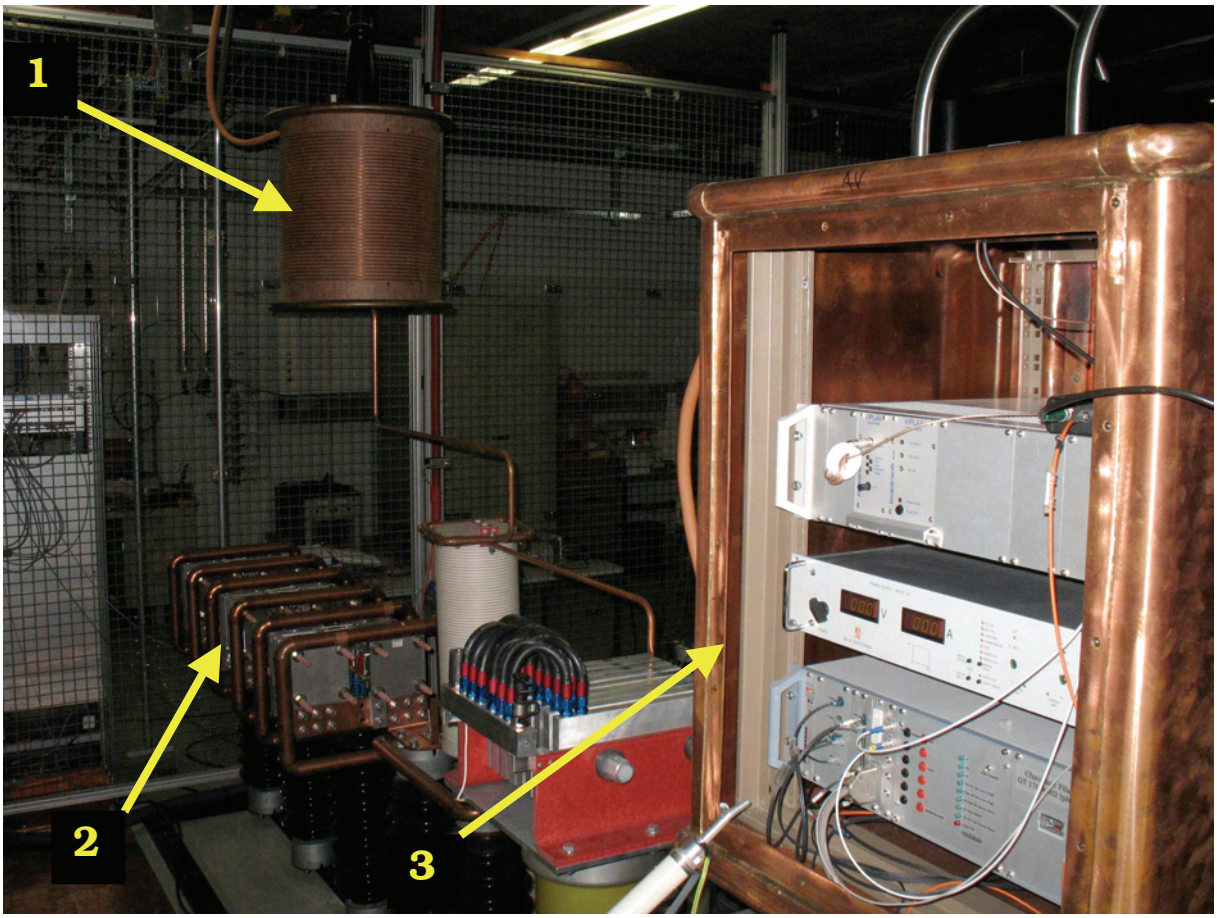

Fig. 4.3.1 *High voltage room of the gyrotron test stand. (1) Matching passive components; (2) Thyristor crow bar; (3) Gyrotron power supplies.*

Main HV Power Supply (MHVPS)

This power supply to be connected to the gyrotron cathode will replace the existing RHVPS mentioned above. This new equipment will be able to operate continuously in order to comply with the development of the CW ITER gyrotrons. CRPP is responsible for following the procurement contract passed with industry (OCEM, I). This task implies regularly reviewing the design choices proposed by industry, to ensure on-site integration, to follow the acceptance tests and to participate to the progress meetings foreseen in the framework of the contract agreement.

During 2008, the delivery previously foreseen in July has been delayed for two reasons:

- The multi-secondary transformers, part of the delivery but subcontracted to a second company (MF Trasformatori, I), met some design problems during the factory tests. More precisely at the time when the short-circuit tests have been applied in a specialised laboratory equipped to fulfil such testing procedure, HV secondary connections have been removed due to the electromechanical forces during the tests, as in a second rush an overheat of one of the secondaries damaged the isolation resin. The transformer must be returned at factory for repair and improvements.
- The gyrotron testing period has been extended to September 2008. Since it would have been difficult, even impossible, to operate the gyrotron at the

same time the MHVPS was installed on-site, it has been decided to shift the MHVPS delivery of several months.

Finally, the power supply delivery should take place at the beginning of 2009.

For the time being, the MHVPS equipment is assembled at the factory. Preliminary tests are applied on a dummy load, in order to verify the requirements specified and to prepare the future acceptance tests at factory which are foreseen in December 2008.

In the meantime, preparation work has been made on-site and will continue by the end of the year in view of the MHVPS installation. The commissioning should take place in January 2009, the final acceptance tests in February. Then, the whole supply structure would be available to be prepared for the next gyrotron operation period starting in the middle of 2009.

4.3.2 Data acquisiton system and gyrotron pulse control

A data acquisition system has been integrated into the gyrotron control system. It comprises four D-TACQ acq196 cards and one D-TACQ acq216 card. These cards provide 296 channels of slow data (1kHz) acquisition, 96 channels of medium rate (125kHz) acquisition and 16 channels of fast (5MHz) acquisition.

The data acquisition is integrated into the test facility control system and its arming, triggering and clocking are embedded into the gyrotron pulse cycle.

A gyrotron shot cycle has been implemented that allows simultaneous tracking of pulse number, plant state before and after the pulse and quasi-real-time monitoring of all acquired signals. In case of a fault in any of the gyrotron ancillary systems or subsystems the pulse is aborted. At the same time data acquisition on the four acq196 cards is stopped while, simultaneously, the acq216 acquisition card is triggered. In this way the gyrotron is protected against fault, the volume of acquired data is not wasteful and highly resolved data is acquired around the time of the fault. Dependent upon the gyrotron pulse length, two modes of operation were defined.

The first mode (gts-fast) of operation, for pulses less than 400msec., sees the four acq216 modules armed and triggered simultaneously and data acquired at 125kHz and stored in a MDS tree after the gyrotron pulse.

The second mode (gts-slow) of operation for pulses longer than 400msec and/or for long series of short (<100msec.) conditioning pulses sees three of the acq196 cards triggered and then clocked at 1kHz. The data from these cards (296 channels) is streamed to hard disk and stored in an MDS tree and ready for use, in 1 second long blocks. This allows for quasi-real time calorimetry on gyrotron sub-systems, monitoring of the gyrotron vacuum and measurement of power supply voltages and currents. At the same time the fourth acq196 card is available to acquire bursts of data at 125 kHz, at pre-programmemed times, during the shot. The acq216 card is armed and waiting to be triggered in case of fault.

The mode, gts-slow, has been used extensively throughout 2008. Due to the problems associated with extending the pulse length of the gyrotron, gts-slow has been used to acquire data during long series of short gyrotron pulses. Approximately 15GByte of data has been acquired in approximately 156 shots and the data has been used to estimate thermal loads on certain gyrotron sub-systems.

Indeed, it was in examining the data acquired form the gyrotron collector thermocouples that certain problems associated with the collector sweeping coils were detected; suspicions later confirmed using thermographic techniques.

A MATLAB based graphical user interface (GUI) has been developed to facilitate access to the gyrotron data stored in the MDS trees.

4.4 *The ITER Upper Launcher for Electron Cyclotron Waves*

TW6-TPHE-ECHULB2 is a two year contract for the design and testing of the mm-wave system of the ITER upper launcher started in 2006. In addition, support of the physics analysis associated with NTM stabilization and other ECCD applications is provided.

In ITER, 170GHz electron cyclotron wave launch from upper ports is used to control the NTM. The unstable NTM may limit the performance of ITER. The launcher, known as the Front Steering Upper Launcher (FS-UL), must have the capability to steer the microwave beams in the poloidal direction (±12°). The Associations CRPP, ENEA (I), FZK (D), FOM (NL), IPF-Stuttgart (D) are collaborating to design the UL.

CRPP has been awarded the contract with EFDA to be the principle association involved in the design, analysis and testing of the mm-wave system of the upper launcher. Other associations (CNR and IPF-Stutgart) participate in the mm-wave design aspects offering a cross-check of CRPP's design and collaborating in potential design improvements for better physics performance. This work will continue the launcher development programmeme up until beginning of 2009 and advance the design to a near build-to-print level.

The current design of the antennae system is based on the quasi-optical transmission of eight beams through a system of focussing and plane mirrors to achieve the best possible alignment and absorbtion of the mm-wave power at plasma target locations. The beam steering system has been built as a prototype setup to demonstrate the validity of the mechanically compliant structural concept and to perform dynamic steering and control system optimisation. The test and measurement results have proven the feasibility of the initial design choices and have opened paths for further improvement of the steering performances.

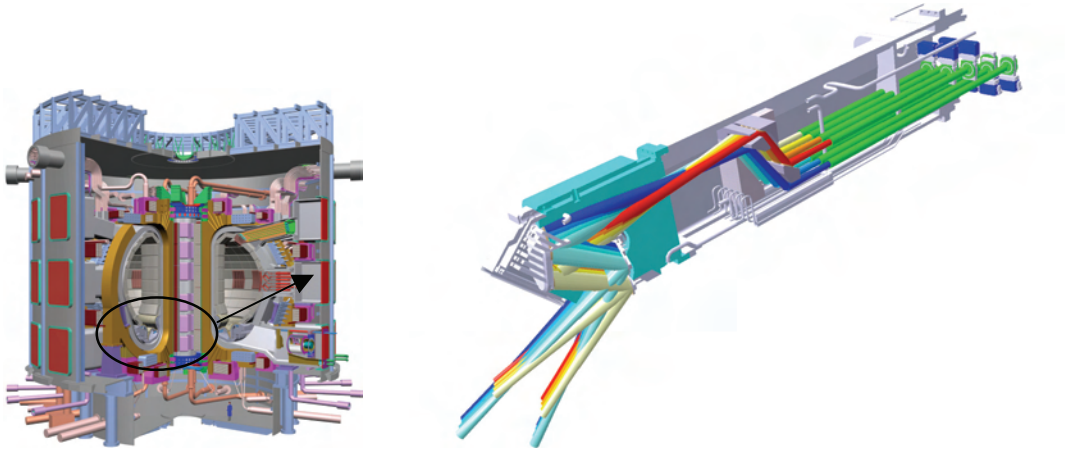

Fig. 4.4.1 *The EC upper launcher.*

4.5 *The use of SULTAN for developing and testing ITER conductors*

The Nb_3Sn CICC's for the toroidal field (TF) coils of ITER have to be qualified by a successful SULTAN sample test. The required current sharing temperature is 5.7K or above at a current of 68kA and a SULTAN background field of 10.78T. In the period under review, the samples JATF3, USTF1 and USTF2 have been tested in the SULTAN facility. In addition, JATF2 and TFPRO2 have been re-tested with an enhanced instrumentation. The sample KOTF2 is under test at the time of writing and the samples RFTF2 and USTF3 are planned to be tested within the end of 2008. The samples tested till summer 2008 are considered R&D samples, those from October 2008 on are Qualification samples. The activities summarized below are all carried out under bilateral contracts with the IO and the DAs.

The samples JATF3 and USTF1 have been assembled and instrumented by the JA and US domestic agencies, respectively. The sample USTF2 (as well as KOTF2, RFTF2 and USTF3) has been heat treated and assembled at CRPP. The additional instrumentation of the re-tested samples JATF2 and TFPRO2 has been mounted at CRPP. The main features of the five SULTAN samples are gathered in the table. For all conductors except USTF1 Alt1 and USTF2 Alt1b, the cabling pattern is ((2sc+1Cu)×3×5+core)×6 (ITER cabling pattern). The alternate cabling pattern of USTF1 Alt1 and USTF2 Alt1b is (((6sc+1Cu)×6+Core1)×5+Core2)×6, where the cabling patterns of Core1 and Core2 are (6+1)Cu and (6+1)Cu×3, respectively.

Sample	**JATF2**		**JATF3**		**TFPRO2**		**USTF1**		**USTF2**	
Conductor	JAB2	JAI2	JAC	JAD	OST2	OST1	Base	Alt1	Alt1b	Opt2
Strand type	Bronze	Int. Sn	Bronze		Internal tin		Internal tin		Internal tin	
Strand identity	He 2539	6005-K	06494-1	LK0003	7878	7567 7603 7730	NT8404	NT8401	9707	9484
Sc strands	900	900	900	900	900	900	900	1080	1080	900
Cu wires	522	522	522	522	522	522	522	456	456	522
Twist pitch, mm	45 85 130 250 447	45 85 130 250 454	80 140 178 300 420		116 182 245 415 520	45 87 126 245 520	45 85 127 254 457	25 127 254 457	25 127 304 508	78 139 190 304 437
Void fraction, %	29.6	29.8	29	29	27.7	29.1	n.a.	n.a.	n.a.	n.a.
Central channel, id × od, mm	6.7 × 9 Spiral		7 × 9 Spiral		7 × 9.1 Spiral		7.5 × 9.5 Perforated pipe			
Cable space, mm	39.28	39.32	39.32	39.32	38.25	38.85	40.2	40.3	40.3	39.6
Conductor, mm	42.68	42.66	42.65	42.65	41.45	42.05	43.7	43.8	43.8	43.7

The reasons to re-test the conductors JATF2 and TFPRO2 with an enhanced instrumentation are closely related to the difficulty to find an accurate current sharing temperature, T_{cs}, from the voltage measurements, see also section 3.7. In general, the re-tests of the TFPRO2 and JATF2 samples confirm the results of the measurements with the initial instrumentation. The T_{cs} results of the re-tests (*italic*) and the measurements with the initial instrumentation (normal) are compared in the table below.

Sample	**TFPRO2**		**JATF2**	
Conductor	OST1	OST2	JAB2	JAI2
T_{cs} Standard voltage taps (K)	6.00	7.39	-	-
T_{cs} Fit to $E = a(T/T_{cs}) + E_c(T/T_{cs})^m$ (K)	6.34	7.37	6.41	5.88
T_{cs} Calorimetry (K)	- / *5.69*	- / *7.24*	6.51 / *6.45*	5.96 / *5.85*
T_{cs} Jacket stars (K)	*6.00*	*7.30*	*6.55*	*5.90*
T_{cs} Crimping ring stars (K)	*5.70*	*7.20*	*6.55*	*6.00*

The critical current of witness strands, heat treated together with the corresponding SULTAN samples, was measured at 4.2K in the field range of 8T to 15T. An electric field criterion of 0.1μV/cm was used to define the critical current (I_c). The main strand characteristics and the results of the witness strand measurements at 12T and 4.2K are gathered in the table. The test of the witness strands is crucial to assess how far the CICC performance is degraded compared to the potential performance deduced from the scaling laws and witness strands results.

Completely solder filled joints are a special feature of the USTF1 sample. In both legs of this sample the current dependent offsets have been found to be very low in any of the various voltage tap pairs. The current sharing temperature of the USTF1 Base conductor, manufactured according to the ITER baseline design, exceeds 6.2K even after 1200 load cycles. The conductor USTF1 Alt1 with a different cabling pattern showed no decrease of the current sharing temperature with cycling and reached an even higher T_{cs} value of 6.69K. To clarify if the smooth behaviour of USTF1 is due either to the solder filled joint or to the load tolerant strand (LUVATA), it has been agreed to assemble a test the USTF3 sample, made from identical conductor sections as USTF1, but assembled at CRPP with the "solder dipped" termination also used in the other samples assembled at CRPP in 2008. The test of USTF3 will be done in December 2008. To quantify the role of solder (coated/dipped/filled) for the current re-distribution, the inter-strand resistance measurements were also launched, see section 2.5.1.

Sample	**JATF2**		**JATF3**		**TFPRO2**		**USTF1**		**USTF2**	
Conductor	JAB2	JAI2	JAC	JAD	OST2	OST1	Base	Alt1	Alt1b	Opt2
Strand Identification	He 2539	6005-K	06494-1	LK0003	7878	7567 7603	NT8404	NT8401	9707	9484
Type	Bronze	Int. Sn	Bronze		Internal tin		Internal tin		Internal tin	
d (mm)	0.826	0.82	0.82	0.82	0.815	0.815	0.82	0.77	0.77	0.82
Cu : non-Cu	1	1	0.96	1.07	1	1	1.05	1.19	1.2	1.08
Twist pitch (mm)	15	10	15	15	17	15	13	14	17	17
I_c @ 12T, 4.2K, A	247	282	239	208	265	303	209	181	233	278
J_c @ 12T, 4.2K, A/mm²	920	1070	890	810	1020	1160	810	850	1100	1100
n at 12T, 4.2K	33	34	31	27	32	23	18.5	18	33	29.5

The procedure to solder fill the termination of Nb_3Sn CICC is routinely applied at CRPP since 2001 for sub-size SULTAN samples. In order to be ready, if necessary, to apply the same technique to the large size ITER conductors, an R&D plan was launched under funding of the IO, including the assembly of a prototype termination: the Cr plating and all the wraps are removed prior of the heat treatment, the cable is swaged into a Cu sleeve electron beam welded to a steel collar, after the heat treatment the termination is solder filled by a siphon and eventually the central channel is restored by drilling out the solder from the 450mm long termination.

One leg of the USTF2 sample has been manufactured with longer twist pitches (Opt2 for ITER), whereas in the other leg again an alternative cabling pattern was used. The initial T_{cs} of USTF2 Opt2 is as high as 7.22K. However, cyclic loading and an additional thermal cycle reduce the T_{cs} to a value of 6.3K. Inspection of the USTF2 Alt1b conductor during sample assembly revealed severe cable damage in the joint region. The lower performance of USTF2 Alt1b seems to reflect this cable damage.

The evolution of the T_{cs} values in the two legs of the JATF3 sample is illustrated in Fig. 4.5.1. The T_{cs} values of both conductor legs have been found to be well below the potential performance (-0.65% strain). An unusually large increase of the T_{cs} for reversed current suggests that the current distribution depends on the current direction, i.e. from the self-field profile. The progressive performance loss suggests that some cable damage is present.

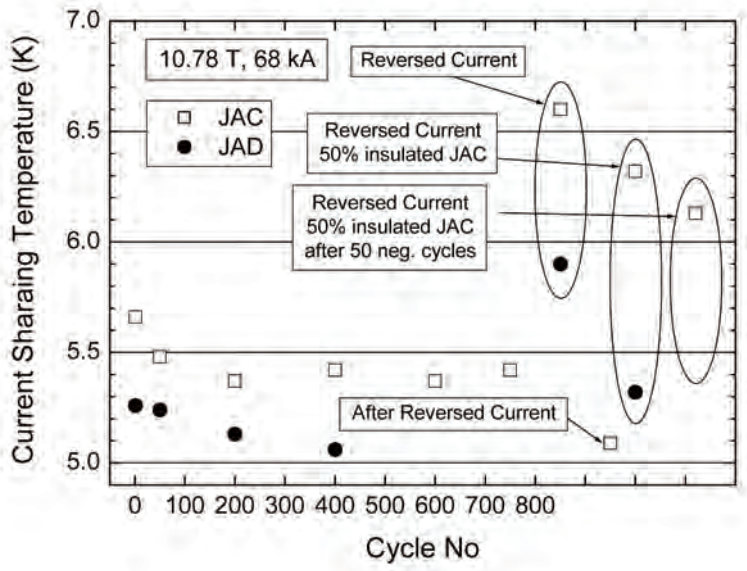

Fig. 4.5.1 *Evolution of T_{cs} in the two legs of JATF3 with the number of load cycles.*

In addition to the DC performance, the AC loss behaviour of the conductors has been investigated using gas flow calorimetry. The results of the AC loss measurements for USTF1 and JATF3 are shown in Fig. 4.5.2. The total AC losses of USTF1 Alt1 are even after cyclic loading considerably larger than those in the Base leg. The AC loss for option2 ITER cables are larger than for option1, as expected from the longer twist pitches of option2. The lines in Fig. 4.5.2 represent different values of the coupling loss constant ($n\tau$). The calculated lines for the coupling loss constant are based on a normalisation of the loss to the Nb_3Sn strand volume.

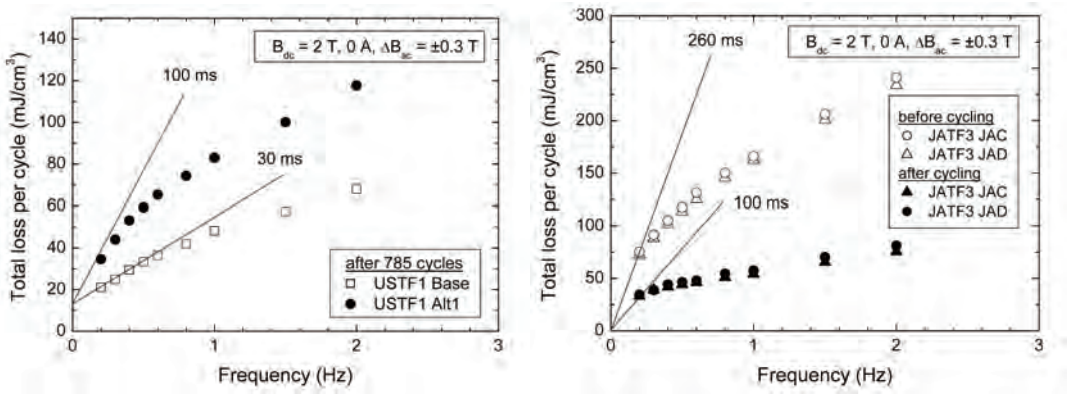

Fig. 4.5.2 *AC loss measured in the two legs of USTF1 (left) and JATF3 (right) before the dc tests and after cyclic loading. The losses, measured before the dc tests, are considerably larger.*

4.6 The development of the ITER magnetics diagnostic

Work continued in 2008 on the development of the ITER magnetics diagnostic, under multiple EFDA tasks, now managed by F4E. These tasks included work on the following topics.

Quantify the noise levels

The probable levels of noise in the stabilising closed loop for vertical position control is required as input to the dimensioning of the active control power supplies. A number of tokamaks have provided input from their own data under ITPA. TCV was shown to have a factor 2 lower noise level than the next best tokamak and a factor 5 better than the worst. Figure 4.6.1 illustrates the method used.

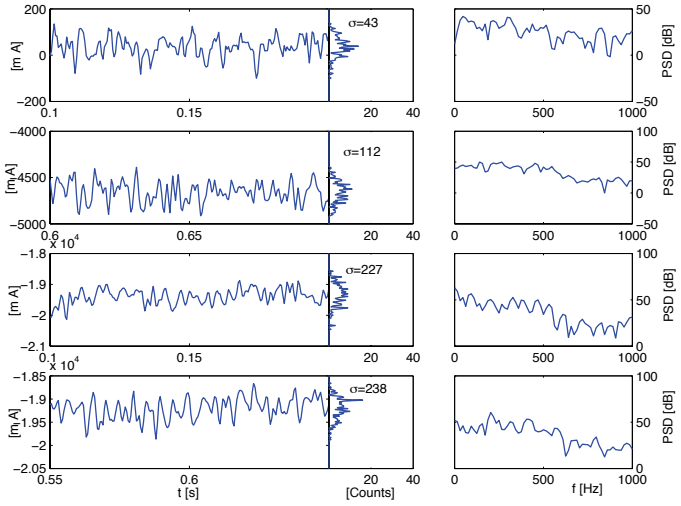

Fig. 4.6.1 *The time traces of Z*Ip for the 4 pulse segments are given in the 1st column starting from the PCS (top row), the stray (2nd from top), the quiet plasma (3rd) and the active MHD plasma (bottom). Attached to the time dependence, the "noise" distribution function is shown together with its standard deviation (σ) The last column shows the spectral density of the frequency response.*

Develop a project plan, work breakdown structure and costing

A full project plan is required for the magnetics diagnostic. This is still in progress. The existing project schedules developed by CEA and RFX have been incorporated into Primavera and the CRPP schedules have been added. A Work Breakdown Structure has been proposed to F4E for this diagnostic. Interfaces are being defined.

Evaluate problems associated with equilibrium reconstruction

CRPP contributed to work carried out mainly by CEA on the likely precision of the reconstruction of the plasma equilibrium.

Develop prototypes for the fast MHD coils inside the ITER vacuum vessel

The mechanical design and stress analysis of MHD coils have been developed, Fig. 4.6.2. In addition, the merits of different placement of these probes for analysing high mode number TAEs, given possible loss of sensors, has been studied.

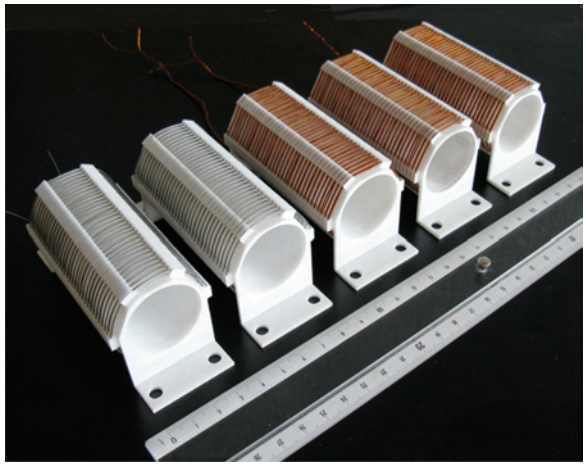

Fig. 4.6.2 *View of several prototype MHD coils developed for ITER.*

Provide coordination of activities carried out by Associations

The CRPP, CEA, Consorzio RFX and CIEMAT Associations have worked together on these EFDA tasks. Progress has been made on the creation of a consortium linking these Associates, with a view to working for future Fusion for Energy contracts.

4.7 The development of the ITER CODAC design

An activity launched in 2005 which began at the beginning of 2006 to develop a conceptual design for the Control, Data Access and Communication for ITER came to an end in February 2008. After a review by all ITER parties in November 2007, the activity was completed with the release of the final version of this conceptual design in February 2008.

4.8 Contributions to the ITPA

CRPP staff participate regularly in the ITPA activities, which in 2008 came under coordination by the ITER IO.

CRPP hosted the diagnostics ITPA meeting in April 2008, and three ITPA groups meeting after the IAEA FEC in October 2008, the Integrated Operational Scenarios, the Energetic Particles and the MHD Stability groups.

4.9 Contributions to ITER committees

Professor MQ Tran has been a member of the ITER STAC in 2008, and Head of the EU ITER STAC delegation.

4.10 ITER scenario modelling

Understanding the non-linearly coupled free-boundary physics between the plasma transport and equilibrium evolution requires a full tokamak discharge simulator which can self-consistently include all the related physics and engineering constraints. In this work, a free-boundary evolution code, DINA-CH (collaboration with Kurchatov and TRINITI, Russian Federal) and an advanced transport code, CRONOS (collaboration with CEA, France), are combined to form a full tokamak discharge simulator and the ability of this simulator is fully demonstrated by successfully simulating the inductive 15MA ITER operation scenario 2 and investigating the feasibility of the scenario in a more complete way.

In the full discharge simulation, the average electron density is assumed to evolve with the plasma current and the ion and impurity density profiles are self-consistently calculated with the effective charge profile which is assumed to decrease monotonically as the electron density increase. The KIAUTO transport model developed in CEA controls the energy confinement and mode transition respecting the confinement time scaling laws. The plasma shape evolution and transition to a diverted configuration are guided by the feed-forward reference coil current waveforms, and finally determined by the non-linear evolution of the plasma equilibrium. A virtual radial position controller initially stabilising the non-linear growth of the plasma column is switched to a shape controller after the plasma shape is fully diverted. Appropriate initial eddy currents in the passive conducting structures are determined by trial. Neutral beam injection (NBI) is applied during the current ramp-up phase to avoid the coil current limits by reducing the resistive ohmic flux consumption. 53MW of additional heating and current drive (H&CD) power is applied during the current flat-top phase to initiate and maintain the plasma burn.

In the simulation, the evolution of plasma poloidal beta, internal inductance and safety factor follows the reference scenario as shown in Fig. 4.10.1. The plasma poloidal beta varies in response to the application of additional power and confinement mode transitions. Although the internal inductance was slightly higher than the reference scenario at the start of flat-top, the vertical instability was stabilized with the present ITER control systems. The central safety factor is reduced fast at the beginning of the plasma current ramp-up, causing an early

onset of sawtooth events. The coil voltage limits are imposed in the control system as saturation voltages and the coil currents are allowed to evolve across the coil current limits as shown in Fig. 4.10.2. Although the CS1 coil current limits are avoided by the application of early NBI, the PF2 coil currents briefly violates its limits at the end of the flat-top phase. However, this violation seems avoidable by either slightly changing the reference plasma shape or increasing the coil current limit itself, as in the recent ITER design review. The poloidal flux consumption during the flat-top phase was slightly less than the reference scenario due to the application of higher H&CD power. The imbalance current flowing in the vertical stabilization converter (VSC) and the total active power of the power supply system were within the operational limits, Fig. 4.10.3. Though the plasma shape evolution was well controlled during the whole simulation, the radial dynamic response of the plasma was underestimated during L-H and H-L mode transitions.

Lower Hybrid (LH) assisted plasma current ramp-up has been simulated to study its capability of reducing the plasma internal inductance and saving the poloidal flux consumption. The early application of 20MW LH during the plasma current ramp-up phase of ITER was effective to reduce the internal inductance down to 0.71 from 1.05 while the poloidal plasma beta was increased up to 0.11 as shown in Fig. 4.10.4. The flux consumption during the plasma current ramp-up was reduced to -81Wb from -124Wb. The saved flux of about 43Wb is equivalent to about 500sec of additional burn duration and all the current limits were safely avoided. The safety factor profile was reversed with high central values delaying the onset of sawtooth events. When the early LH was applied, an additional elongation control was required to make the plasma shape diverted as it was originally intended. [Collaboration with: Kurchatov Inst., Moscow, RU; TRINITI Inst., RU; CEA Cadarache, F]

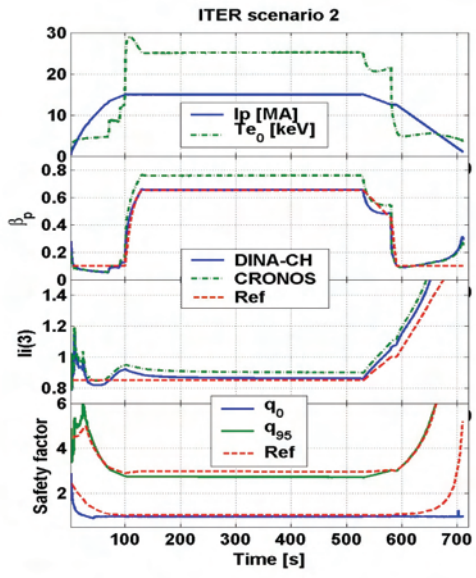

Fig. 4.10.1 *Time trace of plasma parameters, plasma current, central electron temperature, poloidal beta, internal inductance and safety factors (q_0 and q_{95}) (dashed red lines: ITER reference scenario 2).*

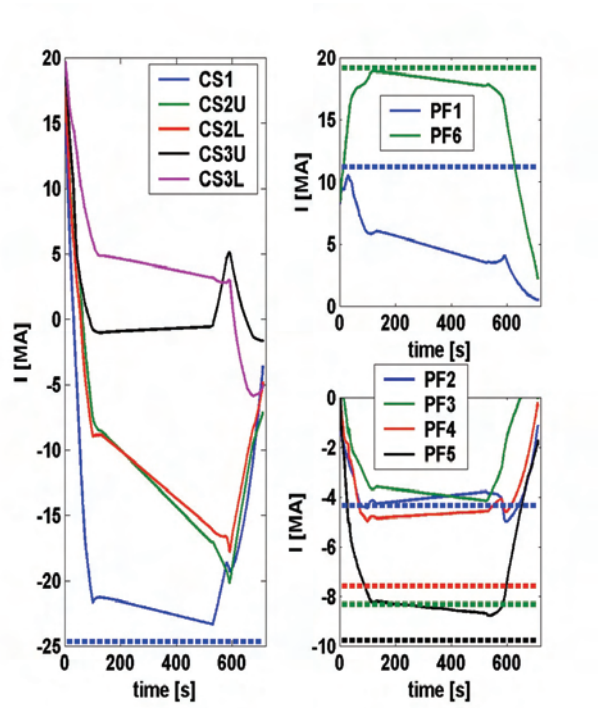

Fig. 4.10.2 *Time trace of coil currents (dashed thick lines: coil current limits).*

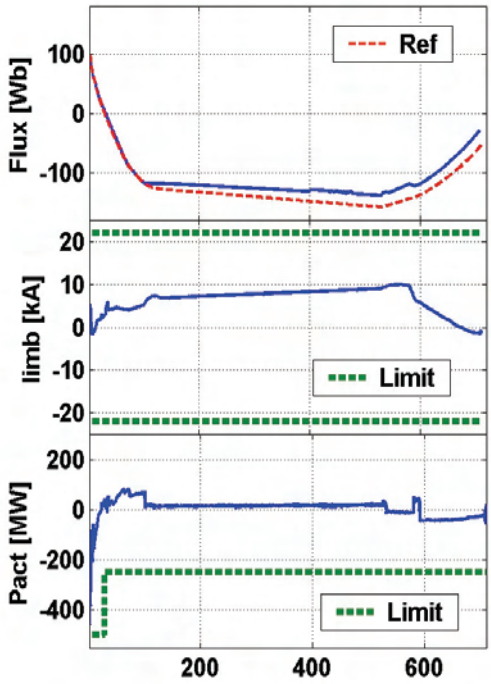

Fig. 4.10.3 *Time trace of poloidal flux at the plasma boundary, imbalance current flowing in the Vertical Stabilization Converter and total active power of the power supply system.*

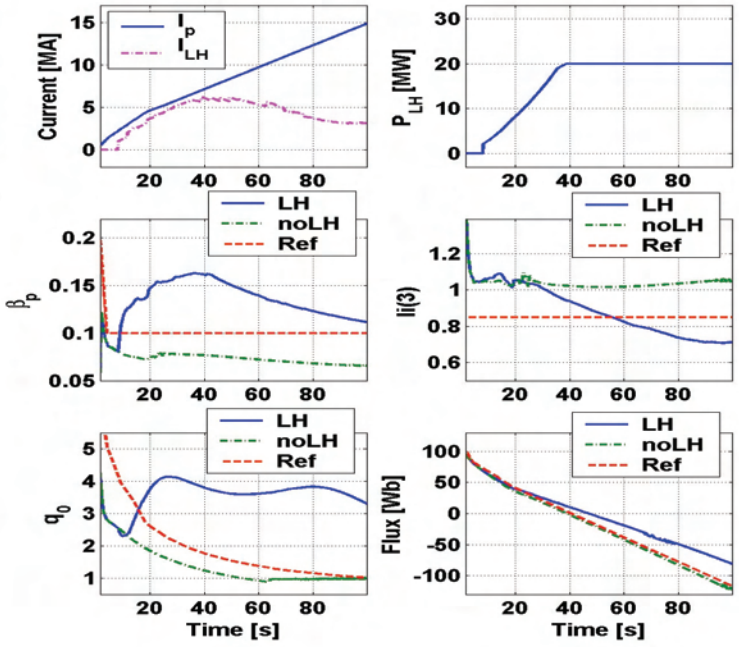

Fig. 4.10.4 *Time trace of plasma parameters, plasma current, poloidal beta, safety factors at the center, LH power, internal inductance and poloidal flux at the plasma boundary (dashed red lines: ITER reference scenario 2)*

Recently, specifications of plasma disturbances anticipated in ITER have been updated to cover a wider range of plasma disturbances observed in present tokamak experiments. Therefore, re-assessment of the ITER control system was requested to investigate if the plasma can be safely recovered from the disturbances with the present control system. This work was performed under EFDA Task, PLASMADYN2. Dynamic plasma responses to the strong disturbances, uncontrolled ELMs and fast H-L mode transitions, has been examined by using a non-linear plasma response modelling code, DINA-CH. In this simulation, a recent version of DINA-CH in which a bug in calculating 2D current profile is fixed was used together with an updated ITER design. The disturbances were generated in a pre-programmemed manner by using a simple routine controlling heat conductivity profiles and the target plasma was obtained from a full tokamak discharge simulation of ITER scenario 2.

The uncontrolled ELMs in an H-mode ITER plasma were simulated by applying high heat conductivity values at the plasma boundary as shown in Fig. 4.10.5. Stored plasma energy of about 20~45MJ was released about in 1ms and recovered in 0.5~1.0s. The decrease of the plasma poloidal beta was about 0.04~0.08, similar to the value given in the disturbance specifications. However, the internal inductance changes were smaller than expected and the slow increase of the internal inductance up to 0.95 at a later time was not observed due to the pre-programmemed recovery of the plasma profiles. Larger plasma energy releases produced larger fluctuations in the total plasma current, radial and vertical position, and minor radius as shown in Fig. 4.10.6. Full recovery of plasma current, position and shape was possible within 4s.

The fast H-L mode transitions in ITER were simulated with different amount of released plasma energy as shown in Fig. 4.10.7. The internal inductance increased

fast as the edge bootstrap current was reduced by the relaxation of the pedestal pressure gradients. For a strong disturbance, the plasma experienced a VDE due to a large inward radial movement which makes the plasma limited and smaller in volume as shown in Fig. 4.10.8. Full recovery of the total plasma current, position and shape was achieved within 10s, unless the plasma experiences a strong disturbance causing a VDE. As the released plasma energy is smaller, the recovery takes less time. [Collaboration with: Kurchatov Inst., Moscow, RU; TRINITI Inst., RU; CEA Cadarache, F]

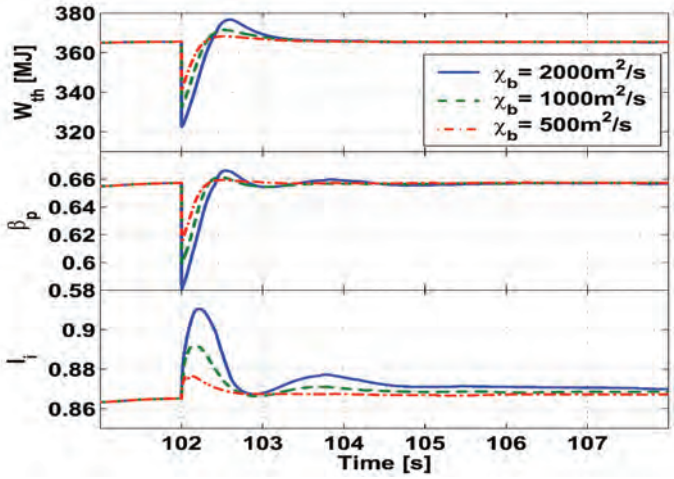

Fig. 4.10.5 *Dynamic plasma responses to pre-programmemed uncontrolled ELMs. The amount of released plasma energy is varied by imposing a heat conductivity at the plasma boundary (*$2000\ m^2/s$, $1000\ m^2/s$ *and* $500\ m^2/s$*). The time traces of stored plasma energy, plasma poloidal beta and internal inductance are compared.*

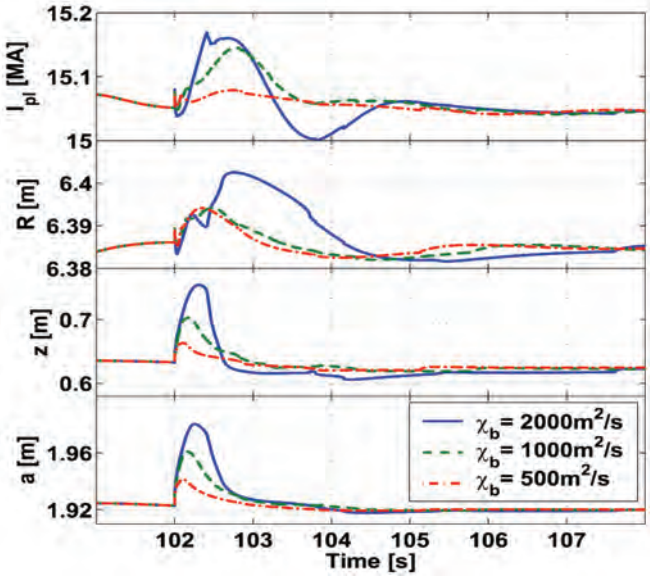

Fig. 4.10.6 *Dynamic plasma responses to pre-programmemed uncontrolled ELMs. The time trace of the total plasma current, plasma centre and minor radius are compared. The fluctuations caused by the disturbances are stabilised quickly within 4s.*

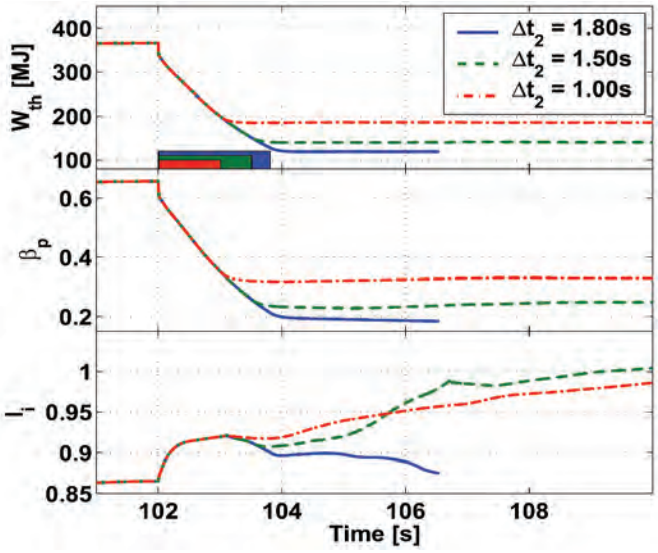

Fig. 4.10.7 *Dynamic plasma responses to pre-programmemed fast H-L mode transitions. The amount of released plasma energy is varied by imposing the duration of slow energy release at second phase, Δt_2. The time traces of stored plasma energy, plasma poloidal beta and internal inductance are compared.*

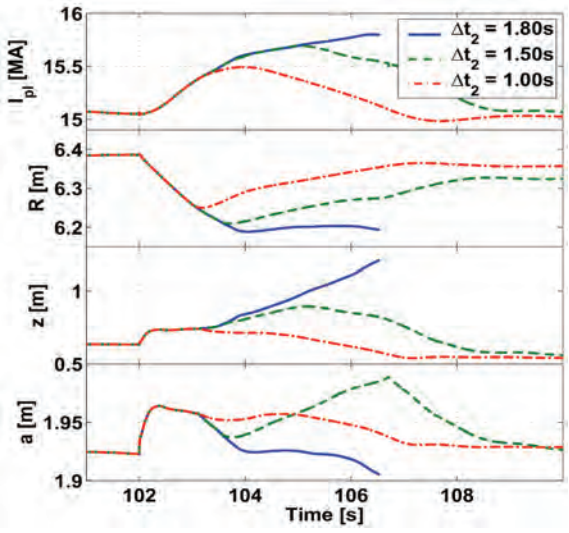

Fig. 4.10.8 *Dynamic plasma responses to pre-programmemed fast H-L mode transitions. The time trace of the total plasma current, plasma centre and minor radius are compared. The fluctuations caused by the disturbances are stabilised within 10s, unless the plasma experience a strong disturbance causing a VDE.*

4.11 Resistive Wall Mode control in ITER

In support of the EFDA Contract TW6-TPO-3DCON "Resistive Wall Modes Control in ITER with 3D Structures" a sensitivity study of beta limits and RWM growth rates with respect to changes in safety factor was initiated. ITER Scenario 4 equilibria with smoothed plasma boundary and variations of the current density

profile in its peak value and in the pedestal were calculated with the CHEASE code. The reduction of the peak results in a lower q_{min} value 2.05 compared to q_{min}=2.35 in the reference equilibrium. The beta limit against the n=1 mode with and without wall stabilization were computed with the KINX code. The n=1 mode normalized beta limit significantly degrades from 3.5 to 2.7 (no wall limit 2.3 to 2.0) due to q_{min} approaching 2. The reduction of the current density in the pedestal region has a weak effect on the n=1 mode limits.

5 INTERNATIONAL AND NATIONAL COLLABORATIONS

5.1 Exploitation of the JET facilities

5.1.1 Control of MHD instabilities

CRPP staff has contributed to both the theoretical and experimental aspects of studies related to the control of MHD instabilities, with particular focus on the development of control mechanisms for the sawtooth instability in JET.

The sawtooth control mechanism in plasmas employing off-axis toroidally propagating ion cyclotron resonance waves in tokamaks has been reinvestigated. The radial drift excursion of energetic passing ions distributed asymmetrically in the velocity parallel to the magnetic field is found to determine stability when the rational q=1 surface resides within a narrow region centred about the Doppler-shifted fundamental cyclotron resonance. This work employs RF wave-field and fast ion distribution function simulations applied to a key demonstration JET discharge with localised off-axis ion cyclotron current drive (ICCD) counter to the ohmic current. Analytical and full numerical calculations of the internal kink mode with the simulated JET fast ion distribution function demonstrate ideal instability when the deposition of the resonating ions is very close to the q=1 radius. Such is the sensitivity to the location of deposition, and the magnitude of the effect, that this fast ion mechanism, i.e. non-MHD mechanism, dominates over the previously assumed classical mechanism relating to the change in the magnetic shear due to the fast ions, and the resulting effect on MHD stability. Based on this theoretical modelling, and in order to distinguish between the two mechanisms described above so as to test the prospects of sawtooth control in ITER using ICCD, experiments in JET have been planned for December 2008 using minority He3, under the leadership of CRPP personnel.

5.1.2 JET, S1 support for NTM avoidance

An experiment has been proposed under the auspices of Task Force M to investigate the mechanism of neoclassical tearing mode (NTM) triggering by sawtooth crashes, and more specifically to explore in detail an apparent discontinuity in the threshold β_N for NTM destabilisation as a function of the sawtooth period. This experiment has been approved and assigned three sessions to be carried out in November 2008 under the leadership of CRPP personnel.

5.1.3 Particle transport and confinement in TCV and JET

Linear gyro-kinetic calculations of the density peaking in JET H-mode plasmas have been run to identify the most important parameters which influence the particle transport properties in tokamaks in order to predict the density profiles behaviour in burning plasma devices, ITER in particular.

After completing the analysis of JET H-mode experimental density profile database in 2007, the focus was put into the comparison between the experimental results and the theoretical predictions made using gyro-kinetic simulations. In excess of 1000 linear electrostatic GS2 calculations were executed on the PLEIADES computer cluster at EPFL, with simulation parameters dedicated to the particle transport study in JET specific plasma conditions. The four most important simulation parameters, T_i/T_e, R/L_n, R/L_{Ti}, ν_{eff} (effective collisionality) were scanned independently in the range of experimental plasma parameters on JET. For each run the linear mode with the highest growth rate was identified and the results, namely the induced heat and particle fluxes, were stored into a database of GS2 results. A separate, smaller set of simulations was produced in a similar way, with variation of R/L_n, ν_{eff} and $\hat{s}$ (local magnetic shear value) parameters to identify the role of the safety factor profile on generated fluxes. The entire JET operating domain is found to be dominated by ITG modes.

As an innovative approach, particle fluxes produced by the fastest growing linear ITG mode were equated to NBI particle fluxes through the mid-radius surface. For a direct comparison with the experiments, $\Gamma'=eT_iS/Q_i$, the particle flux normalised to the ion heat flux, is the key parameter. To facilitate the analysis, simple parameterisations of the output results were produced (Fig. 5.1.1). It was shown that with this method the stationary density gradient predicted by the GS2 simulation is indeed in excellent agreement with the experimental observations, including parametric dependence on the effective collisionality, particle sources, ion to electron temperature ratio and local shear value, as well as the unimportance of the local ion temperature gradient.

The results show that Γ' can be approximated with a good precision by a linear function of the input parameters: $\nu_{eff}^{1/2}$, T_i/T_e, $R/L_n^{3/2}$. In the domain investigated, R/L_{Ti} has no significant effect. Using this parameterisation we were able to predict R/L_n at mid-radius from the experimental values of the other parameters. The experimental Γ' was obtained only from the NBI particle flux and from the ion heat flux through the mid-radius surface. With such an approach the simulation results appeared to be in an excellent agreement with experiment (Fig. 5.1.2). The theoretical dependences on $\nu_{eff}^{1/2}$, T_i/T_e, $R/L_n^{3/2}$, $\hat{s}$ and R/L_{Ti} are all very close to the experimentally observed ones, as obtained using linear regressions. Using the linear simulation results we were able to make a prediction for the ITER density profile. For the relevant collisionality, zero particle source and a fully equi-partitioned plasma ($T_i/T_e=1$), the stationary density profile is expected to be peaked with $R/L_n\sim1.5$, corresponding to $n_{e0}/\langle n_e\rangle\sim1.5$, consistently with empirical extrapolations.

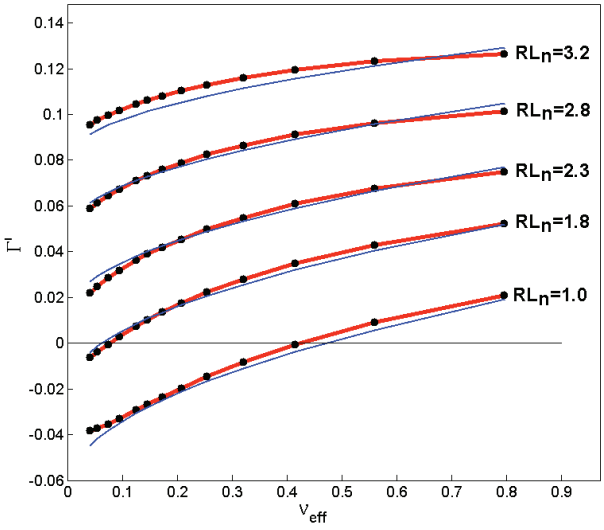

Fig. 5.1.1 *GS2 simulation results for $T_i/T_e=1.0$ and $R/L_{Ti}=6.0$ case (black dots). The blue lines show the parametrisation used for comparison with the experiments.*

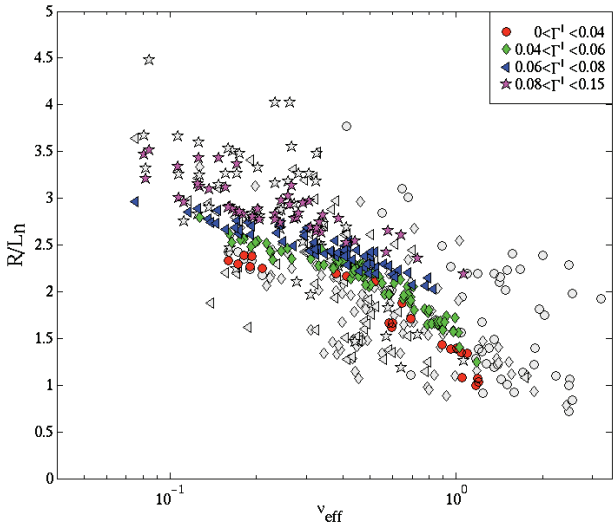

Fig. 5.1.2 *Simulation results for different Γ' ranges (in colour) plotted on top of experimental values (gray). Note the clear trend of decreasing R/L_n for increasing collisionality.*

5.1.4 Edge physics studies

In 2008 a significant contribution was made to the ongoing process of code-experiment and code-code benchmarking by SOLPS5 modelling of two separate JET H-mode pulses. In one case the ELM-free phase of a high-power, high-stored energy JET discharge with large ELMs was analysed, whereas in the second case modelling was performed of the full ELM cycle of a lower power JET H-mode discharge previously examined in detail with the EDGE2D-NIMBUS code package.

The first JET discharge which has been simulated is #70224: this is an un-fuelled pulse at high plasma current and magnetic filed (I_p=3MA, B=3T) with total input power P_{IN}~20MW (supplied mostly by Neutral Beam Injection) and plasma stored energy W_{plasma}~8MJ. The electron density ($n_{e,ped}$) and temperature ($T_{e,ped}$) at the top of the pedestal region reach values of $n_{e,ped}$~$6\times10^{19}m^{-3}$ and $T_{e,ped}$~2.5keV, respectively. This yields ITER-relevant neo-classical pedestal collisionalities in the range ν_e^*=0.03-0.08. This discharge has extremely large, but very sporadic ELMs, with some events approaching an energy loss ΔW_{ELM}~1MJ, and thus being close in amplitude to what is now thought to be the maximum for the avoidance of material damage on ITER. Such a discharge was modelled for the first time with the SOLPS code package. The time independent simulations of the steady state form a good basis on which to perform future ELM simulations.

Upstream, the code is constrained by pedestal profile measurements from the new JET High resolution Thomson Scattering System (HRTS), the Lithium beam, ECE and CXRS diagnostics. To achieve a reasonable match between the code results and the experimental measurements, values of $D_\perp$=0.01m^2s^{-1} and $\chi_{\perp e}$=0.3m^2s^{-1} are required in the pedestal region, and much larger values of $D_\perp$=1m^2s^{-1} and $\chi_{\perp e}$=1m^2s^{-1} are needed in the Scrape-Off Layer (SOL) region, respectively. However, the steep density pedestal profile cannot be matched satisfactorily without the inclusion of an inward particle pinch there. To match the very steep ion temperature (T_i) gradient in the pedestal, $\chi_{\perp i}$=0.03m^2s^{-1} and $\chi_{\perp i}$=1m^2s^{-1} are required in the pedestal and SOL regions, respectively. Variation of the ratio $\chi_{\perp e}/\chi_{\perp i}$ (obtained assuming an ion-electron energy equi-partition) was sufficient to find a reasonable fit to the experimental profiles.

At the targets, simulation results are compared with profiles of n_e and T_e obtained with the JET divertor Langmuir probe (LP) array. The agreement between code and experiment is fair, although the lack of vertical strike point sweeps means that

there are only a few points on the radial LP profiles of T_e and n_e. At these high power levels, there is unfortunately no data in the main SOL region with which to better constrain the transport coefficients there. This inter-ELM solution is a good basis for ELM simulations and efforts are underway to include a time dependent simulation for the ELM itself for comparison with recent PIC kinetic simulations of similar JET discharges.

The code-code benchmark is based on an earlier successful JET H-mode modelling exercise using the EDGE2D-NIMBUS for discharge #58569. This is a close match in shape to the 3MA/3T low fuelling case described above, run however at I_p=2MA with gas fuelling and lower P_{IN}~13MW. In this case, $T_{e,ped}$~1.25keV and $n_{e,ped}$~$4\times10^{19}m^{-3}$ with f_{ELM}~30Hz and ΔW_{ELM}~200kJ. In SOLPS5 simulations, an approximation to the ELM cycle is included via an ad-hoc increase in transport coefficients for a specified ELM duration. This benchmarking exercise is featuring a high level of complexity, including carbon impurities and the full (and multiple) ELM cycle and it is also one of the rare occasions on which a time dependent ELM simulation has been performed with SOLPS5. As for the more recent pulse, the simulations are constrained upstream by experimental n_e, T_e and T_i profiles, but without the benefit of the HRTS system. Unlike the higher power shot, however, this lower I_p discharge was run with a slow vertical sweep, allowing high resolution target profiles of ion flux, n_e and T_e to be generated with the LP array.

The high level of agreement between upstream profiles during the pre-ELM phase and 3ms after the start of the ELM from the two codes is extremely encouraging. As for the previous discharge, a strong inward particle pinch in the pedestal region is found to be necessary to match the steep upstream density pedestal.

The agreement between the two codes for both inter-ELM and ELM profiles at the divertor targets is again reasonable given, for example, the different neutral models. Both are a fair match to the experimental data but both largely over-estimate the target T_e, especially during the ELM. Neither code actually predicts much of a rise in the peak density values at the ELM's times. This is clearly symptomatic of a problem in the ELM model itself and suggests that the conductive ansatz used upstream should be replaced by a more convective transient. The inter-ELM and ELM target heat fluxes were computed assuming a total sheath transmission coefficient of γ=7.5. The peak values during the ELM reach 100 MWm^{-2} and 300MWm^{-2} at the inner and outer targets, respectively.

The SOLPS5 benchmark output has been used to study the energy balance during the ELM cycle. The measured time variation of the diamagnetic stored energy during the ELM cycles is well reproduced by the code, giving the observed value of ΔW_{ELM}~200kJ. This energy is extremely well balanced in the code runs by the calculated energy deposited onto the targets (E_{DEP}~160kJ) and the total radiated energy (E_{RAD}~40kJ). Analysis of the energy balance during the ELM with SOLPS5 shows ~20% of ΔW_{ELM} is radiated, with a 2:1 asymmetry favouring the inner divertor. Although this radiation asymmetry is also seen experimentally, the predicted fractional radiated energy is rather lower than the observed value and the ratio of energy deposited on the targets found in the code favours the outer target, in contradiction to that found experimentally, further demonstrating that the simple model of the ELM used here is incomplete.

The pedestal rotation effects on this ELM simulation have been included by adding the toroidal velocity v_ϕ~$10^5 ms^{-1}$ at the inner core boundary. As these simulations are extremely time-consuming, it is hoped that this ansatz could serve as a simplified approximation of the drift effects (which are very difficult to include in the complex time-dependent simulations).

5.1.5 Collaboration on Alfvén waves and fast particles studies

Our activities on JET have mainly focused on the commissioning of the new Alfvén Eigenmode (AE) diagnostic system (KC1T), on the analysis of the data obtained during the 2007 experimental campaigns, and on the preparation and running of dedicated AE experiments, which have been performed in June and September 2008.

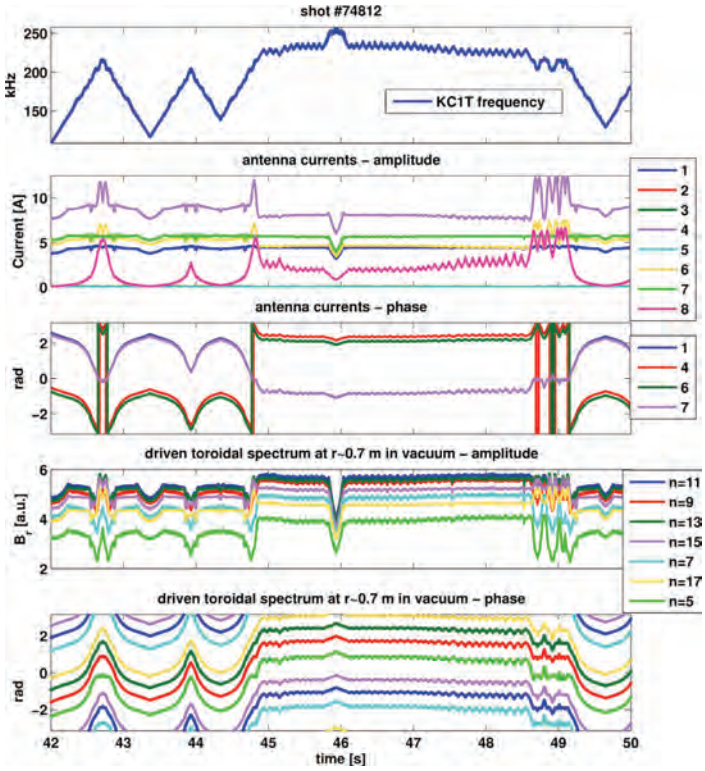

Fig. 5.1.3 *Antenna currents and vacuum spectrum.*

Following the installation of the second set of in-vessel AE antennas, which took place during October 2007, the entire KC1T diagnostic system has had to be re-commissioned for operation on plasmas. Many individual commissioning tasks have been performed, and the system was fully operational during early June 2008, in readiness for the first dedicated experiments. The antenna impedance was measured at various points along the high-voltage transmission path. These measurements revealed a very significant problem of the KC1T system: antennas 5 and 8 (octant 8) appear do be open-circuit in-vessel, most likely because of a fault that occurred during the remote handling installation. Hence, it is not possible to drive current into these antennas, which have now been taken out of service. A matching circuit for the most important frequency band of operation (170-230kHz) was designed, built and it is now ready for use. The operation of the automatic gain control electronics was tested and optimised to increase the driven current up to the maximum operating levels. The full end-to-end calibration of various signals that can be directed to the KC1T system has been done: fast coils, ECE and reflectometry channels. The impedance and polarity of the high frequency coils which are used for the real-time and post-pulse mode detection algorithm was also measured in order to identify possible specific problems for real-time applications. The full antenna field in vacuum and the toroidal spectrum that the measured antenna currents produce have been computed (Fig. 5.1.3).

The SparSpec method was recently implemented as part of the real-time control software within the Alfvén Eigenmode Local Manager. We tested the new software on the bench by simulating operation using selected shots from the past and also ran it on a number of plasma shots. This task is now under way, with the aim of designing an experiment (for execution during the 2009 JET campaigns) to simulate and test on JET plasma possible real-time burn control tools.

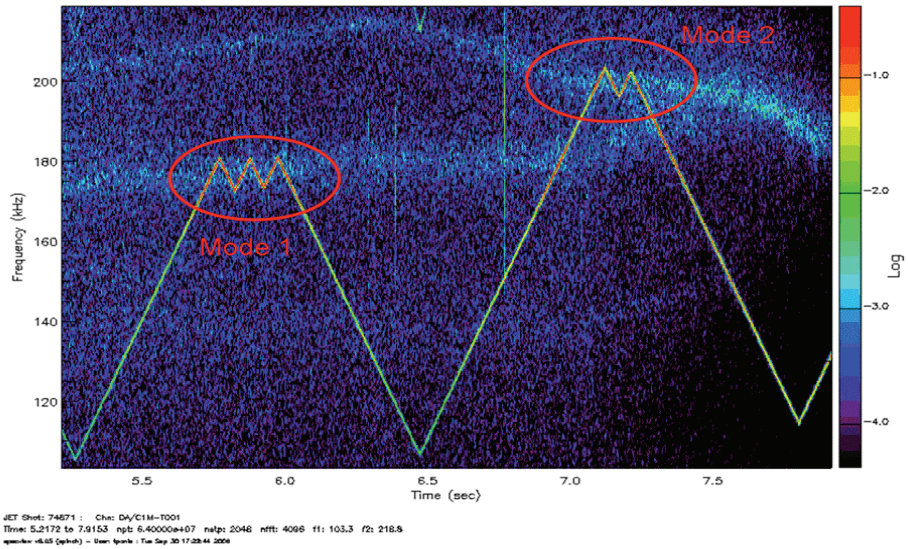

Fig. 5.1.4 *Spectrogram with antenna frequency sweeping and tracking.*

The analysis of the data obtained during the2007 experimental campaigns has been performed using a statistical approach based on a multi-shot database, with the aim to remove possible bias due to single-shot comparisons. This multi-shot statistical analysis has demonstrated that such method does not in fact allow the determination of clear trends in the damping rate measurements for medium-n AEs, as the shot-to-shot variations in the background plasma parameters (such as density and q-profile) are sufficiently large to mask possible dependencies arising from variations in the edge shape and in the properties of the fast ion populations, which were the main target parameters for our analysis. We are now isolating a smaller subset of much more closely matched individual discharges, so as to be able to elucidate the role of individual plasma parameters for the stability of medium-n AEs in JET.

Two dedicated sessions have been run in 2008 to obtain damping rate measurements of stable Alfvén modes of medium and high toroidal mode number n. Moreover, the KC1T diagnostic has been operated parasitically during a significant fraction of the JET experimental time in 2008. Excitation of modes in the medium n range has been demonstrated, as well as tracking (sweep antenna frequency around the mode resonance frequency), as shown in Fig. 5.1.4. The analysis and the interpretation of these results are currently ongoing, with a view to provide stringent test cases for a direct comparison with theoretical models.

5.1.6 Divertor studies: ELM and heat loads

A new, vertically viewing, fast IR diagnostic (KL9) has been installed at the beginning of 2008 on JET, with a sufficient frame-rate to resolve the heat loads

caused by individual ELMs, as well as the filamentary nature of the particle transport at the onset of the instability. A specific task was the assembly of a database originating from as many different ELMy regimes as possible. The goal is a systematic statistical analysis of the data, providing more realistic constraints for the tolerance values for the materials that are foreseen to be used in the ITER divertor. The current prescriptions are limiting the maximum tolerable ELM size to cause an equivalent energy loss of ΔW=1MJ. As the camera commissioning was slightly delayed with respect to the original planning, some data interfaces and software tools were developed in view of this goal, but to achieve the original objectives, the database will need to be processed further in 2009, via remote data processing.

5.2 Collaborations on other fusion experiments

Stability Studies of ARIES Compact Stellarator Reactors - Collaboration with General Atomics, USA

The 3D MHD stability code TERPSICHORE has been applied to investigate the ideal MHD stability properties of the ARIES Compact Stellarator reactor systems. For this purpose, an improved conformal wall has been devised that can handle the more extreme bean-shaped geometrical cross sections that appear in this device. At β=4%, the plasma is virtually stable. At β=6%, a conducting wall scaled by 1.2 times the plasma-vacuum interface stabilises all ideal MHD modes. At β=8%, the plasma remains weakly unstable with a wall right at the plasma edge.

On the possible usage of the T-10 heavy ion beam for poloidal magnetic flux measurements - Collaboration with RRC Kurchatov, Russian Federation

The aim was to investigate whether the heavy ion beam probe on T10 would be able to provide a localised measurement of the poloidal magnetic flux. In a truly axisymmetrical system (an ideal tokamak) this is possible, based on the conservation of canonical momentum. However, in a real tokamak the primary and secondary particles must pass through areas of strong toroidal field ripple outside the plasma. Usage of conservation principles is therefore restricted to the plasma itself and it is necessary that the (strong) effects of TF ripple are calculated and/or calibrated for those parts of the trajectories, which lie between the plasma and the source (for the primaries) and the detector (for the secondaries). The results of the study, which used the heavy ion orbit code developed at Kurchatov, suggest that for a tokamak such as T-10, measurements of the local poloidal flux with accuracies of the order of 10^{-3}Wb are possible in principle, limited by experimental errors, rather than by ripple effects. The achievement of such accuracies will require a careful calibration of the system, in order to correctly evaluate the ripple contribution to the momentum balance, especially for the secondaries on their way from the plasma to the detector. The practical implementation of such a measurement will be a challenging endeavour in terms of new hardware (array detectors) and manpower.

TCV and C-Mod collaboration on rotation inversion with density, MIT, USA

Following results of toroidal rotation reversal with density obtained in TCV, it was proposed to attempt similar experiments on the C-Mod tokamak (MIT, USA) in the frame of the ITPA transport group. After the project submission and acceptance procedure, the CRPP was awarded an operational session in May 2008.

Approximately 20 plasma discharges were performed on the C-Mod machine using prescription of a safety factor ~3 and a high positive triangularity and, for CMod, relatively low plasma densities. The last 3 discharges of the session showed strong evidence for toroidal rotation reversal as a function of increasing plasma density.

Control of ECH polarization – Collaboration with National Institute of Fusion Science, Japan

A collaboration with NIFS (National Institute of Fusion Science) in Japan has been started on the topic of control of polarization of Electron Cyclotron Heating beams. The long-term objective is to realize control methods to guarantee maximal absorption of the beam by the plasma, even under changing conditions or uncertain magnetic configurations at the edge, by adjusting the beam polarization in real-time. This is particularly important in long-pulse devices such as ITER or LHD (Large Helical Device, at NIFS) to avoid excessive wall heating. As a first step, a set of polarizers (one linear and one elliptically polarizing grating mirror) were tested in a low-power test stand at 84GHz. A hill-climber algorithm was implemented and proved capable of reaching the polarization settings necessary for maximal coupling of the EC wave with a horn receiver. A second visit planned in December 2008 will continue this work with new polarizer mirrors and possibly experiments on LHD.

Contribution to JT60-SA [*]

In the context of the negotiation between EU and JA about ITER , it has been agreed that several projects relative to the fusion research will be integrated under the BA concept, in which both partners (EU and Japan) will collaborate in order to accelerate the development of fusion as a source of energy.

Among these projects, one is related to the upgrade of the existing Japanese tokamak JT60, a project called JT60-SA. Several EU countries participate to this project, and the Swiss government decided to support the ECRH part by supplying in kind the procurement of the High Voltage Power Supplies (HVPS) required to power the gyrotrons. Swiss industry is specialized in this type of technology. CRPP will act as RO (Responsible Officer) for EU in the ECRH domain.

Other in-kind procurement is under consideration in the frame of the JT60-SA re-design performed during 2008.

5.3 Plasma surface interactions in collaboration with the University of Basel

Rhodium is considered as one of the most promising materials for the first mirrors of diagnostic systems of ITER, due to its high reflectivity in the visible range and its low sputtering yield. It is thus envisaged to use rhodium coatings on polished metallic substrates. To ensure the reliability of these components in a nuclear fusion environment it is necessary to determine their chemical stability and in particular the reactivity of rhodium towards typical impurities in a tokamak such as carbon, oxygen, beryllium and tungsten. Indeed any change in the surface composition will affect the mirror reflectivity and in turn the signal measured by the diagnostic system.

[*] Part of Swiss Voluntary Contribution to Broader Approach. Not part of the Association workprogrammeme

Co-deposition of rhodium and carbon was carried out to study their reactivity. No chemical bonding was observed between rhodium and carbon whatever the deposition conditions, even at high deposition temperature. The reflectivity of the films decreases linearly with decreasing rhodium concentration and no rhodium with crystalline phase is measured for less 85% of rhodium in the film. All these properties, i.e. no formation of carbide and also no important oxidation in air, show advantages of this material in comparison to molybdenum mirror.

Another point is the possible deterioration of mirrors reflectivity as a result of erosion by ions and deposition of material eroded from the plasma facing components. This represents a serious concern for the reliability of the spectroscopic signals for ITER. Dedicated experiments were initiated in Basel to compare the deposition erosion patterns observed on different materials under similar conditions using laboratory experiments. For this, a new radio frequency plasma source has been developed to provide clean deuterium plasmas in our vacuum chamber. This source has been tested for different plasma conditions. Additionally, an in-situ reflectometry measurement setup with 3 lasers has been developed and installed on the experimental chamber in order to monitor the evolution of the optical characteristics of mirrors exposed to this plasma source.

Test of metallic mirrors (Molybdenum, Copper, Stainless Steel, Rhodium) with a deuterium plasma containing carbon and tungsten impurities are scheduled.

5.4 Organisation of the IAEA-Fusion Energy conference

The CRPP was the local organizer of the 2008 20th IAEA Fusion Energy Conference. The event, hosted by the Swiss government, was held at the United Nations Offices in Geneva (ONU-G) and gathered about 800 participants worldwide. During the conference, ITER Organization and Domestic Agencies organized an exhibition about ITER. A large number satellite meetings were held in parallel during the meeting.

Fig. 5.4.1 *The opening session of the IAEA-FEC*

5.5 Collaborations with other EURATOM Associations

Y. Andrew, JET, Abingdon, UK, *"Plasma rotation measurement comparison between JET and TCV plasmas"*

P. Angelino, X. Garbet, Ph. Ghendrih, V. Grandgirard, G. Falchetto, Association EURATOM-CEA, France, *"Gyrokinetic global turbulence simulations"*

J-F. Artaud, V. Basiuk, Association EURATOM-CEA, France, *"Coupling of the DINA-CH and CRONOS codes to simulate the ITER hybrid scenario"*

K. Avramidis, Association Euratom Hellenic Republic, Greece, *"Studies of high-power gyrotrons for ITER"*

I. Chapman, UKAEA Fusion, UK, *"Sawtooth Stability with Fast Ions"*

A. dellaCorte, Association EURATOM-ENEA, Italy, *"Assembly and instrumentation of a ENEA-broader approach prototype conductor"*

D. Coster, IPP-Garching, Germany, *"SOLPS simulations of scrape-off layer in TCV and JET elmy-H discharges"*

T. Eich, IPP-Garching, Germany, *"Parallel transport dynamics of type-I ELMs in JET and comparison to PIC modelling"*

L.-G. Eriksson, CEA Cadarache, France, *"Ion cyclotron current drive, heating, and sawteeth"*

O.E. Garcia, A. Nielsen, Association EURATOM–Risø National Laboratory, Roskilde, Denmark, *"Modelling and simulation of turbulence interchange dynamics in the TCV tokamak scrape-off layer"*

R. Heller, Association EURATOM-FzK, Germany, *"Final design of HTS current leads for ITER"* (TW4-TDS-CLDES)

M. Hirsch, IPP-Greifswald, **E. Holzhauer,** University of Stuttgart, Germany, *"Loan of two homodyne single-frequency reflectometers and participation in reflectometer measurements and analysis on TCV"*

J. Horacek, Association EURATOM/IPP.CR, Czech Academy of Sciences, Praha, Czech Republic, *"Electrostatic turbulence measurements in the TCV tokamak scrape-off layer"*

F. Jenko, T. Goerler, F. Merz, IPP-Garching, Germany, *"Development and application of the gyrokinetic code GENE"*

T. Johnson, EURATOM-VR Association, Stockholm Univ., Sweden *"Ion cyclotron current drive, heating, and sawteeth"*

A. Koenies, V. Kornilov, A. Mishchenko, S. Sorge, IPP Greifswald, Germany, **A. Bottino, A. Peeters**, IPP Garching, Germany, **R. Hatzky**, Rechenzentrum MPG Garching, Germany *"Linear and nonlinear gyrokinetic code developments and simulations"*

A. Krämer-Flecken, Forschungszentrum Jülich, Germany, *"Fluctuation studies by reflectometry on the TCV and TEXTOR tokamaks"*

H.P. Laqua, IPP Greifswald, Germany, *"Electron Bernstein Waves on TCV"*

E. Lazzaro, **M. Lontano**, **G. Grosso**, EURATOM-ENEA-CNR Association, Italy, *"Development of a linear plasma device for basic wave-particle interactions studies"*

M. Lewandowska, EURATOM-Poland Association, Un. Of Stectin, *"Hydraulic experiments and modeling of CICC"*

Y. Peysson, J. Decker, Association EURATOM-CEA, France, *"Quasilinear Fokker-Planck simulations and modelling of hard X-ray emission in TCV"*

V. Piffl, IPP Prague, Czech Republic, *"Study the carbon ionisation equilibrium using Charge Exchange Spectroscopy and infer transport coefficients for carbon ions"*

J. Rice, JET, Abingdon, UK, *"Plasma rotation reversal measurement comparison between TCV and C-Mod tokamaks"*

A. Rodrigues, N. Cruz, C. Varandas, CFN Lisbon, Portugal, *"Advanced plasma control for TCV"*.

S. Shibaev, Association UKAEA Fusion, UK, *"Data acquisition for fast framing camera on TORPEX and TCV"*

G. Temmerman, UKAEA-MAST, UK, *"Inner-outer divertor power assymetries on TCV (using another fast IR camera we will borrow from MAST for our inner, as yet undiagnosed divertor) & Investigating the effect of optical filters on improving the S/N ratio for infrared divertor measurements"*

I. Tigelis, G. Latsas, Association Euratom Hellenic Republic, Greece, *"Instability calculations in the 170GHz coaxial-cavity-gyrotron beam-duct"*

G. Veres, M. Berta, B. Tal, S. Zoltenik, Association EURATOM-HAS, KFKI Reasearch Inst. For Particle & Nuclear Physics, Budapest, Hungary, *"Plasma imaging and tomography" and "Mitigation disruption studies, particle transport studies in the SOL, high temporal resolution radiation measurements for ELMs"*

C. Wahlberg, EURATOM-VR Association, Uppsala University, Sweden, *"MHD aspects of the sawtooth instability"*

M. Windridge, Association UKAEA Fusion, UK, *"Non-linear modelling of MAST"*

P. Xanthopoulos, P. Helander, IPP-Greifswald, Germany, F. Jenko, IPP-Garching, Germany, *"Geometry interface for Stellarator turbulence"*

L. Zani, Association EURATOM-CEA, France, *"Test of a CEA-broader approach prototype conductor in SULTAN"*

5.6 Other international collaborations

G.A. Cooper, R.S. Peterson, Univ. of the South, Sewanee, TN, USA, *"3D finite element ballooning eigensolvers"*

D. Ernst, Plasma Science and Fusion Center, M.I.T., Cambridge, MA, USA, *"Implementation of a synthetic tangential phase contrast imaging diagnostic in the gyrokinetic code GS2 for TCV"*

R. Ganesh, J. Chowdury, Inst. For Plasma Research, Bhat, Gandhinagar, India, *"Effects of non-adiabatic electron dynamics in gyrokinetic simulations of microinstabilities"*

R. Gruber, EPF-Lausanne, Switzerland, **S.P. Hirshman**, ORNL, USA, **K.Y. Watanabe, H. Yamada, S. Okumara, Y. Narushima**, NIFS, Japan, **K. Yamazaki**, Nagoya Univ., Japan, *"3D anistropic pressure equilibrium and fluid magnetohydrodynamic stability"*

R.W. Harvey, A.P. Smirnov, E. Nelson-Melby, CompX, San Diego, CA, USA, *"Modelling of electron cyclotron wave propagation and electron cyclotron emission in TCV"*

W. Heidbrink, H. Boehmer, UC Irvine, USA, *"Sources for energetic ions for a simple magnetized torus"*

S.P. Hirshman, Oak Ridge National Laboratory, USA, *"Three-dimensional anisotropic pressure free boundary equilibria: the ANIMEC code"*

J. Huettinger, R. Berger, Lawrence Livermore National Laboratory, USA, **E. Valeo**, Princeton University, USA, and *"Development of numerical methods for Vlasov simulations"*

M.Yu. Isaev, Russian Research Centre Kurchatov Institute, Moscow, Russia *"Development of the VENUS-df Code for Bootstrap Current and Neoclassical Transport in Stellarators"*

M.Yu. Isaev, Kurchatov Inst. Moscow, Russia, **H. Maassberg, C. Beidler, J. Nuehrenberg, M. Schmidt, J. Geiger**, IPP-Greifswald, Germany, **A. Bergmann**, IPP Garching, Germany, *"Montecarlo-delta-f neoclassical transport in 3D systems"*

K. Kim, KBSI, South Korea,, *"Assembly and test of the Korean TF conductor qualification sample KOTF2"*

S.Yu. Medvedev, A.A. Martynov, A.A. Ivanov, Yu.Yu. Poshekhonov, Keldysh Institute of Applied Mathematics, Moscow, Russia, **M.Yu. Isaev, V.D. Shafranov, A.A. Subbotin**, RRC Kurchatov Institute, Moscow, Russia, *"Equilibrium and Stability of 2D and 3D plasma configurations"*

M. Mikhailov, A. Subbotin, V.D. Shafranov, M.Yu. Isaev, M. Samitov, Russian Research Centre Kurchatov Institute, Moscow, Russia; J**. Nuehrenberg**, Max Planck Institut fuer Plasma Physik, Greifswald *"Optimisation of Advanced Stellarator Systems"*

J. Miller, ORNL, USA, *"Test of the US TF conductor qualification sample USTF1"*

N. Mitchell, ITER Organisation, *"Instrumentation of the re-test of JATF2 sample", "Assembly and test of the US TF conductor qualification sample USTF2", "Development of a solder filled termination" and "A buoyancy experiment on TF conductor Option2"*

V. Naulin, O.E. Garcia, Risoe, Denmark, *"Adaptation of the ESEL fluid code for modelling of turbulence in the TORPEX device"*

G.R. Odette, Univ. California Santa Barbara (UCSB), Santa Barbara, CA, USA, *"Fracture mechanics and small specimen test technology"*

K. Okuno, JAEA, Japan, *"Assembly and test of the Japanese TF conductor qualification sample JATF3"*

V. Pantsyrny, VNIINM, Russian Fed., *"Assembly and test of the Russian TF conductor qualification sample RFTF2"*

A. Peeters, Y. Camenen, Warwick Univ., UK, *"Modelling of plasma rotation and momentum transport on the TCV tokamak"*

F. Poli, Warwick Univ., UK, *"Characterization of the linear and nonlinear spectral properties of plasma density fluctuations in the TORPEX device in a limited magnetic configuration"*

B. Rogers, Dartmouth College, USA, *"Theoretical characterization of turbulence in TORPEX plasmas"*.

P. Savrukhin, A. Sushkov, D. Kravtsov, RRC Kurchatov Institute, Moscow, Russian Federation, *"Design and fabrication of a tangential X-ray diagnostic for TCV"*

Dr. T.Shimozuma, National Institute of Fusion Science, Japan, *"Real-time control of ECH polarization"*

F. Skiff, Univ. of Iowa, USA, *"Basic wave-particle interactions and turbulence studies in TORPEX"*

P. Smeibidl, HZB, Berlin, Germany, *"Assembly of a SCH High Field conductor sample" and "Design and construction of a SC Cable-in-Conduit coil for a horizontal series-connected hybrid magnet system within the framework of the high field magnet project (HFM) at HZB"*

J. Snipes, R. Parker, M. Porkolab, J. Freidberg, J. Sears, PFSC, MIT, USA, *"Fast particle physics, Alfven waves, and active MHD mode excitation on the Alcator C-Mod tokamak plasma"*

A. Sushkov, Nuclear Fusion Institute, Kurchatov, Moscow, Russia, *"Electron heat transport at switch-off in sawtooth-less TCV discharges"*, and *"Development, commissioning and use of DMPX soft X-ray wire chamber towards Te measurements"* and *"Tangential hard-X-ray imaging"*

D. Tskhakaya, Innsbruck Univ., Austria, *"Comparison of SOLPS and PIC BIT-1 code simulations of the scrape-off layer in TCV and JET elmy-H mode discharges and TCV fast infrared measurements"*

A.D. Turnbull, General Atomics, San Diego, USA, *"Stability studies of ARIES stellarator configurations"*

F. Volpe, General Atomics, San Diego, CA, USA, *"Electron Bernstein wave (EBW) modelling with the ART ray tracing code, planning of EBW experiments on TCV"*

K.Y. Watanabe, S. Okamura, Y. Narushima, H. Yamada, S. Sakakibara, National Institute for Fusion Science, Toki, Japan, *"MHD stability in LHD"*

Y. Wu, ASIPP, P.R. China, *"Assembly and test of the Chinese TF conductor qualification sample CNTF1"*

J. Yu, China Institute of Atomic Energy (CIAE), Beijing, P.R. China, *"Modelling of radiation damage and radiation effects"*

5.7 Other collaborations within Switzerland

E. Cadoni, University of Applied Sciences of Southern Switzerland, Canobbio, *"High strain rate tensile testing of the EUROFER 97 RAFM steel"*

Besides the activities in the field of plasma wall interaction with the University of Basel, of the socio-economics with the LASEN (EPFL) and CEPE (ETHZ), the CRPP also collaborates with the PSI in the field of materials under irradiation.

6 THE EDUCATIONAL ROLE OF THE CRPP

The CRPP plays a role in the education of undergraduate and postgraduate students, particularly in the Faculté des Sciences de Base (FSB) of the EPFL. Advanced education and training in fusion physics and technology and plasma physics topics is carried out as part of the research activities of the Association. Section 6.1 presents the 6 courses given to physics undergraduates and to engineering undergraduates. In their fourth and final year, physics undergraduates spend time with a research group at the EPFL, typically 12 hours per week for the whole year. During this period, they perform experimental or theoretical studies alongside research staff, discovering the differences between formal laboratory experiments and the "real" world of research. After successful completion of the first year of the Master Programmeme (4^{th} year of studies), physics students are required to complete a "master project" with a research group, lasting a full semester. This master project is written up and defended in front of external experts. The CRPP plays a role in all of these phases of an undergraduate's education, detailed in Sections 6.2 and 6.3.

As an academic institution, the CRPP supervises many Ph.D. theses, also in the frame of the Physics Section of the EPFL. 4 PhDs were awarded in 2008. At the end of 2008 we had 39 PhD students supervised by CRPP members of staff, mostly in Lausanne but also at the PSI site in Villigen. Their work is summarised in Section 6.4.

6.1 Undergraduate courses given by CRPP staff

S. Alberti, *Chargé de cours – "Plasma Physics I"*
This course is an introduction to plasma physics aimed at giving an overall view of the essential properties of a plasma and at presenting the approaches commonly used to describe its behaviour. We study single particle motion, the fluid description and the kinetic model. The relation between plasma physics and developing a thermonuclear reactor is presented and illustrated with examples.

N. Baluc, *Professeure titulaire – "Materials Physics"*
Basic course on materials physics, presented as an option to 3^{rd} year Physics students. The course covers the theory of diffusion, dislocations and plasticity as well as the characterization of materials. Ways of production, structures, microstructures, physical and mechanical properties are presented for pure metals, intermetallic alloys, superalloys, shape memory alloys, steels, quasicrystals, glasses, gels, liquid crystals, aggregates, ceramics, composites, polymers, and nuclear materials for fission and fusion reactors.

N. Baluc - Profresseure titulaire**, J. Fikar, G. Lucas, R. Schäublin** - Maître d'Enseignement et Recherche**, P. Spätig** - Maître d'Enseignement et Recherche: *"Fundamentals of radiation damage and effects"*
This 28-hours course is part of the EPFL's Minor in Space Technologies. The objective of this course is to provide a detailed description of fundamental interaction mechanisms between particles and matter, radiation damage and its characterization methods, and radiation effects with emphasis on the relationships between microstructure and mechanical properties. Various types of materials are being considered as well as various examples of applications related to nuclear, semi-conductor and aerospace industries.

A. Fasoli, Professor – *"Plasma physics II"*
One semester option course presented to 4th year Physics students, introducing the theory of hot plasmas via the foundations of kinetic and magnetohydrodynamic theories and using them to describe simple collective phenomena. Coulomb collisions and elementary transport theory are also treated. The students also learn to use various theoretical techniques like perturbation theory, complex analysis, integral transforms and solutions of differential equations.

A. Fasoli, Professor – *"General Physics II"*
This course completes the introduction to mechanics provided in the first semester with the basic concepts of statics, oscillations and special relativity. It also covers the whole of thermodynamics, from the introduction to heat, temperature and kinetic theory to the first and second principles, including entropy and thermal engines, ending with a treatment of transport and non-equilibrium phenomena in open systems.

A. Fasoli, Professor and **M.Q. Tran**, Professor - *"Nuclear fusion and plasma physics"*
The aim of this course is to provide a basic understanding of plasma physics concepts of fusion energy, and of the basic principles of fusion reactors, including the main technological aspects. This course was given within the frame of the Master in Nuclear Engineering.

J.B. Lister, *Maître d'Enseignement et Recherche (MER) – "Plasma Physics III"*
An introduction to controlled fusion, presented as a one semester option to 4th year Physics students. The course covers the basics of controlled fusion energy research. Inertial confinement is summarily treated and the course concentrates on magnetic confinement from the earliest linear experiments through to tokamaks and stellarators, leading to the open questions related to future large scale fusion experiments.

M.Q. Tran, *Professor - "General Physics III and IV"*
This course, given to the Mathematics Section, covers hydrostatic, hydrodynamics waves and electromagnetism (General Physics III) and quantum mechanics (General Physics IV).

L. Villard, *Professeur Titulaire – "Numerical Physics I-II"*
Full year course given to students in their 2nd year in Physics. The course covers various time and space integration techniques for ordinary and partial differential equations, and is applied to various physics problems ranging from particle dynamics, hydrodynamical equilibrium, electromagnetism and waves. It includes a strong practical work aspect.

H. Weisen, Chargé de cours, *"Physique Générale I SV"*
This is a classical mechanics course on basic kinematics and dynamics, systems dynamics and rotation taught during the autumn term to a class of 150 first year life science students. It features two weekly hours of classroom lectures followed by two hours of exercises.

6.2 Undergraduate work performed at the CRPP

EPFL Master students (4th year)

Summer 2008 semester:

Urs Amherd: *"Study of suprathermal electron dynamics in TCV"*

Sébastien Boutinard Rouelle: *"Spectroscopy of thermal plasma spraying"*

Alexandre Bovet: *"Estimation de la température et du potential plasma avec la sonde HEXTIP dans les plasmas de TORPEX"*

Alice Burckel: *"Simulation of fast ions in a toroidal plasma device"*

David Grange: *"Electrical discharge machining"*

Jérôme Guterl: *"Etude experimentale des modes de confinement L et H dans un plasma toroidal simplement magnetise"*

Francis Voutaz: *"Etude du profil de rayonnement X-mou du plasma en présence de grand ELMs"*

Winter 2008-2009 semester

Juliette Audet: *"Etude des oscillations de dents-de-scie sur TCV et prédiction pour ITER"*

Lucie Brocher: *"Beam and thermal ion diamagnetic drifts in a heliotron"*

Aurélien Gallice: *"Diffusion of charged particles in an electrostatic Potential"*

David Martinet: *"Current density measurements in the BAI device"*

Imram Quaine: *"Propriétés spectrales de la turbulence dans TORPEX en présence d'un champ magnétique vertical présentant une courbure radiale"*

Mikael Rancic: *"Calibration in situ de la réponse fréquentielle des sondes magnétiques de TCV"*

Boris Roulet: *"Propriétés statistiques de la turbulence dans TORPEX en présence d'un champ magnétique vertical courbé dans la direction radiale"*

Mathilde Schmitt: *"Propagation of a microwave beam through an optical system using phase reconstruction method, ray matrices and huygens' integral"*

Ralph Schnyder: *"RF breakdown in capacitively coupled reactor"*

6.3 EPFL Master degrees awarded in 2008

Pierre-Henri Chevalley: *"Calibration of the Electron Cyclotron Emission (ECE) radiometry on the TCV Tokamak"*

Lucia Federspeil: *"Investigation of the excitation threshold for pressure gradient driven instabilities in TORPEX plasmas"*

Pierre Kikudji: *"Characterization of the neutron rate in ASDEX Upgrade"*

Etienne Küng: *"Effect of magnetic configuration on fluctuations and turbulence in TORPEX toroidal plasmas"*

Thibaut Vernay: *"Effet des collisions sur les instabilities d'électrons piégés"*

6.4 Postgraduate studies

Postgraduate courses given in 2008

Nadine BALUC, Robin SCHAUBLIN, Philippe SPÄTIG: *"Multiscale Approach of Plastic Deformation of Metals and Alloys"*
This 28-hour course is part of the EPFL Doctoral School in Materials Science and Engineering. It is aimed at introducing the fundamental phenomena of plastic deformation of metals and alloys, and at providing the necessary background to understand the multi-scale nature of the plastic deformation from the atomistic scale up to the continuum one. The course is divided into eight chapters: 1) elasticity, 2) plasticity, 3) finite element simulations, 4) dislocations, 5) strain hardening model, 6) molecular dynamics simulations, 7) kinetic Monte-Carlo simulations, 8) discrete dislocation dynamics simulations.

Trach-Minh TRAN: *"MPI, An Introduction to Parallel Programmeming"*
This course, part of the EPFL Doctoral School programmeme, is organized as a 4-day, intensive, full-time course. It puts emphasis on practical implementation and includes examples and exercises performed on a dedicated PC Linux cluster. After an introduction to various parallelization models such as OpenMP, Pthreads, TBB, PVM, the course focuses on the Message Passing Interface (MPI) standard. The topics covered include: point-to-point communications; collective communications; derived types; communicators, groups and topologies; development aid tools for MPI programmeming; introduction to MPI-2; parallel numerical libraries: ScaLapack, Petsc, FFTW. The course was given 3 times in 2008.

Stephan BRUNNER, Jean-Marc MORET: *"Advanced Theory of Plasmas"*
This course is part of the EPFL Doctoral School Physics Programmeme. It aims at completing the theoretical knowledge in plasma physics, in particular of PhD students. It covers the following advanced topics: kinetic theory of gases and plasmas; collisional transport theory; nonlinear effects in plasmas; microinstabilities and waves in inhomogeneous plasmas. It is a full semester course with 2h/week lecture and 2h/week exercises, totalling 56 hours.

Doctorate degrees awarded during 2008

Lukas DERENDINGER: *"Design, Characterisation and Modelling of a High Current DC Arc Plasma Source for Silicon and Silicon Carbide Processing at Low Pressure"* (EPFL thesis No. 4238 (2008))

In the frame of this thesis, two similar high current DC arc (HCDCA) plasma sources were investigated in a low gas pressure regime (10^{-3}–10^{-2}mbar). One of them was initially designed for the epitaxial growth of silicon and silicon germanium (LEP), the other for the industrial deposition of diamond (BAI).

The LEP source was analysed using pure argon plasmas. Measurements of the ion saturation current were performed with a custom-built multi-Langmuir probe to analyse plasma density homogeneity. Plasma instabilities at 50Hz were observed and studied by different means. One source of the instability is the AC current used for the filament heating, whereas lower frequency instabilities are due to the use of a ring shaped anode. A sensitive Hall sensor was used to measure the magnetic field induced by the discharge current. It was found that depending on the plasma parameters gas pressure and external magnetic field the current tends to attach at different points on the anode, leading to a complete loss of reactor symmetry. The installation of an additional cusp field around the reactor chamber lead to an increase of the overall homogeneity of the plasma density, but it could not resolve the problems of current attachment. In the following the ring anode was replaced by a point anode and the maximum external magnetic field strength was increased by a factor of ten.

With a novel multi-Hall probe the current density of the now columnar shaped plasma was measured, showing a strongly peaked current density profile, when an external magnetic field is applied. Together with ion saturation current measurements made with a Langmuir probe, the electron temperature inside the plasma column was estimated to be about 4eV.

In earlier works made on the BAI reactor the high dissociation efficiency of the HCDCA plasma source has already been shown. Optical emission spectra were compared between RF plasmas, low pressure (1.5mbar) HCDCA plasmas and our very low pressure (10^{-3}–10^{-2}mbar) HCDCA plasmas. The dominating species found in RF plasma spectra are molecular, the spectra of low pressure HCDCA plasmas are dominated by atomic species and the spectra of very low pressure HCDCA plasmas are dominated by ions, emphasising the high dissociation efficiency of this system.

Silane and Methane were used as precursor gases in the BAI reactor for the deposition of silicon carbide films. Promising high deposition rates up to 9nm/s were found, but FTIR spectroscopy showed high hydrogen and oxygen concentrations in the porous films, making the not optimised deposited material useless for the application of wear-resistant coatings.

Microcrystalline hydrogenated silicon (μc-Si:H) is viewed as a cost- and energy-effective alternative to crystalline silicon for the production of solar cells. A detailed analysis of the deposition rate and the Raman crystallinity of μc-Si:H films deposited in the BAI reactor showed deposition rates up to 6.5nm/s and a wide range of crystallinity from 0–80%. Film thickness inhomogeneity in silicon solar cells has to be less than 5%. To meet this standard a first substantial improvement was achieved with the installation of a linear gas injection along the plasma column. Tests on large surface glasses ($47\times37cm^2$) revealed strong diffusive effects, which could be reproduced with a simple gas diffusion model. The model showed the necessity to reduce the dead volume around the plasma and to set the substrates as close as possible to the plasma column in order to minimise film thickness inhomogeneity due to diffusion. Deposition rate measurements made in these conditions confirmed the results of the model.

The development of a method to estimate the dissociation efficiency of the plasma by simple pressure measurements showed also an important increase of the silane

dissociation from 75% to 92% when the plasma is confined in a smaller volume. Therefore, compared to the reactor with a large dead volume, only a third of the initial silane is lost to the pumps.

Illy PAVLOV: *"Analysis of Plasma Dynamic Response to Modulated Electron Cyclotron Heating in TCV Tokamak"* (EPFL Thesis No. 4086(2008))
This thesis presents the analysis and interpretation of perturbative Modulated Electron Cyclotron Heating (MECH) experiments performed in the TCV tokamak with particular attention paid to the non-linear phase coupling of heat waves. A new analysis method for the characterization of the plasma non-linear dynamic response to modulated heating was developed on the basis of Higher Order Spectral Analysis (HOSA) technique. This method was applied to signals from different diagnostics, such as electron cyclotron emission and soft X-ray measurements, and was extensively used to quantitatively characterize the effect of nonlinear phase coupling.
In sawtooth free discharges a detailed analysis of the propagation of heat waves demonstrated that their phase coupling is solely related to properties of heat sources. It was shown that coupled heat waves loose their phase coherence while propagating in the plasma. The dissipation of phase coupling is due to different phase velocities of heat waves and their diffusive damping.
In cases when MECH is applied to sawtoothing plasmas a direct experimental evidence of MECH-sawtooth nonlinear phase coupling has been demonstrated using HOSA techniques, in particular bispectrum and bicoherence profiles. The detailed analysis demonstrates a periodic modification of sawtooth behaviour by modulated ECH. It was shown that a simple diffusive model for the perturbed electron temperature with MECH source term cannot be used for transport analysis in the presence of MECH-sawtooth coupling. Self-consistent time dependant transport simulations including a sawtooth relaxation model are capable of properly reproducing the effect of MECH-sawtooth phase coupling and can be used for transport analysis. On the basis of these simulations, a hypothesis for MECH-sawtooth coupling based on periodic modifications of the magnetic shear was proposed. Additional information provided by HOSA analysis enabled a correct interpretation of the plasma dynamic response to modulated heating in the presence of MECH-sawtooth coupling.

Amuthan RAMAR: *"On the Relationship Between the Microstructure and the Mechanical Properties of an ODS Ferritic/Martensitic Steel"* (EPFL Thesis No. 4213(2008))
In the quest for materials for the first wall of the future fusion reactor, it has been shown that Oxide Dispersion Strengthened (ODS) ferritic / martensitic (F/M) steels appear to be promising candidates. Their inherent properties, good thermal conductivity, swelling resistance and low radiation damage accumulation, deriving from the base material EUROFER 97, are further enhanced by the presence of oxide particles. They would allow, in principle, for a higher operating temperature of the fusion reactor, thereby improving its thermal efficiency. In effect, their strength remains higher than the base material with increasing temperature. EUROFER97 is a reduced activation F/M steel, whose chemical composition is 8.9wt.%Cr, 1.1wt.% W, 0.47wt.%Mn, 0.2wt.%V, 0.14wt.%Ta and 0.11wt.%C and Fe for the balance. EUROFER97 has a tempered martensitic structure.
As a part of development of ODS based EUROFER97, a new ODS F/M steel based on EUROFER 97 was developed with the strengthening materials as Y_2O_3 maintained at 0.3wt%. The ODS powder was produced by powder metallurgy route. The EUROFER97 atomized powder with particle sizes around 45μm was ball milled in argon atmosphere in a planetary ball mill together with yttria particles with sizes about 10 to 30 nm and also with 0.3wt% of yttria and 0.3wt% of Ti. The ball milling

is conducted until the EUROFER97 particles reach their minimum size. A detailed examination was carried about the solubility of yttria in the EUROFER97 matrix. It was found that yttria is not dissolved in the matrix of EUROFER97, whereas it got embedded in the particles of EUROFER97.
The milled powders were then compacted by HIPing at 1150°C for 2.5hrs at a pressure of 190MPa. A detailed study was carried out to identify the mechanism behind the alloy densification. It was found that temperature has more influence than pressure, which confirms that densification is mainly through diffusion, such as surface, lattice and grain boundary diffusion. The heat treatment of normalization and tempering was given to all the alloys in order to have a consistency in the microstructure. TEM observations showed that Casted EUROFER97, atomized EUROFER97, ball milled EUROFER97 and ODS Yttria present microstructure morphologies typical of tempered martensite, whereas ODS Ti presents a nano sized grain microstructure with an average grain size of 200nm. In ODS Yttria, yttria presents an average particle size distribution of 25nm. In ODS Ti, Y-Ti-O presents an average particle size distribution of 7nm.
Dispersion barrier strengthening model was used to understand and to define the hardening due to the yttria particle in the EUROFER97 matrix. A new model was proposed to identify the total alloy hardening when more than one mechanism is acting at a time. It was found in the heat treatment studies that the hardening due to dispersed oxide is more pronounced for the heat treatment up to 800°C in both ODS Yttria and ODS Ti, whereas the influence of the particles in alloy hardening is unpronounced for heat treatment at 1000°C due to the raise in the dislocation and lath boundary density.
In the mechanical property analysis, it was found that the ODS yttria and ODS Ti present higher strength than all series of EUROFER97. In EUROFER97, ball milled EUROFER97 presents higher strength. The total elongation is higher for EUROFER97 than ODS series. To understand the significant hardening observed in EUROFER97 by oxide addition in relation to microstructure, HRTEM technique was used. HRTEM results showed that the oxide particles are not coherent with the matrix, indicating that it is hard for the moving dislocation to pass through the yttria particles and thus resulting in higher strength. TEM in situ heating experiments were performed on ODS yttria and ODS Ti to understand thermal stability of the oxides and carbides existing in the EUROFER97 matrix. It was found that the yttria particles are very stable without any change in shape and size for temperatures up to 1000°C, whereas particle dissolution and coarsening is observed above 500°C in Y-Ti-O particle. Differential strain rate experiments were performed to understand the types of deformation mechanism happening in ODS Yttria and ODS Ti. At low temperature the deformation was caused by the formation of the Orowans loop around the yttria particle, whereas at high temperature it is dislocation climb that is responsible for the deformation.

Gang YU: *"Analysis of Nano-Sized Irradiation-Induced Defects in Fe-base Materials by Means of Small Angle Neutron Scattering and Molecular Dynamics Simulations"* (EPFL Thesis No. 4279(2008))
Thermonuclear fusion of light atoms is considered since decades as an unlimited, safe and reliable source of energy that could eventually replace classical sources based on fossile fuel or nuclear fuel. Fusion reactor technology and materials studies are important parts of the fusion energy development programme. For the time being, the most promising materials for structural applications in the future fusion power reactors are the Reduced Activation Ferritic/Martensitic (RAFM) steels for which the greatest technology maturity has been achieved, i.e., qualified fabrication routes, welding technology and a general industrial experience are almost available. The most important issues concerning the future use of RAFM steels in fusion power reactors are derived from their irradiation by 14 MeV neutrons that are the product, together with 3.5 MeV helium ions, of the envisaged

fusion reactions between deuterium and tritium nuclei. Indeed, exposure of metallic materials to intense fluxes of 14 MeV neutrons will result in the formation of severe displacement damage (about 20-30 dpa per year) and high amounts of helium, which are at the origin of significant changes in the physical and mechanical of materials, such as hardening and embrittlement effects, for instance.

This PhD Thesis work was aimed at investigating how far the Small Angle Neutron Scattering (SANS) technique could be used for detecting and characterizing nano-sized irradiation-induced defects in RAFM steels. Indeed, the resolution limit of Transmission Electron Microscopy (TEM) is about 1 nm in weak beam TEM imaging, and it is usually thought that a large number of irradiation-induced effects have a size below 1 nm in RAFM steels and that these very small defects actually contribute to the irradiation-induced hardening and embrittlement of RAFM steels occurring at irradiation temperatures below about 400°C.

The aim of this work was achieved by combining SANS experiments on unirradiated and irradiated specimens of RAFM steels with Molecular Dynamics (MD) simulations of main expected nano-sized defects in irradiated pure Fe and Fe-He alloys, as model materials for RAFM steels, and simulations of their corresponding TEM images and SANS signals. In particular, the SANS signal of various types of defects was simulated *for the first time*.

The methodology used in this work was the following:

SANS experiments were performed by applying a strong saturating magnetic field to unirradiated and irradiated specimens of three types of RAFM steels, namely the European EUROFER 97, the Japanese F82H and the Swiss OPTIMAX A steels. The available irradiated specimens included specimens which had been irradiated with 590 MeV protons in the Proton IRradiation EXperiment (PIREX) facility at the Paul Scherrer Institute (PSI) at temperatures in the range of 50-350°C to doses in the range of 0.3-2.0 dpa. SANS spectra as well as values of the so-called *A* ratio, which represents the ratio of the total scattered intensity to the nuclear scattered intensity, were obtained for the various irradiation doses and temperatures investigated.

MD simulations of atomic displacement cascades in pure Fe and in Fe-He alloys were performed using Embedded Atom Method (EAM) many-body interatomic potentials. The main nano-sized defects that should be produced in RAFM steels under irradiation were created by means of MD in pure Fe. These included dislocation loops of various types, voids, helium bubbles with various He concentration and Cr precipitates.

TEM images of cascade damage and all the defects created by MD were simulated in the dark field/weak beam imaging modes by using the Electron Microscopy Software (EMS) developed by P.A. Stadelmann (EPFL) and analyzed in terms of variations of contrast intensities versus depth inside the specimen.

The SANS signal provided by cascade damage and all the defects created by MD was simulated by using a slightly modified version of EMS, accounting for neutrons instead of electrons.

In this work the SANS technique has proven to be a very powerful tool for detecting nano-sized irradiation-induced defects and a tool well complementary to TEM for characterizing such very small irradiation-induced defects. Indeed, TEM appears most adapted to investigate structural defects, such as dislocation loops and helium bubbles with high helium concentration, which yield significant lattice deformation of the surrounding matrix, while SANS is most adapted to investigate phase defects, such as voids, helium bubbles with low helium concentration and Cr precipitates. By combining the results of SANS experiments with those of MD simulations, TEM image simulations and SANS signal simulations, the nano-sized irradiation-induced defects were tentatively identified as small helium bubbles. While the radiation hardening measured for RAFM steels cannot be explained by accounting only for the defects observed in TEM, it could be successfully modeled by accounting also for a reasonable number density of the nano-sized defects evidenced using the SANS technique.

Ph.D. Theses supervised by CRPP staff at the end of 2008

Mattia ALBERGANTE: *"Anomalous transport of energetic particles driven by ITG turbulence"*
This thesis is dedicated to the study of the turbulent transport of energetic particles, modelled as Maxwellian tracers, by means of the GENE code. Several simulations were performed, mainly focusing on the particle transport of Helium populations characterized by $T_{He} >> T_e$. Two potentially dangerous characteristics have been, namely the inward particle flux for low temperature distributions and the non vanishing high temperature diffusivities. Although these two phenomena were observed in a wide range of parameters, only the latter affected a modelled ITER discharge, where no pinch was observed. An estimate of the diffusivity for this scenario has shown that $D_{fast} = 0.15 * D_i$ at $T_{fast} = 50 * T_i$, suggesting that gyroaveraging effects might not be sufficient for suppressing the particle transport. Phase space investigations show that the particle flux is mainly driven by the low energy region of the distribution. However, the phase space resolution may not be able to probe narrow regions, and further studies are needed. Finally, an interface for mapping GENE turbulent fields onto general tokamak geometry has been written and the HMGC code, dedicated to the study of the single particle motion, has been ported to the Pleiades2 cluster. The main objective for 2009 is to improve the understanding of the mechanism driving the transport, employing both the Eulerian and the Lagrangian approaches.

Alessandro BORTOLON: *"Plasma rotation and momentum transport studies in the TCV Tokamak based on Charge Exchange Spectroscopy measurements"*.
With the restart of TCV experimental activity, a considerable effort has been devoted to the commissioning of the newly upgraded CXRS diagnostic, facing some unexpected issues, e.g. the accidental exposure of in-vessel mirrors to glow discharge and electric fault of one of CCD detectors. The diagnostic alignment could be verified by reconstructing the ray path from out-vessel measured references. Data have been validated finding consistency between measurement by different CXRS systems and former measurement on similar experiments. Specific experimental activity focused on plasma rotation in limited L-mode. The test case of inversion of toroidal rotation u_ϕ has been studied with the improved diagnostic capabilities. The effect of low edge safety factor q_e has been addressed in plasmas with q_e down to 2.2. While former results have been confirmed, the higher spatial resolution permitted an accurate measurement of the velocity gradient and the direct observation of the core acceleration in co-current direction (Δu_ϕ=2-5 km/s) induced by the sawtooth instability. This effect remains the dominant intrinsic rotation source in plasmas with $q_e<2.5$, where, in contrast with previously proposed scaling laws, u_ϕ appears close to zero in the region $0.6<\rho<0.95$ and practically insensitive to density/collisionality. The simultaneous measurements of u_ϕ and u_θ allowed us to estimate the radial electric field E_r profile, that in L-mode discharges may exceed 4 kV/m and abruptly change sign in case of rotation inversion.

Loïc CURCHOD: *"Heating of High Density Plasmas in the TCV Tokamak"*
The extension of the TCV operation domain to high density heated plasmas is being explored with central Electron Bernstein Wave (EBW) heating. In these experiments, an optimum coupling of the injected O2 power to the EBW requires a steep edge density gradient. Thomson scattering shows that these conditions are met at the edge of low-*q* shaped H-mode plasmas in ELM-free phases. Unfortunately, operating at low-*q* implies strong central sawtooth activity, which makes the standard Fast Fourier Transform (FFT) analysis unreliable for the power deposition location of

modulated EBW heating. Recently, the Break-In-Slope (BIS) analysis method has been investigated to circumvent this difficulty. The simplest form of the BIS analysis assumes that, if the heating power modulation is fast enough, the electron temperature T_e has a prompt linear response to steps in the ECH power. At each heating power step time, the jump in the slope of a T_e time trace gives thus an estimation of the local variation of the absorbed power. The BIS analysis allows resolving the power deposition location with a time rate as high as the power modulation frequency whereas FFT analysis needs longer time intervals. Moreover, the BIS analysis allows selecting EC power pulses at times without sawtooth perturbations, yielding an estimation of the deposition profiles where the FFT and correlation analyses failed. In view of future modulated EBW heating central deposition experiments, the BIS method has been successfully tested on the signal of a high space and time resolution soft X-ray detector to determine the power deposition location in different X2 heating scenarios. The results are in very good agreement with the TORAY ray-tracing code as well as with the LUKE ray-tracing and Fokker-Planck equation solver code.
A reception antenna for the EM waves in the 0.5-1.5GHz range has been recently installed on TCV. It is meant for the detection, frequency spectrum analysis and monitoring of the lower-hybrid parametric instability decay waves generated at the slow-extraordinary to Bernstein (SX-B) mode conversion. This non-linear three-wave interaction is a potential loss channel for the O-SX-B electron Bernstein wave heating and its study will help optimizing the EC-EBW coupling with, in particular, optimum injection angles for the O-SX conversion. The antenna has been connected to an analog spectrum analyzer remotely controlled. The spectrum is continuously scanned in the frequency range of interest and digitized such that a complete spectrum is available every 10 to 100ms. The full equipment has been successfully tested with an artificial signal.

Cornelis DE MEIJERE: *"Experimental study of turbulence in the edge region of TCV plasmas"*
Over the past year, work was mainly conducted on the simple reflectometer system on loan from the W7-AS stellarator device at the Max-Planck-Institute for Plasmaphyisk in Garching, Germany. Lab testing of two newly acquired broad band antennas showed that these antennas do not meet design specifications, and have to be remade. A definitive mechanical support for the reflectometer system was put into place and the diagnostic was readied for operation, to commence at the end of 2008. The principles of the Doppler reflectometry technique were studied, and the possibility of improving the resolution in wave-vector space was investigated. Finally, some additional analysis software was developed.
The principal part of this thesis, however, will be a detailed study of edge turbulence in TCV, using the new tangential phase contrast imaging (PCI) system. This system is planned to become operational in 2009. The system will enable spatially localized measurements of plasma density fluctuations having wavelengths between 0.1-7 cm with high spatial and temporal resolution.

Emiliano FABLE: *"Particle transport theory"*
A quasi-linear gyrokinetic model is developed to predict stationary values of the density logarithmic gradient for electrons and ions. The contributions to the off-diagonal convective term composing the turbulent particle flux are derived from first principles and evaluated with numerical parameters scan. The application of the model and the numerical scans have allowed a theory-experiment comparison where qualitative trends seen in the experiment are found in the theory. A 'universal' behaviour of the density peaking, through the pinch coefficients, in terms of the dominant microinstabilities is discussed in detail. As a second

application, the model has been applied successfully to interpret the observations on particle transport from the eITB scenario in TCV.

Lucia FEDERSPIEL: *"Study of electrostatic instabilities in TORPEX plasmas"*
The thesis project started in September 2008. In the first months, the research was focused on deepening the Master Project topic (February 2008), which investigated the existence of an excitation threshold for pressure gradient driven instabilities in TORPEX plasmas. Experiments with Argon plasmas were carried out as a consequence of the very promising results obtained with this gas at the end of the Master Project.

Federico FELICI: *"Control of ECH systems in Tokamaks aimed at Neoclassical Tearing Mode suppression"*
In preparation for experiments on tearing mode stability on TCV, the effect of localised current drive on classical tearing mode stability was analysed using a cylindrical stability code coupled to the CHEASE equilibrium solver. Preliminary results show that co/counter current drive can be stabilizing or destabilizing depending on whether the current is deposited inside or outside the rational surface. Separately, work is under way to operate the ECH system in real-time feedback mode, allowing it to respond to effects in the plasma during the discharge. As a first experimental verification, the peak of the x-ray emission profile -determined from the DMPX diagnostic- was controlled in feedback by varying the angles of the ECH launcher. Also, a set of algorithms was developed for real-time multichannel x-ray diagnostic signal processing. These algorithms allows one to detect the sawtooth inversion radius, the location of magnetic islands, and to determine profile information. Finally, in collaboration with the NIFS (National Institute of Fusion Science) in Japan, work has been done on the control of ECH beam polarization for maximal absorption. As a first step, a polarizer mirror set-up in a low power stand was used to test real-time control algorithms envisaged for use on LHD (Large Helical Device). In later stages, a measure of the absorption efficiency will be used to adjust the polarization in response to changes in the plasma. Also, an EFDA bid for real-time polarization control experiments on TCV was successful, which will incorporate the use of fast polarizers in the TCV X2 transmission line as well as low-power tests on RF Control Unit for the European 2MW ITER Gyrotron.

Silvano GNESIN: *"Suprathermal electron dynamics in the TCV tokamak"*
Resonant wave heating and current drive in the TCV tokamak can generate a significant suprathermal electron population in an energy range from a few tens to hundreds of keV, resulting in hard-X ray bremsstrahlung emission. Understanding suprathermal electron generation and dynamics is key to achieving advanced plasma scenarios and to controlling MHD instabilities. To address this issue a new spectroscopic HXR camera system has been proposed and designed; this system is envisioned to comprise up to 4 cameras of typically 25 detectors each, distributed around the poloidal plane to provide the possibility of a 2D tomographic inversion. The detectors chosen are CdTe semiconductor diodes, with radiation to be collimated by tungsten metal foils in a modified Soller collimator configuration. A complete conceptual design has been performed, resulting in a comprehensive white paper. A first test camera is in an advanced mechanical design stage, with fabrication of vacuum components already well underway. The expected signal to the detectors has been studied by employing the EGSnrc Monte Carlo code, particularly to determine the expected parasitic detection and minimize its impact by opportune design. The expected suprathermal electron population in a given TCV plasma is modelled by the use of the LUKE Fokker Planck code. Work is

currently underway with LUKE to simulate the EC power deposition and the attendant suprathermal electron generation and radial transport for comparison with data obtained in past TCV experiments.

Alexandr GUDOZHNIK: *"Numerical and experimental validation of sawtooth control using ECCD"*
TCV discharges have been analyzed using the ASTRA transport code, showing fast sawtooth stabilization (i.e. very rapid transition from small (~2.5 ms) to large (20-40 ms) sawtooth period) during toroidal scans of ECCD injection angle.
Numerical simulations of different profiles (q, Te, ne) transformation during sawtooth crash using full and partial reconnection model have been performed.
A MATLAB user-friendly interface has been developped for the spectral analysis of ECE. It contains various functions such as detrending, filtering, cross-correlation analysis, FFT/PSD/CSD and wavelets. This tool is useful for discovering weak or localized modes in signals with high level of noise.

Barbora GULEJOVA: *"Exploitation of the new AXUV diagnostic"*
The successful time-dependent simulation of the TCV Type III ELM event using the coupled fluid-Monte Carlo SOLPS5 code, was encouraging in terms of absolute agreement with experimental upstream and target measurements. However, a closer look at the time evolution of target electron and ion temperatures has been undertaken, because the decrease in simulated ion temperature after the ELM "switch-off" is significantly faster than expected on the basis of ion sonic transit time from upstream to target. The flux limitors used in the SOLPS simulations play a role in the discrepancies in the time evolution of target temperatures. Results of the kinetic BIT1 code show a strong time-dependence of the flux limitors and this needs to be taken into account.
A significant part of the research programme in 2008 was devoted to JET. Contributions were made to the ongoing process of code-experiment and code-code benchmarking. Two separate H-mode pulses were modeled by SOLPS5. In one case the ELM-free phase of a high power/stored energy discharge with large ELMs was simulated. Such a discharge has ELMs approaching an energy loss, ΔW_{ELM}~1MJ which is close to the maximum allowed for the avoidance of material damage on ITER. A reasonable match between code and experiment is achieved upstream and fair match at the targets. This inter-ELM solution is a good basis for ELM simulations and efforts are underway to include a time dependent simulation for the ELM itself for comparison with recent PIC kinetic simulations of similar JET discharges.
In the second case, the full ELM cycle of a lower power H-mode discharge with ΔW_{ELM}~200kJ, examined previously in detail with the EDGE2D-NIMBUS code package, was simulated. There is a high level agreement between the two codes for both inter-ELM and ELM profiles upstream and at the targets. As for the previous discharge, a strong inward particle pinch in the pedestal region is found to be necessary to match the steep upstream density pedestal. The SOLPS5 benchmark output has been used to study the energy balance during the ELM cycle. Although the in-out radiation asymmetry matches the experiment, the predicted fractional radiated energy is lower than observed. In addition, the ratio of energy deposited on the targets found in the code favours the outer target, in contradiction to that found experimentally. This demonstrates that the simple model of the ELM used here is incomplete.

Seyed Masood HAFEZ HAGHIGHAT: *"Multiscale modeling of irradiation induced effects on the plasticity of Fe and Fe-Cr alloys"*
Understanding of the effect of irradiation on the plasticity of Fe and Fe alloys is of main importance for the development of future fusion reactors. This work is aimed

at determining as precisely as possible the plasticity mechanisms and their amplitude influenced by irradiation-induced effects at the nanoscale level, by molecular dynamics (MD), and microscale level, by dislocation dynamics (DD) simulations. MD calculations were used to simulate the interaction between a moving dislocation and a defect, such as a void, a He bubble or a Cr precipitate, to obtain the influence of various defects on the plasticity of ferritic base steels at different temperatures. It appears that a 2nm Cr precipitate is an easy defect for an edge dislocation relative to a 2nm void. Temperature gives a pronounced effect on the softening of a void in comparison with a Cr precipitate. However, a He bubble can hold a complex strengthening behaviour in pure Fe depending on the bubble density. The strength of various defects obtained from MD calculations is used to simulate their influence in the presence of dislocation population by DD modeling. This work is in progress to clarify the effects of those defects on the plasticity of pure Fe.

Davoud IRAJI: *"Turbulence imaging in a toroidal magnetised plasma"*
To improve quality of the imaging system the noise level of the obtained images was decreased by cooling the camera with a continuous air flow and also using an optical fiber to transfer the data from the camera to the computer.
To fix the camera at desired positions and alignments a holder with three degrees of freedom was developed.
Different plasma scenarios and the influence of various parameters like vertical magnetic field (B_z), magnetron power and neutral gas pressure on the light emission were studied. Obtained results clearly show the dependence of mean values of light intensity to neutral gas pressure and plasma density. But due to the low level of light emissions, first attempts to interpret the light fluctuations as plasma density fluctuations failed. To overcome this problem the development of a gas puffing system was considered. As the first step, the gas puffing system including a fast piezoelectric valve and ceramic tube having a 200μm nozzle were calibrated in a test bench and then installed in TORPEX. The first results of gas puff imaging clearly show an improvement of the level of the camera signals which enables acquiring at higher acquisition frequencies up to 50k frames per second. So the interpretation of the light fluctuations as density fluctuations is possible now.

Sudheer Kumar JAWLA: "*Phase Retrieval of Gyrotron Microwave Beam from Intensity Measurements*"
Measurements were performed on the first prototype of "EU 170GHz / 2MW coaxial cavity gyrotron for ITER" to measure the beam profile of the output microwave beam. A microwave leak tight RF box was designed and used to perform the free space beam profile measurements of the gyrotron RF output using an infrared thermographic technique. The diagnostic consists in an IR camera and a target material placed on an optical bench. During the measurements, the gyrotron was operated below its nominal parameters. A frequency diagnostic was also set to verify the correct excitation of the nominal gyrotron operating mode $TE_{34,19}$. Data processing was also a necessary step before the data could be used in the phase retrieval algorithm. The measurements of beam intensity profile showed very good agreement with the simulations. The correlation between the simulation and measured beam intensity profile was more than 90%.
Further, a detailed theoretical analysis of the Iterative Phase Retrieval Approach for determining the phase profile of the output microwave beam from known intensity patterns was performed emphasizing on the field propagation techniques. The analysis provides more insight into Rayleigh-Sommerfeld diffraction integral propagation method in terms of field discretization and provides almost accurate results with the measured beam profile data. The phase retrieval algorithm provides

an excellent agreement between measured, theoretical and reconstructed intensity and phase profile with a reconstruction efficiency of 0.996.
A theoretical study is underway to analyze the intermodal decomposition of the quasi optical RF beams to characterize the Gaussian mode content of the RF output of the gyrotron.

Sébastien JOLLIET: *"Gyrokinetic Particle-In-Cell Global Simulations of Ion-Temperature-Gradient and Collisionless-Trapped-Electron-Mode Turbulence in Tokamaks"*
Gyrokinetic theory is a useful tool for studying microinstabilities, such as ITG and TEM modes, which are commonly held responsible for anomalous transport observed in tokamaks. The aim of this work is to develop the gyrokinetic global PIC code ORB5. The fluctuation entropy diagnostic has been implemented. It shows that the noise-control algorithm allows a true steady state, while simulations without this algorithm exhibit a quasi-steady state and unavoidably suffer from statistical noise accumulation. It has also been showed that the v-parallel nonlinearity, previously reported as potentially important for ITG transport, has in fact no influence as long as the numerical noise is low. Finally, first statistically converged, long global simulations of TEM turbulence reveal an effect of the zonal flow for the selected physical parameters.

Martin JUCKER: *"Toroidal precession drift frequency in anisotropic pressure equilibria"*
En route to a numerical study the effects of Ion Cyclotron Resonant Heating (ICRH) on the fast particle distribution function in general plasma geometries, three codes have been coupled: VMEC generates a general(2D or 3D) MHD equilibrium including full shaping and pressure anisotropy. This equilibrium is then mapped into Boozer coordinates and interfaced with two other codes. The full-wave code LEMan calculates the power deposition and electromagnetic field strength of a wave field generated by a chosen antenna using a warm model. Here, modifications to the dielectric tensor for circumpassing effects of a realistic anisotropic bi-Maxwellian have been performed. The single particle Hamiltonian code VENUS combines the outputs of the two previous codes in order to calculate the evolution of the distribution function. Monte Carlo operators for Coulomb collisions of the fast particles with the background plasma have been implemented, accounting for pitch angle and energy scattering. ICRH is simulated using Monte Carlo operators on the Doppler shifted resonant layer. The latter operators act in velocity space and induce a change of perpendicular and parallel velocity depending on the electric field strength and the corresponding wave vector. New statistical modules have been added for being able to re-construct the distribution function and from there new inputs to VMEC and LEMan, making the circle complete. If this procedure is iterated a sufficient number of times, a self-consistent solution can be found. So far one complete iteration could be obtained. This model is an enhancement of previous studies in that it is able to include full 3D effects such as magnetic ripple, treat the effects of non-zero orbit width consistently and inlcude the generation and effects of pressure anisotropy.

Sun Hee KIM: *"Full tokamak discharge simulations using DINA-CH"*
An inductive 15MA ITER operation scenario has been successfully simulated by using a full tokamak discharge simulator, the combined DINA-CH and CRONOS simulator. The feasibility of the ITER operation scenario is investigated considering all the related physical and engineering constraints, such as the vertical stability, fusion burn duration, and poloidal field (PF) coil voltage and current limits. In the simulation, the vertical instability was stabilized with the present ITER control

systems and the required fusion burn duration was achieved with 53MW of additional heating and current drive applied during the current flat-top phase. The PF coil limits were avoided by applying an early heating during the plasma current ramp-up. Lower Hybrid (LH) assisted plasma current ramp-up was additionally studied to investigate the capability of reducing the plasma internal inductance and saving the poloidal flux consumption. LH applied from the initial phase of plasma current ramp-up was effective for both. However, an additional elongation control was required to make the plasma shape diverted as it was originally intended.
Dynamic plasma responses to the disturbances anticipated in ITER have been examined by using a recent version of DINA-CH in which a bug in calculating 2D current profile was fixed. The fast H-L mode transition was identified as a dangerous disturbance which can make the plasma touch the inboard wall in ITER.
Magnetic triggering of ELMs in TCV and ASDEX Upgrade has been re-investigated in detail to find a clue for the observed opposite behaviour between the two tokamaks. A stability analysis conducted by an ideal MHD stability code, KINX, showed that the squareness increase in the low field side (LFS) and upper half plane of the poloidal cross-section in ASDEX Upgrade can destabilise the edge. This agrees with the previous simulation study done by using DINA-CH. In this study, similar local plasma shape deformations were observed near the upper G-coil set in TCV and near the upper passive stabilization loop (PSL) in ASDEX Upgrade for opposite plasma movement. To investigate further the plasma shape deformation effect, additional experiments were conducted in ASDEX Upgrade. Although the plasma shape was easily deformed with the radial plasma movement, ELMs were not triggered. KINX stability analysis on this plasma showed that the plasma boundary curvature change is related to the edge stability.

Etienne KUENG: *"Fluctuations on TORPEX in closed field lines geometry"*
We have investigated a new magnetic configuration in the TORPEX device in which a current is induced in the plasma, thus closing the magnetic field lines. A plasma configuration was achieved in which the current is in equilibrium for approximately 25 ms. Preliminary measurements of density fluctuations have been performed, with a focus on their spectral and statistical properties. In the future, different measurements will be explored to study density fluctuations in the closed field lines magnetic configuration.

Xavier LAPILLONNE: "Effects of geometry on linear and non-linear gyrokinetic simulations and development of a global version of the GENE code"
In order to clarify the observed differences between gyrokinetic simulations using the reduced s-α equilibrium model and a more realistic MHD equilibrium, further analysis considering both linear and non-linear simulations with the flux-tube gyrokinetic code GENE were carried out. In particular, for the Cyclone base case parameters, the ion heat flux was found to differ by nearly a factor two using the different equilibria. It was shown that these discrepancies result primarily from the approximation made in the standard implementation of the s-α model, in which the straight field line angle is identified to the poloidal angle, leading to inconsistencies of order ε (ε=a/R is the inverse aspect ratio, a the minor radius and R the major radius).
Using the previously developed interface with the equilibrium code CHEASE the effects of shaping on microinstabilies was studied with GENE. In the case of ITG modes, the main dependence of both the linear growth rate and the ion heat flux on elongation was identified to result from the modification of the effective flux surface-averaged gradient. The effect of triangularly can also partly be attributed to the modification of the spatial gradient, however further analysis is required concerning effects from this geometrical parameter.

Finally, in order to address the issue of non-local effects in turbulent transport, a global version of the GENE code is under development. As a first step towards this goal and in order to allow for radial variation of equilibrium quantities, the original Fourier representation for the radial direction was replaced by a real space treatment. This modification has required to adapt the radial derivatives, the gyro-averaging and the field solver, as well as the anti-aliasing procedure used when dealing with the non-linear term.

Boris LEGRADIC: *"Parasitic Plasmas in Very Large Area Plasma Enhanced Chemical Vapour Deposition Reactors"*
The race for more powerful and larger area reactors for plasma enhanced chemical vapour deposition (PECVD) brings current designs to their limits. Parasitic plasmas and arcing become more common and can damage or even destroy these reactors. A better understanding of these phenomena is crucial for the development of new reactor generations. In PECVD reactors there are a few areas where no plasma should form, but where the surfaces are still exposed to high RF voltages and the gases used during deposition and cleaning. To understand the possibly complex reasons for the occasional arcing event, it was decided to start with parallel plate breakdown experiments, and to slowly increase the complexity of the geometry until finally arriving at an exact copy of part of the showerhead. The experiments show a possible deviation from the Paschen-curve at small electrode gaps.

Bin LONG: *"Investigation of LBE Embrittlement Effects on the Fracture Properties of T91"*
The objective of this thesis work is to carry out a series of mechanical tests on both un-irradiated and irradiated martensitic steels in LBE (lead-bismuth eutectic) environment to quantify the degradation effects by LBE on the fracture properties of these steels. In 2008 mechanical tests (slow-strain rate tensile test and 3-point bending test) have been done on irradiated ferritic/martensitic steels T91 and F82H. Tensile tests results on T91 and F82H specimens which were irradiated in STIPs programmes show that the liquid metal embrittlement (LME) effect was observed in the temperature range of 200–450°C, consistently with our previous tests performed on specimens which were hardened by a different heat treatment. The results of 3-point bending tests revealed that with the presenting of LBE at the crack-tip of T91 specimens, the fracture toughness value reduced about 50% comparing with the tests performed in argon environment. Those aforementioned results indicate that irradiation induced hardening could increase the sensitivity to LBE embrittlement effect of martensitic steels.

Alessandro MARINONI: *"Experimental study of plasma fluctuations in tokamaks"*
The main aim of this work is to investigate plasma density fluctuations in the core region of the tokamak TCV. This is to be accomplished through a tangential laser imaging diagnostic employing the phase contrast (PCI) method. The work of this year has been divided between the finalization of the diagnostic and the refinement of a theoretical study employing non-linear gyrokinetic (NLGK) simulations. Concerning the first part, the ex-vessel design has been completed, the associated components have been procured and their installation is currently being finalized. In parallel, dedicated MATLAB routines have been developed for data analysis. The diagnostic is expected to be operational at the restart of TCV campaigns.
The second part, consisting of the NLGK modeling of an experimental study of the dependence of confinement on triangularity in TCV, resulted in a satisfactory reproduction of the main experimental findings.

Janos MARKI: *"TCV divertor infrared measurements"*
After the 2007 shutdown, the VIR diagnostic has seen an upgrade of its optics, as well as a number of improvements: a new, more refined black-body calibration, a re-adjusting of the optical elements for better image quality and better temporal precision. During this procedure, the phenomenon of radiation-enhanced absorption was observed on the calibration bench and during the 2008 October bakeout (on the torus as well, hence), however, the extent of the effect remains tolerable during TCV discharges. The diagnostic was involved in the day-to-day operations during the restart, and some new ELM data was collected. A 1-month secondment at JET was spent on the analysis of data from the new, vertically viewing KL9 infrared system, with the aim of establishing an inter-machine database of individual ELM parameters from different plasma conditions. An EU priority support project was launched to receive a similar IR camera on loan from MAST, with a view on the inner divertor, and together with the existing outer divertor-viewing VIR and bolometry, this will enable power balance- and ELM power deposition studies on a fast timescale (> 20 kHz). The hardware preparations of this project have already been completed, however, due to scheduling issues and the unfortunate TCV transformator problem in early November, the actual experiments will be performed in 2009.

Mikhail MASLOV: *"Particle transport and confinement in TCV and JET"*
The aim of this work is to identify the key parameters which influence the particle transport properties in tokamaks in order to predict the density profiles behaviour in
burning plasma devices, ITER in particular.
After completing the analysis of JET H-mode experimental density profile database last year, the focus was the comparison of the experimental results with theoretical predictions using gyrokinetic simulations. In excess of 1000 linear electrostatic GS2 calculations were executed on the PLEIADES computer cluster at EPFL. For each run the linear mode with the highest growth rate was identified and the results, namely the induced heat and particle fluxes were stored into a database.
To facilitate the analysis, simple parameterizations of the output results were produced. It was shown that Γ' (normalized particle flux) can be approximated with a good precision by a linear function of the input parameters: $\nu_{eff}^{1/2}$, T_i/T_e, $R/L_n^{3/2}$. Using this parameterization one is able to predict R/L_n at mid-radius from the experimental values of the other parameters. The experimental Γ' was obtained only from the NBI particle flux and from the ion heat flux through the mid-radius surface. With such an approach the simulation results appeared to be in an excellent agreement with experiment, including the same dependence on collisionality, ion to electron temperature ratio, local shear value and core particle source. GS2 simulations also predicted the insignificance of the ion temperature gradient for JET H-mode plasma conditions, which is consistent with experimental observations.

Nicolas MELLET: *"Extension of the LEMAN code to include finite temperature effects in the dielectric tensor to resolve singular mode structures and study effects of mode conversion without having to include gyroradius effects as in the PENN code"*
The convolution method implemented in the LEMan code has permitted to achieve simulations in 3D configurations like LHD and display some dependence of the TAE frequency on the temperature. Studies have shown a good convergence in the LHD configuration. The present model being not adapted to the ICRH domain, a new method has been developed where the value of the parallel wave vector is computed by iterations. Good agreement has been found in the Alfvén range of frequencies with full model results in JET-like equilibria and straight helix. New terms have been added to the dielectric tensor in order to model the effect of fast ions taking

their distribution function as a bi-Maxwellian. It has been shown that it affects the absorbed power profile.

Pablo Federico MUELLER: *"Fracture study on reduced activation tempered martensitic steels"*
Size effect of fracture toughness is a main concern in nuclear technology. Only a limited number of small specimens can be tested in current and future materials irradiation facilities due to space limitations. Our fracture toughness data of Eurofer97 and F82H reduced activation tempered martensitic steels obtained in the ductile-to-brittle transition temperature range show a significantly stronger size effect than that predicted by the commonly used ASTM-E1921 standard. Based on our results with three different sub-sized compact tension specimens, we demonstrated that the ASTM-E1921 specimen size limit yields non-conservative transition temperature determinations for these materials. We proposed a modified specimen size limit to avoid this problem. 3D finite elements simulations were used to study the loss of constraint phenomenon that causes this strong size effect. A local approach model, based on the attainment of a critical stress over a critical volume, was used to predict the loss of constraint and subsequent apparent high toughness, which is observed experimentally when specimens smaller than the modified size limit are used.

Theodoros PANIS: *"Alfvén Eigenmode stability in tokamak plasmas"*
The work during the past year concerned the optimization of the performance of the TAE antenna system on JET, which is used to study properties of the Alfvén Eigenmodes in tokamak plasmas. It was understood that the electrical model which had been developed during the last months of 2006 was in disagreement with some of the impedance measurements on various stages of the system and therefore, it should be improved in order to proceed to an efficient matching unit design. Using measurements taken on the distribution and isolation units, it was possible to build transformer equivalent models in the frequency range of interest and thus enhance the overall performance of a new four-antenna model that was in good agreement with the impedance measurements. Comparison of the electrical model with the voltage and current measurements on various points of the system revealed important inconsistencies of the measured quantities. This led to recalibration of the corresponding signals and to new measurements so as to ascertain the reliability of the voltage and current measurements. A solution to the matching problem was then investigated. Three resonant matching circuits were designed for the bands 60–90, 120–160 and 170–230kHz. It was shown that various constraints which are due to the system structure (e.g., the antennas are in-vessel) and to the JET operation (e.g., restricted access to the space near the torus) impose significant limitations on the matching possibilities. Finally, a more complete model has been lately constructed in which it is possible to study the effects of the inductive coupling between the closely-spaced antennas. The most important effect predicted by the model is the fact that, in a frequency band around 200 kHz, the antenna currents do not have the phasing combination imposed at the distribution unit. This effect is critical for the ability of exciting and detecting a mode in the plasma and various ways of dealing with it are being considered.

Francesco PIRAS: *"Plasma shape control of TCV"*
Breakdown optimisation: The magnetic field structure during the breakdown phase have been analysed using an electro-magnetic model of TCV. The main parameters that characterise the breakdown have been estimated for different configurations (single-null, double-null for doublet shaped plasmas). The role played by these parameters has been studied by means of a database based on 15000 breakdown

exepriments. One of the most interesting results is related to the reliability of the breakdown as a function of the connection length. For a large magnetic null, the connection length is big and the probability to succeed in both the ionization phase and the ramp-up phase increases.
Snowflake divertor: A preliminary study on the possibility to create a snowflake divertor on TCV has shown the compatibility of our tokamak with this innovative configuration. New experiments are planned to investigate the proprieties of this configuration.
Doublet: The axisymmetric stability of a doublet configuration has been studied. Using the CAXE free-boundary equilibrium code, different doublet configurations can be generated. A rigid model has been developed to analyse the stability of the plasma displacement (RZIP2 model). The results have been then compared with the KINX code. There are mainly two vertically unstable modes. The first one, characterised by two plasmas moving in the same direction, can be well represented with the rigid model. The results in the second unstable mode (plasmas moving in opposite directions) are not in a good agreement with the KINX results. Further studies are necessary to understand this particular instability for a doublet.
Plasma shape and position control system: Preliminary studies of a new plasma shape and position control system have been carried out. Using the new DSP hardware installed in TCV and a D-TACQ card, the flux inside the vacuum vessel at a given number of points will be controlled changing the currents in the external coils.

Andreas PITSCHKE: *"Improvements in data analysis for the TCV Thomson scattering system and ideal MHD-stability simulations of the edge barrier in X3-heated ELMy H-mode discharges at TCV"*
The routine analysis of the TCV Thomson scattering system, providing electron temperature and density, has been revised. The previously simple and fast algorithm, based on the usage of look-up tables and signal ratio evaluation, has been replaced by a more sophisticated and robust least square fitting method. The results show that the data quality has highly improved in plasma regimes where the signal-to-noise ratio is low, i.e. low electron density and high temperature.
The highly improved data quality from the TCV Thomson edge scattering system opens the possibility of a better study of the electron temperature and density edge barriers in ELMy H-mode discharges. To investigate the role of the pressure gradient and the bootstrap current on the MHD-stability of the plasma edge, MHD-stability diagrams as function of MHD α and parallel current density were calculated for X3-heated and compared with those of purely ohmically heated ELMy H-mode discharges. The simulations show that the additional heating of the plasma by X3, i.e. higher edge gradient and larger edge barrier width and thus higher bootstrap current fraction, moves the operational point of ELMy H-mode discharges at TCV towards the region of second MHD-stability. Furthermore, the additional heating by X3 has a destabilizing effect on the toroidal mode numbers n=10-25, whereas the region of ballooning instability is only marginal affected. This effect could explain the observation of larger and less frequent ELM's when applying additional heating.

Gennady PLYUSHCHEV: *"Investigation of the interaction of turbulence with suprathermal ions in a low temperature toroidal plasma"*
The first fast ion experiments with plasma on TORPEX were carried out with ion energies of 300eV and 600eV in a source free region. The fast ion current profiles were measured with a double gridded energy analyzer. Synchronous data detection was used to increase a signal to noise ratio. The experiments showed that, as compared to the beam propagation in vacuum, the fast ion current profile in the plasma is more spread, vertically elongated, and the maximum of current profiles

slightly shifts down. This behaviour was qualitatively predicted with earlier simulations and could be explained by a toroidal drift of scattered fast ions. In the source region the noise from the detector is much higher than the signal limits the fast ion current profile measurements.

Marina RICCI: *"Chemistry of powder produced organosilicon deposition plasmas"*
A dusty plasma is a plasma containing nanometer or micrometer-sized particles suspended in it. The formation of these particles imposes an upper limit on the deposition rate. That is the reason why it is important to study the powder formation, in particular in SiO_x deposition plasmas. Three different organosilicon compounds having a similar chemical structure, such as HMDSO, TMS and HMDSN, in various amounts of oxygen mixture, have been studied. The analysis performed with Time Resolved in-situ FTIR show that at the beginning the particle formation is induced by polymerization, after that the particles grow. Their radius rise (and density) seems to be linked with the increase of oxygen content in the gas mixture.

Jonathan ROSSEL: *"Design of saddle coil system for TCV"*
A saddle coil system is planned as a future upgrade for TCV. This system will be used for the application of resonant magnetic perturbations (with toroidal mode number 2 or 4), in order to mitigate or suppress ELMs in H-mode operation, for error field correction and vertical control of the plasma. This year has been spent on developing an optimal coil design to fulfill these aims. Models have also been developed to caracterize the electrical properties and requirements of the retained design. They include an assessment of the inductance of the system and the forces that it will have to withstand. Finally, methods have been developed to determine optimal current distributions in the coil system

Christian SCHLATTER: *"Ion physics on TCV"*
Ion-acoustic turbulence was elucidated as being responsible for the production of a suprathermal ion population in ECCD discharges on TCV. The mechanism was modeled by means of a kinetic code which was developed in 2007. New experiments are currently scheduled to explore the findings of the simulations. For this purpose the Compact Neutral Particle Analyzer was upgraded to probe the plasma along two different directions, as the modeling is indicating a spatially anisotropic fast ion distribution. A programmemable spectrum analyser was successfully implemented to be remotely controlled on TCV. The signal picked up by the LHPI antenna (see the TCV tokamak chapter) is connected to the device and the measured frequency spectrum is hoped to provide insight into the turbulence activity around the ion-acoustic frequency.

Christian THEILER: *"Propagation of plasma filaments in TORPEX"*
Filamentary structures of increased plasma density, that look like blobs in the plane perpendicular to the magnetic field, are observed in virtually all toroidal confinement devices. A rather clear picture of their formation in TOPREX has emerged in the last year. In this year, we have undertaken dedicated experiments to study the propagation properties of these filaments once they are formed. We have inserted limiters of different materials (conducting, insulating) to study the role of the boundary conditions on blob motion. Further, we have varied other parameters, such as the ion mass, the neutral background pressure and the pitch angle of the magnetic field. While not all experimental findings are yet understood, we have a good understanding for blobs limited by the conducting plate. Both currents along the magnetic field and perpendicular to it play a significant role. We have derived a

scaling which relates the vertical size of a blob to its radial speed. This formula, which interpolates between previously published expressions for blob speed versus size, agrees nicely with experimental results.

Robert TYE: *"Vertical ECE Measurements on TCV"*
Electron Cyclotron Emission (ECE) can be used for the diagnosis of relativistic electron populations, and if the plasma can be viewed along a line of approximately constant magnetic field then the interpretation is greatly simplified; this is the case when making Vertical ECE (VECE) measurements. Work was carried out to characterize a microwave telescope purchased for use in the VECE system over a range of frequencies from 70-100 GHz. Other parts of the VECE system, such as an ellipsoidal mirror, were also tested ready for installation on the TCV with a view to start measurements in early 2009. Work was also carried out on creating a Graphical User Interface (GUI) for GENRAY, a ray tracing code capable of calculating emission spectra, Electron Cyclotron Current Drive (ECCD) efficiency and power absorption from Electron Cyclotron Resonance Heating (ECRH). GENRAY can use distribution functions calculated internally or provided externally by the CQL3D Fokker-Planck code. Emission spectra calculated using GENRAY will be compared to results obtained from the VECE diagnostic.

Lyubomira VELEVA: *"Development and Characterization of Tungsten-Base Materials for Fusion Applications"*
Recent activities were focused on manufacturing W-(0.3-1.0-2.0)Y_2O_3 and W-(0.3-1.0-2.0)Y materials (in weight percent) by conventional powder metallurgy methods including dry mechanical alloying of elemental powders in Ar atmosphere, cold pressing in air using a pressure in the range of 150-250 MPa, and compaction by either sintering at 1800°C in vacuum or Ar atmosphere, or hot isostatic pressing at 1300°C under a pressure of 200 MPa. The mechanical alloying time was optimized by means of X-ray diffractometry and scanning electron microscopy analyses of the particles. It was found that it should not exceed 15 hours, in order to obtain small and homogeneous particle and crystallite sizes and to avoid important oxygen contamination and formation of WC impurities. The density of the sintered specimens was found to increase with Y_2O_3 and Y contents. The highest density was obtained for the W-2Y material: it is about 90% after sintering and 97% after hot isostatic pressing. The highest microhardness of 1790 $HV_{0.2}$ was measured for the W-2Y_2O_3 material after sintering, due to the presence of the hard Y_2O_3 particles.

Thibaud VERNAY: *"A new CHEASE interface for ORB5 and collisions in PIC methods"*
- Work on the gyrokinetic code ORB5: development of a new interface for the code CHEASE, which provides MHD equilibria. Instead of the usual Ad Hoc equilibrium, ORB5 can run with a MHD equilibrium given by an external code. Such an interface already existed, but it did not make a direct link between the magnetic coordinates of ORB5 and CHEASE. The new interface aims at avoiding the use of (r,z) coordinates in order to get directly the MHD equilibrium in terms of the straight-field-line angle coordinate. The interface has been tested in the linear version of ORB5.
- Electron-Ion collisions: following the implementation of the Lorentz operator into ORB5 using a Langevin approach, performed for a master project finished at the beginning of the year, some work has been done about a new way to deal with such collisions. In numerical codes based on the Particle-In-Cell approach, since we discretize the distribution function into N markers, the standard way to implement the Lorentz operator is to act on the marker trajectories by adding a stochastic motion coming from the diffusion part of the collision operator (Langevin

approach). Such a random walk method has the important disadvantage that it generates an unavoidable weight spreading, leading to an increased numerical noise. Since the noise is one of the strongest ennemies for PIC codes, one understands all the problems such an implementation can create. Thus we explored the possibility to act on the weight evolution instead on the marker trajectories, in a code which simulates the evolution of the perturbation distribution in the pitch angle space. If the results are encouraging, an implementation into ORB5 could be considered.

David WAGNER: *"Particle and impurity transport studies"*
Core transport phenomena, especially impuritiy transport, is particulary important to understand on the way towards fusion. A fast valve has been mounted on TCV this year, whose commissioning is about to finish now. This device can be used to puff different gases, as impurities, into the tokamak and their behaviour can be studied. Helium measurements are planned with the Charge Exchange (CXRS) diagnostics. The chain of the CXRS data analysis and the use of the above-mentioned valve was mastered, as well.

Alexandra ZHUCHKOVA: *"Faraday rotation measurements of the poloidal magnetic field in the TCV Tokamak, using a far-infrared polarimeter"*
A new far-infrared (FIR) polarimeter diagnostic is currently under construction and installation on TCV. The Faraday rotation measurements will improve the accuracy of the equilibrium reconstruction by the LIUQE equilibrium code. It will provide a measurement of the poloidal magnetic field and hence the current density profile in TCV plasmas. The current density j(r) is linked to the safety factor q which is a key parameter for the transport models as well as for the magnetohydrodynamic (MHD) stability theory of tearing modes, sawteeth and disruptions. The diagnostic will measure the Faraday rotation angle of FIR laser beams along 10 vertical lines of sight across the poloidal cross section of the tokamak. During 2008 the work has been directed mostly toward component manufacturing and testing, installation, alignment and system integration. This work included the installation of the following components: waveguides from the laser room to the torus, a beam splitter below the TCV vessel which divides the original beam into 5 parts and a detector assembly above the tokamak. The detector electronics and the control system for semi-automatic operation of the CO_2-FIR laser system have been designed, built and installed. The diagnostic is planned to be operational in early 2009.

Costanza ZUCCA: *"Safety-factor profile tailoring by improved electron cyclotron system for sawtooth control and reverse shear scenarios in ITER"*
The effect of the predicted local electron cyclotron current driven by the optimized electron cyclotron system on ITER was studied. A design variant was recently proposed to enlarge the physics programme covered by the upper and equatorial launchers. By extending the functionality range of the upper launcher, significant control capabilities of the sawtooth period can be obtained. The upper launcher improvement still allows for enough margin above the requirements for neoclassical tearing mode stabilization, for which it was originally designed. The analysis of the sawtooth control was carried out with the ASTRA transport code, coupled with the threshold model by Porcelli, to study the control capabilities of the improved upper launcher on the sawtooth instability. The simulations take into account the significant stabilizing effect of the fusion alpha particles. The sawtooth period can be increased by a factor of 1.5 with co-ECCD outside the q=1 surface, and decreased by at least 30% with co-ECCD inside q=1.
The present ITER base-line design has the electron cyclotron launchers providing only co-ECCD. The variant for the equatorial launcher proposes the possibility to

drive counter-ECCD with one of the three rows of mirrors: the counter-ECCD can, then, be balanced with co-ECCD and provide pure ECH with no net driven current. The difference between full co-ECCD off-axis using all 20MW from the equatorial launcher and 20MW co-ECCD driven by 2/3 from the equatorial launcher and 1/3 from the upper launcher has been shown to be negligible. Counter-ECCD also offers greater control of the plasma current density, therefore this analysis addressed the performance of the equatorial launcher to control the central q profile. The equatorial launcher has been shown to control very efficiently the value of $q(\rho=0.2)$-q_{min} in advanced scenarios, if one row provides counter-ECCD.

7 PUBLIC RELATION ACTIVITIES IN 2008

The public relation activities usualy set up by the CRPP all over the year were doubled, in 2008, by the organisation of the 22nd IAEA fusion energy conference. Especial coverage of this event was made by different media as described below. The usual activities were mainly dedicated to the general public and undergraduate students in the form of visits. The CRPP also participated in some events throuhout 2008.

7.1 Public relations activities related to the IAEA conference

The IAEA conference was held from October 12th to 18th at the UNO, in Geneva. The local organising committee was formed by CRPP's collaborators.

To publicise the event, all major swiss media were invited to a 'media day' which was held the week before the conference. About 15 media, among them 'Télévision Suisse Romande', 'Radio Suisse Romande', '24 Heures' gathered at the CRPP for presentations on fusion, CRPP's activities and ITER, the latter having been given by one of ITER Orgnisation Deputy Director General C. Alejaldre. A few newspaper articles have been published in the days following this 'media day'.

A press conference was held at the end of the opening ceremony of the conference. The salient point of this event was the signature of the agreement between the IAEA and ITER. It was signed by MM Sokolov (DDG IAEA) and Ikeda (DG ITER), with Mr Capouet (EU) presiding the event.

The 'Télévision Suisse Italienne' came to the UNO for interviewing Prof. A. Fasoli (Executive Director of CRPP).

An ITER and commercial exhibition was organised in the UNO premises. Almost all ITER parties presented their participation in the project with somtimed impressive booths. This exhibition was located in front of the 'Assembly Hall' in the 'Hall des Pas Perdus' a higly attended crossing point.

7.2 Public relation activities throughout the year

More than 1200 persons visited the CRPP in 2008. Most of them were adults belonging to professionnal or political groups which either were invited or asked for a visit. Besides that, one major event is the visit of 300 children (12-13 years old) in one morning. Classes visit different laboratories in the EPFL and the CRPP is a 'must go' destination !

General posters on fusion and ITER were prepared for and manned at different events such as the 'Research Day' at the EPFL and at the 'Nuclear Forum' at the Olympic Museum(Lausanne).

Several documents on fusion and CRPP'a activities were prepared for politicians at the swiss governement level.

A few talks were given at different large public meetings.

A 45 minutes interview of a TCV physicist was broadcasted by the 'Radio Suisse Romande' and the EPFL, in collaboration with the CRPP, prepared a B-roll on fusion which has been made available to the media.

APPENDICES

APPENDIX A Articles published in Refereed Scientific Reviews during 2009

(see CRPP archives at http://crppwww.epfl.ch/archives)

S. Alberti, F. Albajar, K.A. Avramides, P. Benin, W. Bin, T. Bonicelli, A. Bruschi, S. Cirant, E. Droz, O. Dumbrajs, D. Fasel, F. Gandini, J.P. Hogge, B. Marletaz, P. Marmillod, I. Pagonakis, A. Perez, B. Piosczyk, L. Porte, T. Rzesnicki, U. Siravo, M. Thumm, M.Q. Tran, *Status of Development of the 2mw, 170ghz Coaxial-Cavity Gyrotron for ITER,* 2008 33rd Int. Conf. on Infrared, millimeter and Terahertz waves **1-2**, 311 (2008).

Y. Andrew, T.M. Biewer, K. Crombe, et al., Y.R. Martin, *H-Mode Access on JET and Implications for ITER,* Plasma Phys. Control. Fusion **50**, 124053 (2008).

Z.N. Andrushchenko, M. Jucker, V.P. Pavlenko, *Self-Consistent Model of Electron Drift Mode Turbulence,* J. Plasma Phys. **74**, (2008).

P. Angelino, X. Garbet, L. Villard, A. Bottino, S. Jolliet, P. Ghendrih, V. Grandgirard, B.F. McMillan, Y. Sarazin, G. Dif-Pradalier, T.M. Tran, *The Role of Plasma Elongation on the Linear Damping of Zonal Flows,* Phys. Plasmas **15**, Art. No. 062306 (2008).

E. Asp, J.H. Kim, W. Horton, L. Porte, S. Alberti, A. Karpushov, Y. Martin, O. Sauter, G. Turri, T.C.V. Team, *Electron Thermal Transport Analysis in Tokamak a Configuration Variable,* Phys. Plasmas **15**, 082317 (2008).

M. Bagnasco, L. Bottura, P. Bruzzone, M. Lewandowska, C. Marinucci, F. Staehli, *Pressure Drop of Cable-in-Conduit Conductors with Different Void Fraction,* Advances in Cryogenic Engineering **53A and 53B**, 1317 (2008).

P. Bauer, P. Bruzzone, F. Cau, K. Weiss, A. Portone, E. Salpietro, M. Vogel, A. Vostner, *Solder-Filling of a Cic Cable for the EFDA Dipole Magnet,* Advances in Cryogenic Engineering Materials, ICMC **54**, 151 (2008).

F. Bellina, P. Bruzzone, *The Thelma Model of the Joint Resistance Distribution Tests with Jordi,* IEEE T. Appl. Supercon. **18**, 1092 (2008).

M.N.A. Beurskens, G. Arnoux, A.S. Brezinsek, et al., R.A. Pitts, *Pedestal and ELM Response to Impurity Seeding in JET Advanced Scenario Plasmas,* Nucl. Fusion **48**, 095004 (2008).

R. Bonade, P. Mueller, P. Spaetig, *Fracture Toughness Behavior in the Ductile-Brittle Transition Region of the Tempered Martensitic Eurofer97 Steel: Experiments and Modeling,* Eng. Fract. Mech. **75**, 3985 (2008).

R. Bonade, P. Spaetig, *The Evolution of the Mobile Dislocation Density During Successive Stress Relaxation Transients,* Mat. Sci. Eng. A **483-484**, 203 (2008).

L. Bottura, C. Marinucci, *A Porous Medium Analogy for the Helium Flow in Ciccs,* Int. J. Heat Mass Tran. **51**, 2494 (2008).

V.R. Bovshuk, W.A. Cooper, M.I. Mikhailov, J. Nuehrenberg, V.D. Shafranov, *Search for Very-High-Beta MHD Stability Quasi-Isodynamic Configurations,* Plasma Fusion Res.: Regular Articles **3**, S1046 (2008).

P. Bruzzone, M. Bagnasco, M. Calvi, F. Cau, D. Ciazynski, A. Della Corte, A. Di Zenobio, L. Muzzi, A. Nijhuis, E. Salpietro, L.S. Richard, S. Turtu, A. Vostner,

R. Wesche, R. Zanino, *Test Results of Two European ITER TF Conductor Samples in Sultan,* IEEE T. Appl. Supercon. **18**, 1088 (2008).

P. Bruzzone, M. Bagnasco, F. Cau, B. Stepanov, R. Wesche, *Development of a React and Wind Conductor for the ITER Toroidal Field Coils,* IEEE Trans. Appl. Supercond. **18**, 467 (2008).

P. Bruzzone, B. Stepanov, E. Salpietro, R. Wesche, A. Vostner, K. Okuno, T. Isono, Y. Takahashi, H.C. Kim, K. Kim, A.K. Shikov, V.E. Sytnikov, *Results of a New Generation of ITER TF Conductor Samples in Sultan,* IEEE T. Appl. Supercon. **18**, 459 (2008).

M. Calvi, A. Bagnasco, P. Bruzzone, F. Cau, R. Herzog, C. Marinucci, B. Stepanov, M. Vogel, R. Wesche, *Preparatory Work to Host the EDIPO Test Facility at Crpp,* IEEE T. Appl. Supercon. **18**, 204 (2008).

F. Cau, M. Bagnasco, P. Bruzzone, M. Calvi, F. Roth, *Inter-Strand Resistance in the Termination of ITER Conductors,* IEEE T. Appl. Supercon. **18**, 1101 (2008).

I.T. Chapman, I. Jenkins, R.V. Budny, J.P. Graves, S.D. Pinches, S. Saarelma, *Sawtooth Control Using Off-Axis NBI,* Plasma Phys. Control. Fusion **50**, 045006 (2008).

J. Chowdhury, R. Ganesh, P. Angelino, J. Vaclavik, L. Villard, S. Brunner, *Role of Nonadiabatic Untrapped Electrons in Global Electrostatic Ion Temperature Gradient Driven Modes in a Tokamak,* Phys. Plasmas **15**, 072117 (2008).

D. Ciazynski, L. Zani, P. Bruzzone, B. Stepanov, R. Wesche, R. Zanino, L. Savoldi-Richard, A. Nijhuis, Y. Ilyin, S. Turtu, V. Corato, G. Demarzi, G.M. Polli, *Influence of Cable Layout on the Performance of ITER-Like Nb3Sn Conductor,* Journal of Physics Conference Series **97**, 012027 (2008).

S. Coda, *Diagnostic Techniques for Measuring Suprathermal Electron Dynamics in Plasmas,* Rev. Sci. Instrum. **79**, 10F501 (2008).

Y. Corre, E. Joffrin, P. Monier-Garbet, et al., O. Sauter, JET EFDA contributors, *Hybrid H-Mode Scenario with Nitrogen Seeding and Type III ELMs in JET,* Plasma Phys. Control. Fusion **50**, 115012 (2008).

N. Cruz, A.P. Rodrigues, B. Santos, C.A.R. Varandas, B.P. Duval, J.M. Moret, J. Berrino, Y. Martin, X. Llobet, *The Integration of the New Advanced Digital Plasma Control System in TCV,* Fusion Eng. Des. **83**, 215 (2008).

T. Dannert, S. Guenter, T. Hauff, F. Jenko, X. Lapillonne, P. Lauber, *Turbulent Transport of Beam Ions,* Phys. Plasmas **15**, 062508 (2008).

G. De Temmerman, R.A. Pitts, *Substrate-Dependent Deposition Efficiency on Mirrors Exposed in the TCV Divertor,* Fusion Eng. Des. **83**, 10.1016/j.fusengdes.2007.04.044 (2008).

A. Descoeudres, C. Hollenstein, G. Waelder, R. Demellayer, R. Perez, *Time- and Spatially-Resolved Characterization of Electrical Discharge Machining Plasma,* Plasma Sources Science and Technology **17**, 024008 (2008).

A. Diallo, A. Fasoli, I. Furno, B. Labit, M. Podesta, C. Theiler, *Dynamics of Plasma Blobs in a Shear Flow,* Phys. Rev. Lett. **101**, 115005 (2008).

A.J.H. Donne, C.J. Barth, H. Weisen, *Laser-Aided Plasma Diagnostics,* Fusion Sci. Technol. **53**, 397 (2008).

B.P. Duval, A. Bortolon, A. Karpushov, R.A. Pitts, A. Pochelon, O. Sauter, A. Scarabosio, G. Turri, *Spontaneous L-Mode Plasma Rotation Scaling in the TCV Tokamak,* Phys. Plasmas **15**, 056113 (2008).

D. Elbeze, J.L. Segui, A. Macor, D. Molina, J. Decker, M. Goniche, V.S. Udintsev, *Correlation ECE Diagnostic on Tore Supra to Study MHD Instabilities Related to Fast Particle Dynamics,* (2008).

E. Fable, C. Angioni, O. Sauter, *Gyrokinetic Calculations of Steady-State Particle Transport in Electron Internal Transport Barriers,* Plasma Phys. Control. Fusion **50**, 115005 (2008).

G.L. Falchetto, B.D. Scott, P. Angelino, et al., T. Dannert, S. Jolliet, B.F. McMillan, *The European Turbulence Code Benchmarking Effort: Turbulence Driven by Thermal Gradients in Magnetically Confined Plasmas,* Plasma Phys. Control. Fusion **50**, 124015 (2008).

D. Fasel, T. Bonicelli, M.A. Henderson, M.Q. Tran, *Electrical Powering Concept for ITER Electron Cyclotron Radio-Frequency Sources,* Fusion Sci. Technol. **53**, 246 (2008).

A. Fasoli, for the TCV Team, *Overview of TCV Results,* Nucl. Fusion **48**, 034001 (2008).

W. Fundamenski, D.P. Coster, M. Airila, et al., B. Gulejova, R.A. Pitts, EFDA JET Contributors, *Progress in Edge Plasma Transport Modeling on JET,* Contrib. Plasma Phys. **48**, 190 (2008).

I. Furno, B. Labit, A. Fasoli, F.M. Poli, P. Ricci, C. Theiler, S. Brunner, A. Diallo, J.P. Graves, M. Podesta, S.H. Mueller, *Mechanism for Blob Generation in the TORPEX Toroidal Plasma,*

I. Furno, B. Labit, M. Podesta, A. Fasoli, S.H. Mueller, F.M. Poli, P. Ricci, C. Theiler, *Experimental Observation of the Blob-Generation Mechanism from Interchange Waves in a Plasma,* Phys. Rev. Lett. **100**, (2008).

S. Gnesin, S. Coda, J. Decker, Y. Peysson, *Suprathermal Electron Studies in the TCV Tokamak: Design of a Tomographic Hard-X-Ray Spectrometer,* Rev. Sci. Instrum. **79**, 10F504 (2008).

M. Goniche, G.T.A. Huysmans, F. Turco, et al., V. Udintsev, *Identification of Fast Particle Triggered Modes by Means of Correlation Electron Cyclotron Emission on Tore Supra,* Fusion Sci. Technol. **53**, 88 (2008).

T.P. Goodman, and the TCV Team, *Experience in Integrated Control of the Multi-Megawatt Electron Cyclotron Heating System on the TCV Tokamak: The First Decade,* Nucl. Fusion **48**, 054011 (2008).

T.P. Goodman, V.S. Udintsev, I. Klimanov, A. Mueck, O. Sauter, C. Schlatter, *First Measurements of Oblique ECE with a Real-Time Movable Line of Sight on TCV,* Fusion Sci. Technol. **53**, 196 (2008).

P.P. Granieri, M. Calvi, P. Xydi, D. Bocian, L. Bottura, M. Breschi, A. Siemko, *Stability Analysis of the LCH Cables for Transient Heat Depositions,* IEEE T. Appl. Supercon. **18**, 1257 (2008).

B. Guillerminet, M. Airaj, P. Huynh, et al., J.B. Lister, *Integrated Tokamak Modelling: Infrastructure and Software Integration Project,* Fusion Eng. Des. **83**, 442 (2008).

S.M. Hafez Haghighat, J. Fikar, R. Schaeublin, *Effect of Interatomic Potential on the Behavior of Dislocation-Defect Interaction Simulation in a-Fe,* J. Nucl. Mater. **382**, 147 (2008).

S.M.H. Haghighat, A.K. Taheri, *Investigation of Limiting Grain Size and Microstructure Homogeneity in the Presence of Second Phase Particles Using the Monte Carlo Method,* J. Mater. Process. Tech. **195**, 195 (2008).

R.W. Harvey, A.P. Smirnov, E. Nelson-Melby, G. Taylor, S. Coda, A.K. Ram, *Nonthermal Electron Bernstein Emission in NSTX-Like Discharges,* Fusion Sci. Technol. **53**, 237 (2008).

M.A. Henderson, R. Chavan, R. Bertizzolo, D. Campbell, J. Duron, F. Dolizy, R. Heidinger, J.D. Landis, G. Saibene, F. Sanchez, A. Serikov, H. Shidara, P. Spaeh, *Critical Design Issues of the ITER ECH Front Steering Upper Launcher,* Fusion Sci. Technol. **53**, 139 (2008).

M.A. Henderson, R. Heidinger, D. Strauss, et al., R. Bertizzolo, R. Chavan, A. Collazos, F. Dolizy, J. Duron, F. Sanchez, O. Sauter, H. Shidara, V.S. Udintsev, C. Zucca, *Overview of the ITER EC Upper Launcher,* Nucl. Fusion **48**, 054013 (2008).

M.A. Henderson, C.P. Moeller, *Possible Improvements to a Remote Steering Launcher for Localized Electron Cyclotron Current Drive,* Fusion Sci. Technol. **53**, 220 (2008).

M.A. Henderson, G. Saibene, *Critical Interface Issues Associated with the ITER EC System,* Nucl. Fusion **48**, 054017 (2008).

R. Herzog, R. Wesche, P. Bruzzone, *Field and Temperature Dependence of Critical Currents in Industrially Manufactured High-Tc Wires and Tapes,* Journal of Physics Conference Series **97**, 012206 (2008).

C. Hollenstein, J.L. Dorier, *Micro-Plasma Formation During Opening of a Low Current Electrical Contact,* J. Phys. D Appl. Phys. **41**, 035207 (2008).

T. Intrator, X. Sun, L. Dorf, I. Furno, G. Lapenta, *A Three Dimensional Probe Positioner,* A three dimensional probe positioner **79**, 10F129 (2008).

D. Iraji, A. Diallo, A. Fasoli, I. Furno, S. Shibaev, *Fast Visible Imaging of Turbulent Plasma in TORPEX,* Rev. Sci. Instrum. **79**, 10F508 (2008).

M.Y. Isaev, K.Y. Watanabe, M. Yokoyama, N. Ohyabu, C.D. Beidler, H. Maassberg, W.A. Cooper, T.M. Tran, M.I. Mikhailov, *LHD Bootstrap Current Coefficient Calculations with the Venus+Df Code,* Plasma Fusion Res.: Regular Articles **3**, 036 (2008).

M. Jucker, J.P. Graves, G.A. Cooper, W.A. Cooper, *Impact of Pressure Anisotropy on Tokamak Equilibria and the Toroidal Magnetic Precession,* Plasma Phys. Control. Fusion **50**, 065009 (2008).

A. Karpushov, Y. Andrèbe, B.P. Duval, A. Bortolon, *The Diagnostic Neutral Beam Injector with Arc-Discharge Plasma Source on the TCV Tokamak,* Fusion Eng. Des. (2008).

H.C. Kim, D.K. Oh, S.H. Park, K. Kim, P. Bruzzone, *Development and Sultan Test Result of ITER Conductor Samples of Korea,* IEEE T. Appl. Supercon. **18**, 1084 (2008).

A. Klein, H. Carfantan, D. Testa, A. Fasoli, J. Snipes, *A Sparsity-Based Method for the Analysis of Magnetic Fluctuations in Unevenly-Spaced Mirnov Coils,* Plasma Phys. Control. Fusion **50**, 125005 (2008).

V. Kotov, D. Reiter, R.A. Pitts, S. Jachmich, A. Huber, D.P. Coster, *Numerical Modelling of High Density JET Divertor Plasma with the SOLPS4.2 (B2-EIRENE) Code,* Plasma Phys. Control. Fusion **50**, 105012 (2008).

K. Kurihara, J.B. Lister, D.A. Humphreys, J.R. Ferron, W. Treutterer, F. Sartori, R. Felton, S. Bremond, P. Moreau, *Plasma Control Systems Relevant to ITER and Fusion Power Plants,* Fusion Eng. Des. **83**, 959 (2008).

B. Labit, I. Furno, M. Podesta, A. Fasoli, *Two-Dimensional Time Resolved Measurements of Toroidal Velocity Correlated with Density Blobs in Magnetized Plasmas,* Rev. Sci. Instrum. **79**, 086104 (2008).

J.D. Landis, R. Chavan, R. Bertizzolo, A. Collazos, F. Sanchez, M. Henderson, *Design Status of the ITER ECRH Upper Launcher mm-Wave System,* (2008).

N. Lazarev, C. Abromeit, R. Schaeublin, R. Gotthardt, *Atomic-Scale Simulation of Martensitic Phase Transformations in Nial,* Materials Science and Engineering a Structural Materials Properties Microstructure and Processing **481**, 205 (2008).

N. Lazarev, C. Abromeit, R. Schaeublin, R. Gotthart, *Atomic-Scale Simulation of Martensitic Phase Transormations in Nial,* Mat. Sci. Eng. A **481-482**, 481 (2008).

J.B. Lister, J.W. Farthing, M. Greenwald, I. Yonekawa, *The Status of the ITER CODAC Conceptual Design,* Fusion Eng. Des. **83**, 164 (2008).

G. Lucas, R. Schaeublin, *Helium Effects on Displacement Cascades in Alpha-Iron,* Journal of Physics Condensed Matter **20**, 415206 (2008).

G. Manduchi, F. Iannone, F. Imbeaux, G. Huysmans, J.B. Lister, B. Guillerminet, P. Strand, L.G. Eriksson, M. Romanelli, *A Universal Access Layer for the Integrated Tokamak Modelling Task Force,* Fusion Eng. Des. **83**, 462 (2008).

R. Mantica, G. Corrigan, X. Garbet, et al., H. Weisen, *Chapter 10 - Core Transport Studies in JET,* Fusion Sci. Technol. **53**, 1152 (2008).

C. Marinucci, M. Calvi, L. Bottura, P. Bruzzone, R. Herzog, *Quench Analysis of the European High Field Superconducting Dipole Magnet EDIPO,* IEEE T. Appl. Supercon. **18**, 200 (2008).

P. Marmy, T. Kruml, *Low Cycle Fatigue of Eurofer 97,* J. Nucl. Mater. **377**, 52 (2008).

Y. Martin, *Power Requirements for Accessing the H-Mode in ITER,* Journal of Physics: Conference Series **123**, 012033 (2008).

Y.R. Martin, T. Takizuka, ITPA DDBM Group, *Power Requirement for Accessing the H-Mode in ITER,* Journal of Physics: Conference Series **123**, 012033 (2008).

B.F. McMillan, S. Jolliet, T.M. Tran, L. Villard, A. Bottino, P. Angelino, *Long Global Gyrokinetic Simulations: Source Terms and Particle Noise Control,* Phys. Plasmas **15**, 052308 (2008).

P. Mueller, R. Bonade, P. Spaetig, *Fracture Properties of Notched and Pre-Cracked Specimens of a Tempered Martensitic Steel at Low Temperature,* Mat. Sci. Eng. A **483-484**, 346 (2008).

P. Mueller, R. Bonade, P. Spaetig, *Fracture Properties of Notched and Pre-Cracked Specimens of a Tempered Martensitic Steel at Low Temperature,* Materials Science and Engineering a Structural Materials Properties Microstructure and Processing **483**, 346 (2008).

S.K. Nielsen, H. Bindslev, L. Porte, et al., *Temporal Evolution of Confined Fast-Ion Velocity Distributions Measured by Collective Thomson Scattering in TEXTOR,* Phys. Rev. E **77**, 016407 Part 2 (2008).

G.S. Nusinovich, A.N. Vlasov, T.M. Antonsen, J. Lohr, B.G. Danly, J.P. Hogge, *Excitation of Parasitic Modes in Gyrotrons with Fast Voltage Rise,* Phys. Plasmas **15**, 103101 (2008).

Z. Oksiuta, N. Baluc, *Microstructure and Charpy Impact Properties of 12-14Cr Oxide Dispersion-Strengthened Ferritic Steels,* J. Nucl. Mater. **374**, 178 (2008).

I.G. Pagonakis, S. Illy, M. Silva, J.P. Hogge, S. Alberti, K.A. Avramides, B. Piosczyk, F. Albajar, T. Bonicelli, *Parameterization Technique for the*

Preliminary Gun Design of the EU 170ghz 1mw Conventional Cavity Gyrotron for ITER, 2008 33rd Int. Conf. on Infrared, millimeter and Terahertz waves **1-2**, 199 (2008).

L.G. Pagonakis, J.P. Hogge, S. Alberti, K.A. Avramides, J.L. Vomvoridis, *A New Concept for the Collection of an Electron Beam Configured by an Externally Applied Axial Magnetic Field,* IEEE T. Plasma Sci. **36**, 469 (2008).

L. Pangione, J.B. Lister, *Matlab Modeling of ITER CODAC,* Fusion Eng. Des. **83**, 545 (2008).

M. Parlinska-Wojtan, R. Schaeublin, R. Gotthardt, *Relaxation Mechanisms in Martensitic Niti(Cu): Internal Friction Measurements Correlated to in Situ TEM Straining,* Materials Science and Technology **24**, 913 (2008).

M. Podesta, A. Fasoli, B. Labit, I. Furno, P. Ricci, F.M. Poli, A. Diallo, S.H. Mueller, C. Theiler, *Cross-Field Transport by Instabilities and Blobs in a Magnetized Toroidal Plasma,* Phys. Rev. Lett. **101**, 045001 (2008).

F.M. Poli, P. Ricci, A. Fasoli, M. Podesta, *Transition from Drift to Interchange Instabilities in an Open Magnetic Field Line Configuration,* Phys. Plasmas **15**, (2008).

A. Portone, W. Baker, E. Salpietro, et al., P. Bruzzone, F. Cau, *Design and Procurement of the European Dipole (EDIPO) Superconducting Magnet,* IEEE T. Appl. Supercon. **18**, 499 (2008).

A. Portone, P. Bruzzone, M. Calvi, M. Bagnasco, F. Cau, *Winding Configurations Studies for the EFDA Dipole Test Facility EDIPO,* IEEE T. Appl. Supercon. **18**, 196 (2008).

A. Ramar, R. Schaeublin, *Analysis of Basic Mechanisms of Hardening in ODS EUROFER97 Steel Using in-Situ TEM,* Materials Science **2**, 475 (2008).

A. Ramar, P. Spaetig, R. Schaeublin, *Analysis of High Temperature Deformation Mechanism in ODS EUROFER97 Alloy,* J. Nucl. Mater. **8**, (2008).

A. Ramar, P. Spaetig, R. Schaeublin, *Analysis of High Temperature Deformation Mechanism in ODS EUROFER97 Alloy,* J. Nucl. Mater. **382**, 210 (2008).

G. Ramponi, D. Farina, M.A. Henderson, E. Poli, O. Sauter, G. Saibene, H. Zohm, C. Zucca, *Physics Analysis of the ITER ECW System for Optimized Performance,* Nucl. Fusion **48**, 054012 (2008).

P. Ricci, B.N. Rogers, S. Brunner, *High- and Low-Confinement Modes in Simple Magnetized Toroidal Plasmas,* Phys. Rev. Lett. **100**, 225002 (2008).

A.P. Rodrigues, N. Cruz, B. Santos, C.A.F. Varandas, J.M. Moret, J. Berrino, B. Duval, *TCV Advanced Plasma Control System Software Architecture and Preliminary Results,* IEEE T. Nucl. Sci. **55**, 316 (2008).

D.M.S. Ronden, M. Van Den Berg, W.A. Bongers, et al., M.A. Henderson, *Mechanical Design Aspects of A "Long-Waveguide" Version of the Remote Steering ECRH Upper Port Launcher for ITER,* Fusion Sci. Technol. **53**, 104 (2008).

R. Schaeublin, J. Henry, Y. Dai, *Helium and Point Defect Accumulation: (I) Microstructure and Mechanical Behaviour,* Comptes Rendus Physique **9**, 389 (2008).

S. Sharapov, A. Fasoli, D. Testa, *Burning Plasma Studies at JET,* Fusion Sci. Technol. **53**, 989 (2008).

A. Shikov, V. Pantsyrny, A. Vorobieva, et al., P. Bruzzone, *Development of a New RF Produced Internal Tin ITER TF Conductor Sample for Testing in Sultan Facility,* IEEE T. Appl. Supercon. **18**, 1076 (2008).

E.R. Solano, S. Jachmich, F. Villone, et al., R.A. Pitts, *ELMs and Strike Point Movements,* Nucl. Fusion **48**, 065005 (2008).

B. Stepanov, P. Bruzzone, R. Wesche, M. Bagnasco, M. Vogel, D. Ciazynski, N.N. Martovetsky, *Re-Test of the TFAS1 Sample with Solder Filled Extremities,* IEEE T. Appl. Supercon. **18**, 1080 (2008).

J.D. Strachan, J. Likonen, P. Coad, et al., R.A. Pitts, *Modelling of Carbon Migration During JET C-13 Injection Experiments,* Nucl. Fusion **48**, 105002 (2008).

B. Strahm, C. Hollenstein, A. Howling, *Uniformity of Silicon Microcrystallinity in Large Area RF Capacitive Reactors,* Progress in Photovoltaics **16**, 687 (2008).

E.J. Strait, E.D. Fredrickson, J.M. Moret, M. Takechi, *Magnetic Diagnostics,* Fusion Sci. Technol. **53**, 304 (2008).

X. Sun, T.P. Intrator, L. Dorf, I. Furno, G. Lapenta, *Transition of MHD Kink-Stability Properties between Line-Tied and Non-Line-Tied Boundary Conditions,* Phys. Rev. Lett. **100**, 1 (2008).

A. Sushkov, V. Andreev, Y. Camenen, A. Pochelon, I. Klimanov, A. Scarabosio, H. Weisen, *High-Resolution Multiwire Proportional Soft X-Ray Diagnostic Measurements on TCV,* Rev. Sci. Instrum. **79**, 023506 (2008).

Y. Takahashi, T. Isono, N. Koizumi, et al., B. Stepanov, P. Bruzzone, *Performance of Japanese Nb3Sn Conductors for ITER Toroidal Field Coils,* IEEE T. Appl. Supercon. **18**, 471 (2008).

P. Testoni, F. Cau, A. Fanni, A. Portone, P. Sonato, *Static and Transient Electromagnetic Features of the EFDA Dipole,* IEEE Trans. Appl. Supercond. **18**, 188 (2008).

C. Theiler, A. Diallo, A. Fasoli, I. Furno, B. Labit, M. Podesta, F.M. Poli, P. Ricci, *The Role of the Density Gradient on Intermittent Cross-Field Transport Events in a Simple Magnetized Toroidal Plasma,* Phys. Plasmas **15**, (2008).

D. Tskhakaya, F. Subba, X. Bonnin, D.P. Coster, W. Fundamenski, R.A. Pitts, *On Kinetic Effects During Parallel Transport in the SOL,* Contrib. Plasma Phys. **48**, 89 (2008).

G. Turri, S. Coda, J.M. Moret, Y. Martin, O. Sauter, *The Effect of MHD Noise on the Vertical Observer in Tokamaks,* Plasma Phys. Control. Fusion **50**, 035012 (2008).

G. Turri, O. Sauter, L. Porte, S. Alberti, E. Asp, T.P. Goodman, Y.R. Martin, V.S. Udintsev, C. Zucca, *The Role of MHD in the Sustainment of Electron Internal Transport Barriers and H-Mode in TCV,* Journal of Physics Conference Series **123**, (2008).

G. Turri, V.S. Udintsev, O. Sauter, T.P. Goodman, E. Fable, *MHD as Trigger of Electron Temperature Oscillations in ECCD Discharges in TCV,* Plasma Phys. Control. Fusion **50**, 065010 (2008).

V.S. Udintsev, O. Sauter, E. Asp, E. Fable, T.P. Goodman, G. Turri, J.P. Graves, A. Scarabosio, G. Zhuang, C. Zucca, T. And the Tcv, *Global Plasma Oscillations in Electron Internal Transport Barriers in TCV,* Plasma Phys. Control. Fusion **50**, 124052 (2008).

L. Veleva, R. Schaeublin, A. Ramar, Z. Oksiuta, N. Baluc, *Focused Ion Beam Application on the Investigation of Tungsten-Based Materials for Fusion Application,* Materials Science **2**, 503 (2008).

U.B. Vetrella, A. Della Corte, G. De Marzi, A. Di Zenobio, L. Muzzi, L. Reccia, S. Turtu, A. Baldini, P. Bruzzone, E. Salpietro, A. Vostner, *Manufacturing of the ITER TF Full Size Prototype Conductor,* IEEE T. Appl. Supercon. **18**, 1105 (2008).

A. Vostner, P. Bauer, R. Wesche, U.B. Vetrella, B. Stepanov, A. Della Corte, A. Portone, E. Salpietro, P. Bruzzone, *Development of the EFDA Dipole High Field Conductor,* IEEE T. Appl. Supercon. **18**, 544 (2008).

R. Wesche, R. Herzog, P. Bruzzone, *Comparison of the Performances of the Cs Model Coil and the Good Joint Sultan Sample,* Supercond. Sci. Technol. **21**, 054001 (2008).

APPENDIX B Conferences and Seminars

(see CRPP archives at http://crppwww.epfl.ch/archives)

B.1 Conference and conference proceedings published in 2008

M. Albergante, J.P. Graves, T. Dannert, A. Fasoli, F. Zonca, S. Briguglio, G. Vlad, G. Fogaccia, *Interaction between Fast Particles and Turbulence,* Joint Varenna Lausanne International Workshop on Theory of Fusion Plasmas, Varenna, ITALY, August 25-29, 2008, Theory of Fusion Plasmas **1069**, 240-246 (2008).

P. Angelino, X. Garbet, L. Villard, A. Bottino, S. Jolliet, P. Ghendrih, V. Grandgirard, B.F. McMillan, Y. Sarazin, G. Dif-Pradalier, T.M. Tran, *Effects of Plasma Current on Drift Wave Turbulence,* 35th European Physical Society (EPS) Conference on Plasma Physics, Hersonissos, Crete, Greece, June 9-13, 2008, ECA **32D**, P-4.033 (2008).

M. Bagnasco, *Calorimetric Method Results for Current Sharing Temperature Measurements in ITER Conductor Samples in Sultan,* 25th SOFT, Symposium on Fusion Technology, Rostock, Germany, September 15-19, 2008.

M. Bagnasco, M. Levandowska, *Pressure Drop Measurements in Cable-in-Conduit Conductors (CICC) with Different Layouts,* Int Cryogenic Engineering Conf. 22, and Int. Cryogenic Engineering Conf. 22, Seoul, Korea, July 21-25, 2008.

R. Bertizzolo, R. Chavan, A. Collazos, F. Dolizy, M. Henderson, J.D. Landis, F. Sanchez, *Design and Test of a Pressure Controlled Bellows Actuator for the Angular Positioning of the Steering Mirror in the ITER ECRH Upper Port Plug,* 25th SOFT, Symposium on Fusion Technology, Rostock, Germany, September 15-19, 2008.

A. Bortolon, B.P. Duval, A. Karpushov, Y. Andrebe, *Intrinsic Rotation and Radial Electric Field in TCV Plasmas,* 50th APS Division of Plasma Physics Meeting, Dallas, Texas, USA, November 17-21, 2008.

V.R. Bovshuk, W.A. Cooper, M.I. Mikhailov, J. Nuehrenberg, V.D. Shafranov, *Exploration of Configurational Space for Quasi-Isodynamic Stellarators with Poloidally Closed Contours of the Magnetic Field Strength,* 22nd IAEA Fusion Energy Conf. (FEC) 50th Anniversary of Controlled Nuclear Fusion Research, Geneva, Switzerland, October 10-18, 2008.

P. Bruzzone, B. Spepanov, R. Wesche, A. Della Corte, L. Affinito, M. Napolitano, A. Vostner, *Test Results of a Nb3Sn Cable-in-Conduit Conductor with Variable Pitch Sequence,* ASC 2008 Applied Superconductivity Conference, Chicago, Illinois, USA, August 17-22, 2008.

P. Bruzzone, B. Stepanov, R. Wesche, F. Cau, M. Bagnasco, M. Calvi, R. Herzog, *Qualification Tests for ITER TF Conductors in Sultan,* 25th SOFT, Symposium on Fusion Technology, Rostock, Germany, September 15-19, 2008.

P. Bruzzone, B. Stepanov, R. Wesche, F. Cau, M. Bagnasco, M. Calvi, R. Herzog, *Qualification Tests and Facilities for ITER TF Superconductors,* 22nd IAEA Fusion Energy Conf. (FEC) 50th Anniversary of Controlled Nuclear Fusion Research, Geneva, Switzerland, October 10-18, 2008.

P. Bruzzone, B. Stepanov, R. Wesche, Y. Ilyin, R. Herzog, M. Calvi, M. Bagnasco, F. Cau, *Methods, Accuracy and Reliability of ITER Conductor Tests in Sultan,* ASC 2008 Applied Superconductivity Conference, Chicago, Illinois, USA, August 17-22, 2008.

R.J. Buttery, S. Gerhardt, A. Isayama, R.J. La Haye, E.J. Strait, D.P. Brennan, P. Buratti, D. Chandra, S. Coda, J. De Grassie, P. Gohil, M. Gryaznevich, D.F. Howell, G. Jackson, C. Holcomb, M. Maraschek, A. Polevoi, H. Reimerdes, D. Raju, S. Sabbagh, S. Saarelma, M. Schaffer, A. Sen, J.-E. Contributors, JET-EFDA contributors, The DIII-D, JT-60 and NSTX Teams, *Multimachine Extrapolation of Neoclassical Tearing Mode Physics to ITER,* 22nd IAEA Fusion Energy Conf. (FEC) 50th Anniversary of Controlled Nuclear Fusion Research, Geneva, Switzerland, October 13-18, 2008, Proceedings of the 22nd IAEA Fusion Energy Conference, IT/P6-8 (2008).

M. Calvi, L. Bottura, C. Marinucci, *Validation of Supermagnet with PFI Results,* CHATS AS, Applied Superconductivity, Tsukuba, Japan, October 30-November 1, 2008.

F. Cau, M. Bagnasco, P. Bruzzone, M. Calvi, F. Roth, *Interstrand Resistance and Current Redistribution in a Cable-in-Conduit Conductor (CICC) Termination,* ASC 2008 Applied Superconductivity Conference, Chicago, Illinois, USA, August 17-22, 2008.

F. Cau, P. Bruzzone, *AC Loss Measurements in CICC with Different Aspect Ratio,* ASC 2008 Applied Superconductivity Conference, Chicago, Illinois, USA, August 17-22, 2008.

F. Cau, P. Bruzzone, F. Staehli, *AC Loss Measurements on Cable in Conduit Conductor with Random-Changing Magnetic Fields,* 25th SOFT, Symposium on Fusion Technology, Rostock, Germany, September 15-19, 2008.

R. Chavan, G. Chitarin, R.S. Delogu, A. Encheva, E. Hodgson, C. Ingesson, A. Le-Luyer, J.B. Lister, P. Moreau, J.M. Moret, S. Peruzzo, D. Testa, G. Vayakis, R. Vila, *The Magnetic Diagnostics Set for ITER,* 25th SOFT, Symposium on Fusion Technology, Rostock, Germany, September 15-19, 2008.

S. Coda, A. Marinoni, R. Chavan, J.C. Magnin, G. Pochon, *Design of a Tangential Phase Contrast Imaging Diagnostic for the TCV Tokamak,* 50th APS Division of Plasma Physics Meeting, Dallas, Texas, USA, November 17-21, 2008, Bull. Am. Phys. Soc. **53**, TP6.00057 (2008).

S. Coda, O. Sauter, M.A. Henderson, T.P. Goodman, *Full Bootstrap Discharge Sustainment in Steady State in the TCV Tokamak,* 22nd IAEA Fusion Energy Conference, Geneva, 13-18 October 2008, Proceedings of the 22nd IAEA Fusion Energy Conference, EX/2-3 (2008).

A. Collazos, M. Henderson, R. Chavan, F. Felici, J.D. Landis, F. Dolizy, R. Bertizzolo, F. Sanchez, *Progress on the ITER ECRH Upper Launcher Control System,* 25th SOFT, Symposium on Fusion Technology, Rostock, Germany, September 15-19, 2008.

A. Collazos, V. Udintsev, M.A. Henderson, R. Chavan, F. Felici, F. Dolizy, H. Shidara, *Progress on the ITER Upper Launcher Millimeter Wave Design and Testing,* EC 15 Joint workshop on ECE and ECRH, Yosemite Park, California, USA, March 3-13, 2008.

W.A. Cooper, J.P. Graves, S.P. Hirshman, P. Merkel, *Three-Dimensional Free-Boundary Anisotropic Pressure Equilibria,* 35th European Physical Society (EPS) Conference on Plasma Physics, Hersonissos, Crete, Greece, June 9-13, 2008, ECA **32D**, P-4.061 (2008).

W.A. Cooper, J.P. Graves, S.P. Hirshman, P. Merkel, J. Kisslinger, H.F.G. Wobig, K.Y. Watanabe, Y. Narushima, *3d Plasma Equilibrium and Stability with Hot Particle Anisotropic Pressure,* Joint Varenna Lausanne International Workshop on Theory of Fusion Plasmas, Varenna, ITALY, August 25-29, 2008, Theory of Plasma Physics **1069**, 40-52 (2008).

T. Dannert, S. Guenter, T. Hauff, F. Jenko, X. Lapillonne, P. Lauber, *Turbulent Transport of Beam Ions,* 21st US TTF, US Transport Taskforce Workshop, Boulder, CO, USA, March 25-28, 2008.

J. Decker, A.K. Ram, Y. Peysson, S. Coda, L. Curchod, A. Pochelon, *Electron Bernstein Wave Heating and Current Drive in Axisymmetric Toroidal Plasmas,* 35th European Physical Society (EPS) Conference on Plasma Physics, Hersonissos, Crete, Greece, June 9-13, 2008, ECA **32D**, P-1.099 (2008).

I.R. Dixon, M.D. Bird, P. Bruzzone, B. Stepanov, *Current Sharing and AC Loss Measurements of Cable-in-Conduit Conductor with Nb3Sn Strands for the High Field Section of the Series-Connected Hybrid Outsert Coil,* ASC 2008 Applied Superconductivity Conference, Chicago, Illinois, USA, August 17-22, 2008.

J.L. Dorier, P. Guittienne, C. Hollenstein, M. Gindrat, A. Refke, *Thin and Thick Film Coating Using Liquid and Gaseous Precursors with Low Pressure Plasma Spraying Equipment,* S2TS 2¬∞ Int Workshop on Suspension and Solution Thermal Spraying, Tours, France, June 5-7, 2008.

B.P. Duval, A. Bortolon, A. Karpushov, A. Pochelon, O. Sauter, G. Turri, *Effect of Sawteeth on the Spontaneous TCV Plasma Rotation,* 35th European Physical Society (EPS) Conference on Plasma Physics, Hersonissos, Crete, Greece, June 9-13, 2008, ECA **32D**, P-2.020 (2008).

E. Fable, C. Angloni, O. Sauter, *Parametric Dependence of Particle Pinch Coefficients for Electron Particle Transport in Linear Gyrokinetic Theory,* Joint Varenna Lausanne International Workshop on Theory of Fusion Plasmas, Varenna, ITALY, August 25-29, 2008, THEORY OF FUSION PLASMAS **1069**, 64-75 (2008).

E. Fable, H. Weisen, et al., *Convective Carbon Transport in TCV L-Modes,* 22nd IAEA Fusion Energy Conf. (FEC) 50th Anniversary of Controlled Nuclear Fusion Research, Geneva, Switzerland, October 13-18, 2008.

A. Fasoli, TCVT. And The, *Overview of Physics Research on the TCV Tokamak,* 22nd IAEA Fusion Energy Conf. (FEC) 50th Anniversary of Controlled Nuclear Fusion Research, Geneva, Switzerland, October 10-18, 2008, ECA **32D**, OV/1-1 (2008).

A. Fasoli, A. Diallo, I. Furno, D. Iraji, B. Labit, S. Mueller, M. Podesta, F.M. Poli, *Fluctuations, Turbulence and Related Transport in the TORPEX,* 35th European Physical Society (EPS) Conference on Plasma Physics, Hersonissos, Crete, Greece, June 9-13, 2008, ECA **32D**, P-1.184 (2008).

A. Fasoli, A. Diallo, I. Furno, D. Iraji, B. Labit, G. Plyushchev, P. Ricci, C. Theiler, S. Mueller, M. Podesta, F. Poli, *Fluctuations, Turbulence and Related Transport in the TORPEX Simple Magnetized Toroidal Plasma,* 21st US TTF, US Transport Taskforce workshop, Boulder, CO, USA, March 25-28, 2008.

A. Fasoli, A. Diallo, I. Furno, D. Iraji, B. Labit, G. Plyushchev, P. Ricci, C. Theiler, S. Mueller, M. Podesta, F. Poli, *Analysis of Fluctuations, Turbulence and Related Transport in the TORPEX Simple Magnetized Toroidal Plasma,* International Sherwood Fusion Theory Conference, Boulder, CO, USA, March 30-April 2, 2008.

A. Fasoli, et al., *Instabilities, Blobs and Transport in TORPEX Simple Magnetized Toroidal Plasmas,* 50th APS Division of Plasma Physics Meeting, Dallas, Texas, USA, November 17-21, 2008.

F. Felici, E. Asp, S. Coda, E. Fable, T.P. Goodman, J. Graves, M. Henderson, J. Paley, F. Piras, O. Sauter, G. Turri, V. Udintsev, C. Zucca, TCV Team, *Recent Results of ECRH/ECCD Experiments on TCV,* 18th International Toki Conference (ITC18), Ceratopia Toki, Toki Gifu, Japan, December 9-12, 2008.

F. Felici, O. Sauter, C. Zucca, T.P. Goodman, *Safety Factor Profile Influence on Tearing Mode Stability in TCV,* Annual Meeting of the Swiss Physical Society, Geneva, Switzerland, March 26-27, 2008.

I. Furno, A. Diallo, A. Fasoli, D. Iraji, B. Labit, S.H. Mueller, G. Plyushchev, M. Podesta, F.M. Poli, P. Ricci, C. Theiler, *Turbulence and Transport in Simple Magnetized Toroidal Plasmas,* 22nd IAEA Fusion Energy Conf. (FEC) 50th Anniversary of Controlled Nuclear Fusion Research, Geneva, Switzerland, October 13-18, 2008, Paper EX/P5-41 (2008).

I. Furno, A. Fasoli, B. Labit, M. Podesta, P. Ricci, C. Theiler, *Investigation of the Existence of an Improved Confinement Regime in Simple Magnetized Toroidal Plasmas,* 35th European Physical Society (EPS) Conference on Plasma Physics, Hersonissos, Crete, Greece, June 9-13, 2008, ECA **32D**, P-2.182 (2008).

S. Gnesin, S. Coda, *Design of a Tomographic Hard X-Ray Spectrometer for Suprathermal Electron Studies with ECRH,* International Conference on Burning Plasma Diagnostics, Varenna, ITALY, September 24-28, 2007, AIP Conference proceedings **988**, 222-225 (2008).

T.P. Goodman, F. Albajar, S. Alberti, P. Benin, S. Bethuys, T. Bonicelli, *First Experimental Results from the EU 2MW Coaxial Cavity ITER Gyrotron Prototypie,* EC 15 Joint Workshop on ECE and ECRH, Yosemite Park, California, USA, March 10-13, 2008.

J.P. Graves, I. Chapman, S. Coda, L.G. Eriksson, T. Johnson, *Sawtooth Control Mechanism Using Counter Current Propagating ICRH in JET,* 35th European Physical Society (EPS) Conference on Plasma Physics, Hersonissos, Crete, Greece, June 9-13, 2008, ECA **32D**, P-5.062 (2008).

B. Gulejova, R.A. Pitts, D. Coster, X. Bonnin, M. Beurskens, S. Jachmich, A. Kallenbach, *Solps5 Simulations of Type I Elming H-Mode at JET,* 18th International Conference on Plasma Surface Interactions (PSI), Toledo, Spain, May 26-30, 2008.

M.A. Henderson, S. Alberti, R. Chavan, D. Fasel, T.P. Goodman, I.G. Pagonakis, O. Sauter, U. Siravo, V.S. Udintsev, C. Zucca, G. Saibene, F. Albajar, T. Bonicelli, S. Cirant, D. Farina, G. Ramponi, R. Heidinger, B. Piosczyk, M. Thumm, *A Revised ITER EC System Baseline Design Proposal,* EC 15 Joint Workshop on ECE and ECRH, Yosemite Park, California, USA, March 10-13, 2008.

M.A. Henderson, R. Chavan, R. Bertizzolo, A. Collazos, F. Dolizy, J.D. Landis, F. Sanchez, V.S. Udintsev, G. Saibene, M. Cavinato, A. Bruschi, S. Cirant, D. Farina, A. Moro, P. Platana, G. Ramponi, C. Sozzi, E. Poli, H. Zohm, B. Blaum, W. Kasparek, *Progress in the ITER Upper Launcher Mm-Wave,* EC 15 Joint Workshop on ECE and ECRH, Yosemite Park, California, USA, March 10-13, 2008.

R. Herzog, M. Calvi, C. Marinucci, P. Bruzzone, *Helium Flow-Reversal in 3 M Long, Partially Heated Sections of Dual-Channel CICC for ITER,* ASC 2008 Applied Superconductivity Conference, Chicago, Illinois, USA, August 17-22, 2008.

R. Herzog, R. Wesche, P. Bruzzone, *Ic Measurements on Nb3Sn Strands Extracted from ITER CICC Prototypes,* ASC 2008 Applied Superconductivity Conference, Chicago, Illinois, USA, August 17-22, 2008.

J.P. Hogge, S. Alberti, F. Albajar, K. Avramides, P. Benin, T. Bonicelli, et al., *Status of Development of the 2MW, 170ghz Coaxial-Cavity Gyrotron for ITER,* ICOPS, 35th IEEE International Conference on Plasma Science, Karlsruhe, Germany, June 15-19, 2008 (2008).

J. Horacek, A.H. Nielsen, R.A. Pitts, J. Zajac, J. Seidl, O.E. Garcia, B. Gulejova, *Fast Temperature Fluctuation Measurements in SOL of Tokamak TCV,* EFTSOMP2008 11th Workshop on Electric Fields, Turbulence and Self

Organisation in Magnetized Plasmas, Satellite meeting of the 35th EPS Plasma Physics Conference, Hersonissos, Crete, Greece, June 12-18, 2008.

A.A. Howling, B. Strahm, C. Hollenstein, *Non-Intrusive Plasma Diagnostics for Deposition of Large Area Thin Film Silicon,* E MRS, European Materials Research Society Symposium, Strasbourg, France, May 26-30, 2008.

A. Huber, R.A. Pitts, A. Loarte, JET EFDA Contributors, *Plasma Radiation During Transient Events in JET,* 35th European Physical Society (EPS) Conference on Plasma Physics, Hersonissos, Crete, Greece, June 9-13, 2008, ECA **32D**, O-4.033 (2008).

F. Imbeaux, J.B. Lister, G.T.A. Huysmans, et al., ITM-TF Contributors, *Data Structure for the European Integrated Tokamak Modelling Task Force,* 35th European Physical Society (EPS) Conference on Plasma Physics, Hersonissos, Crete, Greece, June 9-13, 2008, ECA **32D**, P-2.112 (2008).

S. Jawla, J.P. Hogge, S. Alberti, T.P. Goodman, B. Piosczyk, T. Rzesnicki, C. Lievin, *Infrared Measurements and Phase Retrieval Analysis of the RF-Beam of the 2MW/170ghz Coaxial Cavity Gyrotron for ITER,* ICOPS, 35th IEEE International Conference on Plasma Science, Karlsruhe, Germany, June 15-19, 2008.

S. Jolliet, B.F. McMillan, T.M. Tran, X. Lapillonne, L. Villard, A. Bottino, P. Angelino, *Global Nonlinear Simulations of Ion and Electron Turbulence Using a Particle-in-Cell Approach,* 22nd IAEA Fusion Energy Conf. (FEC) 50th Anniversary of Controlled Nuclear Fusion Research, Geneva, Switzerland, October 10-18, 2008.

M. Jucker, J.P. Graves, W.A. Cooper, N. Mellet, S. Brunner, *Monte Carlo ICRH Simulations in Fully Shaped Anisotropic Plasmas,* Joint Varenna Lausanne International Workshop on Theory of Fusion Plasmas, Varenna, ITALY, August 25-29, 2008, THEORY OF FUSION PLASMAS **1069**, 283-288 (2008).

A.N. Karpushov, B.P. Duval, C. Schlatter, *Ion Temperature Fluctuations in ELMy H-Mode of the X3 EC-Heated Plasmas on TCV,* PLASMA 2007: International Conference on Research and Applications of Plasmas; 4th German Polish Conference on Plasma Diagnostics for Fusion and Applications; 6th French Polish Seminar on Thermal Plasma in Space and Laboratory, Greifswald, GERMANY, October 16-19, 2007, AIP Conference Proceedings **993**, 219-222 (2008).

S.H. Kim, J.F. Artaud, V. Basiuk, V. Dokouka, F. Imbeaux, R.R. Khayrutdinov, J.B. Lister, V.E. Lukash, *Full Tokamak Simulation of ITER Scenario 2 Using the Combined DINA-Ch and CRONOS Simulator,* 35th European Physical Society (EPS) Conference on Plasma Physics, Hersonissos, Crete, Greece, June 9-13, 2008, ECA **32D**, O-2.004 (2008).

A. Klein, D. Testa, J. Snipes, A. Fasoli, H. Carfantan, JET EFDA Contributors, *Toroidal Mode Number Analysis of Degenerate Alfven Eigenmodes in the Active MHD Spectroscopy on JET,* 35th European Physical Society (EPS) Conference on Plasma Physics, Hersonissos, Crete, Greece, June 9-13, 2008, ECA **32D**, P-5.083 (2008).

B. Labit, A. Fasoli, I. Furno, P. Ricci, C. Theiler, *Correlation between Toroidal Rotation and Density Blobs in the TORPEX Magnetized Plasmas,* 13th EU US TTF workshop, Copenhagen, Denmark, September 1-9, 2008.

X. Lapillonne, T. Dannert, S. Brunner, A. Marinoni, S. Jolliet, L. Villard, F. Jenko, T. Goerler, F. Merz, *Effects of Geometry on Linear and Non-Linear Gyrokinetic Simulations, and Development of a Global Version of the Gene Code,* Joint Varenna Lausanne International Workshop on Theory of Fusion Plasmas, Varenna, ITALY, August 25-29, 2008.

A. Marinoni, S. Brunner, Y. Camenen, S. Coda, J. Graves, X. Lapillonne, A. Pochelon, O. Sauter, L. Villard, *The Effect of Plasma Triangularity on Turbulent Transport: Modelling TCV Experiments by Linear and Non Linear Gyrokinetic*

Simulations, 50th APS Division of Plasma Physics Meeting, Dallas, Texas, USA, November 17-21, 2008, Bull. Am. Phys. Soc. **53**, GP6.00106 (2008).

C. Marinucci, L. Bottura, M. Calvi, *A Parametric AC Loss Model of the ITER Coils for Control Optimization,* CHATS AS, Applied Superconductivity, Tsukuba, Japan, October 30-November 1, 2008.

J. Marki, R.A. Pitts, J. Horacek, G. Turri, D. Tskhakaya, *ELM Induced Divertor Heat Loads on TCV,* Annual Meeting of the Swiss Physical Society, Geneva, Switzerland, March 26-27, 2008.

J. Marki, R.A. Pitts, J. Horacek, G. Turri, D. Tskhakaya, TCV Team, *ELM Induced Divertor Heat Loads on TCV,* 18th International Conference on Plasma Surface Interactions, PSI, Toledo, Spain, May 26-30, 2008.

N.N. Martovetsky, D.R. Hatfield, J.R. Miller, C.Y. Gung, J.S. Schultz, N. Cheggour, L.F. Goodrich, P. Bruzzone, B. Stepanov, *Test Results of the First US ITER TF Conductors in Sultan,* ASC 2008 Applied Superconductivity Conference, Chicago, Illinois, USA, August 17-22, 2008.

A.A. Martynov, S.Y. Medvedev, L. Villard, *Tokamaks with Reversed Current Density: Stability of Equilibria with Axisymmetric Islands,* 35th European Physical Society (EPS) Conference on Plasma Physics, Hersonissos, Crete, Greece, June 9-13, 2008.

M. Maslov, H. Weisen, C. Angioni, *Density Profile Behavior in JET H-Mode Plasmas,* 22nd IAEA Fusion Energy Conf. (FEC) 50th Anniversary of Controlled Nuclear Fusion Research, Geneva, Switzerland, October 13-18, 2008.

K. Matsui, T. Isono, Y. Nunoya, T. Hemmi, Y. Nabara, Y. Okui, M. Oshikiri, N. Koizumi, Y. Takahashi, K. Okuno, B. Stepanov, P. Bruzzone, *Test Results of Japanese Sultan Sample and Conductor Procurement in Japan for ITER TF Coils,* ASC 2008 Applied Superconductivity Conference, Chicago, Illinois, USA, August 17-22, 2008.

B.F. McMillan, S. Jolliet, T.M. Tran, A. Bottino, P. Angelino, L. Villard, *Avalanche-Like Bursts in Global Gyrokinetic Simulations,* 35th European Physical Society (EPS) Conference on Plasma Physics, Hersonissos, Crete, Greece, June 9-13, 2008, ECA **32D**, P-1.019 (2008).

S.Y. Medvedev, A.A. Ivanov, A.A. Martynov, Y.Y. Poshekhonov, R. Behn, Y.R. Martin, A. Pochelon, O. Sauter, L. Villard, *Beta Limits and Edge Stability for Negative Triangularity Plasma in TCV Tokamak,* 35th European Physical Society (EPS) Conference on Plasma Physics, Hersonissos, Crete, Greece, June 9-13, 2008, ECA **32D**, P-1.072 (2008).

N. Mellet, W.A. Cooper, M. Jucker, J.P. Graves, L. Villard, *A New Iterative Method to Compute the Dielectric Tensor in the Low-Frequency Wave Code Leman,* 50th APS Division of Plasma Physics Meeting, Dallas, Texas, USA, November 17-21, 2008.

P. Moreau, F. Saint-Laurent, J.B. Lister, *Drift Free Magnetic Equilibrium Reconstruction Using Neural Network,* 50th APS Division of Plasma Physics Meeting, Dallas, Texas, USA, November 17-21, 2008.

Y. Narushima, K.Y. Watanabe, R. Sakamoto, Y. Suzuki, S. Sakakibara, S. Ohdachi, H. Yamada, E.G. Lhd, W.A. Cooper, V.R. Jacobo, *Characteristics of Magnetohydrodynamics of IDB Plasma in LHD,* ICPP 2008 ‚Äî Int. Congress on Plasma Physics, Fukuoka, Japan, September 8-12, 2008.

Y. Narushima, K.Y. Watanabe, R. Sakamoto, I. Yamada, K. Narihara, Y. Suzuki, S. Sakakibara, S. Ohdachi, H. Yamada, E.G. Lhd, W.A. Cooper, J. Varela Rodriguez, *MHD Stability Analysis of IDB Plasma in LHD,* ICPP 2008 ‚Äî Int. Congress on Plasma Physics, Fukuoka, Japan, September 8-12, 2008.

I.G. Pagonakis, J.P. Hogge, S. Alberti, A. Avramides, J.L. Vomvoridis, *Optimization Study of the Gyrotron Collector System Optimization Study of the Gyrotron Collector System Based on the ExB Electron Drift,* IRMMW THz 2008, 33rd International Conference on Infrared, Millimeter, and Terahertz Waves, Caltech, Pasadena, CA, USA, September 15-19, 2008.

J.I. Paley, F. Felici, J. Berrino, S. Coda, N. Cruz, B.P. Duval, T.P. Goodman, Y. Martin, J.M. Moret, F. Piras, A.P. Rodrigues, B. Santos, C.A.F. Varandas, TCVT. The, *Real Time Control of Plasmas and ECRH Systems on TCV,* 22nd IAEA Fusion Energy Conf. (FEC) 50th Anniversary of Controlled Nuclear Fusion Research, Geneva, Switzerland, October 13-18, 2008, Proceedings of the 22nd IAEA Fusion Energy Conference, EX/P6-16 (2008).

J.I. Paley, F. Felici, T. Goodman, F. Piras, S. Coda, TCV Team, *Real Time Feedback Control of the Sawtooth Period Using ECRH Launchers,* 50th APS Division of Plasma Physics Meeting, Dallas, Texas, USA, November 17-21, 2008, Bull. Am. Phys. Soc. **53**, NO3.00005 (2008).

B. Piosczyk, S. Alberti, F. Albajar, et al., D. Fasel, T.P. Goodman, J.P. Hogge, S. Jawla, I.G. Pagonakis, M.Q. Tran, *Status of the European 2 MW, 170 GHz Coaxial Cavity Gyrotron for ITER (Invited Paper),* 7th Int. Workshop on Strong Microwaves: Sources and Applications, Nizhny Novgorod, Russia, July 27-August 2, 2008.

R.A. Pitts, A. Alonso, G. Arnoux, S. Brezinsek, M. Beurskens, T. Eich, H.G. Esser, W. Fundamenski, A. Huber, B. Gulejova, S. Jachmich, A. Kreter, A. Loarte, E. De La Luna, J. Marki, G.F. Metthews, V. Philipps, E. Solano, M.F. Stamp, J.E. And, *The Impact of Large ELMs on JET,* 18th International Conference on Plasma Surface Interactions, PSI, Toledo, Spain, May 26-30, 2008.

R.A. Pitts, A. Bencze, G. Gulejova, J. Horacek, J. Marki, D. Tskhakaya, R. Tye, G. Veres, *SOL Transport in TCV,* 22nd IAEA Fusion Energy Conf. (FEC) 50th Anniversary of Controlled Nuclear Fusion Research, Geneva, Switzerland, October 13-18, 2008.

G. Plyushchev, A. Fasoli, I. Furno, B. Labit, P. Ricci, C. Theiler, *Interaction of Fast Ion Beam with Plasma Turbulence in the TORPEX Simple Magnetized Toroidal Plasma,* 50th APS Division of Plasma Physics Meeting, Dallas, Texas, USA, November 17-21, 2008.

A. Pochelon, S. Brunner, Y. Camenen, S. Coda, J. Graves, A. Marinoni, A. Martynov, H. Reimerdes, O. Sauter, A. Scarabosio, S. Alberti, P. Angelino, R. Behn, A. Bortolon, A. Bottino, L. Curchod, K. Daouk, B.P. Duval, A. Fasoli, I. Furno, T.P. Goodman, M.A. Henderson, F. Hofmann, A. Karpushov, X. Lapillonne, J.B. Lister, Y. Martin, J.M. Moret, S. Medvedev, J.I. Paley, R.A. Pitts, F. Piras, L. Porte, F. Ryter, L. Sulmoni, A. Sushkov, L. Villard, M.Q. Tran, H. Weisen, TCV Team, *Physics Insight and Performance Benefit from Plasma Shaping Experiments in MHD and Energy Transport in the TCV Tokamak,* 22nd IAEA Fusion Energy Conf. (FEC) 50th Anniversary of Controlled Nuclear Fusion Research, Geneva, Switzerland, October 13-18, 2008, Proceedings of the 22nd IAEA Fusion Energy Conference, EX/P5-15 (2008).

A. Portone, W. Baker, E. Salpietro, P. Testoni, A. Vostner, P. Bruzzone, E. Theisen, A. Della Corte, A. Baldini, *Status of the EDIPO Project,* ASC 2008 Applied Superconductivity Conference, Chicago, Illinois, USA, August 17-22, 2008.

P. Ricci, B.N. Rogers, S. Brunner, *High- and Low-Confinement Modes in Simple Magnetized Toroidal Plasmas,* 21st US TTF, US Transport Taskforce Workshop, Boulder, CO, USA.

F. Sanchez, R. Bertizzolo, R. Chavan, A. Collazos, M. Henderson, J.D. Landis, *Design and Manufacturing of the ITER ECRH Upper Launcher Mirrors,* 25th SOFT, Symposium on Fusion Technology, Rostock, Germany, September 15-19, 2008.

Y. Sarazin, G. Dif-Pradalier, V. Grandgirard, et al., S. Jolliet, B.F. McMillan, T.M. Tran, L. Villard, *Global Gyrokinetic Simulations of Rho* and Nu* Scalings of Turbulent Transport,* 22nd IAEA Fusion Energy Conf. (FEC) 50th Anniversary of Controlled Nuclear Fusion Research, Geneva, Switzerland, October 10-18, 2008, Proceedings of the 22nd IAEA Fusion Energy Conference, TH/P8-46 (2008).

M. Silva, S. Alberti, J.P. Ansermet, K.A. Avramides, G. Bodenhausen, J.P. Hogge, I.G. Pagonakis, D. Wagner, *Design of a Low-Power High-Frequency Gyrotron for DNP-Enhanced NMR Spectroscopy,* ICOPS, 35th IEEE International Conference on Plasma Science, Karlsruhe, Germany, June 15-19, 2008.

B. Strahm, A.A. Howling, C. Hollenstein, *Crystallinity Uniformity of Microcrystalline Silicon Thin Films Deposited in Large Area Radio Frequency Capacitively-Coupled Reactors,* Symposium on Amorphous and Polycrystalline Thin Film Silicon Science and Technology held at the 2008 MRS Spring Meeting, San Francisco, CA, March 25-28, 2008, AMORPHOUS AND POLYCRYSTALLINE THIN-FILM SILICON SCIENCE AND TECHNOLOGY-2008 **1066**, 3-14 (2008).

C. Theiler, A. Diallo, A. Fasoli, I. Furno, B. Labit, S.H. Mueller, M. Podesta, F.M. Poli, P. Ricci, *Intermittent Transport Events and Blobs in a Simple Magnetized Toroidal Plasma,* 13th EU US TTF workshop, Copenhagen, Denmark, September 1-9, 2008.

G. Turri, O. Sauter, V.S. Udintsev, T.P. Goodman, E. Asp, E. Fable, C. Zucca, TCVT. And The, *Global Plasma Oscillations in Electron Internal Transport Barriers in TCV,* 22nd IAEA Fusion Energy Conf. (FEC) 50th Anniversary of Controlled Nuclear Fusion Research, Geneva, Switzerland, October 10-18, 2008, paper EX/P3-6 (2008).

R. Tye, J. Horacek, R.A. Pitts, *ELM Filament Characteristics on TCV,* MRS Material Research Society, San Francisco, CA, USA, March 24-28, 2008.

R. Tye, J. Horacek, R.A. Pitts, *ELM Filament Characteristics on TCV,* Annual Meeting of the Swiss Physical Society, Geneva, Switzerland, March 26-27, 2008.

V.S. Udintsev, E. Asp, T.P. Goodman, J.P. Graves, O. Sauter, G. Turri, *Control of Global Plasma Oscillations in TCV,* EC 15 Joint Workshop on ECE and ECRH, Yosemite Park, California, USA, March 10-13, 2008.

G. Veres, R.A. Pitts, A. Bencze, J. Marki, R. Tye, TCVT. And The, *Fast Radiation Dynamics During ELMs on TCV,* 18th International Conference on Plasma Surface Interactions, PSI, Toledo, Spain, May 26-30, 2008.

A.E. Vorobieva, A.K. Shikov, V.I. Pantsyrny, E.A. Dergunova, L.I. Vozhdaev, N.I. Kozlenkova, V.E. Sytnikov, A.V. Taran, A.V. Rychagov, P. Bruzzone, *Development of Nb3Sn Bronze TF Conductor Sample for Testing in Sultan Facility,* ASC 2008 Applied Superconductivity Conference, Chicago, Illinois, USA, August 17-22, 2008.

R. Wesche, M. Bagnasco, P. Bruzzone, M. Calvi, F. Cau, R. Herzog, C. Marinucci, B. Stepanov, *Results of Conductor Testing in Sultan: A Review,* Wamsdo, Cern, Geneva, Switzerland, May 19-23, 2008.

M.J. Windridge, G. Cunningham, V. Dokuka, T.C. Hender, R. Khayrutdinov, J.B. Lister, V. Lukash, *MAST Plasma Response Investigations Using DINA-Ch,* 35th European Physical Society (EPS) Conference on Plasma Physics, Hersonissos, Crete, Greece, June 9-13, 2008, ECA **32D**, P-4.066 (2008).

A. Zhuchkova, H. Weisen, R. Behn, P. Blanchard, C. Zucca, Y. Andrebe, *A New Far-Infrared Polarimeter on The "Tokamak a Configuration Variable",* ICOPS, 35th

IEEE International Conference on Plasma Science, Karlsruhe, Germany, June 15-19, 2008.

S. Zoletnik, D. Dunai, A.R. Field, et al., R.A. Pitts, M.T. And The, *Observations of ELM Pre-Cursor Structures Using Beam Emission Spectroscopy in MAST,* 35th European Physical Society (EPS) Conference on Plasma Physics, Hersonissos, Crete, Greece, June 9-13, 2008, ECA **32D**, O-4.031 (2008).

C. Zucca, O. Sauter, M.A. Henderson, E. Fable, D. Farina, A. Polevoi, G. Ramponi, G. Saibene, H. Zohm, *Safety-Factor Profile Tailoring by Improved Electron Cyclotron System for Sawtooth Control and Reverse Shear Scenarios in ITER,* Joint Varenna Lausanne International Workshop on Theory of Fusion Plasmas, Varenna, ITALY, August 25-29, 2008, THEORY OF FUSION PLASMAS **1069**, 361-367 (2008).

B.2 Seminars presented at the CRPP in 2008

Dr. K. Appert, CRPP-EPFL, Lausanne, Switzerland, *"CLEAN advection based on a COOL idea and semi-Lagrangian time integration"*

F. Jenko, IPP-Garching, Germany, *"Non-linear saturation of trapped electron modes via perpendicular particle diffusion"*

T. Goerler, IPP-Garching, Germany, *"Gyrokinetic multi-scale simulatins of coupled ITG/TEM and ETG turbulence"*

Dr. T. Stoltzfus-Dueck, Princeton Plasma Physics Labortory, Princeton, USA, *"Blobs and near-adiabatic tokamak edge turbulence"*

Dr. F. Zonca, Dr. M. Valisa, Dr. G. Granucci, Dr. A. Tuccillo, ENEA Frascati, Italy, *"The Fusion Advanced Studies Torus: A proposal for a setellite facility in support of the development of fusion energy"*

Dr. Ch. Wahlberg, Dept. of Astronomy and Space Physics, Uppsala Univ., Uppsala, Sweden, *"A new geodesic acoustic mode induced by toroidal rotation in tokamaks"*

Th. Vernay, Diplômant EPFL, Lausanne, Switzerland, *"Les collisions électron-ion dans le code gyrocinétique ORB5"*

I. Pavlov, CRPP-EPFL, *"Analysis of plasma dynamic response to modulated electron cyclotron heating in TCV tokamak"*

D. Wagner, Budapest Univ. of Technology & Economics, Budapest, Hungary, *"Quasi two-dimensional simulation of pellet ablation and plasmoid expansion"*

E. Küng, Diplômant EPFL, Lausanne, Switzerland, *"Effect of magnetic configuration on fluctuations and turbulence in TORPEX toroidal plasmas"*

Prof. J.-P. Bœuf, LAPLACE, Univ. Paul Sabatier, Toulouse, France, *"Surface dielectric barrier discharges and applications to flow control"*

L. Federspiel, Diplômant EPFL, Lausanne, Switzerland, *"Investigation of the excitation threshold for pressure gradient driven instabilities in TORPEX plasmas"*

V. Belmondo, Univ. of Torino, Italy, *"Study of the automatic control of the ITER ion cyclotron heating and current drive system (ICH&CD system)"*

Dr. I. Kaganovich, Princeton Plasma Physics Lab., Princeton, USA, *"Collective excitations in intense beam pulses propagating through background plasma"*

Dr. P. Scarin, Consorzio RFX, Associazione ENEA-Euratom, Padova, Italy, *"Analysis of edge turbulence in RFX-mod from GPI data and comparison with other toroidal devices"*

F. Giordano, Univ. of Bologna, Italy, *"Reconstruction of cosmic muons in the CMS experiment at LHC and muongraphy of the cavern"*

Dr. A.S. Ware, Univ. of Montana, USA, *"Modeling of flow generation and transport barriers in plasmas"*

Dr. S. Alberti, CRPP-EPFL, Lausanne, Switzerland, *"Gyrotron physics for applicatins from fusion to NMR spectroscopy"*

K. Besseghir, Etudiant EPFL, Lausanne, Switzerland, *"Mécanique quantique PT-symétrique et calcul de l'opérateur C"*

Dr. A. Koenies, Max-Planck-Institute für Plasmaphysik, Greifswald, Germany, *"Global gyrokinetic simulations with PIC codes in tokamaks and stellarators"*

Dr. M.J. Hole, Australian National University, Canberra, Australia, *"Equilibria and stability of a partially relaxed 3D MHD model with KAM surfaces"*

Dr. A. Macor, Univ. de Provence, Physique des Interactions Ioniques et Moléculaires, Groupe Plasma-Surface, Marseille, France, *"Redistribution of suprathermal electrons due to fishbone frequency jumps"*

Dr. D. Testa, CRPP-EPF Lausanne, Switzerland, *"Astrophysics and fusion plasmas: Application of the SparSpec algorithm to the data analysis and design of the ITER high-frequency Mirnov coil diagnostic system"*

Drs M. Spolaore & N. Vianello, Consorzio RFX, Ass. Euratom-ENEA, Padova, Italy, *"Magnetic and electrostatic structures measured in the edge region of the RFX-mod experiment"*

Dr. L. Marot, Dept. Of Physics, Univ. Basel, Switzerland, *"Coated mirrors for ITER"*

Dr. F.P. Poli, Univ. of Warwick, UK, *"Using wavelets to extract the spectral features of edge localised modes"*

APPENDIX C External activities of CRPP Staff during 2008

C.1 National and international committees and ad-hoc groups

MEMBERSHIP

N. Baluc	Scientific and Technical Advisory Committee (STAC), Euratom Member of the HPC-FF board International Organizing Committee of the SOFT Conference (Symposium on Fusion Technology) International Advisory Committee of the ICFRM Conference (International Conference on Fusion Reactor Materials) IEA Annex II Executive Committee IEA Fusion Materials Agreement Executive Committee Steering Committee CRPP-PSI on Materials for Nuclear Applications (SCMATNUC). Swiss Society for Optics and Microscopy (SSOM) Task Coordinator of the Euratom Task TTMS-003 entitled ' Compatibility of Steels with Hydrogen and Liquids' of the Tritium Breeding and Materials Programme of EFDA Task Coordinator of the subproject entitled 'Radiation-Resistant Materials' of the EXTREMAT Integrated Project (IP) of the 6th European Framework Programmeme
P. Bruzzone	International Magnet Technology Conference Organizing Committee European Magnet Expert Group 21st Magnet Technology Conference, Programme Committee SST-1 (India), Magnet Review Group Series Connected Hubrid Magnet, Project Review Group GSI Magnet Advisory Group
J.-L. Dorier	Member of the commitee of the Swiss Vacuum Society
A. Fasoli	Visiting Professor, MIT Physics Department EFDA Steering Committee ASDEX Upgrade Programme Committee, Germany International Tokamak Physics Activities: Energetic Particles Topical Group Scientific Committee, 12th IAEA Technical Meeting on Energetic Particles in Magnetic Confinement Systems, 2008 Expert for the Review of projects submitted to the French National Agency for Research (ANR) Member of the International Review Panel for US Department of Energy Theory 2008 Review Member of visiting Committee for the Laboratory of Plasma Physics of the Ecole Polytecnique Paris (fusion of LPTP and CETP) President of a Committee for a nation wide search for researchers in plasma physics with the Italian National Research Council Member of Scientific Committee of the EFDA Transport Topical Group Scientific Expert for EFDA in the EU Facilities Review Member of the APS-DPP Programme Committee
Ivo Furno	Member of the SPS Committee
Ch. Hollenstein	Member of the Wissenschaftlicher Beirat Leibniz-Institut für Oberflächenmodifizierung Leipzig Editorial Board Plasma Chemistry and Plasma Processing Kluwer Academic/Plenum Publisher Member of the IUVSTA Plasma Division

	President of the Swiss Vacuum society
J.B. Lister	International Tokamak Physics Activities: MHD, Disruption and Control Topical Group 35th EPS Conference Programme Committee, Crete 2008
C. Marinucci	CHATS-AS, Board
P.J. Paris	Member of the CCEF
R.A. Pitts	Leader of the EFDA-JET Exhaust Physics Task Force (TF-E) CRPP Representative of the EFDA EU Task Force on Plasma-Wall Interactions
A. Pochelon	Member of the Committee of the SWISS NUCLEAR FORUM Member of the Commission for Training and Formation of the Swiss Nuclear Forum "Aussschuss Wissenschaft" Member of the FORATOM Committee, in particular of the "Research and Development Task Force (R&D.TF)
O.Sauter	Member of ITPA on Transport Physic
R. Schäublin	Member of the board of the Swiss Society for optics and microscopy
M.Q. Tran	Director of the Inst. of Physics of Energy and Particle, EPFL Consultative Committee for the Euratom Specific Research and Training Programme in the field of Nuclear Energy, Fusion (CCE-FU) Chairman of the Technical Advisory Panel of the Joint Undertaking Fusion for Energy (F4E) Swiss delegate to the Governing Board of F4E Member of the Core Commission for the nomination of Max-Planck Plasma Physics Director Standing Committee of the International Symposium on Fusion Nuclear Technology Expert on the IAEA International Fusion Research Council Member of the Steering Committee of the Center of Competence on Energy and Mobility of the the CEPF Member of the International Committee of the IRMWW and THZ conference Swiss delegate at the Fusion Power Coordinating Committee Head of EU Delegation to ITER STAC
L. Villard	Expert Group on High Performance Computing, EFDA Special working group 1 of the HPC-IFERC-Broader Approach
H. Weisen	Coordinator for particle transport at the JET Transport Task Force Coordinator for particle transport ('spokesperson') of the working group on particle transport within the ITPA database and modelling workgroup Member of the Diagnostics Working Group within the ITPA Member of the ad'hoc expert group for the application for preferential support for the proposal "Enabling a programme of ITER relevant plasma studies by transferring and installing COMPASS-D to the Institute of Plasma Physics AS CR, Association EURATOM-IPP.CR" Member of the expert panel for evaluating PhD and post-doc research proposals submitted to the Fonds National de la Recherche, Luxembourg

PARTICIPATION

B. Duval	Remote Participation Users Group, EFDA-JET 36th EPS Local Organising Committee
C. Coda	Programme Committee EPS 2009, Sofia, Bulgaria

Y.R. Martin	International Tokamak Physics Activity: Confinement Database and Modelling Topical Group Vice-chairman of the 22nd IAEA-Fusion Energy Conference, Geneva 2008, Local-committee
M.Q. Tran	Chairman of the 22nd IAEA-Fusion Energy Conference, Geneva 2008, Local-committee
R.A. Pitts	International Tokamak Physics Activity: SOL & Divertor Topical Group

C.2 Editorial and society boards

S. Coda	Editorial Board of Plasma Physics and Controlled Fusion
Ch. Hollenstein	Editorial Board Plasma Chemistry and Plasma Processing Kluwer Academic/Plenum Publisher
J.B. Lister	Chairman of the European Physical Society Plasma Physics Division Member of the International Advisory Board of Plasma Physics and Controlled Fusion
Y.R. Martin	Chairman of the Association Vaudoise des Chercheurs en Physique
P.J. Paris	EFDA Information Network (PIG) "Fédération Romande de l'Energie" Committee Chairman of the "International Association of Specialists in Energy" (AISEN)
A. Pochelon	Auditor of the Swiss Physical Society Committee

C.3 EPFL committees and commissions

N. Baluc	Commission Ecole Doctorale en Science et Génie des Matériaux
J-L. Dorier	Commission du Doctorat de la Section de Physique, FSB-EPFL
A. Fasoli	Commission d'Enseignement de la Section de Physique, FSB-EPFL Commission Stratégique de la Physique, EPFL Comité de nomination "Professeur de Théorie des Plasmas"
J-Ph. Hogge	Commission du Doctorat de la Section de Physique, FSB-EPFL
O. Sauter	Commission du Doctorat de la Section de Physique, FSB-EPFL
M.Q. Tran	Commission du Doctorat de la Section de Physique, FSB-EPFL Commission stratégique de la Section de Physique, EPFL Membre du Comité de Sélection du Prix de la meilleure thèse EPFL Comité de nomination "Professeur de Théorie des Plasmas"
T.M. Tran	Groupe de travail technique du Comité de Pilotage HPC/MPC, EPFL
L. Villard	Délégué à la mobilité, Section de physique, FSB-EPFL Commission d'Ethique, EPFL Commission d'Enseignement de la Section de Physique, FSB-EPFL Groupe de travail technique HPC (High Performance Computing) – EPFL Steering Committee, HPC (High Performance Computing) – EPFL Steering Committee, Blue Gene Project - EPFL

APPENDIX D The basis of controlled fusion

D.1 Fusion as a sustainable energy source

Research into controlled fusion aims to demonstrate that it is a valid option for generating power in the long term future in an environmentally, politically and economically acceptable way. Controlled fusion is a process in which light nuclei fuse together to form heavier ones: during this process a very large amount of energy is released. For a fusion reactor it is planned to use the two isotopes of hydrogen: deuterium (D) and tritium (T), which fuse together much more readily than any other combination of light nuclei according to the following reaction:

$$D^2 + T^3 \rightarrow He^4 + n + 17.6MeV$$

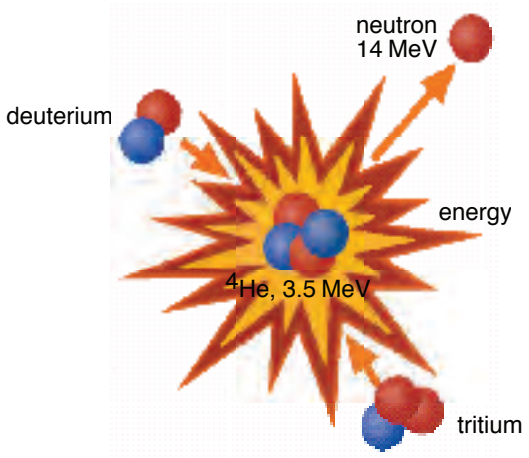

Fig. D.1 *Schematic of a fusion reaction between deuterium and tritium nuclei. The products are 3.5MeV ^{4}He, the common isotope of helium, and a 14MeV free neutron.*

The end products are helium and neutrons (n). The total energy liberated by fusing one gram of a 50:50% mixture of deuterium and tritium is 94000kWh, which is 10 million times more than from the same mass of oil. 80% of this energy is carried by the neutrons with an energy of 14MeV while the remaining 20% is carried by the helium nucleus. Most of this energy eventually becomes heat to be stored or converted by conventional means into electricity.

The temperature at which fusion reactions start to become significant are above a few tens of millions of degrees. For the D-T reaction, the optimal temperature is of the order of 70-200 million degrees. At such temperatures the D-T fuel is in the plasma state.

Deuterium is very abundant on the earth and can be extracted from water (0.034g/l). Tritium does not occur naturally, since its half-life is only 12.3 years, but it can be regenerated from lithium using the neutrons produced by the D-T fusion reactions. The two isotopes of natural lithium contribute to this breeding of tritium according to the reactions:

$$Li^6 + n \rightarrow He^4 + T^3 + 4.8MeV$$

$$Li^7 + n \rightarrow He^4 + T^3 + n - 2.5MeV$$

The relative abundance of the two lithium isotopes Li^6 and Li^7 are 7.4% and 92.6%, respectively. The known geological resources of lithium both in the earth and in the sea water are large enough to provide energy for an unlimited time.

D.2 Attractiveness of fusion as an energy source

The inherent advantages of fusion as an energy source are:

- The fuels are plentiful and their costs are negligible because of the enormous energy yield of the reaction;
- The end product of the reaction is helium, an inert gas;
- No chain reaction is possible: at any time only a very small amount of fuel is in the reacting chamber and any malfunction would cause an immediate drop of temperature and the reaction would stop;
- No after-heat problem can lead to thermal runaway;
- None of the materials required by a fusion power plant are subject to the provisions of the non-proliferation treaties.

Its further potential advantages are:

- Radioactivity of the reactor structure, caused by neutrons, can be minimised by careful selection of low-activation materials resulting in a manageable quantity of long lived radioactive waste;
- The release of tritium in normal operation can be kept at a very low level. The inventory of tritium in the breeding section of the reactor and on the site can be sufficiently small so that the worst possible accident could not lead to a harmful release to the environment requiring evacuation of the nearby population.

APPENDIX E Sources of Financial Support

The work carried out at the CRPP and presented in this annual report was financed from several sources. The major financial support is provided by the Ecole Polytechnique Fédérale de Lausanne (EPFL), EURATOM, the Paul Scherrer Institute (PSI), which hosts the supraconductivity and materials science activities, and the Swiss National Science Foundation and the Centre de Compétence "Energie-Mobilité" of the CEPF. Other public and private organisations which contributed funding for our research in 2008 include, in alphabetical order: Charmilles SA,, OC Oerlikon, Ruag, the Secrétariat d'Etat à l'Education et à la Recherche (SER), Sulzer Metco AG, the Swiss Commission pour la Technologie et l'Innovation (CTI), Swiss Electric AG and Tetra Pak SA.

The CRPP is the Host of Euratom Fellows:

- Dr. I. Pagonakis whose fellowship is entitled *"Design of the collector system for the coaxial gyrotron 170GHz/2MW/CW"*,
- Dr. J. Paley, whose fellowship is entitled *"Real-time control of multi-beam ECRH-ECCD in the TCV tokamak"*,
- Dr. P. Ricci, whose fellowship is *entitled "Plasma turbulence: comparison between theory simulations and the basic plasma physics experiments TORPEX"*, and
- Dr. G. Turri, whose fellowship is entitled *"MHD spectroscopy in the TCV tokamak, in particular to determine current density profiles"*.
- MM. A. Collazos and M. da Silva, EC-TECH "Electron cyclotron system technology for ITER"
- F. Cau, M. Bagnasco, MATEFU "Magnet Technology for Fusion"

APPENDIX F Glossary

A general purpose glossary for the field of controlled fusion and plasma physics is provided in the CRPP Annual Report every two years. Since it was part of the Annual Report 2007, it will not be provided here.